SPIN DYNAMICS OF POLARONS AND POLARON PAIRS IN A RANDOM HYPERFINE FIELD

by

Robert C. Roundy

A dissertation submitted to the faculty of
The University of Utah
in partial fulfillment of the requirements for the degree of

Doctor of Philosophy

in

Physics

Department of Physics and Astronomy

The University of Utah

December 2015

The University of Utah Graduate School

STATEMENT OF DISSERTATION APPROVAL

The dissertation of **Robert C. Roundy**

has been approved by the following supervisory committee members:

Mikhail Raikh	, Chair	**02/11/2014** Date Approved
Zeev Valentine Vardeny	, Member	**02/11/2014** Date Approved
Yong-Shi Wu	, Member	**02/11/2014** Date Approved
Oleg Starykh	, Member	**02/11/2014** Date Approved
Alexander Balk	, Member	**02/11/2014** Date Approved

and by **Carleton DeTar** , Chair/Dean of

the Department/College/School of **Physics and Astronomy**

and by David B. Kieda, Dean of The Graduate School.

ABSTRACT

Spin-dependent recombination of polaron pairs and spin relaxation of a single polaron are the most fundamental processes are responsible for the performance of organic-spintronics-based devices such as light-emitting diodes and organic spin valves1. In organic materials, with no spin-orbit coupling, both processes are due to random hyperfine fields created by protons neighboring the polaron sites.

The essence of spin-dependent recombination is that in order to recombine the pair must be in the singlet state. Hyperfine fields acting on the electron and hole govern the spin-dynamics of localized pairs during the waiting time for recombination. We demonstrate that for certain domain of trapping configurations of hyperfine fields, crossover to the singlet state is quenched. This leads to the blocking of current. The phenomenon of organic magnetoresistance (OMAR) is described by counting the weights of trapping configurations as a function of magnetic field. This explains the universality of the lineshapes of the OMAR curves. In finite samples incomplete averaging over the hyperfine fields gives rise to mesoscopic fluctuations of the current response. We also demonstrate that under the condition of magnetic resonance, new trapping configurations emerge. This leads to nontrivial evolution of current through the sample with microwave power.

When discussing spin-relaxation two questions can be asked: (a) How does the local spin polarization decay as a function of distance from the spin-polarized injector? (b) How does the injected spin decay as a function of time after spatial averaging? With regard to (a), we demonstrate that, while decaying exponentially on average, local spin-polarization exhibits giant fluctuations from point to point. Concerning (b), we find that for a spin-carrier which moves diffusively in low dimensions the decay is faster than a simple exponent. The underlying physics for both findings is that in describing spin evolution it is necessary to add up amplitudes for partial spin-rotations in hyperfine fields on different sites.

CONTENTS

LIST OF FIGURES

ACKNOWLEDGEMENTS

The creation of something new is not accomplished by the intellect but by the play instinct acting from inner necessity. The creative mind plays with the objects it loves.

Carl Jung

This dissertation would not be possible without the support of many people. Firstly, I would like to acknowledge the love and support of my beautiful wife and children. Secondly, I would like to acknowledge the MRSEC, who through the grant MRSEC DMR-112125 funded the research. The connection to MRSEC was quite informal. In fact, the present dissertation is an outgrowth of experimental effort conducted in the department under the auspices of the MRSEC. Moreover, I had the unique opportunity to see the predictions made in this dissertation tested experimentally. I am grateful to Dr. Boehme for showing his results to me prior to publication. Thirdly, I would like to thank my advisor, Dr. Mikhail Raikh, without whose tireless efforts and sage advice on all matters the present work would not exist. I would be a poorer scientist and a poorer human being had I not had the chance to get to know him. I would also like to thank all of the members of my supervisory committee for their time invested into committee meetings and studying my dissertation. The skills which were necessary to perform the research here, I learned under the tutelage of Dr. Yong-Shi Wu, to whom I am deeply grateful.

Finally, I would like to dedicate this to my brother, James Clayton Roundy, who tragically passed away while I was working on this dissertation.

PART I

SPIN-DEPENDENT RECOMBINATION AND ORGANIC MAGNETORESISTANCE

CHAPTER 1

INTRODUCTION

The present dissertation is not an outgrowth of fundamental discoveries, like the quantum Hall effect or superconductivity. It arises, instead, from prominent semi-applied discoveries in material science which were made in the last two decades and are listed below:

- It would be fair to date the emergence of the field of spintronics from the experimental observation of the giant magnetoresistance (GMR) effect [1, 2] in the late 1980s. The most impressive consequence of this discovery is that it was quickly followed by fabrication of spin valves, with scores of applications in consumer electronics.

  A spin valve is a device in which a thin nonmagnetic layer is sandwiched between two ferromagnetic electrodes. In the simplest geometry, current is passed through the sandwich, and resistance is measured. The essence of the GMR effect is that the resistance is different if the magnetization in the two ferromagnetic ends are aligned parallel or antiparallel to each other.

  The GMR effect, and specifically, spin-valves were quickly leveraged technologically, leading to, among other things, GMR-based computer hard disks (HDD) and magnetic random access memory (MRAM). For example, in hard disks each logical bit is encoded in the magnetization direction of a small domain on a spinning platter. As the disk spins around a read head hovers over the platter. The read head consists of the spacer layer and a ferromagnetic electrode. Current passes through the disk and into the read head. By measuring the resistance, the direction of magnetization is identified, and the logical state is recovered [3].

  In Fig. 1.1, adapted from Ref. [3], the performance of an MRAM is illustrated. The elemental unit of an MRAM is again the spin valve. An idealized MRAM is simply a trilayer spin-valve structure, a fixed ferromagnetic layer, a thin spacer layer, and another ferromagnetic layer. In the last layer the magnetization direction can be

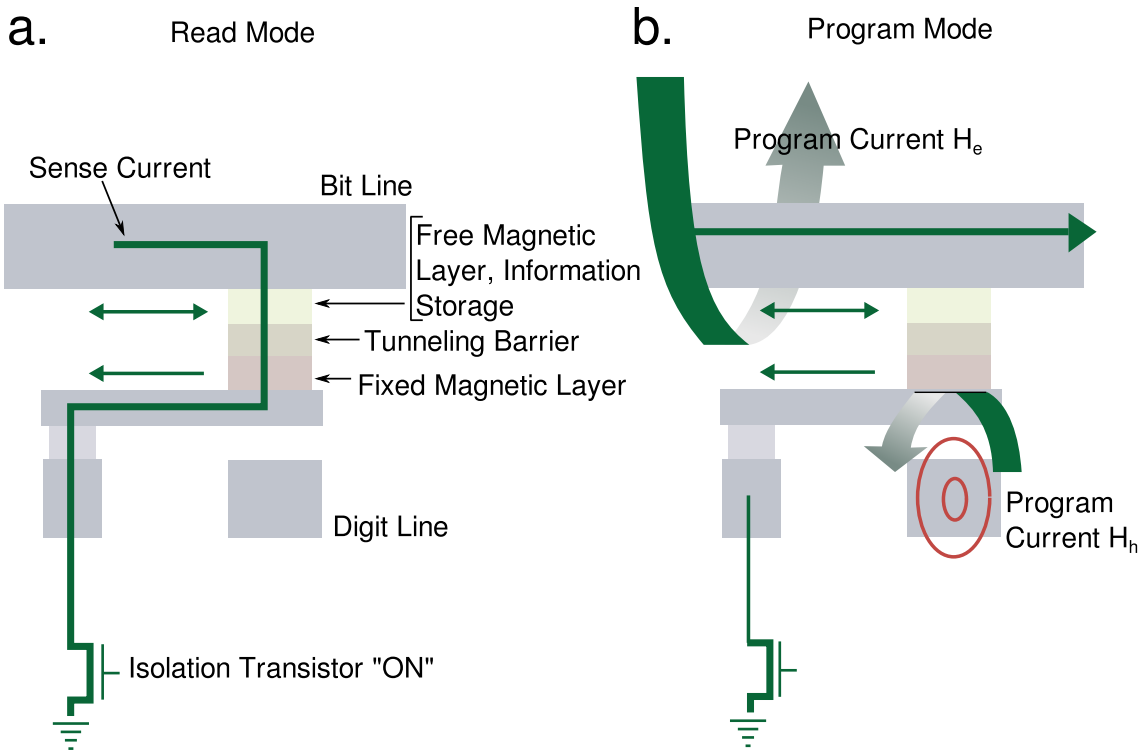

Figure 1.1: A schematic illustration of a reading (a) and writing (b) mode of operation of an MRAM cell is shown. The crucial ingredient is the colored stack which makes up an elementary spin valve. The bit is read by passage of current (in green) through the spin valve. To write one bit of information current is passed (large green arrow) which creates a magnetic field sufficient to magnetize the domain where the logical bit is stored. Adapted from Ref. [3].

changed by an external current-induced magnetic field, and it is the direction of this magnetization that encodes the logical bit. A real MRAM device is a collection of such simple cells, one for each bit. To read the state of one cell, current is passed through the stack and like in the case of the HDD, resistance is measured.

- The first spin valve using an organic polymer was reported in 2004 [4]. In this seminal paper the authors reported a spin valve effect, measured as $\Delta R/R = (R_{\text{anti-parallel}} - R_{\text{parallel}})/R_{\text{anti-parallel}}$, where R_{parallel} is the resistance when the ferromagnetic electrodes are aligned in the same direction, which was as high as 40%, see Fig. 1.2.

  The organic compound for the active layer in Ref. [4], was Alq_3, which was sandwiched between $La_{0.67}Sr_{0.33}MnO_3$ (LSMO) and Co. The thickness of the Alq_3 was ~ 175nm. All of the experiments were performed at low temperatures, the spin valve effect was reported to be as high as 40% at 11K, while at high enough temperatures the spin valve effect vanished.

- In 2004, Francis et al. [5] discovered that even with nonmagnetic electrodes, the resistance of a three-layer structure is strongly sensitive to *weak* magnetic fields even at room temperature. The active layer of the device in [5] was PFO[1], which was sandwiched between e.g., PEDOT[2] and Ca. The relative change, $\Delta R/R = (R(B) - R(0))/R(0)$, of the resistance reported in [5] was as high as 10% at room temperature for applied field, B, as low as 10mT, see Fig. 1.3. In the same paper it was shown similar results hold for various electrode materials and polymer thicknesses.

  In the Abstract of [5], the authors throw down the metaphorical gauntlet:

  > .... To the best of our knowledge, the discovered effect is not adequately described by any of the MR mechanisms known to date.

The unifying theme of the present thesis is the role of random nuclear (hyperfine) magnetic field in organic spintronics. The body of the thesis can be conveniently divided into two parts: the phenomenon of organic magnetoresistance, (Part I, Chapters 1-3) and the physics of organic spin-valves (Part II, Chapters 4-8). More specifically, in Part I we study the fundamental aspects of spin physics of *pairs* of carriers. It is now commonly accepted [6] that it is pairs of carriers which are responsible for the phenomenon of organic

[1] PFO is the organic compound poly(9,9-dioctylfluorenyl-2,7-diyl).

[2] PEDOT is the compound poly(3,4-ethylenedioxythiophene) poly(styrenesulfonate).

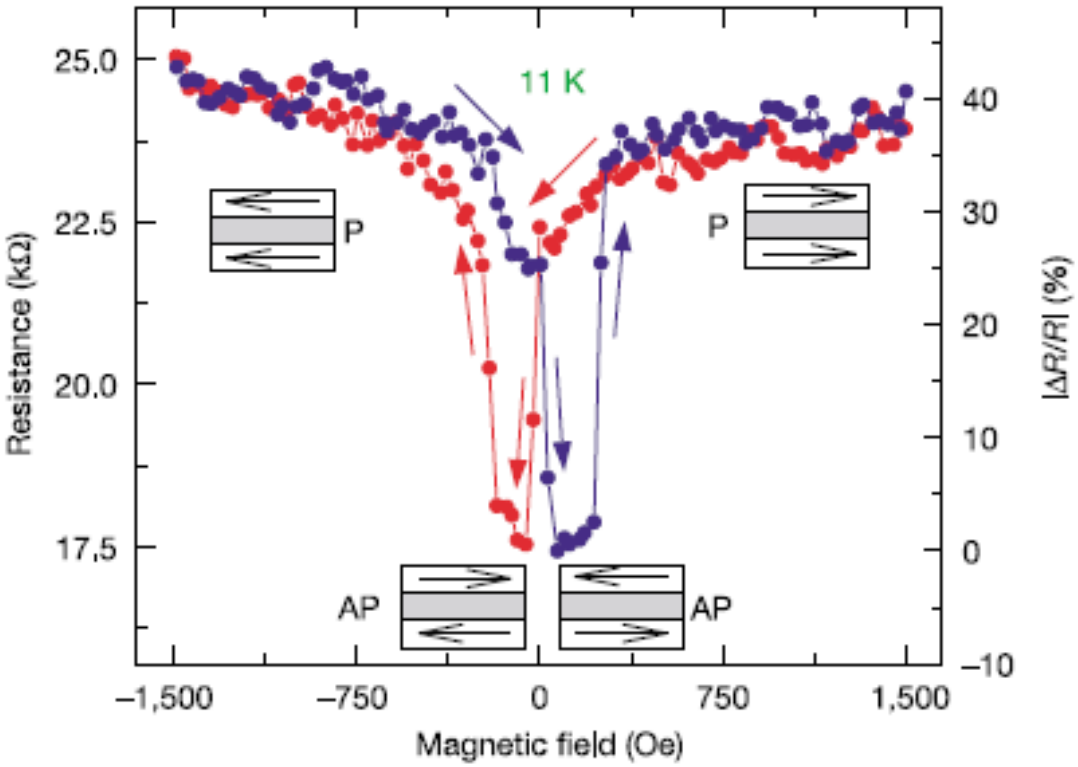

Figure 1.2: The magnetotransport response of the OSE spin-valve device. The GMR loop of a LSMO (100 nm)/Alq3 (130 nm)/Co (3.5 nm) spin-valve device was measured at 11 K. The blue (red) curve denotes GMR measurements made while increasing (decreasing) H. The antiparallel (AP) and parallel (P) configurations of the FM magnetization orientations are shown in the insets at low and high H, respectively. The electrical resistance of the device is higher when the magnetization directions in FM1 and FM2 films are parallel to each other. Adapted from Ref. [4].

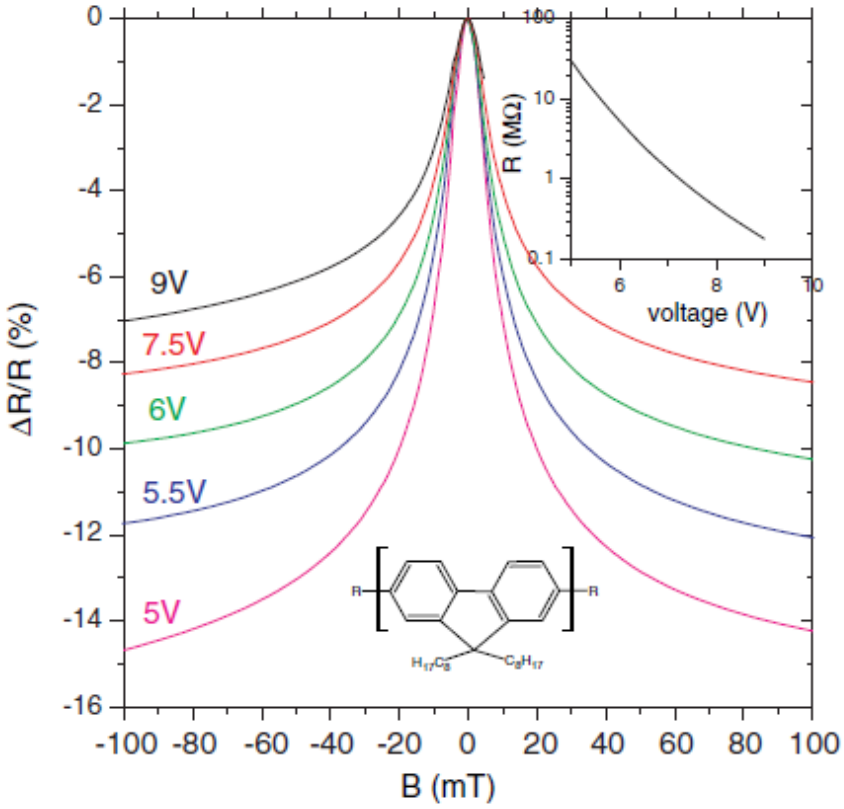

Figure 1.3: Magnetoresistance, $\Delta R/R$ curves, measured at room temperature in an ITO (30 nm)/PEDOT (.100 nm)/PFO (.100 nm)/Ca (.50 nm including capping layer) device at different voltages. The inset shows the device resistance as a function of the applied voltage. Adapted from Ref. [5].

magnetoresistance. Part II is devoted to the spin dynamics of a *single* carrier in a random hyperfine field. More specifically, we uncover profound aspects of spin-memory loss due to random hyperfine fields. This is a central issue of organic spintronics because the common mechanism responsible for spin-memory loss in metal-based spin valves, namely, spin-orbit coupling, is inefficient in organic materials which are made of light atoms. Therefore, the random spin rotation in hyperfine fields is a dominant mechanism for spin-memory loss. On the other hand, spin-memory loss is a *fundamental* process which limits the performance of organic spin-valves. In more prosaic terms one cannot make the active layer of a spin-valve thicker than the spin-diffusion length in the material constituting the active layer.

Both the fundamental physical picture and the mathematical techniques employed to obtain the main results in Part I and Part II are different. Therefore, each part is preceded by a special section in which the physical framework and mathematical foundations are introduced and discussed.

In general, the very intention to develop a theory of transport in organic materials is discouraging. This is because the microscopic picture of transport is vastly ambiguous. It cannot be approximated either by simple diffusion, as in a metal, nor by thermally activated hopping, as in an amorphous insulator. What is known for sure is that the carrier mobilities are very low, these mobilities do not exhibit well defined activation energies, and that the motion of carriers along the chains and between the chains is accompanied by strong distortion of the backbone (polaronic effects). What makes matters even worse, is that organic materials are strongly inhomogeneous. As a result, one cannot judge from experimental current-voltage characteristics whether the current flows through the sample homogeneously or is restricted to a few of the most conductive paths.

There is, however, an argument which outweighs the above concerns. It can be found in the literature on chemical reactions, which is nearly four decades old [7]. This simple argument states that spin selection rules are superior to all the above complications. For example, if the chemical reaction involves the recombination of an exciton, then the pair partners, which constitute the exciton, can recombine only if they are in the singlet state, S. On the other hand, they are generated in all possible spin states, T_0, T_+, T_-, and S. In a medium with spin-orbit interaction the spin-selection rules for recombination do not make any difference because the spin-orbit instantaneously mixes all spin components of the pair. Conversely, without spin-orbit, the memory about the initial spin orientations survives for a long time, regardless of how many times a carrier was scattered prior to recombination. Since the recombination is only from S, the exciton assembled from two

carriers, say, in T_+, will never recombine. It is the mixing of spin components caused by the random magnetic fields created by the protons which surround the pair partners that allows the recombination.

A key idea of Ref. [7] rests on the fact that the typical number of these protons is big. Thus their cumulative hyperfine field can be treated as *static*, and, moreover, as a *classical* Gaussian random variable. This opens an avenue to develop a quantitative theory predicting the yield of a chemical reaction as a function of time. Calculating this yield requires ensemble averaging over random hyperfine fields. Remarkably, as was demonstrated in Ref. [7], this averaging can be performed analytically. The authors of Ref. [7] calculated the time dependence of the probability for a pair of spins to cross from S to T, where T is any of triplet states, by treating the nuclear bath as a static Gaussian field, compared the analytical result with numerical solution in which the nuclear spins were treated quantum-mechanically, and found excellent agreement. In Ref. [7] only very weak and very strong magnetic fields were considered. Generalization to the arbitrary fields can be found in Ref. [8].

With the discovery of the phenomenon of Organic Magnetoresistance (OMAR) there was much confusion about its interpretation. This confusion has essentially been dissipated after the model of Ref. [6] was put forward. We understand the reasoning in Ref. [6] as follows: Current passage can be envisioned as carrier hops over the sites. On the way between the electrodes, the carrier encounters the situation when it has to hop on the site which is already occupied by another carrier. The Pauli principle dictates that the final state after this hop is the singlet state of the two carriers (pair-partners). Since in the initial state the pair can be found with equal probability in all spin states, the scenario of the hop is very different depending on the initial state. If the initial state is S, the waiting time for the hop will be same as it would be in the absence of spin. On the contrary, if the initial state is T, the hop will take place much later. Indeed, the pair should first "wait" to find itself in S, and only then will the hop be allowed. Therefore, the essence of the OMAR phenomenon is the sensitivity of the "mixing efficiency" to the external field. More specifically, the higher is the magnetic field, the lower is the "mixing efficiency" for the T_+ and T_- states. Summarizing, the OMAR phenomenon is the consequence of the lifting of the spin-blocking due to the hyperfine field.

Nothing changes in the above scenario when one of the electrodes supplies electrons, while the other one supplies holes. Then, instead of occupying the same site, the pair partners recombine. Still, the recombination is allowed only when the pair is a singlet.

Note now, that calculating the yield of chemical reactions and calculating the probability

of either a hop or recombination involve the very same averaging over the hyperfine fields. This is why the breakthrough made in Ref. [7] ensures that the OMAR phenomenon can be described quantitatively.

The above scenario is certainly a strong strong simplification of OMAR physics. In reality it is impossible to rigorously separate the "waiting" for a recombination and the recombination act itself. Rigorous analysis is carried out in Chapter 3, where it is shown that recombination exerts a feedback on the pair spin dynamics. It might be that the above scenario is incomplete, however, it does allow us to make *quantitative* predictions for the observables which can be verified experimentally. Namely, we predict a mesoscopic effect in OMAR, which is random fluctuations of the resistance of a small sample with magnetic field due to incomplete averaging over the hyperfine fields. We also predict a nonmonotonic dependence of the current response under the condition of magnetic resonance. These predictions are the subject of Chapters 4 and 5, respectively.

1.1 Averaged pair dynamics in a random hyperfine field

In this section we will present a rederivation of results which were originally obtained in Ref. [7]. In the original paper these results are presented in a compressed form. On the other hand, all of the theory which we develop in later chapters rests on this foundation. For this reason, we present the results in a more systematic, pedagogical, and detailed fashion. A second motivation for presenting the theoretical treatment of Ref. [7], is that we extend it to include a finite external field, which is crucial for the theory of OMAR developed in the subsequent chapters.

We wish to calculate the probability of a system to be in a singlet state if we start it out in a singlet state and let it evolve with time. We assume that the two independent spin 1/2 particles, $i = 1, 2$, are weakly coupled and evolve under a constant applied field, $\boldsymbol{B}$, and a random hyperfine field, $\boldsymbol{b}_i$. The total field of a pair partner is given by $\boldsymbol{\Omega}_i = \boldsymbol{B} + \boldsymbol{b}_i$.

In the present section we use the Dirac notation. Let us label the spin-states as $|S\rangle = \frac{1}{\sqrt{2}}\left(|\uparrow\downarrow\rangle - |\downarrow\uparrow\rangle\right), |T_+\rangle = |\uparrow\uparrow\rangle$, and so on. The wave function is $|\psi(t)\rangle$ which satisfies the Schrödinger equation

$$i\frac{d\,|\psi(t)\rangle}{dt} = H\,|\psi(t)\rangle\,, \quad |\psi(0)\rangle = |S\rangle\,. \tag{1.1}$$

We are only interested in the degrees of freedom associated with the spin states. Therefore we adopt the simplest Hamiltonian,

$$H = H_1 + H_2 = \boldsymbol{S}_1 \cdot \boldsymbol{\Omega}_1 + \boldsymbol{S}_2 \cdot \boldsymbol{\Omega}_2, \tag{1.2}$$

where $\boldsymbol{S}$ is the vector of spin angular momentum $S^i = \sigma^i/2$. We have, for notational simplicity, taken units in which $\hbar = 1$.

To find the probability that we are in the state $|S\rangle$ at some time later we find the amplitude $A_S(t) = \langle S|\,\psi(t)\rangle$, and the probability $P_S(t) = |A_S(t)|^2 = \langle S|\,\psi(t)\rangle\,\langle\psi(t)|\,S\rangle$. For the present, we will rewrite this as the expectation value for the operator $\Pi_S = |S\rangle\,\langle S|$. The operator Π_S is the projection operator onto the singlet subspace. Reordering the expression for $P_S(t)$, yields the equivalent expression, $P_S(t) = \langle\psi(t)|\,\Pi_S\,|\psi(t)\rangle$.

It will be convenient to evaluate $P_S(t)$ by "switching to the Heisenberg picture." In the Heisenberg picture the states remain fixed while the operators evolve in time. In this picture we write $P_S(t) = \langle\psi(0)|\,\Pi_S(t)\,|\psi(0)\rangle$. We wish also to note that $P_S(t)$ can be written as the trace of the compound operator

$$P_S(t) = \mathrm{Tr}\Big(|\psi(0)\rangle\,\langle\psi(0)|\,\Pi_S(t)\Big) = \mathrm{Tr}\Big(\Pi_S(0)\Pi_S(t)\Big). \tag{1.3}$$

Here, we used the initial condition $|\psi(0)\rangle = |S\rangle$ to recognize $|\psi(0)\rangle\,\langle\psi(0)| = \Pi_S(0)$.

To evaluate $P_S(t)$ we use the operator identity $\Pi_S(t) = \frac{1}{4}\mathbf{1} - \boldsymbol{S}_1(t)\cdot\boldsymbol{S}_2(t)$, which can be easily verified by checking that both sides have the same action on the basis states. Expanding Eq. (1.3) yields

$$P_S(t) = \frac{1}{16}\mathrm{Tr}(\mathbf{1}) - \frac{1}{4}\mathrm{Tr}(\boldsymbol{S}_1(0)\cdot\boldsymbol{S}_2(0)) - \frac{1}{4}\mathrm{Tr}(\boldsymbol{S}_1(t)\cdot\boldsymbol{S}_2(t)) + \mathrm{Tr}\left(\boldsymbol{S}_1(0)\cdot\boldsymbol{S}_2(0)\,\boldsymbol{S}_1(t)\cdot\boldsymbol{S}_2(t)\right). \tag{1.4}$$

The above expression is simplified upon noticing that $\mathrm{Tr}(\boldsymbol{S}_1(t)\cdot\boldsymbol{S}_2(t)) = 0$ at all times t. The result in component notation reads

$$P_S(t) = 1/4 + \mathrm{Tr}\left(S_1^i(0)S_{2i}(0)S_1^j(t)S_{2j}(t)\right) = 1/4 + \mathrm{Tr}\left(S_1^i(0)S_1^j(t)S_{2i}(0)S_{2j}(t)\right). \tag{1.5}$$

To proceed further, notice that the trace over the subspaces corresponding to pair partner 1 and pair partner 2 can be performed independently:

$$P_S(t) = 1/4 + \mathrm{Tr}_1\left(S_1^i(0)S_1^j(t)\right)\mathrm{Tr}_2\left(S_{2i}(0)S_{2j}(t)\right) = 1/4 + {T_1}^{ij}T_{2ij}. \tag{1.6}$$

Here, we have introduced the notation Tr_1 to denote a trace only over the spin-space corresponding to pair partner 1. We have also defined the time dependent tensors

$$T_1^{ij}(t) = \mathrm{Tr}(S_1^i(0)S_1^j(t)). \tag{1.7}$$

Analogous notations are presumed for pair partner 2.

For the simple system described by Eq. (1.2) we can go further. The Heisenberg equation of motion for $\boldsymbol{S}_1$ reads

$$i\frac{dS_1^i}{dt} = [S_1^i, H] = [S_1^i, S_1^j\Omega_{1j} + S_2^j\Omega_{2j}] = i\epsilon^{ijk}S_{1k}\Omega_{1j}. \tag{1.8}$$

Upon reverting to vector notation we recover the well known result

$$\frac{d\boldsymbol{S}}{dt} = \boldsymbol{\Omega} \times \boldsymbol{S}. \tag{1.9}$$

When $\boldsymbol{\Omega}$ is constant this is a linear first order ODE. It will admit a fundamental solution in terms of the initial conditions $\boldsymbol{S}(0)$ and a time dependent matrix $M(t)$,

$$\boldsymbol{S}(t) = M(t)\boldsymbol{S}(0). \tag{1.10}$$

In terms of the fundamental solution $M(t)$ we have

$$T^{ij}(t) = \mathrm{Tr}(S^i(0)S^j(t)) = \mathrm{Tr}(S^i(0)M_k^j(t)S^k(0)) = M_k^j(t)\mathrm{Tr}(S^i(0)S^k(0)). \tag{1.11}$$

We are allowed to remove the real numbers $M_k^j(t)$ from the trace in the last equality due to the linearity of the trace operation.

For spin 1/2 particles we can use the well known property of the Pauli matrices, $\sigma_i\sigma_j = \delta_{ij} + i\epsilon_{ijk}\sigma^k$.

$$\mathrm{Tr}\left(S^i(0)S^k(0)\right) = \frac{1}{4}\mathrm{Tr}(\sigma^i\sigma^k) = \frac{1}{4}\mathrm{Tr}(\delta^{ik} + i\epsilon^{ijl}\sigma_l) = \frac{1}{2}\delta^{ik}. \tag{1.12}$$

The final result for the tensor T^{ij} in terms of the matrix M reads

$$T^{ij} = M_k^j(t)\frac{1}{2}\delta^{ik} = \frac{1}{2}M^{ji}. \tag{1.13}$$

This immediately yiels $P_S(t)$ also in terms of the matrices M_1 and M_2 as

$$P_S(t) = \frac{1}{4}\left(1 + M_1^{ji}(t)M_{2ji}(t)\right). \tag{1.14}$$

At this point we would like to note that we have reduced the quantum mechanical calculation of $P_S(t)$ to solutions of the classical equation of a magnetic moment in a magnetic field. Solutions to the latter are, of course, well known. For completeness we present a solution here in the case of constant $\boldsymbol{\Omega}_1$ and $\boldsymbol{\Omega}_2$.

We can solve Eq. (1.9) in the following way. Take a second time derivative of both sides of Eq. (1.9)

$$\ddot{\boldsymbol{S}} = \boldsymbol{\Omega} \times \dot{\boldsymbol{S}} = \boldsymbol{\Omega} \times (\boldsymbol{\Omega} \times \boldsymbol{S}) = \boldsymbol{\Omega}(\boldsymbol{\Omega} \cdot \boldsymbol{S}) - \boldsymbol{S}\Omega^2 \tag{1.15}$$

The term $\boldsymbol{\Omega} \cdot \boldsymbol{S}$ is really a constant, to see it take Eq. (1.9) and take the dot product with $\boldsymbol{\Omega}$, $\boldsymbol{\Omega} \cdot \boldsymbol{S}(t) = \boldsymbol{\Omega} \cdot \boldsymbol{S}(0)$. Physically this tells us that the vector $\boldsymbol{S}$ is tracing out a cone with respect to $\boldsymbol{\Omega}$.

The remaining second order ODE is

$$\ddot{\boldsymbol{S}} = -\Omega^2 \boldsymbol{S} + \boldsymbol{\Omega}(\boldsymbol{\Omega} \cdot \boldsymbol{S}_0). \tag{1.16}$$

The initial conditions are $\boldsymbol{S}(0) = \boldsymbol{S}_0$, and $\dot{\boldsymbol{S}}(0) = \boldsymbol{\Omega} \times \boldsymbol{S}_0$. This is solved with the ansatz,

$$\boldsymbol{S} = \boldsymbol{E}\cos(\Omega t) + \boldsymbol{F}\sin(\Omega t) + \boldsymbol{G}, \tag{1.17}$$

where $\boldsymbol{E}, \boldsymbol{F}$, and $\boldsymbol{G}$ are constant vectors fixed by the initial conditions. The inital conditions give the following solution,

$$\boldsymbol{S} = \left(\boldsymbol{S}_0 - \frac{(\boldsymbol{\Omega} \cdot \boldsymbol{S}_0)\boldsymbol{\Omega}}{\Omega^2}\right)\cos(\Omega t) + \frac{\boldsymbol{\Omega} \times \boldsymbol{S}_0}{\Omega}\sin(\Omega t) + \frac{(\boldsymbol{\Omega} \cdot \boldsymbol{S}_0)\boldsymbol{\Omega}}{\Omega^2}. \tag{1.18}$$

Writing this in components,

$$S^i = \left[\left(\delta^{ij} - \frac{\Omega^i\Omega^j}{\Omega^2}\right)\cos(\Omega t) + \frac{\epsilon^{ikj}\Omega_k}{\Omega}\sin(\Omega t) + \frac{\Omega^i\Omega^j}{\Omega^2}\right] S_{0j} \tag{1.19}$$

allows us to extract the matrix $M(t)$. To separate out the effects due to the magnitude and orientation of $\boldsymbol{\Omega}$ we write $\boldsymbol{\Omega} = \Omega\boldsymbol{n}$.

$$M^{ij}(t) = \left(\delta^{ij} - n^i n^j\right)\cos(\Omega t) - \epsilon^{ijk} n_k \sin(\Omega t) + n^i n^j. \tag{1.20}$$

Now we can explicitly write down the probability, $P_S(t)$, for two particles in constant magnetic fields to be in the singlet state when they started in the singlet state by inserting Eq. (1.20) into Eq. (1.14). Note, that M has a symmetric part and an antisymmetric part, which for the present derivation we call P and Q, $M = P + Q$. P and Q are given by

$$P^{ij} = (\delta^{ij} - n^i n^j)\cos(\Omega t) + n^i n^j = P^{ji}, \tag{1.21}$$

$$Q^{ij} = -\epsilon^{ijk} n_k \sin(\Omega t) = -Q^{ji}. \tag{1.22}$$

The trace specified in Eq. (1.14) is simplified in terms of P and Q as

$$M_1{}^{ij} M_{2ij} = (P_1{}^{ij} + Q_1{}^{ij})(P_{2ij} + Q_{2ij}) = P_1{}^{ij} P_{2ij} + Q_1{}^{ij} Q_{2ij}. \tag{1.23}$$

These are, in turn, found from routine calculation

$$\begin{aligned} P_1{}^{ij} P_{2ij} &= \left((\delta^{ij} - n_1^i n_1^j)\cos(\Omega_1 t) + n_1^i n_1^j\right)\left((\delta_{ij} - n_{2i} n_{2j})\cos(\Omega_2 t) + n_{2i} n_{2j}\right) \\ &= (1 + (\boldsymbol{n}_1 \cdot \boldsymbol{n}_2)^2)\cos(\Omega_1 t)\cos(\Omega_2 t) \\ &\quad + (1 - (\boldsymbol{n}_1 \cdot \boldsymbol{n}_2)^2)(\cos(\Omega_1 t) + \cos(\Omega_2 t)) + (\boldsymbol{n}_1 \cdot \boldsymbol{n}_2)^2, \end{aligned} \tag{1.24}$$

for the symmetric part P, and

$$Q_1{}^{ij} Q_{2i} j = (-\epsilon^{ijk} n_k \sin(\Omega_1 t))(-\epsilon_{ijl} n^l \sin(\Omega_2 t))$$

$$= 2(\boldsymbol{n}_1 \cdot \boldsymbol{n}_2)\sin(\Omega_1 t)\sin(\Omega_2 t), \tag{1.25}$$

for the antisymmetric part Q.

Using Eqs. (1.24), (1.25), (1.23), and (1.14) we can write down the full expression for $P_S(t)$,

$$\begin{aligned} P_S(t) = \frac{1}{4}\Big\{ &\left[1 + (\boldsymbol{n}_1 \cdot \boldsymbol{n}_2)^2\right](1 + \cos(\Omega_1 t)\cos(\Omega_2 t)) \\ &+ \left[1 - (\boldsymbol{n}_1 \cdot \boldsymbol{n}_2)^2\right](\cos(\Omega_1 t) + \cos(\Omega_2 t)) \\ &+ 2(\boldsymbol{n}_1 \cdot \boldsymbol{n}_2)\sin(\Omega_1 t)\sin(\Omega_2 t)\Big\}. \end{aligned} \tag{1.26}$$

In order to understand Eq. (1.26) we can consider several special cases. Suppose $\boldsymbol{\Omega_1}$ is perpendicular to $\boldsymbol{\Omega}_2$ so that $\boldsymbol{n}_1 \cdot \boldsymbol{n}_2 = 0$. Then we see

$$P_S^{\perp}(t) = \frac{1}{4}\left\{\cos\left[\frac{(\Omega_1 + \Omega_2)t}{2}\right] + \cos\left[\frac{(\Omega_1 - \Omega_2)t}{2}\right]\right\}^2. \tag{1.27}$$

At this point we would like to notice that something interesting happens when $\Omega_1 = \Omega_2$. In the previous equation one of the terms disappears. In general, the condition $\Omega_1 = \Omega_2$ will have an important role to play[3]. We dub such configurations *soft pairs*.

The second particular case important for the next chapter is when $\boldsymbol{\Omega}_1$ is parallel to $\boldsymbol{\Omega}_2$ so that $\boldsymbol{n}_1 \cdot \boldsymbol{n}_2 = 1$,

$$P_S^{||} = \cos^2\left(\frac{(\Omega_1 - \Omega_2)t}{2}\right). \tag{1.28}$$

From Eq. (1.28) we see that unless Ω_1 and Ω_2 are equal $P_S(t)$ is an oscillating function taking all values between 0 and 1. For the special case of soft pairs, however, $P_S(t)$ is identically 1. Figs (1.4) and (1.5) show Eq. (1.26) plotted for several choices of parameters, at two different relative orientations of $\boldsymbol{\Omega}_1$ and $\boldsymbol{\Omega}_2$.

1.1.1 Averaging over random orientations of hyperfine fields

As was discussed above, the hyperfine field can be described as a Gaussian random variable. Explicitly, the probability of the hyperfine field to have magnitude b and direction specified by the spherical angles θ, ϕ is

$$P(b, \theta, \phi) = (\tau^2/4/\pi)^{(3/2)}\exp(-\frac{1}{4}b^2\tau^2). \tag{1.29}$$

Since we will be averaging expressions that are spherically symmetric, it will be convenient to break up the probability density function as

$$P(b, \theta, \phi) = P_b(b)P_{\theta,\phi}(\theta, \phi), \tag{1.30}$$

---

[3]See Chapter 2.

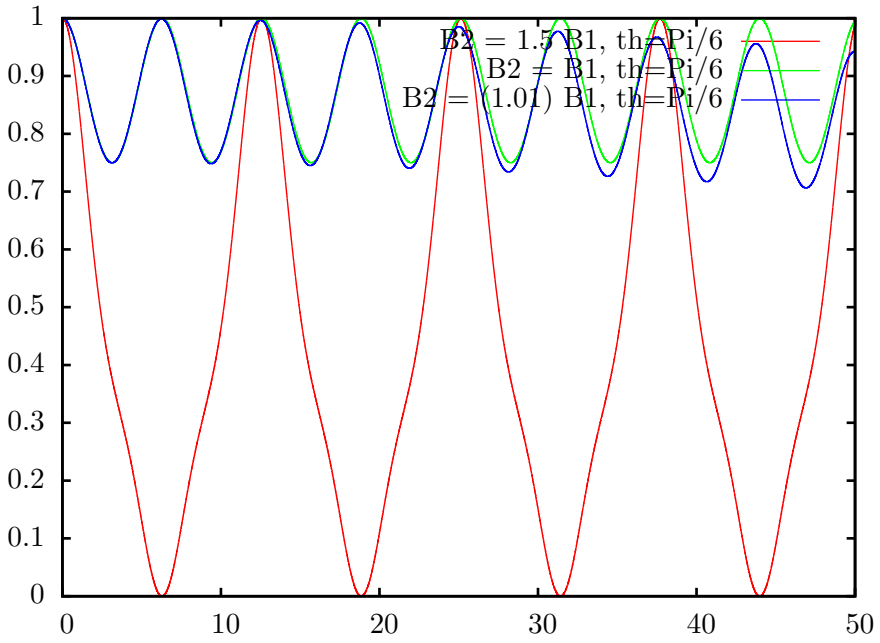

Figure 1.4: $P_S(t)$ calculated from Eq. (1.26). $\mathbf{\Omega}_1$ and $\mathbf{\Omega}_2$ are offset by the angle, $\pi/6$ is plotted for three choices of the ratio Ω_1/Ω_2. $\Omega_1/\Omega_2 = 1$ (green), 1.01 (blue), 1.5 (red).

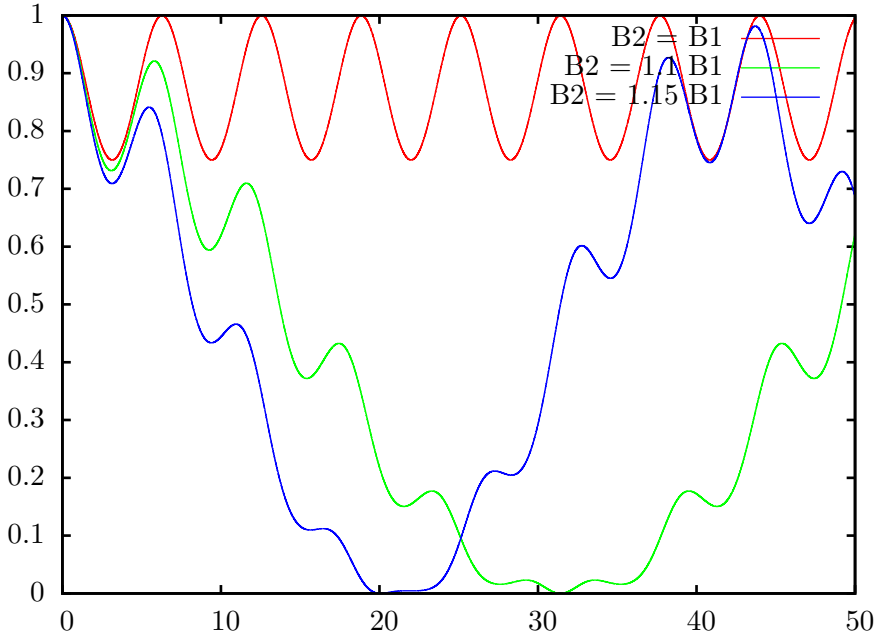

Figure 1.5: $P_S(t)$ calculated from Eq. (1.26). $\mathbf{\Omega}_1$ and $\mathbf{\Omega}_2$ are aligned parallel to each other. $P_S(t)$ is plotted for three choices of the ratio Ω_1/Ω_2. $\Omega_1/\Omega_2 = 1$ (red), 1.1 (green), 1.15 (blue).

with

$$P_b(b) = 4\pi b^2(\tau^2/4/\pi)^{(3/2)} \exp(-\frac{1}{4}b^2\tau^2), \tag{1.31}$$

which is normalized so that

$$\int_0^\infty P_b(b)db = 1. \tag{1.32}$$

While the angles are uniformly distributed,

$$P_{\theta,\phi}(\theta,\phi) = \frac{1}{4\pi}, \quad \text{normalized so that } \int P_{\theta,\phi}(\theta,\phi)d\Omega = 1. \tag{1.33}$$

At this point it behooves us to test the machinery we have developed, and reproduce the results of Ref. [7], exactly. In that work the authors were interested in averaging the quantity $P_T(t) = 1 - P_S(t)$, i.e. the probability to be in the triplet subspace at time t having started from a singlet state, or more casually, the crossover probability. We will only show the results here for the special cases $B = 0$ and $B \to \infty$.

For $B = 0$ and from Eq. (1.26) we have the expression

$$\begin{aligned} P_T(t) = 1 - P_S(t) = 1 - \frac{1}{4}((1 + (\boldsymbol{n}_1 \cdot \boldsymbol{n}_2)^2)(1 - \cos(b_1 t)\cos(b_2 t)) \\ + (1 - (\boldsymbol{n}_1 \cdot \boldsymbol{n}_2)^2)(\cos(b_1 t) + \cos(b_2 t)) + 2\,\boldsymbol{n_1} \cdot \boldsymbol{n_2} \sin(b_1 t)\sin(b_2 t)). \end{aligned} \tag{1.34}$$

The advantage of the notation is that we can average the angles and magnitudes separately in this case. Explicitly, when $B = 0$ the vector $\boldsymbol{n}_i$ consists of just the spherical angles of $\boldsymbol{b}_i$. It is obvious that

$$\langle \boldsymbol{n}_1 \cdot \boldsymbol{n}_2 \rangle = 0, \tag{1.35}$$

since the averages over 1 and 2 are independent. More interestingly,

$$\left\langle (\boldsymbol{n}_1 \cdot \boldsymbol{n}_2)^2 \right\rangle = \left\langle n_1^\alpha n_1^\beta \right\rangle_1 \left\langle n_{2\alpha} n_{2\beta} \right\rangle_2, \tag{1.36}$$

this can be performed by noticing $\langle n_\alpha n_\beta \rangle = 0$ unless $\alpha = \beta$, and further by symmetry $\langle n_x n_x \rangle = \langle n_y n_y \rangle = \langle n_z n_z \rangle = \frac{1}{3}\langle n^2 \rangle = \frac{1}{3}$. So that

$$\left\langle (\boldsymbol{n}_1 \cdot \boldsymbol{n}_2)^2 \right\rangle = \left\langle n_1^\alpha n_1^\beta \right\rangle_1 \left\langle n_{2\alpha} n_{2\beta} \right\rangle_2, = \frac{1}{9}\delta_{\alpha\beta}\delta^{\alpha\beta} = \frac{1}{3}. \tag{1.37}$$

All that remains is to perform the integral,

$$\langle \cos(bt) \rangle = \int_0^\infty \cos(bt) \left[4\pi \left(\frac{\tau^2}{4\pi} \right)^{(3/2)} b^2 \exp(-\frac{1}{4}b^2\tau^2) \right] db \tag{1.38}$$

$$= \left(1 - 2\frac{t^2}{\tau^2} \right) e^{-\frac{t^2}{\tau^2}} = C(t^2/\tau^2). \tag{1.39}$$

Here we have introduced the auxiliary function, $C(x) = (1-2x^2)\exp(-x^2)$, through which the authors of Ref. [7] express their results. At $B = 0$ the crossover probability is given by

$$\langle P_T(t)\rangle = 1 - \frac{1}{4}\left[\left(1+\frac{1}{3}\right)(1+C_1C_2) + \left(1-\frac{1}{3}\right)(C_1+C_2)\right] \tag{1.40}$$

$$= 1 - \frac{1}{4}\left[\frac{4}{3} + \frac{4}{3}C_1C_2 + \frac{2}{3}(C_1+C_2)\right]. \tag{1.41}$$

Here we have introduced the short-hand notation C_1 for the particle 1 and C_2 for the particle 2. We have now also allowed the possibility that $P_b(b)$ be different for partners 1 and 2, specifically that τ, which is a measure of the average hyperfine field strength, might be different for each partner. This will be explored further in the following chapters.

To present the result in the final form it is convenient to introduce yet another auxiliary function $g(x) = \frac{1}{3}(1+2C(x))$. In terms of g_1 and g_2 the crossover probability reads

$$P_T(t) = \frac{3}{4} - \frac{3}{4}g_1g_2. \tag{1.42}$$

In this form we have reproduced the $B = 0$ result of Ref. [7].

At this point we pass to the limit of large B. It is interesting to see how B falls out of the result in the high fields. Take $\boldsymbol{B}$ to be $B\boldsymbol{k}$, then $\boldsymbol{n} \approx \boldsymbol{k}$ and $B \approx B_z + b_z$, i.e., we can essentially neglect the in-plane components of $\boldsymbol{b}$ in comparison with $\boldsymbol{B}$. Eq. (1.26) simplifies in this case to be

$$P_T(t) = \frac{1}{2} - \frac{1}{2}\cos((b_{1z} - b_{2z})t). \tag{1.43}$$

The average over the components b_z offer no surprises and the result is

$$P_T(t) = \frac{1}{2} - \frac{1}{2}\exp(-t^2/\tau_1^2)\exp(-t^2/\tau_2^2). \tag{1.44}$$

In this sense we have completed the goal stated at the start of this section. By far the most interesting result is Eq. (1.26), from which we can reason about the averages when B takes a finite value. Such integrations are cumbersome, but we will return to similar results in later chapters.

1.2 Explicit crossover probabilities

Following we present an alternate derivation of Eq. (1.26) and generalizations detailing the structure of the crossover probabilities from S to the other three states. We take as the starting point, the single particle Hamiltonian which describes a magnetic moment in

a constant field Ω, $\mathcal{H} = \boldsymbol{S} \cdot \boldsymbol{\Omega}$. This is time independent so the solution to the Schrödinger equation is formally given by

$$|\psi(t)\rangle = \exp(-i\mathcal{H}t)\,|\psi(0)\rangle = \exp(-i\boldsymbol{S}\cdot\boldsymbol{\Omega}t)\,|\psi(0)\rangle\,. \tag{1.45}$$

This formal solution is analytically tractable because of the property of the Pauli matrices, namely, $\exp(i\boldsymbol{n}\cdot\boldsymbol{\sigma}\,\theta) = \cos(\theta) + i\boldsymbol{n}\cdot\boldsymbol{\sigma}\sin(\theta)$, which holds for any unit vector $\boldsymbol{n}$. This allows us to write the time-evolution operator, $U = \exp(-i\mathcal{H}t)$, as

$$U = \cos\frac{\Omega t}{2}\begin{pmatrix}1 & 0\\ 0 & 1\end{pmatrix} - i\left(n_x\begin{pmatrix}0 & 1\\ 1 & 0\end{pmatrix} + n_y\begin{pmatrix}0 & -i\\ i & 0\end{pmatrix} + n_z\begin{pmatrix}1 & 0\\ 0 & -1\end{pmatrix}\right)\sin\frac{\Omega t}{2} \tag{1.46}$$

$$= \begin{pmatrix}\cos\frac{\Omega t}{2} - in_z\sin\frac{\Omega t}{2} & -in_-\sin\frac{\Omega t}{2}\\ -in_+\sin\frac{\Omega t}{2} & \cos\frac{\Omega t}{2} + in_z\sin\frac{\Omega t}{2}\end{pmatrix}; \tag{1.47}$$

here, we have introduced the oft used notations $n_\pm = n_x \pm in_y$. Due to the calculations which follow, it will be convenient to go even further and introduce the short-hand c and s for $\cos\frac{\Omega t}{2}$ and $\sin\frac{\Omega t}{2}$. In this short-hand U is

$$U = \begin{pmatrix}c - in_z s & -in_- s\\ -in_+ s & c + in_z s\end{pmatrix}. \tag{1.48}$$

Using these matrices we can explicitly calculate the quantities we are interested in. We start with $\frac{1}{\sqrt{2}}\langle S|\,U\,|{\uparrow\downarrow}\rangle$, which is essentially the amplitude for a starting from the product state $|{\uparrow\downarrow}\rangle$ to be measured at a time t later to be in the state $|S\rangle$. We present the following calculation:

$$\begin{aligned}\frac{1}{\sqrt{2}}\langle S|\,U\,|{\uparrow\downarrow}\rangle &= \frac{1}{\sqrt{2}}\langle S|\,(U^1\,|{\uparrow}\rangle)(U^2\,|{\downarrow}\rangle)\\ &= \frac{1}{\sqrt{2}}\langle S|\,[(c_1 - in_{1z}s_1)\,|{\uparrow}\rangle + (-in_{1+}s_1)\,|{\downarrow}\rangle]\,[(-in_{2-}s_2)\,|{\uparrow}\rangle + (c_2 + in_{2z}s_2)\,|{\downarrow}\rangle]\\ &= \frac{1}{\sqrt{2}}\langle S|\,(\xi\,|{\uparrow\uparrow}\rangle + (c_1 - in_{1z}s_1)(c_2 + in_{2z}s_2)\,|{\uparrow\downarrow}\rangle - (n_{1+}n_{2-}s_1s_2)\,|{\downarrow\uparrow}\rangle + \xi'\,|{\downarrow\downarrow}\rangle)\\ &= \frac{1}{2}((c_1 - in_{1z}s_1)(c_2 + in_{2z}s_2) + n_{1+}n_{2-}s_1s_2).\end{aligned} \tag{1.49}$$

In a similar fashion we may calculate

$$\frac{1}{\sqrt{2}}\langle S|\,U\,|{\downarrow\uparrow}\rangle = \frac{1}{2}(-(n_{1-}n_{2+}s_1s_2) - (c_1 + in_{1z}s_1)(c_2 - in_{2z}s_2)). \tag{1.50}$$

This allows us to write the amplitude for the $S \to S$ process. Namely,

$$\begin{aligned}A_S(t) = \langle S|\,U\,|S\rangle &= \langle S|\left(\frac{1}{\sqrt{2}}\,(|{\uparrow\downarrow}\rangle - |{\downarrow\uparrow}\rangle)\right)\\ &= c_1c_2 + (n_{1x}n_{2x} + n_{1y}n_{2y} + n_{1z}n_{2z})s_1s_2\\ &= \cos\left(\frac{\Omega_1 t}{2}\right)\cos\left(\frac{\Omega_2 t}{2}\right) + (\boldsymbol{n}_1\cdot\boldsymbol{n}_2)\sin\left(\frac{\Omega_1 t}{2}\right)\sin\left(\frac{\Omega_2 t}{2}\right).\end{aligned} \tag{1.51}$$

To arrive at the probability $P_S(t)$ we need to square the amplitude

$$P_S(t) = \left(\cos\left(\frac{\Omega_1 t}{2}\right)\cos\left(\frac{\Omega_2 t}{2}\right) + (\boldsymbol{n}_1\cdot\boldsymbol{n}_2)\sin\left(\frac{\Omega_1 t}{2}\right)\sin\left(\frac{\Omega_2 t}{2}\right)\right)^2, \tag{1.52}$$

expanding this out yields

$$\begin{aligned} P_S(t) = \cos^2\left(\frac{\Omega_1 t}{2}\right)\cos^2\left(\frac{\Omega_2 t}{2}\right) + (\boldsymbol{n}_1\cdot\boldsymbol{n}_2)^2\sin^2\left(\frac{\Omega_1 t}{2}\right)\sin^2\left(\frac{\Omega_1 t}{2}\right) \\ + 2(\boldsymbol{n}_1\cdot\boldsymbol{n}_2)\sin\left(\frac{\Omega_1 t}{2}\right)\cos\left(\frac{\Omega_1 t}{2}\right)\sin\left(\frac{\Omega_2 t}{2}\right)\cos\left(\frac{\Omega_2 t}{2}\right). \end{aligned} \tag{1.53}$$

Upon using a simple trigonometric identity we reproduce Eq. (1.26).

At this point we will work out the three probabilities corresponding to starting in each of the spin states, T_+, T_-, and T_0, and being measured in state S at time t.

From a theoretical standpoint it is important to notice that there seem to be three important vectors which can enter into the probability. The vectors $\boldsymbol{n}_1$ and $\boldsymbol{n}_2$, which tell us the direction of the local hyperfine fields, and $\boldsymbol{k}$ the quantization axis. (Usually taken along the applied field $\boldsymbol{B}$, but it does not have to be.) The formulae considerably simplify if we take the quantization axis along either $\boldsymbol{n}_1$ or $\boldsymbol{n}_2$. However, this choice is not optimal, as we will demonstrate in the next chapter.

The first probability to tackle is for the process $T_+ \to S$, and we turn to that now

$$\begin{aligned} U(t)\left|\uparrow\uparrow\right\rangle &= \left(U_1\left|\uparrow\right\rangle\right)\left(U_2\left|\uparrow\right\rangle\right) \\ &= \left(\left(c_1 - in_{1z}s_1\right)\left|\uparrow\right\rangle + \left(-in_{1+}s_1\right)\left|\downarrow\right\rangle\right)\left(\left(c_2 - in_{2z}s_2\right)\left|\uparrow\right\rangle + \left(-in_{2+}s_2\right)\left|\downarrow\right\rangle\right) \\ &= \xi^{\uparrow\uparrow}_{\uparrow\uparrow}\left|\uparrow\uparrow\right\rangle + (c_1 - in_{1z}s_1)(-in_{2+}s_2)\left|\uparrow\downarrow\right\rangle + (-in_{1+}s_1)(c_2 - in_{2z}s_2)\left|\downarrow\uparrow\right\rangle + \xi^{\uparrow\uparrow}_{\downarrow\downarrow}\left|\downarrow\downarrow\right\rangle. \end{aligned} \tag{1.54}$$

Here ξ are constants which will turn out to be inessential for the probability that we need. The amplitude of the process is given by

$$\begin{aligned} A_{T_+} &= \left\langle S\right| U(t)\left|T_+\right\rangle \\ &= \frac{-i}{\sqrt{2}}\left[(c_1 - in_{1z}s_1)(n_{2+}s_2) - (n_{1+}s_1)(c_2 - in_{2z}s_2)\right] \\ &= \frac{-i}{\sqrt{2}}\left[n_{2+}c_1s_2 - n_{1+}s_1c_2 + i(n_{1+}n_{2z} - n_{1z}n_{2+})s_1s_2\right]. \end{aligned} \tag{1.55}$$

To proceed further we notice that the combination $n_{1+}n_{2z} - n_{1z}n_{2+}$ can be simplified via

$$\begin{aligned} (n_{1x} + in_{1y})(n_{2z}) - n_{1z}(n_{2x} + in_{2y}) &= (n_{1x}n_{2z} - n_{1z}n_{2x}) + i(n_{1y}n_{2z} - n_{1z}n_{2y}) \\ &= -(\boldsymbol{n}_1\times\boldsymbol{n}_2)_y + i(\boldsymbol{n}_1\times\boldsymbol{n}_2)_x = i(\boldsymbol{n}_1\times\boldsymbol{n}_2)_+. \end{aligned} \tag{1.56}$$

At this point introduce a new vector $\boldsymbol{m}$ defined as $\boldsymbol{m} = \boldsymbol{n}_1 \times \boldsymbol{n}_2$ then

$$A_{T_+} = \frac{-i}{\sqrt{2}} \left[n_{2+} c_1 s_2 - n_{1+} s_1 c_2 - m_+ s_1 s_2 \right]. \tag{1.57}$$

In the usual way we calculate the modulus squared to get the probability

$$P_{T_+} = \frac{1}{2} \left[n_{2+} c_1 s_2 - n_{1+} s_1 c_2 - m_+ s_1 s_2 \right] \left[n_{2-} c_1 s_2 - n_{1-} s_1 c_2 - m_- s_1 s_2 \right]. \tag{1.58}$$

We write this in all detail,

$$\begin{aligned} P_{T_+} = \frac{1}{2} \big[& n_{2+} n_{2-} c_1^2 s_2^2 + n_{1+} n_{1-} s_1^2 c_2^2 + m_+ m_- s_1^2 s_2^2 \\ & - (n_{2+} n_{1-} + n_{2-} n_{1+}) c_1 s_1 c_2 s_2 - (n_{2+} m_- + n_{2-} m_+) c_1 s_1 s_2^2 \\ & + (n_{1+} m_- + n_{1-} m_+) s_1^2 c_2 s_2 \big]. \end{aligned} \tag{1.59}$$

This can be simplified more by noticing the following properties of the combinations + and −, which show up as $n_\pm$ or $m_\pm$,

$$\begin{aligned} a_+ a_- &= (a_x + i a_y)(a_x - i a_y) = a_x^2 + a_y^2 = a^2 - a_z^2, \\ a_+ b_- + a_- b_+ &= 2\mathrm{Re}\left((a_x + i a_y)(b_x - i b_y) \right) = 2(a_x b_x + a_y b_y) \\ &= 2(\boldsymbol{a} \cdot \boldsymbol{b} - a_z b_z). \end{aligned} \tag{1.60}$$

The fact that the $\boldsymbol{n}_i$ are unit vectors which are orthogonal to $\boldsymbol{m}$ allows us to simplify the probability P_{T_+}.

$$\begin{aligned} P_{T_+} = \frac{1}{2} \big[& (1 - n_{2z}^2) c_1^2 s_2^2 + (1 - n_{1z}^2) s_1^2 c_2^2 + (m^2 - m_z^2) s_1^2 s_2^2 \\ & - 2(\boldsymbol{n}_1 \cdot \boldsymbol{n}_2 - n_{1z} n_{2z}) c_1 s_1 c_2 s_2 + 2(n_{2z} m_z) c_1 s_1 s_2^2 - 2(n_{1z} m_z) s_1^2 c_2 s_2 \big]. \end{aligned} \tag{1.61}$$

Further,

$$m^2 = (\boldsymbol{n}_1 \times \boldsymbol{n}_2) \cdot (\boldsymbol{n}_1 \times \boldsymbol{n}_2) = n_1^2 n_2^2 - (\boldsymbol{n}_1 \cdot \boldsymbol{n}_2)^2 = 1 - (\boldsymbol{n}_1 \cdot \boldsymbol{n}_2)^2. \tag{1.62}$$

This gives the final form of the result

$$\begin{aligned} P_{T_+} = \frac{1}{2} \Bigg[& (1 - n_{2z}^2) \cos^2\left(\frac{\Omega_1 t}{2}\right) \sin^2\left(\frac{\Omega_2 t}{2}\right) \\ & + (1 - n_{1z}^2) \sin^2\left(\frac{\Omega_1 t}{2}\right) \cos^2\left(\frac{\Omega_2 t}{2}\right) \\ & + \left[1 - (\boldsymbol{n}_1 \cdot \boldsymbol{n}_2)^2 - (\boldsymbol{n}_1 \times \boldsymbol{n}_2)_z^2 \right] \sin^2\left(\frac{\Omega_1 t}{2}\right) \sin^2\left(\frac{\Omega_2 t}{2}\right) \\ & - 2(\boldsymbol{n}_1 \cdot \boldsymbol{n}_2 - n_{1z} n_{2z}) \cos\left(\frac{\Omega_1 t}{2}\right) \sin\left(\frac{\Omega_1 t}{2}\right) \cos\left(\frac{\Omega_2 t}{2}\right) \sin\left(\frac{\Omega_2 t}{2}\right) \\ & + 2 \left(n_{2z} (\boldsymbol{n}_1 \times \boldsymbol{n}_2)_z \right) \cos\left(\frac{\Omega_1 t}{2}\right) \sin\left(\frac{\Omega_1 t}{2}\right) \sin^2\left(\frac{\Omega_2 t}{2}\right) \end{aligned}$$

$$-2\left(n_{1z}(\boldsymbol{n}_1\times\boldsymbol{n}_2)_z\right)\sin^2\left(\frac{\Omega_1 t}{2}\right)\cos\left(\frac{\Omega_2 t}{2}\right)\sin\left(\frac{\Omega_2 t}{2}\right)\Big]. \quad (1.63)$$

The next probability we wish to calculate is for the process $T_-\to S$. Writing

$$\begin{aligned}U(t)\left|\downarrow\downarrow\right\rangle &= \left(U_1\left|\downarrow\right\rangle\right)\left(U_2\left|\downarrow\right\rangle\right)\\ &= \left(\left(-in_{1-}s_1\right)\left|\uparrow\right\rangle+\left(c_1+in_{1z}s_1\right)\left|\downarrow\right\rangle\right)\left(\left(-in_{2-}s_2\right)\left|\uparrow\right\rangle+\left(c_2+in_{2z}s_2\right)\left|\downarrow\right\rangle\right), \quad (1.64)\end{aligned}$$

yields the amplitude

$$A_{T_-}=\langle S|\,U\,|T_-\rangle=\frac{-i}{\sqrt{2}}\left[(n_{1-}s_1)(c_2+in_{2z}s_2)-(n_{2-}s_2)(c_1+in_{1z}s_1)\right]=A^*_{T_+}, \quad (1.65)$$

and thus

$$P_{T_-}=P_{T_+}. \quad (1.66)$$

In a similar manner we derive the probability for the process $T_0\to S$ which is

$$\begin{aligned}P_{T_0}=\Bigg(n_{1z}\sin\left(\frac{\Omega_1 t}{2}\right)\cos\left(\frac{\Omega_2 t}{2}\right)-n_{2z}\sin\left(\frac{\Omega_1 t}{2}\right)\cos\left(\frac{\Omega_2 t}{2}\right)\\ +\left(\boldsymbol{n}_1\times\boldsymbol{n}_2\right)_z\sin\left(\frac{\Omega_1 t}{2}\right)\sin\left(\frac{\Omega_2 t}{2}\right)\Bigg)^2. \quad (1.67)\end{aligned}$$

With the derivations of the equations Eqs. (1.53), (1.63), (1.66), and (1.67) we have essentially completed the goal which was laid out at the beginning of the section. Before we move on, however, it is helpful to consider some simplifications.

Suppose our quantization axis is taken along $\boldsymbol{n}_1$, in this case the formulae simplify drastically since $n_{1+}=0=n_{1-}$. In this case the results can be written in the form

$$P_{T_+}=\frac{1}{2}(1-(\boldsymbol{n}_1\cdot\boldsymbol{n}_2)^2)\sin^2\left(\frac{\Omega_2 t}{2}\right), \quad (1.68)$$

$$P_{T_-}=\frac{1}{2}(1-(\boldsymbol{n}_1\cdot\boldsymbol{n}_2)^2)\sin^2\left(\frac{\Omega_2 t}{2}\right), \quad (1.69)$$

$$P_{T_0}=\left(\sin\left(\frac{\Omega_1 t}{2}\right)\cos\left(\frac{\Omega_2 t}{2}\right)-(\boldsymbol{n}_1\cdot\boldsymbol{n}_2)\cos\left(\frac{\Omega_1 t}{2}\right)\sin\left(\frac{\Omega_2 t}{2}\right)\right)^2, \quad (1.70)$$

$$P_S=\left(\cos\left(\frac{\Omega_1 t}{2}\right)\cos\left(\frac{\Omega_2 t}{2}\right)+(\boldsymbol{n}_1\cdot\boldsymbol{n}_2)\sin\left(\frac{\Omega_1 t}{2}\right)\sin\left(\frac{\Omega_2 t}{2}\right)\right)^2. \quad (1.71)$$

For the sake of consistency, it is simple to check that these sum to 1. We can also see they have the correct limit high B fields. In the high field $\boldsymbol{n}_1\cdot\boldsymbol{n}_2=1$ so these simplify to

$$P_{T_+}=0, \quad (1.72)$$

$$P_{T_-}=0, \quad (1.73)$$

$$P_{T_0}=(s_1c_2-c_1s_2)^2=\sin^2\left[\frac{(\Omega_1-\Omega_2)\,t}{2}\right], \quad (1.74)$$

$$P_S = (c_1c_2 + s_1s_2)^2 = \cos^2\left[\frac{(\Omega_1 - \Omega_2)\,t}{2}\right]. \tag{1.75}$$

In the next section we will again examine the high field limit, from yet another point of view.

1.3 High field limit as a two state problem

We again look at the noninteracting pair problem described by the Hamiltonian $\mathcal{H} = \boldsymbol{S}_1 \cdot \boldsymbol{\Omega}_1 + \boldsymbol{S}_2 \cdot \boldsymbol{\Omega}_2$. The vector space of states is the tensor product of the two noninteracting state spaces. Thus, we have a four-dimensional Hilbert space. It is convenient to represent $\mathcal{H}$ as a matrix acting on these states.

If we work out the matrix elements in the product basis $\mathcal{H}$ is given by

$$\mathcal{H} = \begin{array}{c} \\ \langle\uparrow\uparrow| \\ \langle\uparrow\downarrow| \\ \langle\downarrow\uparrow| \\ \langle\downarrow\downarrow| \end{array} \begin{array}{c} \begin{array}{cccc} |\uparrow\uparrow\rangle & |\uparrow\downarrow\rangle & |\downarrow\uparrow\rangle & |\downarrow\downarrow\rangle \end{array} \\ \begin{pmatrix} \frac{\Omega_{1z}+\Omega_{2z}}{2} & \frac{\Omega_{2-}}{2} & \frac{\Omega_{1-}}{2} & 0 \\ \frac{\Omega_{2+}}{2} & \frac{\Omega_{1z}-\Omega_{2z}}{2} & 0 & \frac{\Omega_{1-}}{2} \\ \frac{\Omega_{1+}}{2} & 0 & \frac{-(\Omega_{1z}-\Omega_{2z})}{2} & \frac{\Omega_{2-}}{2} \\ 0 & \frac{\Omega_{1+}}{2} & \frac{\Omega_{2+}}{2} & \frac{-(\Omega_{1z}+\Omega_{2z})}{2} \end{pmatrix} \end{array}. \tag{1.76}$$

This is easily converted into the basis S, T_+, T_-, and T_0. In that basis $\mathcal{H}$ reads

$$\mathcal{H} = \begin{array}{c} \\ \langle T_+| \\ \langle S| \\ \langle T_0| \\ \langle T_-| \end{array} \begin{array}{c} \begin{array}{cccc} |T_+\rangle & |S\rangle & |T_0\rangle & |T_-\rangle \end{array} \\ \begin{pmatrix} \frac{\Omega_{1z}+\Omega_{2z}}{2} & \frac{-(\Omega_{1-}-\Omega_{2-})}{2\sqrt{2}} & \frac{\Omega_{1-}+\Omega_{2-}}{2\sqrt{2}} & 0 \\ \frac{-(\Omega_{1+}-\Omega_{2+})}{2\sqrt{2}} & 0 & \frac{\Omega_{1z}-\Omega_{2z}}{2} & \frac{\Omega_{1-}-\Omega_{2-}}{2\sqrt{2}} \\ \frac{\Omega_{1+}+\Omega_{2+}}{2\sqrt{2}} & \frac{\Omega_{1z}-\Omega_{2z}}{2} & 0 & \frac{\Omega_{1-}+\Omega_{2-}}{2\sqrt{2}} \\ 0 & \frac{\Omega_{1+}-\Omega_{2+}}{2\sqrt{2}} & \frac{\Omega_{1+}+\Omega_{2+}}{2\sqrt{2}} & \frac{-(\Omega_{1z}+\Omega_{2z})}{2} \end{pmatrix} \end{array}. \tag{1.77}$$

When the applied field B is very large, as we have seen above, we can neglect $\Omega_{1x}, \Omega_{1y}, \Omega_{2x}$, and Ω_{2y} compared to the z components. The high field limit of $\mathcal{H}$ is given by the matrix

$$\mathcal{H}_{\text{high field}} = \begin{array}{c} \\ \langle T_+| \\ \langle S| \\ \langle T_0| \\ \langle T_-| \end{array} \begin{array}{c} \begin{array}{cccc} |T_+\rangle & |S\rangle & |T_0\rangle & |T_-\rangle \end{array} \\ \begin{pmatrix} \frac{\Omega_{1z}+\Omega_{2z}}{2} & 0 & 0 & 0 \\ 0 & 0 & \frac{\Omega_{1z}-\Omega_{2z}}{2} & 0 \\ 0 & \frac{\Omega_{1z}-\Omega_{2z}}{2} & 0 & 0 \\ 0 & 0 & 0 & \frac{-(\Omega_{1z}+\Omega_{2z})}{2} \end{pmatrix} \end{array}. \tag{1.78}$$

Notice that in Eq. (1.78) the T_+ and T_- states are completely decoupled from the S and T_0 states. The interesting dynamics, therefore, occur between the latter two states. As the applied field gets bigger it is a better approximation to treat the states S and T_0 as essentially degenerate. This fact will be shown to have important repercussions in the next chapter.

To find the behavior of a wavefunction we take a generic state (restricted to the two-dimensional subspace spanned by S and T_0)

$$|\psi(t)\rangle = a(t)\,|S\rangle + b(t)\,|T_0\rangle \tag{1.79}$$

and introduce the notation

$$\Delta = \frac{\Omega_1 - \Omega_2}{2}, \tag{1.80}$$

for the difference in field strengths for the pair partners.

In matrix form, then, the high-field hamiltonian is given by

$$\mathcal{H}_{\rm hf} = \begin{pmatrix} 0 & \Delta \\ \Delta & 0 \end{pmatrix}. \tag{1.81}$$

Schrödinger's equation for the amplitudes (coefficients) a and b reads

$$\begin{aligned} i\,\dot{a} &= \Delta b, \\ i\,\dot{b} &= \Delta a. \end{aligned} \tag{1.82}$$

This is trivially soluble, take a derivative of the top equation, $i\,\ddot{a} = \Delta\dot{b} = \Delta\left(\frac{\Delta a}{i}\right)$. This gives $\ddot{a} + \Delta^2 a = 0$. So: $a(t) = c_1\cos(\Delta t) + c_2\sin(\Delta t)$, and $b(t) = \frac{i}{\Delta}\dot{a} = -ic_1\sin(\Delta t) + ic_2\cos(\Delta t)$. Plug in initial conditions $a(0) = a_0$ and $b(0) = b_0$ to get the final result,

$$|\psi(t)\rangle = \left(a_0\cos(\Delta t) - ib_0\sin(\Delta t)\right)|S\rangle + \left(-ia_0\sin(\Delta t) + b_0\cos(\Delta t)\right)|T_0\rangle\,. \tag{1.83}$$

To find $P_S(t)$ we take the initial conditions $a_0 = 1$, $b_0 = 0$ and calculate $|a(t)|^2 = |\,\langle S|\psi(t)\rangle\,|^2$. This gives us the result

$$P_S(t) = \cos^2(\Delta t) = \cos^2\left(\frac{(\Omega_1 - \Omega_2)t}{2}\right). \tag{1.84}$$

To arrive at P_{T_0} we follow the same steps mutatis mutandis,

$$P_{T_0}(t) = \sin^2(\Delta t). \tag{1.85}$$

It is from these results we will begin to generalize to describe the physics of recombining pair partners.

1.4 Leaky double well

As a first step towards describing recombining pair partners, we generalize the Schrödinger equation of the last section. At this point we do it heuristically, by adding an imaginary term to the right hand side of the Schrödinger equation, Eq. (1.82), for S.

$$i\dot{a} = -i\gamma a + \Delta b,$$

$$i\dot{b} = \Delta a. \tag{1.86}$$

The physics expressed in Eq. (1.86) are entirely obvious. There are two states, S and T_0, and a probability Δ to go between them. From the state S the particle has a chance to disappear, γ is a measure of the decay rate. Colorfully, this can be thought of as a well with two buckets and a hole in one of them; $a(t)$ and $b(t)$ are then the amplitudes to find a particle in the first or second bucket, respectively.

The question to be solved is the following: Suppose we start in state S. How long is the particle there? If Δ were 0 then starting from state S you have exponential decay with time constant $1/\gamma$, so it makes sense to say the lifetime is approximately $1/\gamma$. Conversely, if you start in T_0 you would stay there for ever so the lifetime is approximately infinite.

To solve Eq. (1.86), we differentiate the first equation and replace from the second. This gives the second order ODE

$$\ddot{a} = -\gamma\dot{a} + \Delta^2 a, \tag{1.87}$$

if the initial conditions are $a(0) = 1$ and $b(0) = 0$, this translates to $a(0) = 1$, $\dot{a}(0) = -\gamma$. The solution to this ODE is trivial

$$a(t) = \frac{1}{2}\left(1 - \frac{\frac{\gamma}{2}}{\sqrt{\frac{\gamma^2}{4} - \Delta^2}}\right) \exp\left[-\left(\frac{\gamma}{2} + \sqrt{\frac{\gamma^2}{4} - \Delta^2}\right) t\right] + \frac{1}{2}\left(1 + \frac{\frac{\gamma}{2}}{\sqrt{\frac{\gamma^2}{4} - \Delta^2}}\right) \exp\left[-\left(\frac{\gamma}{2} - \sqrt{\frac{\gamma^2}{4} - \Delta^2}\right) t\right]. \tag{1.88}$$

Notice that in Eq. (1.88), as $\Delta \to 0$, the exponential factor in the second term approaches unity. This is another indication of a long-living mode which appears for soft pairs. The probability that the particle is still in the system is given by $p(t) = |a(t)|^2 + |b(t)|^2$. This can again be calculated exactly,

$$p(t) = \frac{\exp(-\gamma t)}{\gamma^2 - 4\Delta^2}\left[-4\Delta^2 - \gamma\sqrt{\gamma^2 - 4\Delta^2}\sinh\left(t\sqrt{\gamma^2 - 4\Delta^2}\right) + \gamma^2\cosh\left(t\sqrt{\gamma^2 - 4\Delta^2}\right)\right]. \tag{1.89}$$

The lifetime of a state is given by[4], $\langle t\rangle = \int_0^\infty p(t)\,dt$. When $p(t)$ is given by Eq. (1.89) the lifetime is simply

$$\langle t\rangle_S = \frac{1}{\gamma}. \tag{1.90}$$

Now we turn to the case where the initial conditions are $a(0) = 0$, $b(0) = 1$, i.e., the particle starts in T_0. The solution of the ODE is exactly the same except the constants

[4]For a derivation see Section 2.8.

have to be chosen to match the new initial conditions $a(0) = 0$, $\dot{a}(0) = -i\Delta$. The solution for $a(t)$ is

$$a(t) = \frac{i\frac{\Delta}{2}}{\sqrt{\frac{\gamma^2}{4} - \Delta^2}} \left(\exp\left[-\left(\frac{\gamma}{2} + \sqrt{\frac{\gamma^2}{4} - \Delta^2} \right) t \right] - \exp\left[-\left(\frac{\gamma}{2} - \sqrt{\frac{\gamma^2}{4} - \Delta^2} \right) t \right] \right). \tag{1.91}$$

To calculate the lifetime we again need the probability to be in the system $p(t) = |a(t)|^2 + |b(t)|^2$, which is very similar to the previous case.

$$p(t) = \frac{e^{-\gamma t}}{\gamma^2 - 4\Delta^2} \left(-4\Delta^2 + \gamma\sqrt{\gamma^2 - 4\Delta^2} \sinh\left(t\sqrt{\gamma^2 - 4\Delta^2} \right) + \gamma^2 \cosh\left(t\sqrt{\gamma^2 - 4\Delta^2} \right) \right). \tag{1.92}$$

After integrating this over t we get the lifetime of the T_0 state

$$\langle t \rangle_{T_0} = \frac{1}{\gamma} + \frac{\gamma}{2\Delta^2}. \tag{1.93}$$

If we assume half the time the system starts from state S and half from state T_0, then on average

$$\langle t \rangle = \frac{1}{2}\langle t \rangle_S + \frac{1}{2}\langle t \rangle_{T_0} = \frac{1}{2}\frac{1}{\gamma} + \frac{1}{2}\left(\frac{1}{\gamma} + \frac{\gamma}{2\Delta^2} \right) = \frac{1}{\gamma} + \frac{\gamma}{4\Delta^2}. \tag{1.94}$$

This is the most important result of this section. It indicates that as $\Delta \to 0$ on average the lifetime of states becomes longer and longer, i.e., the *trapping*, which resists the leakage, takes place. This trapping will be at the heart of the phenomenon of OMAR.

1.4.1 Density matrix reformulation

In the high field we can model our Hamiltonian in the singlet-triplet basis as given by Eq. (1.81). If we also include the recombined state, which we label as G (for ground), then the system is defined by the augmented Hamiltonian

$$\mathcal{H} = \begin{array}{c} \begin{matrix} G & S & T_0 \end{matrix} \\ \begin{pmatrix} -E_g & 0 & 0 \\ 0 & 0 & \Delta \\ 0 & \Delta & 0 \end{pmatrix} \end{array}. \tag{1.95}$$

The system can be described by a density matrix which has nine components,

$$\rho = \begin{pmatrix} \rho_{gg} & \rho_{gs} & \rho_{gt} \\ \rho_{sg} & \rho_{ss} & \rho_{st} \\ \rho_{tg} & \rho_{ts} & \rho_{tt} \end{pmatrix}. \tag{1.96}$$

To take into account the incoherent transition from state S to state G with rate 2γ, we will modify the Heisenberg equation of motion. The factor of two is needed to make it

match what was presented in the previous section. The correct modification of Heisenberg's equation is often called the Liouville-Von Neumman-Lindblad equation:

$$\frac{d\rho}{dt} = -i[\mathcal{H}, \rho] + L[\rho]. \tag{1.97}$$

Here, the operator L is picked to correctly describe the nonunitary time evolution. For Markovian processes it is known that L has a simple form.

$$L[\rho] = \frac{1}{2}\sum_{ij}\Gamma^i_j\left\{2\rho_{ii}\left|j\right\rangle\left\langle j\right| - \rho\left|i\right\rangle\left\langle i\right| - \left|i\right\rangle\left\langle i\right|\rho\right\}, \tag{1.98}$$

where Γ^i_j denotes the decoherent transition rate from state i to state j. For the simple system we are considering there is only transitions from state S to state G to be accounted for. In this case L takes the form

$$\begin{aligned} L[\rho] &= \frac{2\gamma}{2}\left[2\rho_{ss}\begin{pmatrix}1&0&0\\0&0&0\\0&0&0\end{pmatrix} - \begin{pmatrix}\rho_{gg}&\rho_{gs}&\rho_{gt}\\\rho_{sg}&\rho_{ss}&\rho_{st}\\\rho_{tg}&\rho_{ts}&\rho_{tt}\end{pmatrix}\begin{pmatrix}0&0&0\\0&1&0\\0&0&0\end{pmatrix} - \begin{pmatrix}0&0&0\\0&1&0\\0&0&0\end{pmatrix}\begin{pmatrix}\rho_{gg}&\rho_{gs}&\rho_{gt}\\\rho_{sg}&\rho_{ss}&\rho_{st}\\\rho_{tg}&\rho_{ts}&\rho_{tt}\end{pmatrix}\right] \\ &= \begin{pmatrix}2\gamma\rho_{ss}&-\gamma\rho_{gs}&0\\-\gamma\rho_{sg}&-2\gamma\rho_{ss}&-\gamma\rho_{st}\\0&-\gamma\rho_{ts}&0\end{pmatrix}. \end{aligned} \tag{1.99}$$

This, in turn, gives us a system of nine differential equations we need to solve. Five that involve the ground state:

$$\begin{aligned} &\dot\rho_{gg} = 2\gamma\rho_{ss}, \\ &\dot\rho_{gs} = i(E_g\rho_{gs} - \Delta\rho_{gt}) - \gamma\rho_{gs}, \\ &\dot\rho_{gt} = i(E_g\rho_{gt} - \Delta\rho_{gs}) - \gamma\rho_{gt}, \end{aligned} \qquad \begin{aligned} &\dot\rho_{sg} = -i(E_g\rho_{sg} + \Delta\rho_{tg}) - \gamma\rho_{sg}, \\ &\dot\rho_{tg} = -i(E_g\rho_{tg} + \Delta\rho_{sg}) - \gamma\rho_{tg}, \end{aligned} \tag{1.100}$$

and four that do not:

$$\begin{aligned} \dot\rho_{ss} &= -i\Delta(\rho_{ts} - \rho_{st}) - 2\gamma\rho_{ss}, & \dot\rho_{ts} &= -i\Delta(\rho_{ss} - \rho_{tt}) - \gamma\rho_{ts}, \\ \dot\rho_{st} &= -i\Delta(\rho_{tt} - \rho_{ss}) - \gamma\rho_{st}, & \dot\rho_{tt} &= -i\Delta(\rho_{st} - \rho_{ts}). \end{aligned} \tag{1.101}$$

The latter four equations are decoupled from the first five and can be solved independently. It is convenient to turn this into a set of algebraic equations. To do so we employ Laplace's transform. The transformed system is:

$$\begin{aligned} (s+2\gamma)\rho_{ss} - i\Delta\rho_{st} + i\Delta\rho_{ts} &= \rho_{ss}(0), \\ -i\Delta\rho_{ss} + (s+\gamma)\rho_{st} + i\Delta\rho_{tt} &= \rho_{st}(0), \\ i\Delta\rho_{ss} + (s+\gamma)\rho_{ts} - i\Delta\rho_{tt} &= \rho_{ts}(0), \\ i\Delta\rho_{st} - i\Delta\rho_{ts} + s\rho_{tt} &= \rho_{tt}(0). \end{aligned} \tag{1.102}$$

Consider the first case $\rho_{ss}(0) = 1$ and $\rho_{st}(0) = \rho_{ts}(0) = \rho_{tt}(0) = 0$. That is, the system starts in the state S. After some algebra we find

$$\rho_{ss}(s) = \frac{s^2 + s\gamma + 2\Delta^2}{(s+\gamma)(s^2 + 2s\gamma + 4\Delta^2)}, \tag{1.103}$$

$$\rho_{tt}(s) = \frac{2\Delta^2}{(s+\gamma)(s^2+2s\gamma+4\Delta^2)}. \tag{1.104}$$

These can be summed to find the (Laplace-space) probability to be in either the state S or the state T_0, i.e., the probability to be in the system.

$$p(s) = \frac{s^2+s\gamma+4\Delta^2}{(s+\gamma)(s^2+2s\gamma+4\Delta^2)}. \tag{1.105}$$

To find the time-domain probability we perform an inverse Laplace transform. All of the poles of $p(s)$ are in the left hand plane so the integral can be taken along the imaginary axis.

$$p(t) = \frac{1}{2\pi i}\int_{-i\infty}^{i\infty} p(s)e^{st}ds. \tag{1.106}$$

To actually perform the contour integral we use the method of residues. Thus, we need to collect the residues of $p(s)e^{st}$ at each of the poles of the integrand. There are only three poles, $-\gamma$, and the solutions of $s^2+2s\gamma+4\Delta^2=0$, namely, $-\gamma\pm\sqrt{\gamma^2+\Delta^2}$. Careful calculation yields

$$\begin{aligned} p(t) = \frac{-4\Delta^2}{\gamma^2-4\Delta^2}\exp\left(-\gamma t\right) \\ + \frac{\gamma^2-\gamma\sqrt{\gamma^2-4\Delta^2}}{2\left(\gamma^2-4\Delta^2\right)}\exp\left(-\left[\gamma-\sqrt{\gamma^2-4\Delta^2}\right]t\right) \\ + \frac{\gamma^2+\gamma\sqrt{\gamma^2-4\Delta^2}}{2\left(\gamma^2-4\Delta^2\right)}\exp\left(-\left[\gamma+\sqrt{\gamma^2-4\Delta^2}\right]t\right). \end{aligned} \tag{1.107}$$

This is the same $p(t)$ derived in the previous subsection for these initial conditions.

To work out $\langle t\rangle_S$, the lifetime, it is more convenient to reason with $p(s)$ since $p(s)|_{s=0} = \int_0^\infty p(t)dt = \langle t\rangle$. We see that for the above case we recover $\langle t\rangle_S = 1/\gamma$.

In the same fashion we can work out $\langle t\rangle_{T_0}$. Due to the linearity of the Laplace transform and the equations of motion we can find the averaged lifetime over initial states by solving the system with initial conditions $\rho_{ss}(0) = 1/2 = \rho_{tt}(0)$. The average lifetime is found by evaluating $p(s) = \rho_{ss}(s) + \rho_{tt}(s)$ at $s = 0$.

The nutshell of the above exercises is that superradiance phenomenon [9] is encoded in the formulae which describe trapping at the point of degeneracy emerged very naturally. It is this phenomenon that will play a dramatic role in the theory of OMAR developed over the next three chapters.

1.5 References

[1] M.N. Baibich, J. M. Broto, A. Fert, F. Nguyen Van Dau, F. Petroff, P. Etienne, G. Creuzet, A. Friederich, and J. Chazelas, Phys. Rev. Lett. **61**, 2472 (1988).

[2] G. Binasch, P. Grnberg, F. Saurenbach, and W. Zinn, Phys. Rev. B 39, 4828 (1989).

[3] S. A. Wolf, D. D. Awschalom, R. A. Buhrman, J. M. Daughton, S. von Molnr, M. L. Roukes, A. Y. Chtchelkanova, and D. M. Treger, Science **294**, 1488 (2001).

[4] Z. H. Xiong, D. Wu, Z. V. Vardeny, and J. Shi, Nature (London) **427**, 821 (2004).

[5] T. L. Francis, Ö. Mermer, G. Veeraraghavan, and M. Wohlgenannt, New J. Phys. **6**, 185 (2004).

[6] P. A. Bobbert, T. D. Nguyen, F. W. A. van Oost, B. Koopmans, and M. Wohlgenannt, Phys. Rev. Lett. **99**, 216801 (2007).

[7] K. Schulten and P. G. Wolynes, J. Chem. Phys. **68**, 3292 (1978).

[8] K. M. Salikhov, Y. N. Molin, R. Z. Sagdeev, and A. L. Buchachenko, in *Spin Polarization and Magnetic Effects in Radical Reactions*, edited by Y. N. Molin (Elsevier, Amsterdam, 1984), pp. 32-116.

[9] R. H. Dicke, Phys. Rev. **93**, 99 (1954).

CHAPTER 2

SLOW DYNAMICS OF SPIN PAIRS IN A RANDOM HYPERFINE FIELD: ROLE OF INEQUIVALENCE OF ELECTRONS AND HOLES IN ORGANIC MAGNETORESISTANCE

2.1 Introduction

Due to the complex structure of organic semiconductors and their spatial inhomogeneity it is nearly impossible to identify a unique scenario of current passage through them. In view of this, it is remarkable that sizable change of current through a device based on organic semiconductor takes place in weak external magnetic fields. This effect, called organic magnetoresistance (OMAR), seems to be robust, i.e., weakly sensitive to the device parameters. Although the first reports on the observation of organic magnetoresistance (OMAR) appeared decades ago [1, 2], systematic experimental study of this effect started relatively recently [5, 6, 7, 8, 9, 10, 11, 12, 13, 14, 15, 16, 17, 18, 19] (see also the review Ref. [20]).

On the theory side, it is now commonly accepted that the origin of OMAR lies in random hyperfine fields created by nuclei surrounding the carriers (polarons). More specifically, the basic unit responsible for OMAR is a pair of sites hosting carriers (polarons); the spin state of the pair is described by the Hamiltonian

$$\widehat{H} = \boldsymbol{\Omega}_1 \cdot \widehat{\boldsymbol{S}}_e + \boldsymbol{\Omega}_2 \cdot \widehat{\boldsymbol{S}}_h. \tag{2.1}$$

Here, $\widehat{\boldsymbol{S}}_e$ are $\widehat{\boldsymbol{S}}_h$ are the spin operators of the pair-partners (we will assume that they are electron and hole, respectively); $\boldsymbol{\Omega}_1 = \boldsymbol{B} + \boldsymbol{b}_e$ and $\boldsymbol{\Omega}_2 = \boldsymbol{B} + \boldsymbol{b}_h$ are the *full* fields acting on the spins. They represent the sums of external, $\boldsymbol{B}$, and respective hyperfine fields, $\boldsymbol{b}_e$ and $\boldsymbol{b}_h$. As was first pointed out by Schulten and Wolynes in Ref. [4], due to the large number of nuclei surrounding each pair-partner and their slow dynamics, $\boldsymbol{b}_e$ and $\boldsymbol{b}_h$ can be viewed as classical random fields with Gaussian distributions.

In order to give rise to OMAR, the Hamiltonian Eq. (2.1) is not sufficient. It should be complemented by some mechanism through which the pair-partners "know" about each other, so their motion is correlated without direct interaction. The simplest example of such a mechanism is spin-dependent recombination, i.e., the requirement that electron and hole can recombine only if their spins are in the singlet, S, state. Then the essence of OMAR can be crudely understood as a redistribution of portions of singlets and triplets upon increasing B. This redistribution affects the net recombination rate. Clearly, the characteristic B for this redistribution is $\sim b_e, b_h$.

Naturally, the specific relation between the current and recombination rate involves also the rate at which the pairs are created. It is important, though, that the latter process is not spin-selective.

Existing theories of OMAR can be divided into two groups which we will call "steady-state" and "dynamical." The theories of the first group [21] appeared earlier. In a nutshell (see Ref. [18] for details), in these theories the right-hand-side of the equation of motion for the density matrix $i\dot{\rho} = [\widehat{H}, \rho]$ with Hamiltonian Eq. (2.1) is complemented with "source" and *spin-selective* "sink" terms. After that, $\dot{\rho}$ is set to zero. In Refs. [15] current is expressed via the steady-state ρ and subsequently averaged numerically over realizations of hyperfine fields.

The "steady-state" approach applies when the pair does not perform many beatings between S and T during its lifetime, since the beating *dynamics* are excluded by setting $\dot{\rho} = 0$.

These beating dynamics have been incorporated into the OMAR theory in Ref. [22], which appeared last year. This theory relies on decades old findings in the field of dynamic spin-chemistry [4, 3]. We briefly summarize these findings.

If an isolated pair is initially in S, it was shown in Ref. [4] that the averaged probability to find it in T after time t is given either by the function

$$p_{ST}(t) = \frac{1}{2}\left(1 - e^{-b_e^2 t^2} e^{-b_h^2 t^2}\right), \tag{2.2}$$

for strong fields $B \gg b_e, b_h$, or by

$$p_{ST}(t) = \frac{3}{4}\left\{1 - \left[\frac{1}{3}\left(1 + 2e^{-b_e^2 t^2} - 4b_e^2 t^2 e^{-b_e^2 t^2}\right)\right] \times \left[\frac{1}{3}\left(1 + 2e^{-b_h^2 t^2} - 4b_h^2 t^2 e^{-b_h^2 t^2}\right)\right]\right\}, \tag{2.3}$$

for $B \ll b_e, b_h$. Here, b_e, b_h are the rms hyperfine fields for electron and hole. Naturally, the probability approaches $3/4$ at small B and $1/2$ at large B.

In the theory of Ref. [22], the B-dependent dynamics described by Eqs. (2.2), (2.3) translates into the B-dependent resistance (OMAR) on the basis of the following reasoning.

The dynamics $p_{ST}(t)$ leads to prolongation of the recombination time (hopping time, τ_h, in the language of Ref. [22]). This prolongation is quantified by

$$\frac{1}{\tau_h} \to \frac{1}{\tau_h} \int dt(1 - 3p_{ST}(t))e^{-t/\tau_h}. \tag{2.4}$$

The meaning of Eq. (2.4) is that a pair should stay in S in order for a hop to take place. Prolongation of hopping time leads to a B-dependent increase of the resistance. The authors of Ref. [22] evaluated $p_{ST}(t)$ for arbitrary B, while in calculation of OMAR they assumed that bare hopping times, τ_h, have an exponentially broad distribution.

Both theories Refs. [18] and [22] take as a starting point a pair with the Hamiltonian Eq. (2.1) describing its spin states and preferential recombination (hopping) from S. The dynamics of this seemingly simple entity, which is crucial for OMAR, possess some nontrivial regimes. Uncovering these regimes is a central goal for the present paper. The other goal is to demonstrate that nontrivial dynamics can manifest itself in OMAR.

To underline that the spin dynamics of two carriers in noncollinear magnetic fields, which can recombine only from S can be highly nontrivial, we note that separation of these dynamics into S-T "beating" stage followed by instantaneous hopping after time τ_h, as in theory [22], is not always possible. It is quite nontrivial that spin-selective recombination of carriers can exert a *feedback* on the spin dynamics. As an illustration of this delicate issue we invoke the example of cooperative photon emission discovered by R. H. Dicke [23]. In the Dicke effect one superradiant state of a group of emitters having a very short lifetime automatically implies that all the remaining states are subradiant and have *anomalously long* radiation times. Below we demonstrate that a similar situation is realized in dynamics of two spins when recombination from S is very fast. We will see that the remaining three modes of the collective spin motion become very "slow."

Our analysis reveals the exceptional role of the "soft" pairs, which are sparse configurations of $\boldsymbol{b}_e$, $\boldsymbol{b}_h$ for which full fields $\boldsymbol{\Omega}_1$, $\boldsymbol{\Omega}_2$ have the same magnitude.

The chapter is organized as follows. In Section 2.2 we cast the eigenmodes of the Hamiltonian Eq. (2.1) in a convenient notation. In Section 2.3 we include recombination and study its effect on the eigenmodes. The consequences of nontrivial dynamics for OMAR are considered in Sections 2.4 and 2.5, where we perform averaging over realizations of hyperfine fields. We establish that inequivalence of rms hyperfine fields for electrons and holes has a dramatic effect on OMAR, when it is governed by soft pairs. Section 2.6 concludes the chapter.

2.2 Dynamics of a pair in the presence of recombination

2.2.1 Isolated pair

We start with reviewing the dynamics of a pair of spins in the absence of recombination. Obviously, this dynamics does not depend on the choice of the quantization axis. However, since we plan to include recombination, the choice of the quantization axis, z, illustrated in Fig. 2.1 appears to be preferential. The axis is chosen to lie in the plane containing the vectors $\mathbf{\Omega}_1$, $\mathbf{\Omega}_2$. Moreover, the orientation of the z-axis is fixed by the condition $\mathbf{\Omega}_{1x} = -\mathbf{\Omega}_{2x}$. Then the angles, θ_1, θ_2, between $\mathbf{\Omega}_1$, $\mathbf{\Omega}_2$ and the z-axis are given by

$$\tan\theta_1 = \frac{|\mathbf{\Omega}_1 \times \mathbf{\Omega}_2|}{\mathbf{\Omega}_2^2 + \mathbf{\Omega}_1 \cdot \mathbf{\Omega}_2}, \quad \tan\theta_2 = \frac{|\mathbf{\Omega}_1 \times \mathbf{\Omega}_2|}{\mathbf{\Omega}_1^2 + \mathbf{\Omega}_1 \cdot \mathbf{\Omega}_2}. \tag{2.5}$$

With this choice, the Schrödinger equation for the amplitudes of S, T_0, T_+, and T_- reduces to the system

$$i\frac{\partial T_+}{\partial t} = \Sigma_z T_+ - \frac{1}{\sqrt{2}}\Delta_x S, \tag{2.6}$$

$$i\frac{\partial S}{\partial t} = \Delta_z T_0 - \frac{1}{\sqrt{2}}\Delta_x T_+ + \frac{1}{\sqrt{2}}\Delta_x T_-, \tag{2.7}$$

$$i\frac{\partial T_0}{\partial t} = \Delta_z S, \tag{2.8}$$

$$i\frac{\partial T_-}{\partial t} = -\Sigma_z T_- + \frac{1}{\sqrt{2}}\Delta_x S, \tag{2.9}$$

where Σ_z, Δ_z, and Δ_x are defined as

$$\Sigma_z = \frac{\Omega_{1z} + \Omega_{2z}}{2}, \tag{2.10}$$

$$\Delta_z = \frac{\Omega_{1z} - \Omega_{2z}}{2}, \tag{2.11}$$

$$\Delta_x = \frac{\Omega_{1x} - \Omega_{2x}}{2}. \tag{2.12}$$

The advantage of our choice of the quantization axis shows in the fact that the state T_0 is coupled exclusively to S. Since recombination is allowed only from S, this will simplify the subsequent analysis of the recombination dynamics.

The eigenvalues, λ_i, of the system Eqs. (2.6)-(2.9) satisfy the quartic equation

$$\lambda_i^2(\lambda_i^2 - \Sigma_z^2) - \lambda_i^2(\Delta_z^2 + \Delta_x^2) + \Delta_z^2\Sigma_z^2 = 0. \tag{2.13}$$

We will enumerate these eigenvalues according to the convention $\lambda_1 = -\lambda_2$ and $\lambda_3 = -\lambda_4$. To find the absolute values λ_1^2, λ_3^2 one does not have to solve Eq. (2.13), since it is obvious

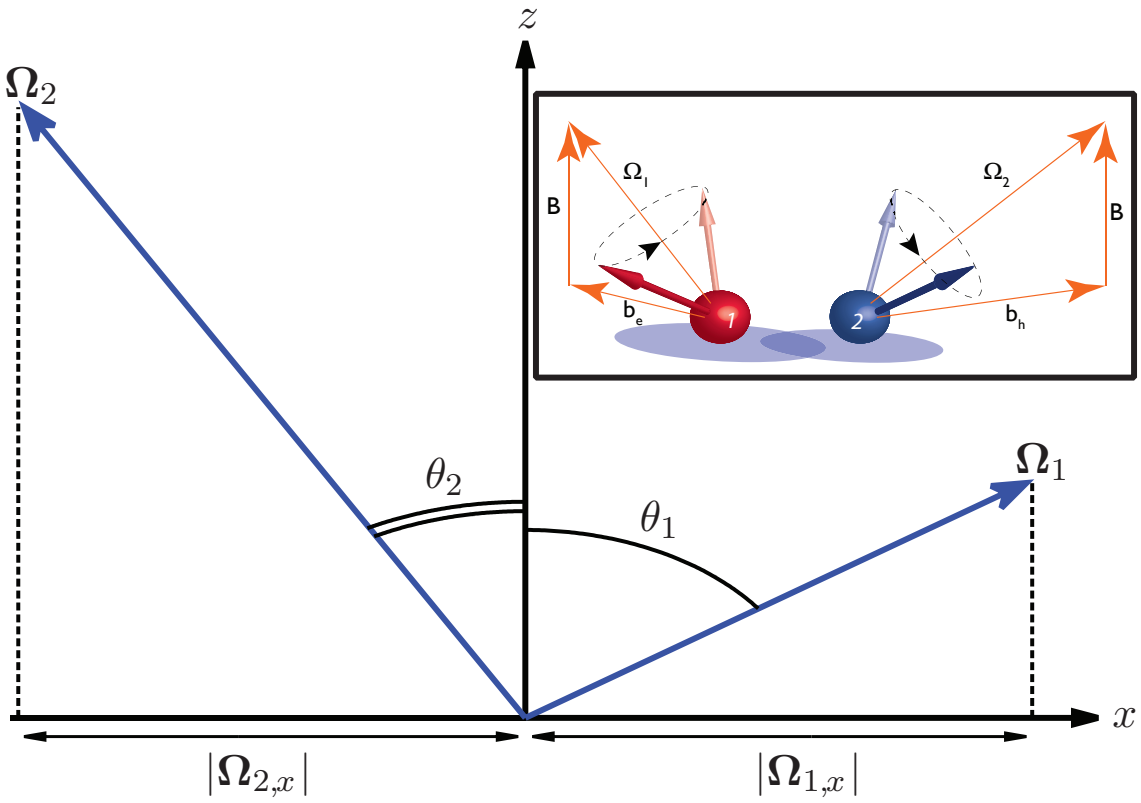

Figure 2.1: Preferential coordinate system used for analysis of the dynamics of the spin pair. Both fields $\mathbf{\Omega}_1$, $\mathbf{\Omega}_2$ reside in the xz-plane. The direction of the quantization axis, z, is fixed by the condition $\mathbf{\Omega}_{1,x} = -\mathbf{\Omega}_{2,x}$.

that for noninteracting spins the eigenvalues are the sums and the differences of individual Zeeman energies

$$\lambda_1^2 = \left(\frac{|\mathbf{\Omega}_1| + |\mathbf{\Omega}_2|}{2}\right)^2, \quad \lambda_3^2 = \left(\frac{|\mathbf{\Omega}_1| - |\mathbf{\Omega}_2|}{2}\right)^2. \tag{2.14}$$

Naturally, λ_1, λ_3 do not depend on the choice of the quantization axis. At the same time, the coefficients in Eq. (2.13) do depend on this choice. To trace how the dependence on the quantization axis disappears in the roots of Eq. (2.13), one should use the following identities

$$\Sigma_z^2 + \Delta_z^2 + \Delta_x^2 = \frac{|\mathbf{\Omega}_1|^2 + |\mathbf{\Omega}_2|^2}{2}, \tag{2.15}$$

$$\Sigma_z^2 \Delta_z^2 = \left(\frac{|\mathbf{\Omega}_1|^2 - |\mathbf{\Omega}_2|^2}{4}\right)^2. \tag{2.16}$$

In terms of the angles θ_1 and θ_2, Fig. 2.1, the corresponding eigenvectors can be expressed as

$$\begin{pmatrix} T_+ \\ S \\ T_0 \\ T_- \end{pmatrix} = \left\{ \begin{pmatrix} \cos\frac{\theta_1}{2}\cos\frac{\theta 2}{2} \\ -\frac{1}{\sqrt{2}}\sin\frac{\theta_1+\theta_2}{2} \\ \frac{1}{\sqrt{2}}\sin\frac{\theta_1-\theta_2}{2} \\ -\sin\frac{\theta_1}{2}\sin\frac{\theta_2}{2} \end{pmatrix}, \begin{pmatrix} -\sin\frac{\theta_1}{2}\sin\frac{\theta_2}{2} \\ -\frac{1}{\sqrt{2}}\sin\frac{\theta_1+\theta_2}{2} \\ -\frac{1}{\sqrt{2}}\sin\frac{\theta_1-\theta_2}{2} \\ \cos\frac{\theta_1}{2}\cos\frac{\theta 2}{2} \end{pmatrix}, \begin{pmatrix} \cos\frac{\theta_1}{2}\sin\frac{\theta 2}{2} \\ \frac{1}{\sqrt{2}}\cos\frac{\theta_1+\theta_2}{2} \\ \frac{1}{\sqrt{2}}\cos\frac{\theta_1-\theta_2}{2} \\ \sin\frac{\theta_1}{2}\cos\frac{\theta_2}{2} \end{pmatrix}, \begin{pmatrix} -\sin\frac{\theta_1}{2}\cos\frac{\theta 2}{2} \\ -\frac{1}{\sqrt{2}}\cos\frac{\theta_1+\theta_2}{2} \\ \frac{1}{\sqrt{2}}\cos\frac{\theta_1-\theta_2}{2} \\ -\cos\frac{\theta_1}{2}\sin\frac{\theta_2}{2} \end{pmatrix} \right\}, \tag{2.17}$$

where the first two correspond to $\lambda_{1,2}$ while the last two correspond to $\lambda_{3,4}$, respectively.

The form of Eq. (2.17) allows us to make the following observation: When the full magnetic fields acting on spins incidentally coincide, we have $|\mathbf{\Omega}_1| = |\mathbf{\Omega}_2|$. Then it follows from Eq. (2.14) that $\lambda_3 = \lambda_4 = 0$, so that the two corresponding eigenstates become degenerate. Under this condition we also have $\theta_1 = \theta_2$. Then the first two eigenvectors Eq. (2.17) have zeros in the rows corresponding to T_0. Concerning the other two eigenvectors, due to their degeneracy, their sum and difference are also eigenvectors. The difference has a zero in the row corresponding to T_0, while the sum consists of the T_0 component, exclusively. Then we conclude that for realizations of hyperfine field for which $|\mathbf{\Omega}_1| = |\mathbf{\Omega}_2|$, the state T_0 is *completely decoupled* from the other three states. This fact has important implications for recombination dynamics, as we will see below.

Including recombination requires the analysis of the full equation for the density matrix

$$i\dot{\rho} = [\widehat{H}, \rho] - \frac{i}{2\tau}\left\{\rho, |S\rangle\langle S|\right\}, \tag{2.18}$$

where τ is the recombination time. The form of the second term ensures that recombination takes place only from S. The matrix corresponding to Eq. (2.18) is 16×16. The 16 eigenvalues can be cast in the form $\lambda_i - \lambda_j^*$, where λ_i and λ_j satisfy the equation

$$\lambda_i\left(\lambda_i + \frac{i}{\tau}\right)(\lambda_i^2 - \Sigma_z^2) - \lambda_i^2(\Delta_z^2 + \Delta_x^2) + \Delta_z^2\Sigma_z^2 = 0. \tag{2.19}$$

The latter equation expresses the condition that λ_i are the eigenvalues of nonhermitian operator $\widehat{H} - \frac{i}{\tau}|S\rangle\langle S|$. In the limit $\tau \to \infty$ this equation reduces to Eq. (2.14). The dynamics of recombination are governed by the imaginary parts of the roots of Eq. (2.19), i.e., decay is described by the exponents $\exp\left[-\left(\mathrm{Im}\,\lambda_i + \mathrm{Im}\,\lambda_j\right)t\right]$, see Fig. 2.2. Less trivial is that finite τ can strongly affect the real parts of λ_i. Physically, the dependence of $\mathrm{Re}\,\lambda_i$ on τ describes the *back-action* of recombination on the dynamics of beating between different eigenstates. In the following two subsections this effect will be analyzed in detail in the two limiting cases.

2.2.2 Slow Recombination

Consider the limit $1/\tau \ll \lambda_i$. In this limit recombination amounts to the small corrections to the bare values of λ_i given by Eq. (2.14). This allows one to set λ_i equal to their bare values in all terms in Eq. (2.19) containing $1/\tau$, and search for solution in the form $\lambda_i + \delta\lambda_i$. Then one gets the following expression for the correction $\delta\lambda_i$

$$\delta\lambda_i = \frac{-i}{\tau}\,\frac{\lambda_i^2 - \Sigma_z^2}{\lambda_i^2 - 2(\Sigma_z^2 + \Delta_z^2 + \Delta_x^2)} = \frac{-i}{2\tau}\,\frac{\lambda_i^2(\lambda_i^2 - \Sigma_z^2)}{\lambda_i^4 - \Sigma_z^2\Delta_z^2}. \tag{2.20}$$

In the last identity we have used the fact that λ_i satisfies the equation Eq. (2.14). The above expression can be greatly simplified with the help of the relations Eq. (2.15). One has

$$\delta\lambda_{1,2} = -\frac{i}{4\tau}\left(1 - \frac{\mathbf{\Omega}_1\cdot\mathbf{\Omega}_2}{|\mathbf{\Omega}_1||\mathbf{\Omega}_2|}\right), \tag{2.21}$$

$$\delta\lambda_{3,4} = -\frac{i}{4\tau}\left(1 + \frac{\mathbf{\Omega}_1\cdot\mathbf{\Omega}_2}{|\mathbf{\Omega}_1||\mathbf{\Omega}_2|}\right). \tag{2.22}$$

The above result suggests that for generic mutual orientations of $\mathbf{\Omega}_1$ and $\mathbf{\Omega}_2$ all modes of a pair decay with characteristic time $\sim\tau$. At the same time, for parallel orientations of $\mathbf{\Omega}_1$, $\mathbf{\Omega}_2$ the modes $\lambda_{1,2}$ have anomalously long lifetime. This long lifetime has its origin in the fact that for $\mathbf{\Omega}_1 \parallel \mathbf{\Omega}_2$, the states T_+ and T_-, which are orthogonal to S, are the eigenstates of the Hamiltonian Eq. (2.1). Formally this can be seen from the general expression Eq. (2.17) for the eigenvectors upon setting $\theta_1 = \theta_2 = 0$. Similarly, for $\mathbf{\Omega}_1$ and $\mathbf{\Omega}_2$ being antiparallel, one can check from Eq. (2.17) that for $\theta_1 = \pi - \theta_2$, the eigenstates λ_3, λ_4 have no S component, so they are long-lived. Note that the existence of long lifetimes for parallel and antiparallel configurations of $\mathbf{\Omega}_1$, $\mathbf{\Omega}_2$ is at the core of the "blocking mechanism" of OMAR proposed in Ref. [15].

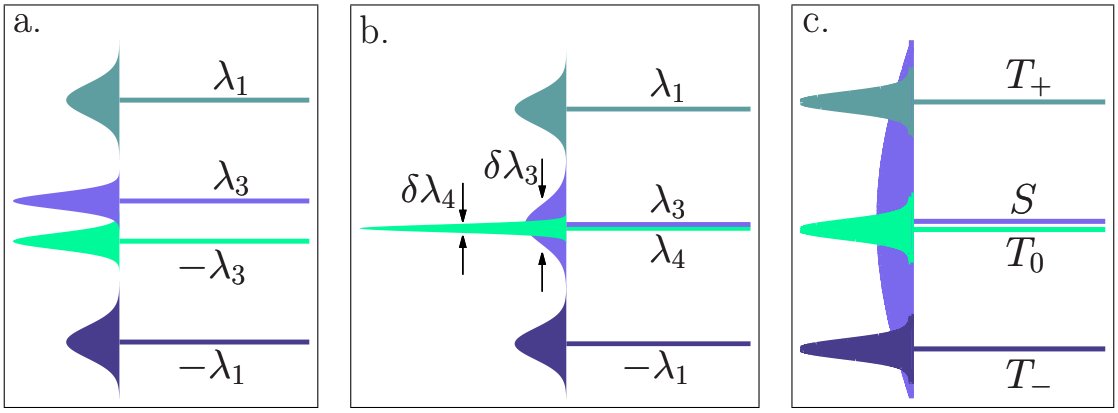

Figure 2.2: Level brodening is illustrated for all three regimes: (a) Slow-recombination regime, $\Omega_{1,2} \gg 1/\tau$. Horizontal lines represent the energy levels Eq. (2.14) of a pair in the absence of recombination. Recombination from S causes the broadening of the levels Eqs. (2.21, 2.22), which, for a typical pair, is of the same order for all levels. (b) Slow-recombination regime. For *soft pairs*, $|\mathbf{\Omega}_1| \approx |\mathbf{\Omega}_2|$, recombination results in splitting Eq. (2.23) of the *widths* of the levels $\lambda_{3,4}$ rather than their positions. (c) Fast-recombination regime, $\Omega_{1,2} \ll 1/\tau$. The eigenstates S, T_0, T_+, and T_- are well-defined. Recombination causes strong broadening, $1/\tau$, of the level S, and weak broadening $\sim \Omega_{1,2}^2\tau$ of the other three levels.

2.2.2.1 Soft pairs

As was pointed out in the Introduction, recombination also has a pronounced effect on the spin dynamics for sparse configurations for which $|\Omega_1| \approx |\Omega_2|$. Indeed, for these configurations, the values λ_3 and λ_4 are anomalously small. Then the basic condition, $1/\tau \ll \lambda_i$, under which Eq. (2.21) was derived, is not satisfied. We dub such realizations as soft pairs. For soft pairs the expressions for $\delta\lambda_1$, $\delta\lambda_2$ remain valid, but the eigenvalues λ_3, λ_4 get strongly modified due to finite recombination time, τ.

Although for soft pairs the terms $\propto 1/\tau$ in Eq. (2.19) cannot be treated as a perturbation, a different simplification becomes possible in this case. We can neglect λ_i^2 compared to Σ_z^2 in the first term and Δ_z^2 compared to Δ_x^2 in the second term. The first simplification is justified, since the typical value of Σ_z is $\sim |\mathbf{\Omega}_1| \approx |\mathbf{\Omega}_2|$ and is much bigger than both $1/\tau$ and $(|\mathbf{\Omega}_1| - |\mathbf{\Omega}_2|)$. Concerning the second simplification, the smallness of $(|\mathbf{\Omega}_1| - |\mathbf{\Omega}_2|)$ automatically implies that Δ_z given by Eq. (2.10) is small. With the above simplifications the eigenvalues $\lambda_{3,4}$ satisfy the quadratic equation

$$(\Sigma_z^2 + \Delta_x^2)\lambda_i^2 + \frac{i}{\tau}\Sigma_z^2\lambda_i - \Delta_z^2\Sigma_z^2 = 0. \tag{2.23}$$

Already from the form of Eq. (2.23) one can make a surprising observation that, even with finite $1/\tau$, one of the roots is *identically* zero when $\Delta_z = 0$, i.e., when $|\mathbf{\Omega}_1|$ and $|\mathbf{\Omega}_2|$ are exactly equal to each other. This suggests that a pair in the state corresponding to this root will never recombine. For a small but finite difference $(|\mathbf{\Omega}_1| - |\mathbf{\Omega}_2|)$ the recombination will eventually take place but *only after time much longer than* τ. Indeed, for the generic case, $|\mathbf{\Omega}_1| \sim |\mathbf{\Omega}_2|$), we have from Eq. (2.23)

$$\lambda_{3,4} = -\frac{i}{2\tau}\left[\Lambda \pm \sqrt{\Lambda^2 - 4\Lambda\Delta_z^2\tau^2}\right], \tag{2.24}$$

where the dimensionless parameter Λ is defined as

$$\Lambda = \frac{\Sigma_z^2}{\Sigma_z^2 + \Delta_x^2}. \tag{2.25}$$

Even when $|\mathbf{\Omega}_1|$ and $|\mathbf{\Omega}_2|$ are close, a typical value of parameter Λ is ~ 1. Then Eq. (2.24) suggests that the anomalously long-living mode exists in the domain $\Delta_z \lesssim 1/\tau$ where its lifetime is $\sim 1/\Delta_z^2\tau$. Note that the lifetime becomes *longer* with a *decrease* of the recombination time.

As the difference $|\mathbf{\Omega}_1| - |\mathbf{\Omega}_2|$ increases, the product $\Delta_z\tau$ becomes big and the expression under the square root in Eq. (2.24) becomes negative. Then the lifetimes of of both states corresponding to λ_3 and λ_4 become equal to τ/Λ. Note that, at the same time, the splitting of the real parts of λ_3 and λ_4 becomes $\sim \Delta_z^2\tau$, which is *much bigger* than $|\mathbf{\Omega}_1| - |\mathbf{\Omega}_2|$.

The above effect can be interpreted as a *repulsion* of the eigenvalues caused by recombination [26]. A more prominent analogy can be found in optics [23]. The signs + and − in Eq. (2.24) can be related to the superradiant and subradiant modes of two identical emitters. The role of τ in this case is played by their radiative lifetime.

Both effects illustrate the back-action of recombination on the dynamics of the pair when the spin levels of pair-partners are nearly degenerate. To track an analogy to this effect one can refer to Refs. [24] and [25], where Eq. (2.24) appeared in connection to resonant tunneling through a pair of nearly degenerate levels, while the role of $1/\tau$ was played by the level width with respect to escape into the leads.

For our choice of the quantization axis, the long-living state corresponds to T_0. For completeness we rewrite the parameter Δ_z, which enters Eq. (2.24), in the coordinate-independent form

$$\Delta_z^2 = \frac{(|\mathbf{\Omega}_1|^2 - |\mathbf{\Omega}_2|^2)^2}{4|\mathbf{\Omega}_1 + \mathbf{\Omega}_2|^2}. \tag{2.26}$$

To establish a coordinate-independent form of parameter Λ we need the combinations Σ_z^2 and $\Sigma_z^2 + \Delta_x^2$, which are given by

$$\Sigma_z^2 = \frac{|\mathbf{\Omega}_1 + \mathbf{\Omega}_2|^2}{4}, \tag{2.27}$$

$$\Sigma_z^2 + \Delta_x^2 = \frac{|\mathbf{\Omega}_1|^2 + |\mathbf{\Omega}_2|^2}{2} - \frac{\left(|\mathbf{\Omega}_1|^2 - |\mathbf{\Omega}_2|^2\right)^2}{4|\mathbf{\Omega}_1 + \mathbf{\Omega}_2|^2}, \tag{2.28}$$

so that Λ can be cast into the form

$$\Lambda = \frac{|\mathbf{\Omega}_1 + \mathbf{\Omega}_2|^4}{|\mathbf{\Omega}_1 + \mathbf{\Omega}_2|^4 + 4|\mathbf{\Omega}_1 \times \mathbf{\Omega}_2|^2}. \tag{2.29}$$

The consequences of "trapping" described by Eq. (2.24) for OMAR will be considered in Sections 2.4 and 2.5. In the subsequent subsection we will see that the similar physics, namely, the emergence of *slow* modes due to *fast* recombination persists also in the domain $|\mathbf{\Omega}_{1,2}|\tau \ll 1$.

2.2.3 Fast Recombination

In the opposite limit, $\tau \ll |\mathbf{\Omega}_{1,2}|^{-1}$, the bracket $(\lambda_i + \frac{i}{\tau})$ in Eq. (2.19) is big. This suggests that three zero-order eigenvalues are

$$\lambda_i = 0, \pm\Sigma_z. \tag{2.30}$$

In the same order, the fourth eigenvalue is $-\frac{i}{\tau}$. Concerning the eigenvectors, in the zeroth order they are simply S, T_+, T_-, and T_0. This follows from the equation

$$i\dot{S} + \frac{i}{\tau}S = \Delta_z T_0 - \frac{1}{\sqrt{2}}T_+ + \frac{1}{\sqrt{2}}T_-. \tag{2.31}$$

Taking τ to zero means that in the zeroth order $S = 0$. Then three other equations in the system Eq. (2.6) get decoupled.

In the first order, the eigenvalues Eq. (2.30) acquire imaginary parts

$$\delta\lambda_i = -i\tau\left(\frac{\lambda_i^2(\Delta_z^2+\Delta_x^2)-\Delta_z^2\Sigma_z^2}{3\lambda_i^2-\Sigma_z^2}\right). \tag{2.32}$$

With the help of Eqs. (2.27) and (2.29) these imaginary parts can be simplified to

$$\delta\lambda_{T_0} = -i\tau\Delta_z^2 = -i\tau\frac{(\Omega_1^2-\Omega_2^2)^2}{4|\mathbf{\Omega}_1+\mathbf{\Omega}_2|^2}, \tag{2.33}$$

$$\delta\lambda_{T_+} = \delta\lambda_{T_-} = -i\tau\frac{\Delta_x^2}{2} = -i\tau\frac{|\mathbf{\Omega}_1\times\mathbf{\Omega}_2|^2}{2|\mathbf{\Omega}_1+\mathbf{\Omega}_2|^2}. \tag{2.34}$$

We see that for a generic situation $|\mathbf{\Omega}_1| \sim |\mathbf{\Omega}_2|$ the lifetime of the modes T_0, T_+, and T_- are $\sim 1/|\mathbf{\Omega}_{1,2}|^2\tau$, i.e., in the regime of fast recombination it is much longer than τ. This is a consequence of effective decoupling of T_0, T_+, and T_- from S in this regime. We also observe from Eq. (2.33) that there is additional prolongation of lifetime for the mode T_0 if the pair is soft. Eq. (2.33) also suggests that lifetimes of the states T_+, T_- are anomalously long when $\mathbf{\Omega}_1$ and $\mathbf{\Omega}_2$ are collinear. This expresses the obvious fact that, for *collinear* effective fields acting on the pair-partners, T_+ and T_- are the eigenstates no matter whether recombination is present or not.

Once the eigenvalues and eigenvectors of a pair in the presence of recombination are established, the next question crucial for transport through the pair is: Suppose that initial state is a random superposition of S, T_0, T_+, and T_-, what is the average (over the coefficients of superposition) waiting time for this state to recombine? Naturally, the answer to this question does not depend on the actual choice of the orthonormal basis. We address this question in the next section.

2.3 Recombination time from a random initial state

2.3.1 Soft pair in a slow recombination regime

To illustrate the peculiarity of the question posed above, we start from an instructive particular case of soft pair in a slow recombination regime. We defined a soft pair as a pair for which the condition $(|\mathbf{\Omega}_1| - |\mathbf{\Omega}_2|) \ll |\mathbf{\Omega}_{1,2}|$ is met. However, in the slow recombination regime, the combination $(|\mathbf{\Omega}_1| - |\mathbf{\Omega}_2|)\tau$ can be either big or small. In both cases there is a strong separation between the absolute values of $\lambda_{1,2}$ and $\lambda_{3,4}$. It can be seen from Eq. (2.24) that in the limit $(|\mathbf{\Omega}_1| - |\mathbf{\Omega}_2|)\tau \gg 1$, the recombination times for states which correspond to λ_3 and λ_4 are given by

$$t_R^{(3)} = \frac{2\tau}{\Lambda} \quad \text{and} \quad t_R^{(4)} = \frac{2\tau}{\Lambda}, \tag{2.35}$$

while in the opposite limit, $(|\mathbf{\Omega}_1| - |\mathbf{\Omega}_2|)\tau \ll 1$, we get

$$t_R^{(3)} = \frac{2\tau}{\Lambda} \quad \text{and} \quad t_R^{(4)} = \frac{1}{\tau\Delta_z^2}. \tag{2.36}$$

We see that the recombination time of λ_3 is $\sim \tau$ for both limits, while the recombination time of λ_4 crosses over from $\sim \tau$ to $\sim 1/\Delta_z^2\tau$ as $(|\mathbf{\Omega}_1| - |\mathbf{\Omega}_2|)\tau$ decreases. Taking into account that for generic case $|\mathbf{\Omega}_1| \sim |\mathbf{\Omega}_2|$ the recombination times corresponding to $\lambda_{1,2}$ are $\sim \tau$, we conclude that for purely random initial conditions the average recombination time is either $\sim \tau$ or it is $\frac{1}{4}$ of $1/\Delta_z^2\tau$.

The major complication for getting exact average recombination time for a soft pair is that the exact eigenstates represent mixtures with weights governed by the recombination time. This follows from Eq. (2.24). In addition, the eigenstates corresponding to λ_3, and λ_4 are not orthogonal to each other. However, for a soft pair these complications can be overcome. The reason is that, there are two small parameters in the problem, $1/\tau|\mathbf{\Omega}_{1,2}|$, and $(|\mathbf{\Omega}_1| - |\mathbf{\Omega}_2|)/|\mathbf{\Omega}_{1,2}|$. The first parameter guarantees slow recombination, while the second ensures that the pair is soft. The presence of these parameters allows us to evaluate $\langle t_R \rangle$ in the closed form using the general formula

$$\langle t_R \rangle = \frac{1}{4} \sum_{i,j} g_{ji} (g_{ji}^{-1})^* \frac{1}{i(\lambda_i - \lambda_j^*)}, \tag{2.37}$$

where $g_{ij} = \langle v_i | v_j \rangle$ is a matrix of inner products of eigenvectors corresponding to *complex* eigenvalues λ_i and λ_j. The above formula becomes absolutely transparent when the eigenvectors are orthonormal. Then the matrix g_{ij} reduces to the Kronecker symbol, δ_{ij}, and $\langle t_R \rangle$ simplifies to

$$\langle t_R \rangle = -\frac{1}{8} \sum_j \frac{1}{\operatorname{Im} \lambda_j}, \tag{2.38}$$

which expresses the fact that for random initial state the average recombination time is the evenly-weighted sum of recombination times from eigenstates.

In the case of a soft pair and slow recombination one should use Eq. (2.37) to evaluate $\langle t_R \rangle$. What enables this evaluation is that, by virtue of small parameters, the eigenvectors corresponding to λ_1 and λ_2 are mutually orthogonal (with accuracy $1/\tau|\mathbf{\Omega}_{1,2}|$), and they are both orthogonal to eigenvectors corresponding to λ_3 and λ_4. Therefore, in evaluating Eq. (2.37), one has to deal only with mutual nonorthogonality of two eigenvectors v_3 and v_4. The straightforward calculation yields

$$\langle t_R \rangle = \frac{\tau}{\Lambda} + \frac{1}{4\Delta_z^2\tau} - \frac{1}{\operatorname{Im} \lambda_1} - \frac{1}{\operatorname{Im} \lambda_2}, \tag{2.39}$$

where $\operatorname{Im} \lambda_1 = \operatorname{Im} \lambda_2$ are given by Eq. (2.21). It is easy to see that in the limiting cases of large and small $(|\mathbf{\Omega}_1| - |\mathbf{\Omega}_2|)\tau$, Eq. (2.39) reproduces Eqs. (2.35) and (2.36), respectively.

While the last two terms in Eq. (2.39) depend weakly on the degree of "softness" of the pair, $\Delta_z \propto (|\mathbf{\Omega}_1| - |\mathbf{\Omega}_2|)$, the second term exhibits *unlimited* growth with decreasing Δ_z. We emphasize the peculiarity of this situation. In conventional quantum mechanics, when the level separation becomes smaller than their width, it should be simply replaced by the width. What makes Eq. (2.39) special is that the smaller is Δ_z, the more the state T_0 becomes isolated. There is direct analogy of this situation with the Dicke effect [23], as was mentioned in the Introduction. By virtue of this analogy, the state T_0 assumes the role of the "subradiant" mode which accompanies the formation of the superradiant mode. In the Dicke effect the formation of superradiant and subradiant states occurs because the bare states are coupled via continuum. In our situation it is recombination that is responsible for "isolation" of T_0. If the pair is not soft, the calculation of the time $\langle t_R \rangle$ in the slow-hopping regime can be performed by simply using Eq. (2.38) and λ_i given by Eqs. (2.21), (2.24). This is because the smallness of $1/\tau$ makes the eigenstates almost orthogonal. However, the Dicke physics becomes even more pronounced in the fast-recombination regime, as demonstrated in the next subsection.

2.3.2 Recombination time in the fast recombination regime

It might seem that under the condition of fast recombination $|\mathbf{\Omega}_{1,2}|\tau \ll 1$ the recombination time from the random initial state should be $\sim \tau$, since spins practically do not precess during the time τ. The fact that recombination takes place only from S, while initial state is a random mixture, already suggests that $\langle t_R \rangle$ is longer than τ. This is because if the initial configuration is different from S it must first cross over into S by spin precession before it recombines. The characteristic time for the spin precession is $\sim |\mathbf{\Omega}_{1,2}|^{-1} \gg \tau$. It turns out that the crossing time is actually much longer than $|\mathbf{\Omega}_{1,2}|^{-1}$. Formally, this fact follows from Eqs. (2.33), (2.34) for $\delta\lambda_i$, which are of the order of $|\mathbf{\Omega}_{1,2}|^2\tau$ rather than $|\mathbf{\Omega}_{1,2}|$. We can now interpret this result by identifying S with superradiant state, while T_0, T_+, and T_- assume the roles of subradiant states. The short lifetime of S isolates it from the rest of the system. Quantitatively, the portion of S in the other eigenvectors is $\sim |\mathbf{\Omega}_{1,2}|\tau$.

What is important for calculation of $\langle t_R \rangle$ is the fact that eigenvectors are orthogonal (with accuracy $\sim 1/|\mathbf{\Omega}_{1,2}|\tau$) in the fast-recombination regime. This allows one to replace the overlap integrals g_{ij} in Eq. (2.37) by δ_{ij} and use Eq. (2.38), which immediately yields for $\langle t_R \rangle$ the result

$$\langle t_R \rangle = -\frac{1}{8}\left(\frac{1}{\operatorname{Im}\lambda_S} + \frac{1}{\operatorname{Im}\lambda_{T_0}} + \frac{1}{\operatorname{Im}\lambda_{T_+}} + \frac{1}{\operatorname{Im}\lambda_{T_-}}\right) \tag{2.40}$$

$$= \frac{1}{8}\left[\tau + \frac{1}{\tau}\left(\frac{1}{\Delta_z^2} + \frac{4}{\Delta_x^2}\right)\right]. \tag{2.41}$$

Substituting the coordinate-independent expressions for Δ_x and Δ_z, we arrive at the final expression for recombination time, which is applicable within the entire fast-recombination regime

$$\langle t_R \rangle = \frac{1}{8}\left[\tau + \frac{4}{\tau}\left(\frac{|\mathbf{\Omega}_1 + \mathbf{\Omega}_2|^2}{\left(|\mathbf{\Omega}_1|^2 - |\mathbf{\Omega}_2|^2\right)^2} + \frac{|\mathbf{\Omega}_1 + \mathbf{\Omega}_2|^2}{|\mathbf{\Omega}_1 \times \mathbf{\Omega}_2|^2}\right)\right]. \tag{2.42}$$

As was already noticed in the previous section, recombination time diverges for two particular configurations: Soft pairs with $|\mathbf{\Omega}_1| = |\mathbf{\Omega}_2|$ and collinear $\mathbf{\Omega}_1$ and $\mathbf{\Omega}_2$. Certainly this divergence will be cut off in the course of calculation of current through a pair to which we now turn.

2.4 Transport model

We adopt the transport model illustrated in Fig. 2.3. For concreteness we will discuss a bipolar device, so that the current is due to electron-hole recombination. As shown in Fig. 2.3, electrons arrive at the pair of sites (enlarged regions in Fig. 2.3) from the left, while holes arrive from the right. Once an electron-hole pair is formed, the spins of the pair-partners undergo precession in the fields $\mathbf{\Omega}_1$ and $\mathbf{\Omega}_2$, respectively, waiting to either recombine or to bypass each other and proceed along their respective current paths. For simplicity we choose the current paths in the form of one-dimensional ($1D$) chains. This choice makes the adopted model of transport very close to the "two-site" model proposed in Ref. [15]. The on-site dynamics of a pair *with recombination* were studied in detail in previous sections. To utilize the results of Section 2.3 for the calculation of current, I, one has to incorporate the stages of formation and dissociation of pairs into the description of transport.

In Fig. 2.4 the formation and dissociation are illustrated with white double-sided arrows. The formation time for all four variants of initial states is assumed to be the same, τ_D. For simplicity we choose the average time for bypassing to be also τ_D. Note that this choice does not limit the generality of the description, provided that τ_D is longer than the recombination time. The middle and the bottom portions in Fig. 2.4 illustrate the spin precession (blue arrows) and recombination (brown arrow) stages, which we studied earlier. Implicit in Fig. 2.4, is that the pair disappears either due to dissociation or by recombination before the next charge carrier arrives. Another way to express this fact is to state that the passage of current proceeds in *cycles*.

Naturally, subsequent cycles are statistically independent. This allows one to express the current along a $1D$ path through the average duration of the cycle, $\bar{t}$. Indeed, $N \gg 1$

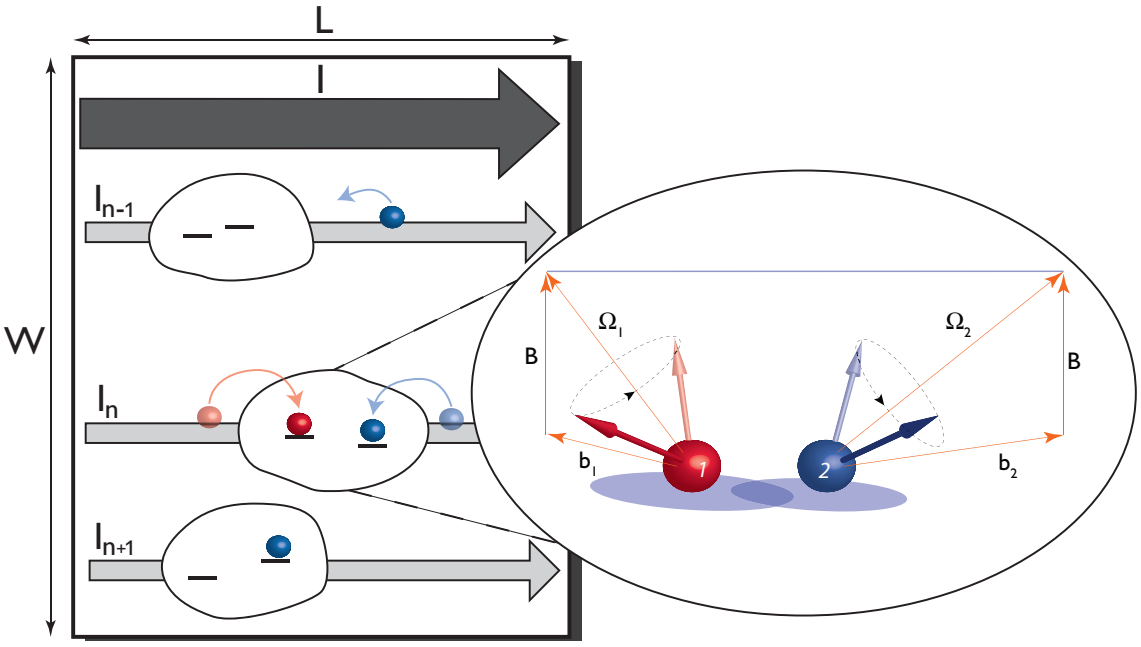

Figure 2.3: The simplest model of transport through a bipolar device in which the currents flow along independent chains. Electrons arrive at the recombination region from the left, while the holes arrive from the right. Blobs enclose the sites from which electron and hole recombine. One of the blobs is enlarged to illustrate the spin precession of the pair partners in their respective fields $\mathbf{\Omega}_1$, $\mathbf{\Omega}_2$. For *soft* pairs the magnitudes of $\mathbf{\Omega}_1$ and $\mathbf{\Omega}_2$ are close to each other.

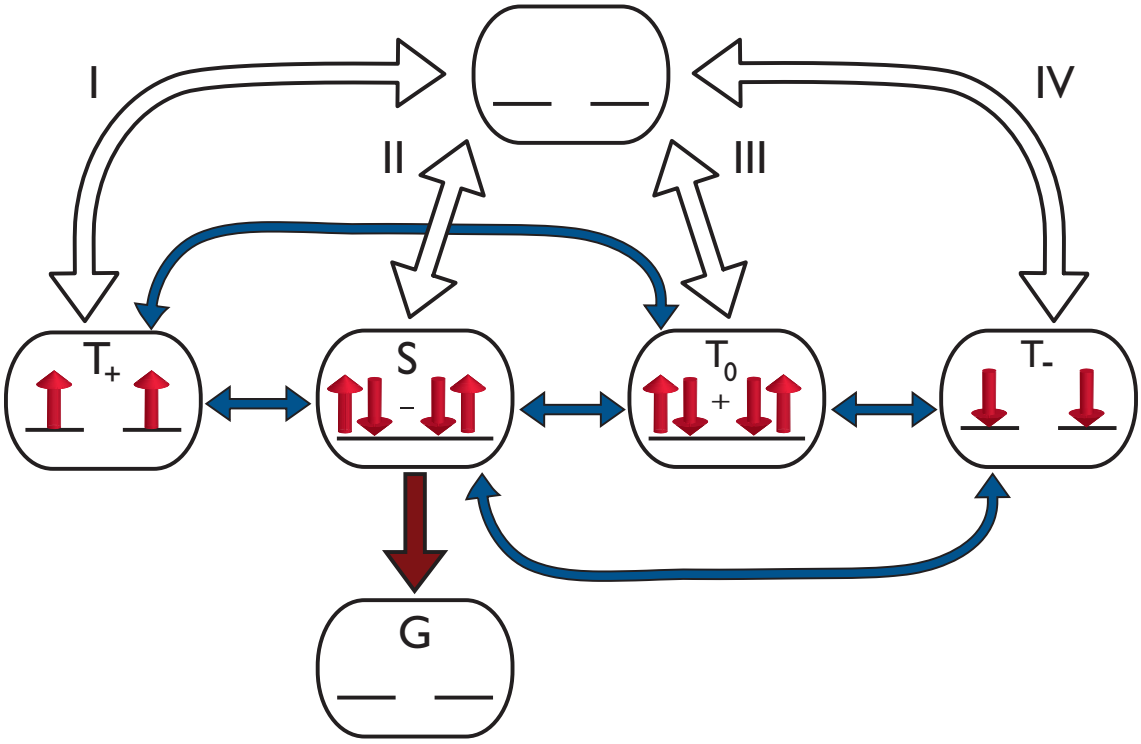

Figure 2.4: Cycles indicated as I, II, III, and IV are possible variants of the current cycle. For each variant the pair is initially created in one of four states. This is followed by time evolution, illustrated by blue double arrows, which mixes the states. Subsequently, the pair either recombines from S (brown arrow) or dissociates. The processes of creation and dissociation are indicated by white double arrows. The current is the inverse duration, $\bar{t}$, of the cycle averaged over initial states, which we assume to have equal probabilities. The time, $\bar{t}$, is given by Eqs. (2.44), (2.45), or (2.46) depending on the recombination regime.

cycles take the time $T_N = t_1 + t_2 + \cdots + t_n$. For large N, this net time acquires a Gaussian distribution centered at $\overline{T_N} = N\bar{t}$. Correspondingly, the current, N/T_N, saturates at the value

$$I = \frac{1}{\bar{t}}. \tag{2.43}$$

Note that Eq. (2.43) constitutes an alternative approach to solving the system of rate equations for the two-site model, as in Ref. [15], or to solving numerically the steady-state density-matrix equations, as in Ref. [16]. Note also that Eq. (2.43) is applicable to such singular realizations as soft pairs, while previous approaches are not. For detailed discussion of this delicate point see Ref. [25].

The remaining task is to express $\bar{t}$ via the average recombination time, $\langle t_R \rangle$ and τ_D. For a typical pair in the regime of slow recombination $\langle t_R \rangle$ is given by Eq. (2.38) upon substitution of Eq. (2.21). Using this expression we get for average duration of the cycle

$$\bar{t} = \tau_D + \frac{1}{4}\left[2\times\frac{1}{\frac{1}{\tau}\left(1-\frac{\boldsymbol{\Omega}_1\cdot\boldsymbol{\Omega}_2}{|\boldsymbol{\Omega}_1||\boldsymbol{\Omega}_2|}\right)+\frac{1}{\tau_D}} + 2\times\frac{1}{\frac{1}{\tau}\left(1+\frac{\boldsymbol{\Omega}_1\cdot\boldsymbol{\Omega}_2}{|\boldsymbol{\Omega}_1||\boldsymbol{\Omega}_2|}\right)+\frac{1}{\tau_D}}\right]. \tag{2.44}$$

The first term captures the formation of the pair, while $1/\tau_D$ in the denominators describes the bypassing. Indeed, if recombination times are $\sim \tau$, one can neglect $1/\tau_D$ in the denominators. On the other hand, as the brackets in denominators in Eq. (2.44) turn to zero, which corresponds to anomalously slow recombination, the second term becomes τ_D. Similarly, for slow recombination with soft pairs, using Eq. (2.39) we get

$$\bar{t} = \tau_D + \frac{1}{4}\left[2\times\frac{1}{\frac{1}{\tau}\left(1-\frac{\boldsymbol{\Omega}_1\cdot\boldsymbol{\Omega}_2}{|\boldsymbol{\Omega}_1||\boldsymbol{\Omega}_2|}\right)+\frac{1}{\tau_D}} + \frac{1}{\frac{1}{\tau}\left(\frac{|\boldsymbol{\Omega}_1+\boldsymbol{\Omega}_2|^4}{|\boldsymbol{\Omega}_1+\boldsymbol{\Omega}_2|^4+4|\boldsymbol{\Omega}_1\times\boldsymbol{\Omega}_2|^2}\right)+\frac{1}{\tau_D}} + \frac{1}{\tau\left(\frac{(|\boldsymbol{\Omega}_1|^2-|\boldsymbol{\Omega}_2|^2)^2}{|\boldsymbol{\Omega}_1+\boldsymbol{\Omega}_2|^2}\right)+\frac{1}{\tau_D}}\right]. \tag{2.45}$$

Finally, in the regime of fast recombination one should use Eq. (2.42) for $\langle t_R \rangle$. This leads to the following expression for $\bar{t}$

$$\bar{t} = \tau_D + \frac{1}{4}\left[\frac{1}{\frac{1}{\tau}+\frac{1}{\tau_D}} + \frac{1}{\tau\left(\frac{(|\boldsymbol{\Omega}_1|^2-|\boldsymbol{\Omega}_2|^2)^2}{4|\boldsymbol{\Omega}_1+\boldsymbol{\Omega}_2|^2}\right)+\frac{1}{\tau_D}} + 2\times\frac{1}{\frac{\tau}{2}\left(\frac{|\boldsymbol{\Omega}_1\times\boldsymbol{\Omega}_2|^2}{|\boldsymbol{\Omega}_1+\boldsymbol{\Omega}_2|^2}\right)+\frac{1}{\tau_D}}\right]. \tag{2.46}$$

Obviously, the dependence of current on external field is encoded in Eqs. (2.44)-(2.46) via the frequencies $\boldsymbol{\Omega}_1 = \boldsymbol{B} + \boldsymbol{b}_e$ and $\boldsymbol{\Omega}_2 = \boldsymbol{B} + \boldsymbol{b}_h$. The observable is the current averaged over realizations of the hyperfine fields $\boldsymbol{b}_e$ and $\boldsymbol{b}_h$. This averaging is performed in the next section.

2.5 Averaging over hyperfine fields

2.5.1 Averaging in the slow-recombination regime

Our basic assumption is that the time, τ_D, of formation and dissociation of a pair is much bigger than the recombination time, τ. Only under this condition will the pair exercise spin dynamics. Using the relation $\tau_D \gg \tau$, we can simplify the expression Eq. (2.44) for $\bar{t}$ of a *typical* pair

$$\bar{t} = \tau_D + \frac{\tau}{1 - \left(\frac{\mathbf{\Omega}_1 \cdot \mathbf{\Omega}_2}{|\mathbf{\Omega}_1||\mathbf{\Omega}_2|}\right)^2}. \tag{2.47}$$

We can also rewrite the current in the form $I = \frac{1}{\tau_D} - \delta I_t(B)$, where the field-dependent correction is defined as

$$\delta I_t(B) = \frac{\tau}{\tau_D^2} \frac{1}{1 - \left(\frac{\mathbf{\Omega}_1 \cdot \mathbf{\Omega}_2}{|\mathbf{\Omega}_1||\mathbf{\Omega}_2|}\right)^2 + \frac{\tau}{\tau_D}} \tag{2.48}$$

As we will see below, the significant change of δI_t with B takes place in the domain where B is much bigger than the hyperfine field. Therefore, we expand Eq. (2.48) with respect to $|\boldsymbol{b}_e|/B$ and $|\boldsymbol{b}_h|/B$. The principal ingredient of this step is the expansion of denominator

$$|\mathbf{\Omega}_1|^2|\mathbf{\Omega}_2|^2 - (\mathbf{\Omega}_1 \cdot \mathbf{\Omega}_2)^2 \approx B^2 \left[|\boldsymbol{b}_e - \boldsymbol{b}_h|^2 - \left(\boldsymbol{b}_e \cdot \frac{\boldsymbol{B}}{B} - \boldsymbol{b}_h \cdot \frac{\boldsymbol{B}}{B} \right)^2 \right]. \tag{2.49}$$

Assuming identical Gaussian distributions of $\boldsymbol{b}_e$, $\boldsymbol{b}_h$

$$\mathcal{P}(\boldsymbol{b}_i) = \frac{1}{(\pi b_0)^{3/2}} \exp(-|\boldsymbol{b}_i|^2/b_0^2), \tag{2.50}$$

and choosing the z-direction along $\boldsymbol{B}$ we get

$$\langle \delta I_t(B) \rangle = \frac{B^2 \tau}{\tau_D^2} \left\langle \frac{1}{(b_{1x} - b_{2x})^2 + (b_{1y} - b_{2y})^2 + \frac{\tau}{\tau_D} B^2} \right\rangle. \tag{2.51}$$

The next step is averaging Eq. (2.51) over the remaining four components of the hyperfine fields. It is easiest to perform this integration by switching to $\boldsymbol{b}_1 \pm \boldsymbol{b}_2$ and introducing the polar coordinates. The integrations over the sum and over the polar angle are elementary. The result can be cast in the form

$$\langle \delta I_t(B) \rangle = \frac{1}{\tau_D} \mathcal{F}\left(\frac{B}{B_c}\right), \tag{2.52}$$

where the characteristic field B_c is given by

$$B_c = \left(\frac{2\tau_D}{\tau}\right)^{1/2} b_0. \tag{2.53}$$

The form of the function $\mathcal{F}$ is the following

$$\mathcal{F}(x) = 2x^2 \int_0^\infty du \, \frac{u}{u^2 + x^2} \, e^{-u^2} = x^2 e^{x^2} \mathrm{E}_1(x^2), \tag{2.54}$$

where $\mathrm{E}_1(z)$ is the exponential integral function. From Eq. (2.53) we see that relation $\tau_D \gg \tau$ ensures that $B_c \gg b_0$, so that the expansion Eq. (2.49) of $\delta I_t(B)$ with respect to hyperfine fields is justified.

The magnetoresistance Eq. (2.52) is plotted in Fig. 2.5. We note that the shape, being a single-parameter function, $\mathcal{F}(x)$, can be very closely approximated with $x^2/(0.8+x^2)$. This approximation, which is also plotted in Fig. 2.5, represents a standard fitting function for experimentally measured magnetoresistance. It can be seen that at $x \ll 1$ there is a small deviation of $\mathcal{F}(x)$ from the approximation. This is due to the singular behavior of $\mathcal{F}(x)$ at small arguments. This singularity translates into the following behavior of $\delta I_t(B)$

$$\delta I_t(B) \underset{b_0<B<B_c}{\approx} \frac{\tau B^2}{2\tau_D^2\, b_0^2} \ln\left(\frac{2\tau_D\, b_0^2}{\tau B^2}\right). \tag{2.55}$$

On the physical level, the fact that the "body" of magnetoresistance lies in the domain $B \gg b_0$ suggests that the origin of the effect are trapping configurations for which $\mathbf{\Omega}_1$ and $\mathbf{\Omega}_2$ are almost parallel or antiparallel. In this regard, Eqs. (2.52) and (2.54) can be viewed as analytical, rather than numerical, as in Ref. [15], treatment of the bipolaron mechanism [15].

Another interesting point is the behavior of $\delta I_t(B)$ in the limit of very small $B \ll b_0$. The value $\delta I_t(0)$ can be averaged over hyperfine fields exactly. Taking into account that $\tau \ll \tau_D$, the result of this averaging reads

$$\delta I_t(0) = \frac{\tau}{2\tau_D^2} \ln\left(\frac{4\tau_D}{\tau}\right), \tag{2.56}$$

and matches Eq. (2.55) at $B \approx b_0$. It is noteworthy that the behavior of the difference $\delta I_t(B) - \delta I_t(0)$ at $B \ll b_0$ is *not* quadratic in B. This is because expansion of the denominator in Eq. (2.48) with respect to B and subsequent Gaussian averaging over hyperfine fields renders the coefficient in front of B^2 to be zero *identically*. Thus, to establish a true behavior of $\delta I_t(B) - \delta I_t(0)$ in the limit $B \to 0$, one has to expand the denominator in Eq. (2.48) up to B^4 and then perform the averaging. This tedious but straightforward calculation, outlined in Appendix 2.9, yields

$$\delta I_t(B) = \delta I_t(0)\left(1 + \frac{7\, B^4}{4\, b_0^4}\right). \tag{2.57}$$

Eq. (2.57) suggests that OMAR has a "flat" region at $B \ll b_0$ preceding the quadratic growth. Note that complete cancelation of the B^2 correction would not be revealed in the numerical simulations. In this regard, we would like to notice that Refs. [16] and [27] report a shallow extremum in the OMAR response at low fields, which was inferred from numerical simulations for certain combinations of parameters similar to our τ and τ_D. Possibly, these extrema result from unavoidable errors in numerical averaging.

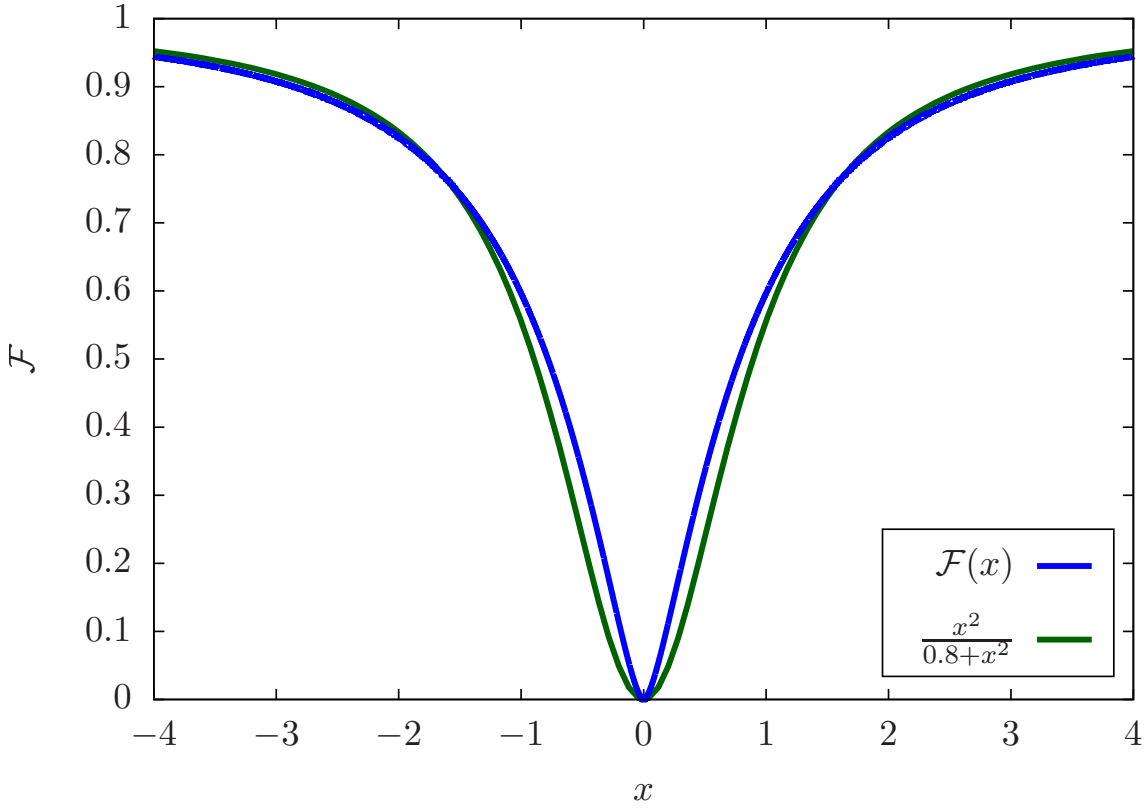

Figure 2.5: The magnetic field response, $\delta I_t(B)$ is shown for the "parallel-antiparallel" blocking mechanism (blue), is plotted from Eq. (2.54) in the units $1/\tau_D$ versus dimensionless magnetic field B/B_c. The fit with conventional lineshape (a Gaussian), $x^2/(0.8+x^2)$, is also plotted (green) for comparison.

2.5.2 Averaging in the soft-pair-dominant regime

Soft pairs are responsible for the second and third terms in the brackets of Eq. (2.45) for $\bar{t}$. The second term becomes big when the sum, $\mathbf{\Omega}_1 + \mathbf{\Omega}_2$, becomes anomalously small. Still it cannot dominate over the contribution from the first term for the following reason. When $\mathbf{\Omega}_1 + \mathbf{\Omega}_2$ is small, the expression in the parenthesis of the second term behaves as $(\mathbf{\Omega}_1 + \mathbf{\Omega}_2)^2/|\mathbf{\Omega}_1|^2$. At the same time, for small $\mathbf{\Omega}_1 - \mathbf{\Omega}_2$, the expression in the parenthesis of the first term behaves as $(\mathbf{\Omega}_1 - \mathbf{\Omega}_2)^2/|\mathbf{\Omega}_1|^2$. In strong fields, the second expression is smaller than the first, leading to the larger δI, while in weak fields the two expressions give the same contribution to δI.

The third term in Eq. (2.45) captures the contribution of the slow modes to the current. Below we will study whether the averaging of this term over hyperfine fields can dominate over the "bipolaron" magnetic-field response given by Eq. (2.55).

Prior to performing averaging, we rewrite the current as $I = \frac{1}{\tau_D} - \delta I_s(B)$, like we did earlier. In the soft-pairs-dominated regime the expression for $\delta I_s(B)$ takes the form

$$\delta I_s(B) = \frac{1}{\tau_D}\left(\frac{1}{1 + \frac{(|\mathbf{\Omega}_1|^2 - |\mathbf{\Omega}_2|^2)^2}{|\mathbf{\Omega}_1 + \mathbf{\Omega}_2|^2}\tau\tau_D}\right). \tag{2.58}$$

For a typical configuration with $|\mathbf{\Omega}_1| \sim |\mathbf{\Omega}_2|$, the second term in the denominator can be estimates as $|\mathbf{\Omega}_1|^2\tau\tau_D$, so that it is large in the slow-recombination regime. This is why the soft pairs with

$$(|\mathbf{\Omega}_1| - |\mathbf{\Omega}_2|) \sim \frac{1}{\sqrt{\tau\tau_D}} \tag{2.59}$$

give the major contribution to the average $\delta I_s(B)$. The latter fact allows one to simplify the averaging procedure. Namely, one can use the fact that for $\epsilon \ll 1$ the combination $\frac{\epsilon}{\epsilon^2 + x^2}$ can be replaced by $\pi\delta(x)$. Thus, the expression to be averaged can be rewritten in the form

$$\delta I_s(B) = \frac{\pi}{\tau_D\sqrt{\tau\tau_D}}\delta\left(\frac{|\mathbf{\Omega}_1|^2 - |\mathbf{\Omega}_2|^2}{|\mathbf{\Omega}_1 + \mathbf{\Omega}_2|}\right). \tag{2.60}$$

The form Eq. (2.60) suggests that characteristic magnetic field determined from zero of the δ-function is $B \sim b_0$, and yields the estimate $1/\tau^{1/2}\tau_D^{3/2}b_0$ for $\delta I_s(B)$. To compare the contribution of soft pairs to that of typical pairs this estimate should be compared to Eq. (2.55) taken at $B \sim b_0$. Soft pairs dominate if the condition

$$\sqrt{\frac{\tau_D}{\tau}} \gg b_0\tau \tag{2.61}$$

is met. Since τ_D is much bigger than τ, this condition is compatible with the condition, $b_0\tau \gg 1$ necessary for slow recombination. Note in passing, that replacement of the

denominator in Eq. (2.48) by a δ-function, as we did for soft pairs, is not permissible. This follows, e.g., from Eq. (2.53) which suggests that the characteristic field B_c is much bigger than b_0. Replacement of the denominator in Eq. (2.48) by a δ-function would automatically fix the characteristic field at $B \sim b_0$.

In averaging of Eq. (2.60) over hyperfine configurations, we will assume from the outset that the characteristic hyperfine fields, b_1 and b_2, for the electron and hole are different, so that

$$\langle \delta I_s(B) \rangle = \frac{1}{\pi^2 b_1^3 b_2^3 \sqrt{\tau \tau_D^3}} \int d^3\boldsymbol{b}_e \int d^3\boldsymbol{b}_h \delta \left(\frac{|\boldsymbol{b}_e + \boldsymbol{B}|^2 - |\boldsymbol{b}_h + \boldsymbol{B}|^2}{|\boldsymbol{b}_e + \boldsymbol{b}_h + 2\boldsymbol{B}|^2} \right) \exp\left(-\frac{|\boldsymbol{b}_e|^2}{b_1^2} - \frac{|\boldsymbol{b}_h|^2}{b_2^2} \right). \tag{2.62}$$

Subsequent analysis will indicate that different b_1 and b_2 is a necessary condition for δI_s to exhibit B-dependence.

The six-fold integral Eq. (2.62) can be reduced to a single integral in three steps. As a first step, we introduce new variables $\boldsymbol{v} = \boldsymbol{b}_e - \boldsymbol{b}_h$ and $\boldsymbol{u} = \boldsymbol{b}_e + \boldsymbol{b}_h + 2\boldsymbol{B}$, so that Eq. (2.62) acquires the form

$$\langle \delta I_s(B) \rangle = \frac{1}{8\pi^2 b_1^3 b_2^3 \sqrt{\tau \tau_D^2}} \int d^3\boldsymbol{u} \int d^3\boldsymbol{v}\, |\boldsymbol{u}|\, \delta(\boldsymbol{u} \cdot \boldsymbol{v}) \times \exp\left(-\alpha(\boldsymbol{u} - 2\boldsymbol{B})^2 + \beta(\boldsymbol{u} - 2\boldsymbol{B}) \cdot \boldsymbol{v} - \alpha|\boldsymbol{v}|^2 \right), \tag{2.63}$$

with parameters α and β defined as

$$\alpha = \frac{1}{4}\left(\frac{1}{b_1^2} + \frac{1}{b_2^2} \right), \quad \beta = \frac{1}{2}\left(\frac{1}{b_1^2} - \frac{1}{b_2^2} \right). \tag{2.64}$$

As a second step, we perform integration over the vector $\boldsymbol{v}$. The reason why this integration can be carried out analytically is that, upon choosing the z-direction along $\boldsymbol{u}$, the δ-function fixes v_z to be zero. The remaining two integrals over v_x and v_y are simply Gaussian integrals, so we get

$$\langle \delta I_s(B) \rangle = \frac{1}{8\pi b_1^3 b_2^3 \alpha \sqrt{\tau \tau_D^3}} \int d^3\boldsymbol{u} \exp\left[-\alpha(\boldsymbol{u} - 2\boldsymbol{B})^2 + \frac{\beta^2}{\alpha}\left(|\boldsymbol{B}|^2 - \frac{(\boldsymbol{B} \cdot \boldsymbol{u})^2}{|\boldsymbol{u}|^2} \right) \right]. \tag{2.65}$$

To perform the integration over $\boldsymbol{u}$, we switch to spherical coordinates with polar axis along $\boldsymbol{B}$. Then the integration over azimuthal angle reduces to multiplication by 2π. The third step is the integration over the polar angle in Eq. (2.65). We have

$$\langle \delta I_s(B) \rangle = \frac{e^{-4\alpha\left(1 - \frac{\beta^2}{4\alpha^2}\right)B^2}}{4 b_1^3 b_2^3 \alpha \sqrt{\tau \tau_D^3}} \int_0^\infty du\, u^2 e^{-\alpha u^2} \int_0^\pi d\theta \sin\theta \exp\left(4\alpha u B \cos\theta - \frac{\beta^2}{\alpha} B^2 \cos^2\theta \right). \tag{2.66}$$

Now we note that the integral over θ can be expressed via the error-functions in the following way

$$\int_{-1}^{1} dx\, e^{-A^2x^2+Cx} = \frac{\sqrt{\pi}}{2A} e^{\frac{C^2}{4A^2}} \left[\mathrm{erf}\left(A+\frac{C}{2A}\right) + \mathrm{erf}\left(A-\frac{C}{2A}\right)\right]. \tag{2.67}$$

We are left with a single integral over u, which can be cast in the form

$$\langle \delta I_s(B)\rangle = \frac{\sqrt{\pi} e^{-4\alpha\left(1-\frac{\beta^2}{4\alpha^2}\right)B^2}}{8b_1^3 b_2^3 \sqrt{\tau\tau_D^3}\sqrt{\alpha}\beta B} \int_0^\infty du\, u^2 \exp\left(-\alpha\left(1-\frac{4\alpha^2}{\beta^2}\right)u^2\right) \times \left[\mathrm{erf}\left(\frac{\beta B}{\sqrt{\alpha}}+\frac{2\alpha^{3/2}u}{\beta}\right) + \mathrm{erf}\left(\frac{\beta B}{\sqrt{\alpha}}-\frac{2\alpha^{3/2}u}{\beta}\right)\right]. \tag{2.68}$$

2.5.3 Analysis of Eq. (2.68)

At this point we make an observation that for $b_1 = b_2$, which is equivalent to $\beta = 0$, the magnetic field drops out of Eq. (2.68). The easiest way to see it is to set $\beta = 0$ at the earlier stage of calculation, namely in Eq. (2.65)

$$\langle \delta I_s(b_1 = b_2)\rangle = \frac{1}{8\pi b_1^3 b_2^3 \alpha\sqrt{\tau\tau_D^3}} \int d^3\boldsymbol{u}\, e^{-\alpha(\boldsymbol{u}-2\boldsymbol{B})^2}, \tag{2.69}$$

which is clearly independent of $\boldsymbol{B}$ after a simple coordinate shift. If we set $b_1 = b_2$, then δI_s is given by

$$\langle \delta I_s(b_1 = b_2)\rangle = \sqrt{\frac{\pi}{2\tau\tau_D^3}}\,\frac{1}{b_1}, \tag{2.70}$$

in agreement with the qualitative estimate above.

Magnetic field dependence of $\langle \delta I_s\rangle$ emerges already at small values of asymmetry parameter defined as

$$\eta = 1 - \frac{b_2^2}{b_1^2}. \tag{2.71}$$

This is illustrated in Fig. 2.6, where $\langle \delta I_s(\eta, B)\rangle - \langle \delta I_s(\eta, 0)\rangle$ in the units of $\langle \delta I_s(\eta = 0)\rangle$, given by Eq. (2.70), is plotted for several values of η. We see that, as η increases, the shape of the curves do not change much. For the saturation value the analysis of Eq. (2.68) yields

$$\frac{\langle \delta I_s(\eta,\infty)\rangle - \langle \delta I_s(\eta, 0)\rangle}{\langle \delta I_s(\eta = 0)\rangle} = \frac{\sqrt{2}\eta^2}{(2-\eta)^{5/2}}. \tag{2.72}$$

The result, Eq. (2.68), can be recast in a more concise form in terms of the Dawson function $D(x) = e^{-x^2}\int_0^x dt\, e^{t^2}$. The corresponding expression reads

$$\frac{\langle \delta I_s(\eta, B)\rangle}{\langle \delta I_s(0,0)\rangle} = \frac{\sqrt{2}}{\sqrt{2-\eta}} - \left(\frac{\eta}{2-\eta}\right)^2 \frac{\sqrt{2}}{2z} D\left(\frac{2z}{\sqrt{2-\eta}}\right), \tag{2.73}$$

where we have introduced $z = B/b_1$.

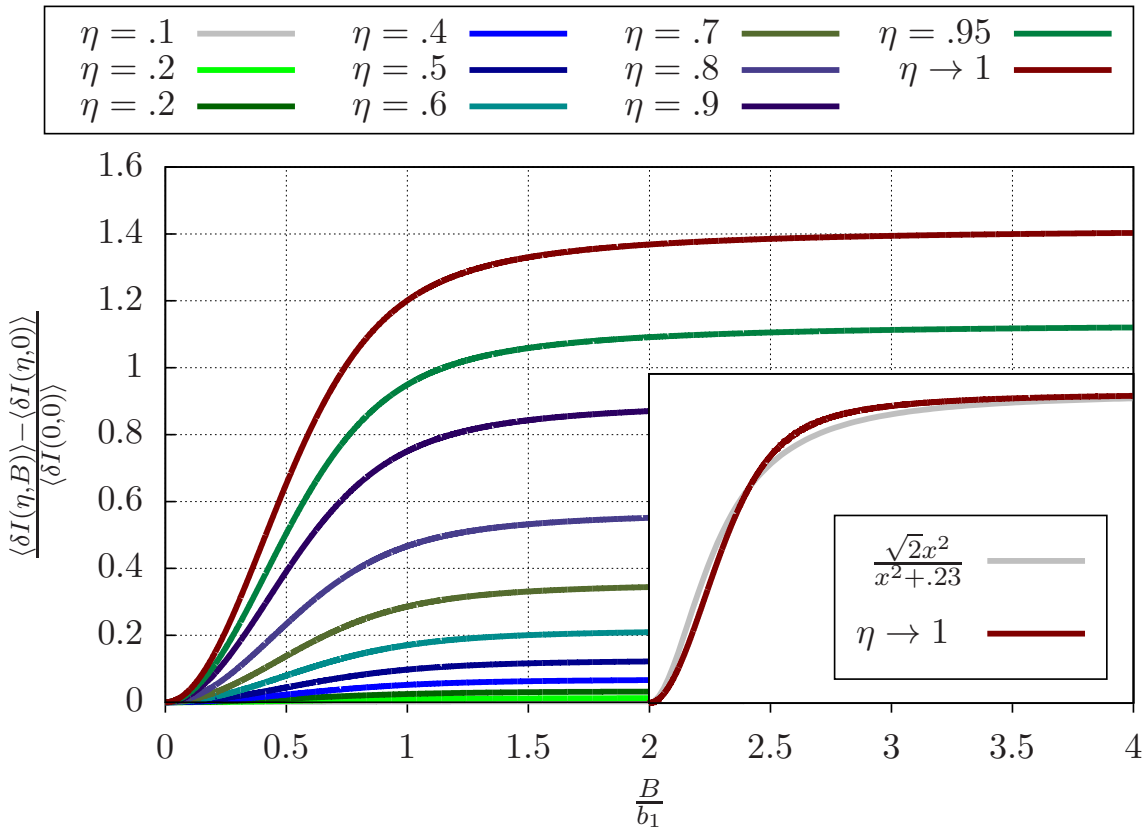

Figure 2.6: Magnetic field response for the "soft-pair" mechanism is plotted from Eq. (2.68) versus magnetic field in the units of the hyperfine field b_1 for different values of the asymmetry parameter η. Inset: fit of the response in the limit of strong asymmetry with conventional lineshape of OMAR, $\sqrt{2}x^2/(0.23 + x^2)$.

In the limit of strong asymmetry, when η is close to 1, one gets a simple analytical expression for $\langle \delta I_s(B) \rangle$

$$\frac{\langle \delta I_s(\eta=1,B) \rangle}{\langle \delta I_s(\eta=0) \rangle} = 2\left(\frac{B}{b_1}\right)^2 \int\limits_{-1}^{1} dx\, \sqrt{1+x}\, \exp\left[-2\left(\frac{B}{b_1}\right)^2 (1-x)\right]. \tag{2.74}$$

At small B the ratio Eq. (2.74) behaves quadratically, while at large B it saturates as $\sqrt{2}\left(1-\frac{b_1^2}{8B^2}\right)$. Overall, similarly to $I_t(B)$, magnetoresistance, Eq. (2.74), can be closely approximated with $\sqrt{2}x^2/(0.23+x^2)$, as illustrated in Fig. 2.6.

2.5.4 Inequivalence of electron and hole g-factors

In the previous subsection we demonstrated that external magnetic field drops out from the general expression, Eq. (2.62), when the variances b_1 and b_2 are equal. Here, we note that averaging does not eliminate the B-dependence even when $b_1 = b_2$, as long as the g-factors of the pair partners are different. Incorporating g_1 and g_2 into Eq. (2.62) is straightforward and amounts to multiplying $\boldsymbol{b}_e + \boldsymbol{B}$ by $1+\kappa$, while $\boldsymbol{b}_h + \boldsymbol{B}$ is multiplied by $1-\kappa$, where κ is the relative difference in the g-factors. The three steps leading from Eq. (2.62) to Eq. (2.68) are exactly the same as for $\kappa = 0$. Finite κ modifies both the prefactor in the integral, Eq. (2.68), and the arguments of the error functions in the integrand. It is convenient to analyze the magnetic field response by considering the ratio $\langle \delta I_s(B;\kappa) \rangle / \langle \delta I_s(\kappa=0) \rangle$, where the denominator is given by Eq. (2.70).

$$\frac{\langle \delta I_s(B;\kappa) \rangle}{\langle \delta I_s(\kappa=0) \rangle} = \frac{\exp\left(-\frac{2z^2}{1+\kappa^2}\right)}{2\sqrt{2}(1+\kappa^2)\kappa z} \int\limits_0^\infty du\, u^2 e^{-\zeta u^2} \left[\mathrm{erf}\left(\frac{\kappa}{1-\kappa^2}(z+\gamma u)\right) + \mathrm{erf}\left(\frac{\kappa}{1-\kappa^2}(z-\gamma u)\right)\right], \tag{2.75}$$

where $z = B/b_1$ is the scaled magnetic field. For notational convenience we introduced the κ-dependent terms ζ and γ, which are defined as

$$\zeta = \frac{1}{2(1-\kappa^2)}\left(1 + \frac{(1-\kappa^2)^3}{2\kappa^2(1+\kappa^2)^2}\right), \tag{2.76}$$

$$\gamma = \frac{1}{1-\kappa^2}\left(1 + \frac{(1-\kappa^2)^3}{\kappa^2(1+\kappa^2)}\right). \tag{2.77}$$

It is seen that the arguments of the error-functions as well as the power in the exponent diverge in the limit $\kappa \to 1$, i.e., when the g-factor of one pair-partner is zero. This divergence signifies that magnetic field response is weak for small $(1-\kappa)$. The underlying reason for this is that the portion of soft pairs goes to zero if the levels of one of the partners are not split by a magnetic field. In Fig. 2.7 we plot the magnetic field response for different values of κ. There are two noteworthy features of this response. Firstly, the *sign* of response is

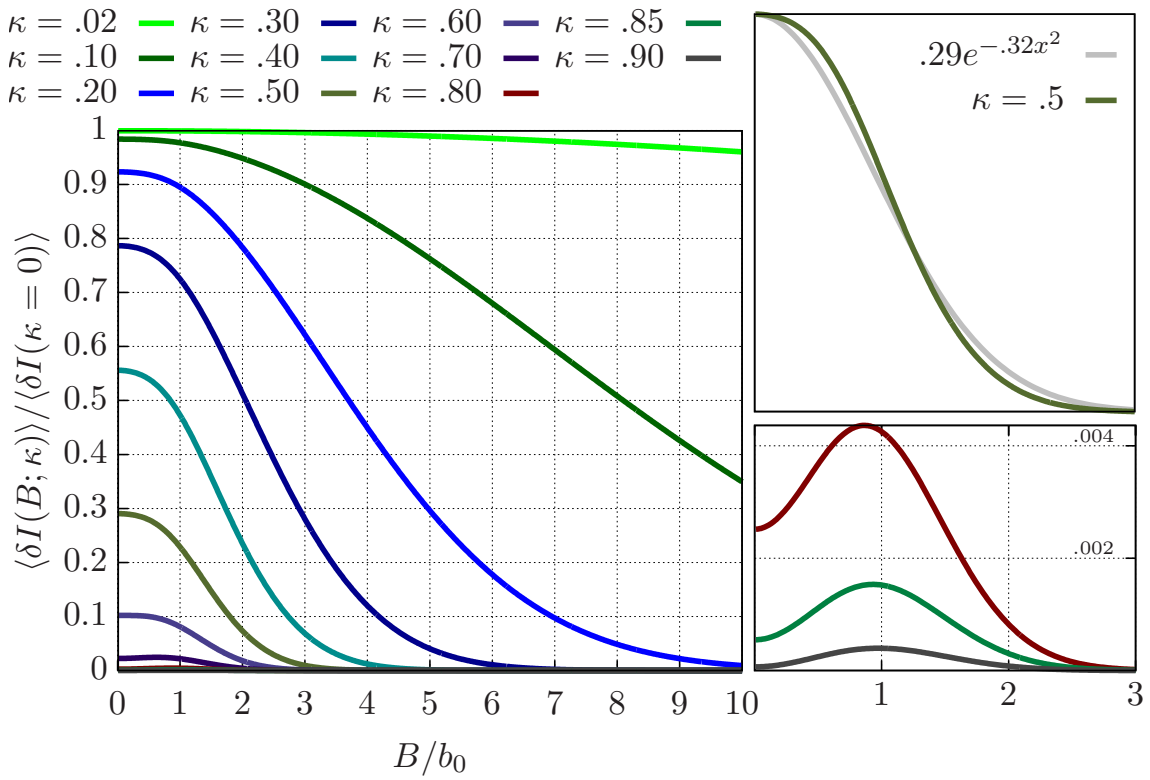

Figure 2.7: Magnetic field response caused by the difference in the g-factors of electron and hole is plotted from Eq. (2.75) for several values of relative difference, κ. Upper inset illustrates that the shape of the response is near-Gaussian. Lower inset illustrates that at κ close to 1 the shape of the response develops a maximum.

opposite to that for inequivalent distributions of electrons and holes, see Fig. 2.6. Secondly, the *shape* of $\delta I_s(B)$ is not Lorentzian anymore. In fact, this shape is close to Gaussian, as illustrated in the inset. Another peculiar feature of $\delta I_s(B)$ which can be seen from Fig. 2.7 is that, for κ close to 1, the response $\delta I(B)$ develops a bump.

2.5.5 Averaging in the fast-recombination regime

Turning to Eq. (2.46) for $\bar{t}$ in the fast-recombination regime we notice that the second term in the square brackets has exactly the same form as the contribution of the soft pairs to $\bar{t}$ in the slow-recombination regime, see Eq. (2.45). The underlying reason is that, similarly to soft pairs, this second term also comes from the slow eigenmode. The origin of this slow eigenmode, i.e., orthogonalization of S-mode to all the other states, was discussed in detail in Section 2.2. Since the configurational averaging for soft pairs was already carried out, we conclude that the magnetic field response in the fast-recombination regime is simply described by Eq. (2.68).

At this point we note that configurational averaging over slow pairs was based on the applicability of the condition $b_0^2\tau\tau_D \gg 1$. Therefore, it is important that this condition is compatible with fast-recombination, $b_0\tau \ll 1$, by virtue of a small parameter τ/τ_D.

In addition to the soft-pair contribution, Eq. (2.46) also contains a term with $|\mathbf{\Omega}_1 \times \mathbf{\Omega}_2|^2$ in the denominator. This term becomes large when $\mathbf{\Omega}_1$ and $\mathbf{\Omega}_2$ are collinear. However, the statistical weight of these configurations is smaller than the statistical weight of the soft-pair contribution. Indeed, in order for the term with $|\mathbf{\Omega}_1 \times \mathbf{\Omega}_2|^2$ in the denominator to become large, the angle between the vectors $\mathbf{\Omega}_1$ and $\mathbf{\Omega}_2$ should be restricted to $\theta_0 \sim 1/b_0\sqrt{\tau\tau_D} \ll 1$. In course of configurational averaging, the integral, $\int d\theta \sin\theta \ldots$, which is small as θ_0^2 emerges.

We now turn to the limit of very weak hyperfine fields for which the parameter $b_0^2\tau\tau_D$ is small. One may expect that magnetic field response is suppressed in this domain. What we demonstrate below is that this suppression is anomalously strong. Namely, the first term of the expansion of Eq. (2.46) with respect to $b_0^2\tau\tau_D$ does not contain the external field *at all*. This first term has the form

$$\bar{t} - 2\tau_D = -\frac{\tau\tau_D^2}{16}\left[\frac{(|\mathbf{\Omega}_1|^2 - |\mathbf{\Omega}_2|^2)^2}{|\mathbf{\Omega}_1 + \mathbf{\Omega}_2|^2} + \frac{4|\mathbf{\Omega}_1 \times \mathbf{\Omega}_2|^2}{|\mathbf{\Omega}_1 + \mathbf{\Omega}_2|^2}\right]. \tag{2.78}$$

To realize that B drops out of the expression in the square brackets it is convenient to first replace $|\mathbf{\Omega}_1 \times \mathbf{\Omega}_2|^2$ by $|\mathbf{\Omega}_1|^2|\mathbf{\Omega}_2|^2 - (\mathbf{\Omega}_1 \cdot \mathbf{\Omega}_2)^2$ and then use the identity

$$|\mathbf{\Omega}_1 + \mathbf{\Omega}_2|^2|\mathbf{\Omega}_1 - \mathbf{\Omega}_2|^2 = (|\mathbf{\Omega}_1|^2 + |\mathbf{\Omega}_2|^2)^2 - 4(\mathbf{\Omega}_1 \cdot \mathbf{\Omega}_2)^2. \tag{2.79}$$

This leads to a drastic simplification of Eq. (2.78), which assumes the form

$$\bar{t} - 2\tau_D = -\frac{\tau\tau_D^2}{16}|\mathbf{\Omega}_1 - \mathbf{\Omega}_2|^2. \tag{2.80}$$

Since $|\mathbf{\Omega}_1 - \mathbf{\Omega}_2| = |\boldsymbol{b}_e - \boldsymbol{b}_h|$, the magnetic field drops out of $\bar{t}$ in the first order in $\tau\tau_D b_0^2$.

2.6 Concluding remarks

- Our findings can be summarized in the form of domains on the plane $(b_0\tau_D, b_0\tau)$, as shown in Fig. 2.8. The fact that for small $b_0^2\tau\tau_D$ the OMAR response is absent is reflected in Fig. 2.8 by leaving the domain lying below the hyperbola uncolored. Large hyperfine fields, $b_0\tau > 1$, correspond to slow recombination. As we have demonstrated, the OMAR for $b_0\tau > 1$ can be dominated either by "typical" pairs or by "soft" pairs. The corresponding regions, I and II, are colored in Fig. 2.8 by pink and gray, respectively. The domains are separated by the curve $b_0\tau = (b_0\tau_D)^{1/3}$. Eq. (2.52) describes OMAR in domain I, while in domain II Eq. (2.68) applies. Note that in domain II only the part above the green line corresponds to slow recombination. The part below the green line corresponds to fast recombination, but Eq. (2.68) applies in both domains. The diagram describes the regimes of OMAR in low applied fields, $B \sim b_0$. As B increases above b_0, the gray domain shrinks.

- The OMAR response from the soft pairs relies exclusively on the asymmetry between the electron and hole. The evidence in favor of such an asymmetry was inferred in Ref. [28] from the analysis of magnetic-resonance data in organic devices. In Ref. [28], the ratio b_2/b_1 was estimated to be close to 3, which leads to the value of the asymmetry parameter $\eta \approx 0.9$. Note that bipolaron mechanism is insensitive to the asymmetry between electron and hole.

- The "parallel-antiparallel" mechanism of Ref. [15] yields the OMAR response on the level of rate equations with the transition rates calculated from the *golden rule*. The applicability of this treatment requires that the separation of Zeeman levels is large compared to their widths. On the other hand, the OMAR response based on soft pairs, studied in the present paper, comes entirely from pairs for which the Zeeman levels are almost aligned. This requires one to go beyond the golden rule. Previously, a similar situation was encountered in Ref. [25] by M. Schultz and F. von Oppen in the study of transport through a nanostructure with almost degenerate levels. The role of spin-selective recombination was played by coupling to the leads, which was strongly different for symmetric and antisymmetric combinations of the wave functions. Ref.

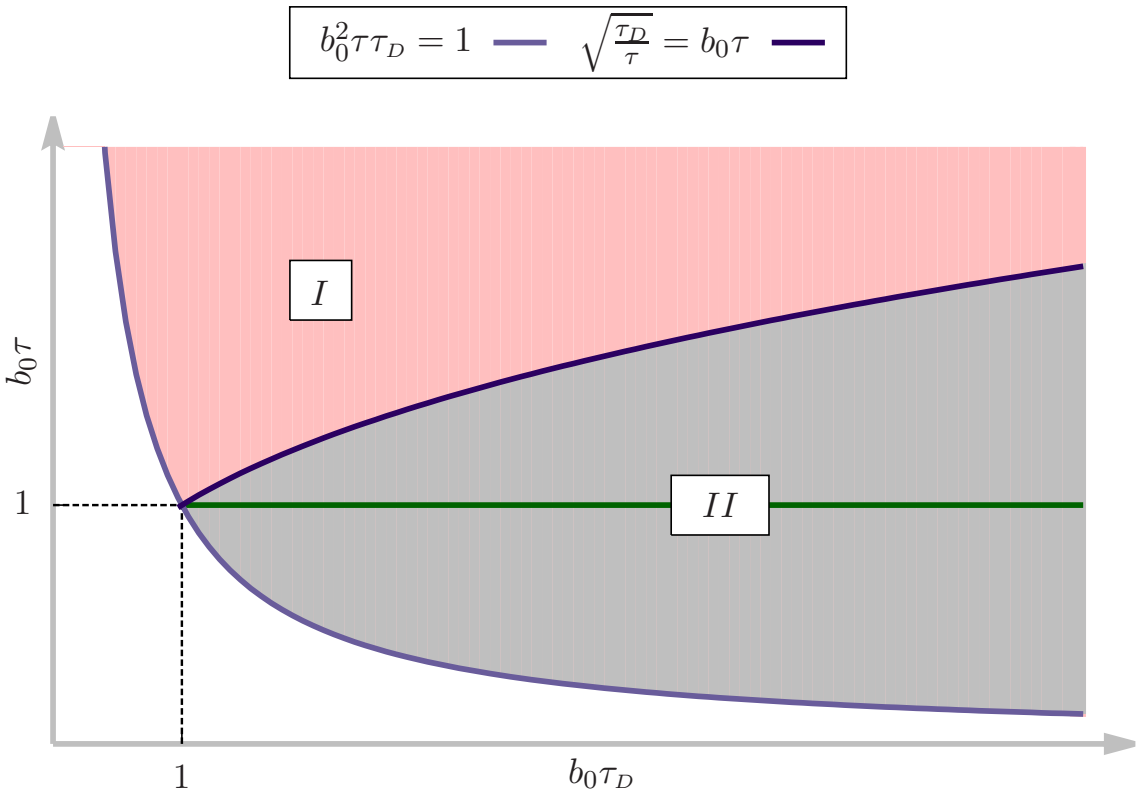

Figure 2.8: Different domains on the plane $(b_0\tau_D,\ b_0\tau)$ illustrate the regions where different OMAR mechanisms dominate. There is no OMAR in the white domain. The pink domain corresponds to slow recombination, and OMAR is given by Eq. (2.52). In both the upper and the lower parts of the gray domain the OMAR is dominated by soft pairs and is described by Eq. (2.68). The green line divides the gray domain into subregions where the recombination is slow (upper part) and fast (lower part). The boundaries of the domains are: $b_0\tau = \frac{1}{b_0\tau_D}$, and $b_0\tau = (b_0\tau_D)^{1/3}$.

[25] pointed out that when two levels are closer in energy than the width of each of them, then the conventional rate-equation-based description is insufficient.

On the physical level, the near-degeneracy implies that some spin configuration is preserved during many precession periods, i.e., the dynamics are important. To account for dynamics, it is intuitively appealing to take the result of Ref. [4], Eqs. (2.2)-(2.3), and multiply it by a factor describing exponential decay of population of states due to recombination. Such an approach was adopted in Ref. [22]. What this approach misses is the *feedback* of recombination on the pair dynamics. It is the central message of the present paper that this effect is strong in certain regimes, since feedback creates long-living modes.

- The "parallel-antiparallel" mechanism of Ref. [15] is based on the picture of incoherent hopping of one of the charge carriers on the site already occupied by the other carrier. We considered the transport model applicable for a bipolar system where the passage of current is due to recombination of electrons and holes. However, the principal ingredients of both models are the same: (a) in both transport models the spins of the carriers precess in their effective magnetic fields, the precession being governed by the same Hamiltonian Eq. (2.1); (b) the passage of current is the sequence of cycles, only one step of each cycle is sensitive to the spin precession; (c) whether it is a hop or recombination, it occurs only from the S-spin configuration; (d) if either the hop or recombination act takes too long, the carriers bypass each other.

- Both the "parallel-antiparallel" pairs and soft pairs create the OMAR response by blocking the current. The origin of this blocking is completely different for the two mechanisms. In the former, the current is blocked due to collinearity of full fields for the pair-partners, while for the latter the blocking is due to coincidence of their absolute values. In general, both contributions are present in the fast-recombination regime. The contribution of soft pairs in this regime dominates by virtue of their statistical weight.

- Another distinctive feature of the soft-pairs mechanism follows from Eq. (2.58). It contains a combination $(|\boldsymbol{\Omega}_1|^2 - |\boldsymbol{\Omega}_2|^2)^2$ in the denominator. As the precession frequencies change with external field, $\boldsymbol{B}$, the pair undergoes evolution from typical to soft (when $|\boldsymbol{\Omega}_1| = |\boldsymbol{\Omega}_2|$) and back to typical. Importantly, this evolution takes place within a narrow interval of $\boldsymbol{B}$, so that at a *given* $\boldsymbol{B}$ only certain sparse pairs

contribute to the current. As demonstrated in Ref. [29], this redistribution of soft pairs gives rise to *mesoscopic* features in $I(B)$ in small samples.

- We have demonstrated above that regardless of whether the OMAR is due to blocking caused by "parallel-antiparallel" configurations, as in Ref. [15], or due to soft pairs, the shape of the response is always close to $B^2/(B^2+B_c^2)$. This result was obtained under the assumption that τ and τ_D are *fixed*. If the values of τ and τ_D are broadly distributed, then the adequate description of transport should be based on the percolative approach [22]. However, within our minimal model, the current is the sum of partial currents through the chains, see Fig. 2.3. Then, with wide spread in cycle durations, $\bar{t}$, the current will be limited by pairs with longest $\bar{t}$ present in each chain.

- There is a certain similarity between OMAR and phonon-assisted electron transport between two spin-blockaded quantum dots, see e.g. Ref. [30]. In both systems the nuclear environment is responsible for the B-dependence of current. Spin-selective recombination, considered above, is similar to the inelastic transitions between dots. To describe the $I(B)$-dependence obtained experimentally [30], The authors of Ref. [31] developed a theory of transport via two quantum dots in the regime of spin blockade. They identified parallel-antiparallel and soft pairs as two distinguished hyperfine-field configurations most sensitive to a magnetic field. Comparison of our results with Ref. [31] is possible in the limit when inelastic interdot transitions are fast. For this limit Ref. [31] considered only parallel-antiparallel contribution to $I(B)$. For this contribution, our result of averaging over hyperfine-field configurations agrees qualitatively with Ref. [31]. Namely, we also find the flat-bottom behavior of $I(B)$.

- The flat-bottom behavior of the OMAR response for the parallel-antiparallel mechanism might manifest itself in an experiment in a very elegant way. Indeed, suppose that this mechanism is dominant, so that $I(B)-I(0)=A_1B^4$. It is natural to assume that the contribution of any other *weaker* mechanism behaves as A_2B^2, at small B. The cumulative effect of both mechanisms is thus, $I(B)-I(0)=A_1B^4+A_2B^2$. Note now, that if A_2 is negative the current response develops a minimum at *small* field, $B=A_2/2|A_1|$, which is much smaller than the hyperfine field. Hence, the appearance of such a minimum can be viewed as evidence of the delicate cancelation of the B^2 term in the parallel-antiparallel mechanism. In fact, such a minimum has been observed experimentally by at least two groups, see Fig. 2.9. An attempt to account for this ultra-small feature theoretically was reported in Ref. [33]. The idea of Ref. [33] is that

at really small magnetic fields the hyperfine-field-configurations for certain pairs will be *both* soft and parallel-antiparallel. Our estimates show that the statistical weight of such doubly-special configurations is too small to account for the experimental data.

2.7 Appendix: Time evolution and the Schrodinger equation

In this appendix we sketch a formal derivation of Eqs. (2.19) and (2.37) starting from the Liouville equation for the density operator, $\widehat{\sigma}$,

$$\frac{\partial\widehat{\sigma}}{\partial t} = -i[\widehat{\mathcal{H}},\widehat{\sigma}] + \widehat{L}(\widehat{\sigma}), \tag{2.81}$$

where the term $\widehat{L}(\widehat{\sigma})$ describes relaxation, which in our case is recombination from S to the ground state, G. The ground state with energy $-\mathcal{E}$ is included into the bare Hamiltonian

$$\widehat{\mathcal{H}} = \widehat{H} + \widehat{H}_G \tag{2.82}$$

$$= \left(\widehat{\boldsymbol{S}}_1\cdot\boldsymbol{B}_1 + \widehat{\boldsymbol{S}}_2\cdot\boldsymbol{B}_2\right) - \mathcal{E}\,|G\rangle\langle G|\,. \tag{2.83}$$

Then the operator $\widehat{L}(\widehat{\sigma})$ cast into conventional Lindblad form [34] reads

$$\widehat{L}(\widehat{\sigma}) = \frac{1}{2}\Gamma\left(2\,|G\rangle\langle S|\,\widehat{\sigma}\,|S\rangle\langle G| - \widehat{\sigma}\,|S\rangle\langle S| - |S\rangle\langle S|\,\widehat{\sigma}\right), \tag{2.84}$$

where $\frac{1}{2}\Gamma = \tau^{-1}$ is the inverse recombination time.

Denote with i, k different spin configurations of the pair prior to recombination. The form, Eq. (2.84), of the dissipation ensures independence of the elements of the density matrix with subindices i, k from the elements containing subindex G. This decoupling follows from the full system of the equations of motion

$$\frac{\partial\sigma_{GG}}{\partial t} = \Gamma\sigma_{SS}, \tag{2.85}$$

$$\frac{\partial\sigma_{Gk}}{\partial t} = -\mathcal{E}\sigma_{Gk} - \sum_i \sigma_{Gi}\mathcal{H}_{ik} - \frac{1}{2}\Gamma\sigma_{Gk}\delta_{Sk}, \tag{2.86}$$

$$\frac{\partial\sigma_{ik}}{\partial t} = -i[\widehat{\mathcal{H}},\widehat{\sigma}]_{ik} - \frac{1}{2}\Gamma\left\{\widehat{\sigma},|S\rangle\langle S|\right\}_{ik}. \tag{2.87}$$

Eq. (2.87) couples only the elements of 4×4 matrix, which we denote with ρ, so that Eq. (2.87) represents equation of motion for ρ. These equations can be rewritten in the form similar to Eq. (2.81)

$$\frac{\partial\widehat{\rho}}{\partial t} = -i[\widehat{H},\widehat{\rho}] + \widehat{L}(\widehat{\rho}), \tag{2.88}$$

with dissipation term redefined as $\widehat{L}(\widehat{\rho}) = -\frac{1}{2}\Gamma\left\{\widehat{\rho},|S\rangle\langle S|\right\}$. To derive Eq. (2.19), we search for solution of Eq. (2.88) in the form

$$\rho(t) = |\psi(t)\rangle\langle\psi(t)|\,, \tag{2.89}$$

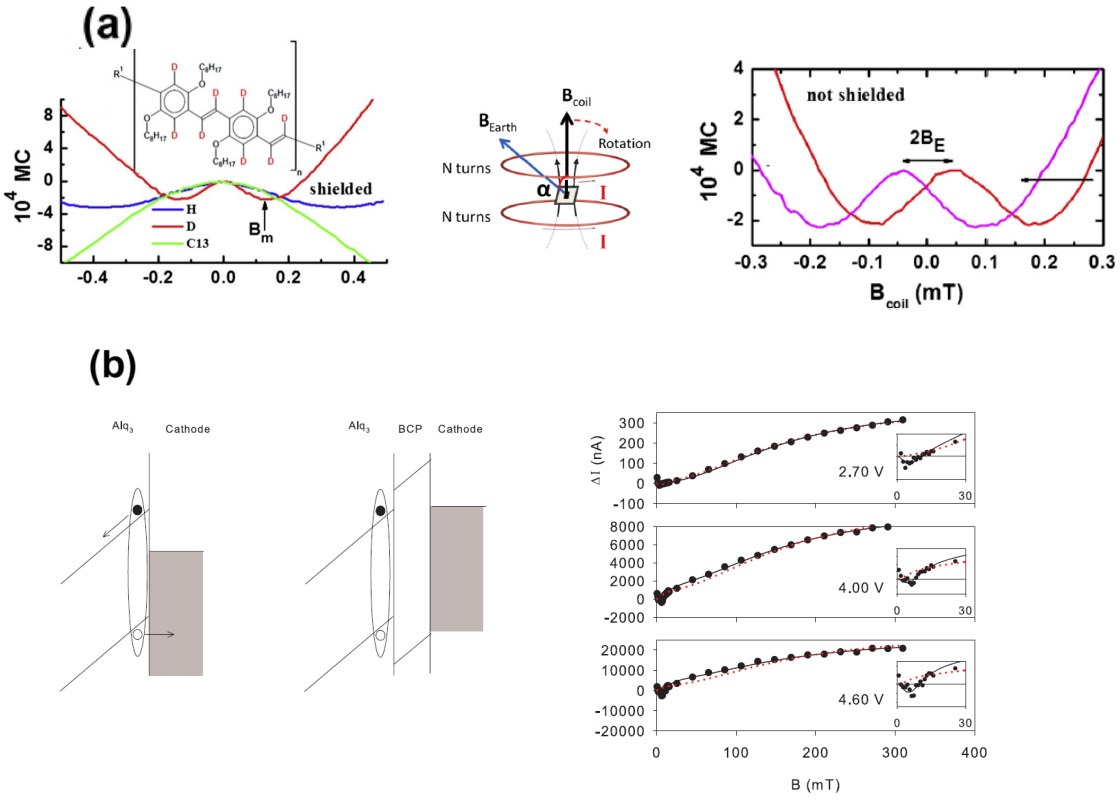

Figure 2.9: Experimental manifestation of the ultra-small field effect in (a) DOO-PPV (adapted from Ref. [32]) and in (b) Alq_3 (adapted from Ref. [9]). In (a) the feature develops at $B \sim 0.1$mT, which is of the order of the earths magnetic field; the position of minimum moves to the right with increasing hyperfine field, b_0. In (b) the feature develops at $B \sim 5$mT.

and find that $\psi(t)$ must satisfy the following nonhermitian Schrödinger equation

$$i\frac{\partial}{\partial t}\left|\psi(t)\right\rangle = \widehat{H}'\left|\psi(t)\right\rangle, \tag{2.90}$$

where $\widehat{H}'$ is defined as $\widehat{H}' = \widehat{H} - i\frac{\Gamma}{2}\left|S\right\rangle\left\langle S\right|$. The fact that decoupling Eq. (2.89) is valid follows from a straightforward calculation

$$\begin{aligned} i\frac{\partial}{\partial t}\left|\psi\right\rangle\left\langle\psi\right| &= \left(i\frac{\partial}{\partial t}\left|\psi\right\rangle\right)\left\langle\psi\right| + \left|\psi\right\rangle\left(i\frac{\partial}{\partial t}\left\langle\psi\right|\right) && (2.91)\\ &= H'\left|\psi\right\rangle\left\langle\psi\right| - \left|\psi\right\rangle\left\langle\psi\right|(H')^{\dagger} && (2.92)\\ &= \left(H - i\frac{\Gamma}{2}\left|S\right\rangle\left\langle S\right|\right)\left|\psi\right\rangle\left\langle\psi\right| - \left|\psi\right\rangle\left\langle\psi\right|\left(H + i\frac{\Gamma}{2}\left|S\right\rangle\left\langle S\right|\right) && (2.93)\\ &= \left[H, \left|\psi\right\rangle\left\langle\psi\right|\right] - i\frac{\Gamma}{2}\left\{\left|S\right\rangle\left\langle S\right|, \left|\psi\right\rangle\left\langle\psi\right|\right\}. && (2.94) \end{aligned}$$

Now Eq. (2.19) immediately emerges as an equation for eigenvalues of the operator $\widehat{H}'$.

2.8 Appendix: Derivation of Eq. (2.37)

To derive Eq. (2.37) for recombination time from *random* initial state, we first find the expression for recombination time, t_{ψ_0}, from a *given* initial state, ψ_0, in terms of the solution of Eq. (2.88) for $\rho(t)$ complemented with condition $\rho(0) = \left|\psi_0\right\rangle\left\langle\psi_0\right|$. The expression for t_{ψ_0} in terms of the full density matrix $\widehat{\sigma}(t)$ reads

$$t_{\psi_0} = \int_0^{\infty}\left(dt\,\frac{\partial\sigma_{GG}}{\partial t}\right)t. \tag{2.95}$$

The meaning of the expression in the brackets is the probability that recombination took place between t and $t + dt$. The expression for t_{ψ_0} in terms of $\rho(t)$ follows from the relation

$$\sigma_{GG} + \operatorname{Tr}\rho = 1. \tag{2.96}$$

Performing integration by parts, we obtain

$$t_{\psi_0} = \int_0^{\infty} dt\,\operatorname{Tr}\rho(t). \tag{2.97}$$

To find the recombination time $\langle t_R\rangle$ from the random initial state, the time t_{ψ_0} should be averaged over initial states. One way to perform this averaging is to fix a certain orthonormal basis, Φ_k, expand ψ_0 as

$$\psi_0 = \sum_k c_k\Phi_k, \tag{2.98}$$

and express t_{ψ_0} as bilinear form in c_k. This yields

$$t_{\psi_0} = \int_0^{\infty} dt\,\operatorname{Tr}\left[\widehat{U}(t)\psi_0^*\psi_0\widehat{U}^{\dagger}(t)\right] \tag{2.99}$$

$$= \int_0^\infty dt \,\mathrm{Tr}\left[\widehat{U}(t)\left[\sum_k c_k\Phi_k\right]\left[\sum_{k'} c_{k'}^*\Phi_{k'}^*\right]\widehat{U}^\dagger(t)\right] \tag{2.100}$$

$$= \sum_{k,k'} c_k c_{k'}^* \int_0^\infty dt \,\mathrm{Tr}\left[\widehat{U}(t)\Phi_k\Phi_{k'}^*\widehat{U}^\dagger(t)\right], \tag{2.101}$$

where $\widehat{U}(t)$ is the nonunitary evolution operator. Now the averaging over initial conditions reduces to averaging over c_k according to the rule $\langle c_k c_{k'}^*\rangle = \frac{1}{4}\delta_{k,k'}$. This averaging is straightforward leading to

$$\langle t_R\rangle = \frac{1}{4}\sum_k \int_0^\infty dt \,\mathrm{Tr}\left[\widehat{U}(t)\Phi_k\Phi_k^*\widehat{U}^\dagger(t)\right]. \tag{2.102}$$

The remaining task is to express the sum, Eq. (2.102), in terms of eigenvalues and eigenvectors of a nonhermitian Schrödinger equation, Eq. (2.90). To accomplish this task we will use the expansion of the solutions ψ_k of Eq. (2.90), which we, for brevity, denote with $|\lambda_k\rangle$, in terms of the orthonormal basis Φ_k, which we denote with $|k\rangle$.

In terms of these new notations, Eq. (2.90) and the time evolution operator can be written as

$$\widehat{H}'\,|\lambda_j\rangle = \lambda_j\,|\lambda_j\rangle\,, \quad \widehat{U}(t)\,|\lambda_j\rangle = e^{-i\lambda_j t}\,|\lambda_j\rangle\,. \tag{2.103}$$

It is also convenient to introduce a matrix, $\widehat{d}$, which relates the elements of the basis to the solutions of Eq. (2.90). Namely,

$$|k\rangle = \sum_l d_{kl}\,|\lambda_l\rangle\,. \tag{2.104}$$

Substituting Eq. (2.104) into Eq. (2.103), we find

$$\widehat{U}(t)\,|k\rangle = \sum_l d_{kl}\widehat{U}(t)\,|\lambda_l\rangle = \sum_l d_{kl}e^{-i\lambda_l t}\,|\lambda_l\rangle\,. \tag{2.105}$$

Next we introduce, $\widehat{g}$, which is the matrix of scalar products

$$g_{ij} = \langle\,\lambda_i|\,\lambda_j\rangle\,. \tag{2.106}$$

Using the definitions Eq. (2.104) and Eq. (2.106) we express $\langle t_R\rangle$, defined by Eq. (2.102), in terms of the matrices $\widehat{d}$ and $\widehat{g}$

$$\langle t_R\rangle = \frac{1}{4}\sum_k \int_0^\infty dt \,\mathrm{Tr}\left[\widehat{U}(t)\,|k\rangle\,\langle k|\,\widehat{U}^\dagger(t)\right], \tag{2.107}$$

$$= \frac{1}{4}\sum_k \int_0^\infty dt \,\mathrm{Tr}\left[\widehat{U}\left(\sum_l d_{kl}\,|\lambda_l\rangle\right)\times\left(\sum_m d_{km}^*\,\langle\lambda_m|\right)\widehat{U}^\dagger\right], \tag{2.108}$$

$$= \frac{1}{4}\sum_{klm}\int_0^\infty dt\, e^{-i(\lambda_l-\lambda_m^*)t} d_{kl}d_{km}^* \mathrm{Tr}\left[|\lambda_l\rangle\langle\lambda_m|\right], \tag{2.109}$$

$$= \frac{1}{4}\sum_{lm}\frac{1}{i(\lambda_l-\lambda_m^*)} g_{ml}\left(\sum_k d_{kl}d_{km}^*\right). \tag{2.110}$$

In the last identity we have isolated the combination of the elements of the matrix $\widehat{d}$. The reason is that this combination can be cast in the form

$$\sum_k d_{kl}d_{km}^* = g_{ml}^{-1*}. \tag{2.111}$$

To prove the latter identity, we start from the matrix relation

$$\langle\lambda_l|\, i\rangle = \sum_j d_{ij}\langle\lambda_l|\,\lambda_j\rangle = \sum_j d_{ij}g_{lj}, \tag{2.112}$$

and invert it to obtain

$$d_{ij} = \sum_l g_{jl}^{-1}\langle\lambda_l|\, i\rangle\,. \tag{2.113}$$

Next we complex conjugate both sides of Eq. (2.113) which yields

$$d_{ij}^* = \sum_l g_{jl}^{-1*}\langle\lambda_l|\, i\rangle^* = \sum_l g_{jl}^{-1*}\langle i|\,\lambda_l\rangle\,. \tag{2.114}$$

Now, the identity Eq. (2.111) emerges as a result of straight-forward calculation

$$\sum_k d_{kl}d_{km}^* = \sum_k\left(\sum_j g_{lj}^{-1}\langle\lambda_j|\, k\rangle\right)\left(\sum_n g_{mn}^{-1*}\langle k|\,\lambda_n\rangle\right), \tag{2.115}$$

$$= \sum_{jk} g_{lj}^{-1}g_{mn}^{-1*}\langle\lambda_j|\left(\sum_k |k\rangle\langle k|\right)|\lambda_n\rangle \tag{2.116}$$

$$= \sum_{jn} g_{lj}^{-1}g_{mn}^{-1*}g_{jn} \tag{2.117}$$

$$= g_{ml}^{-1*}. \tag{2.118}$$

Finally, substituting Eq. (2.111) into Eq. (2.110), we arrive at Eq. (2.37) of the main text.

2.9 Appendix: Derivation of Eq. (2.57)

In this appendix we demonstrate that, upon Gaussian averaging over the hyperfine fields, the B^2 correction to the current

$$\delta I(B) = \frac{\tau}{\tau_D^2}\left\langle\frac{1}{1+\frac{\tau}{\tau_D}-\left(\frac{\mathbf{\Omega}_1\cdot\mathbf{\Omega}_2}{|\mathbf{\Omega}_1||\mathbf{\Omega}_2|}\right)^2}\right\rangle \tag{2.119}$$

vanishes, while B^4 correction is captured by Eq. (2.57). With this in mind, we start with the general expansion of Eq. (2.119) up to the terms $\propto B^4$

$$\delta I(B) = \frac{\tau}{\tau_D^2 \pi^3} \int d^3\Omega_1 \int d^3\Omega_2 \left[\frac{\exp\left(-|\mathbf{\Omega}_1|^2 - |\mathbf{\Omega}_2|^2\right)}{1 + \frac{\tau}{\tau_D} - \left(\frac{\mathbf{\Omega}_1 \cdot \mathbf{\Omega}_2}{|\mathbf{\Omega}_1||\mathbf{\Omega}_2|}\right)^2} \right] \left(1 - 2B^2 + 2B^4\right) \times \left(1 + 2\left[(\mathbf{\Omega}_1 + \mathbf{\Omega}_2)\cdot \boldsymbol{B}\right]^2 + \frac{2^4}{4!}\left[(\mathbf{\Omega}_1 + \mathbf{\Omega}_2)\cdot \boldsymbol{B}\right]^4\right), \quad (2.120)$$

where for economy of notation we have set $b_0 = 1$. Obviously, the terms with odd powers of B average to zero, so Eq. (2.120) reduces to

$$\delta I(B) = \delta I^{(0)} + \delta I^{(2)} + \delta I^{(4)}. \quad (2.121)$$

The $B = 0$ term in Eq. (2.121) is easily evaluated, and in the limit $\tau_D \gg \tau$ reads

$$\delta I^{(0)} = \frac{\tau}{2\tau_D^2} \int_0^\pi d\theta \frac{\sin\theta}{1 + \frac{\tau}{\tau_D} - \cos^2\theta} \approx \frac{\tau}{2\tau_D^2} \ln\left(\frac{4\tau_D}{\tau}\right). \quad (2.122)$$

To trace the cancelation of the quadratic term, we cast it in the convenient form

$$\delta I^{(2)} = \frac{2\tau}{\tau_D^2 \pi^3} \int d^3\Omega_1 \int d^3\Omega_2 \frac{\exp\left(-|\mathbf{\Omega}_1|^2 - |\mathbf{\Omega}_2|^2\right)}{1 + \xi^2 - \cos^2\theta_{12}} \times \left((\mathbf{\Omega}_1 \cdot \boldsymbol{B})^2 + (\mathbf{\Omega}_2 \cdot \boldsymbol{B})^2 + 2(\mathbf{\Omega}_1 \cdot \boldsymbol{B})(\mathbf{\Omega}_2 \cdot \boldsymbol{B}) - |\boldsymbol{B}|^2\right), \quad (2.123)$$

where we have introduced the notation

$$\xi^2 = \frac{\tau}{\tau_D} \ll 1, \quad (2.124)$$

while θ_{12} denotes the angle between $\mathbf{\Omega}_1$ and $\mathbf{\Omega}_2$. Since the result cannot depend on orientation of $\boldsymbol{B}$, we average Eq. (2.123) over all possible orientations using the following identity

$$\frac{1}{4\pi} \iint \sin\theta \, d\theta d\phi \, (\boldsymbol{A} \cdot \boldsymbol{r})(\boldsymbol{C} \cdot \boldsymbol{r}) = \frac{1}{3} r^2 (\boldsymbol{A} \cdot \boldsymbol{C}). \quad (2.125)$$

Upon this averaging Eq. (2.123) assumes the form

$$\delta I^{(2)} = \frac{2\tau |\boldsymbol{B}|^2}{\tau_D^2 \pi^3} \int d^3\Omega_1 \int d^3\Omega_2 \frac{\exp(-|\mathbf{\Omega}_1|^2 - |\mathbf{\Omega}_2|^2)}{1 + \xi^2 - \cos^2\theta_{12}} \left(\frac{1}{3}|\mathbf{\Omega}_1|^2 + \frac{1}{3}|\mathbf{\Omega}_2|^2 + \frac{2}{3}\mathbf{\Omega}_1 \cdot \mathbf{\Omega}_2 - 1\right). \quad (2.126)$$

The product $\mathbf{\Omega}_1 \cdot \mathbf{\Omega}_2$ is odd, and thus drops out. The remaining double integral reads

$$\delta I^{(2)} = \frac{2|\boldsymbol{B}|^2 \tau}{3\tau_D^2 \pi^3} \int d^3\Omega_1 \int d^3\Omega_2 \frac{(2|\mathbf{\Omega}_2|^2 - 3) e^{-(|\mathbf{\Omega}_1|^2 + |\mathbf{\Omega}_2|^2)}}{1 + \xi^2 - \cos^2\theta_{12}}. \quad (2.127)$$

Now the cancelation of $\delta I^{(2)}$ directly follows from the relation

$$\int_0^\infty \Omega_2^2 \, d\Omega_2 \left[2\,\Omega_2^2 - 3\right] e^{-\Omega_2^2} = 0. \quad (2.128)$$

The fourth order correction, $\delta I^{(4)}$, contains three contributions

$$\delta I^{(4)} = \frac{\tau}{\tau_D^2 \pi^3} \int d^3\Omega_1 \int d^3\Omega_2 \frac{e^{-\left(|\mathbf{\Omega}_1|^2+|\mathbf{\Omega}_2|^2\right)}}{1+\xi^2-\cos^2\theta_{12}} \times \left\{ 2|\boldsymbol{B}|^4 - 4|\boldsymbol{B}|^2 \left[(\mathbf{\Omega}_1+\mathbf{\Omega}_2)\cdot\boldsymbol{B}\right]^2 + \frac{2^4}{4!}\left[(\mathbf{\Omega}_1+\mathbf{\Omega}_2)\cdot\boldsymbol{B}\right]^4 \right\}. \quad (2.129)$$

The averaging of the first two contributions involves the same steps as in averaging of $\delta I^{(2)}$, yielding

$$-2|\boldsymbol{B}|^4 \delta I^{(0)}. \quad (2.130)$$

Averaging of the third contribution over orientations of $\boldsymbol{B}$ is now performed with the help of the following identity

$$\frac{1}{4\pi} \iint \sin\theta \, d\theta d\phi \, (\boldsymbol{A}\cdot\boldsymbol{r})^2 (\boldsymbol{C}\cdot\boldsymbol{r})^2 = \frac{r^4}{15}\left(|\boldsymbol{A}|^2|\boldsymbol{C}|^2 + 2(\boldsymbol{A}\cdot\boldsymbol{C})^2\right). \quad (2.131)$$

Then the third contribution acquires the form

$$\sim \frac{|\boldsymbol{B}|^4}{5} \int d^3\Omega_1 \int d^3\Omega_2 \frac{e^{-\left(|\mathbf{\Omega}_1|^2+|\mathbf{\Omega}_2|^2\right)}}{1+\xi^2-\cos^2\theta_{12}} \left[\left(|\mathbf{\Omega}_1|^2+|\mathbf{\Omega}_2|^2\right)^2 + 4(\mathbf{\Omega}_1\cdot\mathbf{\Omega}_2)^2\right]. \quad (2.132)$$

There are four terms in the square brackets of Eq. (2.132). The terms $|\mathbf{\Omega}_1|^4$ and $|\mathbf{\Omega}_2|^4$ give equal contributions, which is evaluated without involving the denominator of Eq. (2.132). The contribution from the term $|\mathbf{\Omega}_1|^2|\mathbf{\Omega}_2|^2$ also does not involve the denominator and can be expressed via $\delta I^{(0)}$. The only term where $\cos\theta_{12}$ in the denominator is important is the term with $(\mathbf{\Omega}_1\cdot\mathbf{\Omega}_2)^2$. The corresponding integration is elementary. Combining Eq. (2.130) and Eq. (2.132) reproduces Eq. (2.57) of the main text.

2.10 References

[1] E. L. Frankevich, I. A. Sokolik, D. I. Kadyrov, and V. M. Kobryanskii, Pis'ma Zh. Eksp. Teor. Fiz. **36**, 401 (1982) [JETP Lett. **36**, 488 (1982)].

[2] E. L. Frankevich, A. A. Lymarev, I. Sokolik, F. E. Karasz, S. Blumstengel, R. H. Baughman, and H. H. Hörhold, Phys. Rev. B **46**, 9320 (1992).

[3] K. M. Salikhov, Y. N. Molin, R. Z. Sagdeev, and A. L. Buchachenko, in *Spin Polarization and Magnetic Effects in Radical Reactions*, edited by Y. N. Molin (Elsevier, Amsterdam, 1984), pp. 32-116, and the review U. E. Steiner and T. Ulrich, Chem. Rev. **89**, 51 (1989).

[4] K. Schulten and P. G. Wolynes, J. Chem. Phys. **68**, 3292 (1978).

[5] T. L. Francis, Ö. Mermer, G. Veeraraghavan, and M. Wohlgenannt, New J. Phys. **6**, 185 (2004).

[6] Ö. Mermer, G. Veeraraghavan, T. L. Francis, Y. Sheng, D. T. Nguyen, M. Wohlgenannt, A. Khler, M. K. Al-Suti, and M. S. Khan, Phys. Rev. B **72**, 205202 (2005).

[7] Y. Sheng, T. D. Nguyen, G. Veeraraghavan, O. Mermer, M. Wohlgenannt, S. Qiu, and U. Scherf, Phys. Rev. B **74**, 045213 (2006).

[8] F. Wang, F. Maciá, M. Wohlgenannt, A. D. Kent, and M. E. Flatté, Phys. Rev. X **2**, 021013 (2012).

[9] P. Desai, P. Shakya, T. Kreouzis, and W. P. Gillin, Phys. Rev. B **76**, 235202 (2007); Sijie Zhang, N. J. Rolfe, P. Desai, P. Shakya, A. J. Drew, T. Kreouzis, and W. P. Gillin, Phys. Rev. B **86**, 075206 (2012).

[10] F. J. Wang, H. Bässler, and Z. Valy Vardeny, Phys. Rev. Lett. **101**, 236805 (2008).

[11] T. D. Nguyen, G. Hukic-Markosian, F. Wang, L. Wojcik, X.-G. Li, E. Ehrenfreund, and Z. V. Vardeny, Nat. Mater. **9**, 345 (2010).

[12] T. D. Nguyen, B. R. Gautam, E. Ehrenfreund, and Z. V. Vardeny, Phys. Rev. Lett. **105**, 166804 (2010).

[13] Tho D. Nguyen, T. P. Basel, Y.-J. Pu, X-G. Li, E. Ehrenfreund, and Z. V. Vardeny, Phys. Rev. B **85**, 245437 (2012).

[14] F. L. Bloom, W. Wagemans, M. Kemerink, and B. Koopmans, Phys. Rev. Lett. **99**, 257201 (2007).

[15] P. A. Bobbert, T. D. Nguyen, F. W. A. van Oost, B. Koopmans, and M. Wohlgenannt, Phys. Rev. Lett. **99**, 216801 (2007).

[16] W. Wagemans, F. L. Bloom, P. A. Bobbert, M. Wohlgenannt, and B. Koopmans, J. Appl. Phys. **103**, 07F303 (2008).

[17] F. L. Bloom, M. Kemerink, W. Wagemans, and B. Koopmans, Phys. Rev. Lett. **103**, 066601 (2009).

[18] S. P. Kersten, A. J. Schellekens, B. Koopmans, and P. A. Bobbert, Phys. Rev. Lett. **106**, 197402 (2011).

[19] W. Wagemans, A. J. Schellekens, M. Kemper, F. L. Bloom, P. A. Bobbert, and B. Koopmans Phys. Rev. Lett. **106**, 196802 (2011).

[20] W. Wagemans and B. Koopmans, Phys. Status Solidi B **248**, 1029 (2011).

[21] V. N. Prigodin, J. D. Bergeson, D. M. Lincoln, and A. J. Epstein, Synth. Met. **156**, 757 (2006).

[22] N. J. Harmon and M. E. Flatté, Phys. Rev. Lett. **108**, 186602 (2012); Phys. Rev. B **85**, 075204 (2012); Rev. B **85**, 245213 (2012).

[23] R. H. Dicke, Phys. Rev. **93**, 99 (1954).

[24] T. V. Shahbazyan and M. E. Raikh, Phys. Rev. B **49**, 17123 (1994).

[25] M. G. Schultz and F. von Oppen, Phys. Rev. B **80**, 033302 (2009).

[26] J. König, Y. Gefen, and G. Schön, Phys. Rev. Lett. **81**, 4468 (1998).

[27] A. J. Schellekens, W. Wagemans, S. P. Kersten, P. A. Bobbert, and B. Koopmans, Phys. Rev. B **84**, 075204 (2011).

[28] D. R. McCamey, K. J. van Schooten, W. J. Baker, S.-Y. Lee, S.-Y. Paik, J. M. Lupton, and C. Boehme, Phys. Rev. Lett. **104**, 017601 (2010); S.-Y. Lee, S.-Y. Paik, D. R. McCamey, J. Yu, P. L. Burn, J. M. Lupton, and C. Boehme, J. Am. Chem. Soc. **133**, 072019 (2011).

[29] R. C. Roundy, Z. V. Vardeny, M. E. Raikh, e-print arXiv:1210.3443v1 (2012).

[30] F. H. L. Koppens, J. A. Folk, J. M. Elzerman, R. Hanson, L. H. Willems van Beveren, I. T. Vink, H. P. Tranitz, W. Wegscheider, L. P. Kouwenhoven, and L. M. K. Vandersypen, Science **309**, 1346 (2005).

[31] O. N. Jouravlev and Y. V. Nazarov, Phys. Rev. Lett. **96**, 176804 (2006).

[32] T. D. Nguyen, E. Ehrenfreund, Z. V. Vardeny, Organic Electronics **14**, 1852 (2013).

[33] J. Danon, X. Wang, and A. Manchon, Phys. Rev. Lett. **111**, 066802 (2013).

[34] G. Lindblad, Commun. Math. Phys. **48**, 119 (1976).

CHAPTER 3

ORGANIC MAGNETORESISTANCE NEAR SATURATION: MESOSCOPIC EFFECTS IN SMALL DEVICES

3.1 Introduction

In the field of "Dynamic Spin Chemistry," a mechanism by which the recombination rate of radical pairs is sensitive to a weak magnetic field, $\boldsymbol{B}$, was established more than four decades ago; see, e.g., the reviews in Ref. [1]. This mechanism relies on the hyperfine interaction of the spin-1/2 pair partners with their respective nuclear spin environments, where the hyperfine field, $\boldsymbol{b}_h$ generated by the nuclei is responsible for the radical spins' dynamics in zero field. In this process, if at time $t = 0$ the radical pair spin state is in a singlet configuration, S, then at finite t it will acquire a triplet (T) component with probability, $P_{ST}(t)$. If recombination is allowed only from S, then $P_{ST}(t)$ dynamic evolution affects the recombination rate. Clearly, $P_{ST}(t)$ depends on $\boldsymbol{B}$ and this sets a small scale, $|\boldsymbol{B}| \sim |\boldsymbol{b}_h|$ that may influence the radical pair recombination rate.

An important advance in the quantitative description of $P_{ST}(t)$ was made by Ref. [2]. They noticed that, due to the large number of nuclei surrounding each radical pair, and slow dynamics of the hyperfine field, the $\boldsymbol{b}_h$ random distribution may be modeled by a Gaussian. Under these conditions the multiplicity of the nuclear spin configurations may be characterized by a single number – namely the width of this distribution, b_0.

The dependence of $P_{ST}(t)$ on $\boldsymbol{B}$ is at the core of organic magnetoresistance (OMAR), which has recently attracted a lot of attention [3, 4, 5, 6, 7, 8, 9, 10, 11, 12, 13, 14, 15, 16, 17, 18]. This is because the current, I, in a biased organic diode involves recombination of the injected e-h polarons (forming polaron pairs, PP); whereas the processes of populating and depopulating of traps are not sensitive to spin dynamics.

The theory of OMAR is conceptually harder than that of spin-magneto-chemistry [1] for two reasons. Firstly, in OMAR the complex dynamics of all four PP spin states, S, T_0, T_+, and T_- needs be incorporated into the calculation of the dc current that is influenced by the

PP. Secondly, each PP is sensitive to the other PPs if they belong to the same current path. Finally, averaging over the nuclear environment should be carried out only at the last step. To bypass these complications several simplifying assumptions concerning both the spin dynamics and current passage scenario were adopted in previous theoretical calculations of the $I(B)$ response [6, 12, 13, 14, 15, 16, 17, 18].

In contrast, in the present paper we do not focus on the entire $I(B)$ response, but rather on the strong B domain, where the OMAR response is close to saturation, see Fig. 3.1.

Our motivation is twofold. Firstly, theory allows a dramatic simplification in this B-domain, since the spin dynamics that are relevant to OMAR involves only the PP S and T_0 states. However, even in this B-domain the OMAR underlying physics is not trivial if the hyperfine field is sufficiently strong; namely when $b_0\tau \gg 1$, which corresponds to the regime of "slow" hopping [16, 18]. Here, τ is a characteristic recombination time, and b_0 is measured in frequency units. Experimentally [13], in organic semiconductors b_0 is $\sim 1\,\mathrm{mT}$, whereas $\tau \sim 1 - 10\,\mu\mathrm{s}$, so that this parameter is $\sim 10^3$. We show that at large $b_0\tau$ the spin dynamics are not "frozen" as B exceeds b_0, but persists in a parametrically broad interval, $b_0^2\tau \gg B \gg b_0$. Our second and central motivation for considering strong fields is that we predict the occurrence of *mesoscopic* properties in this B-domain that would form in small devices that are based on strongly disordered organic active layers. Specifically we predict *reproducible* random fluctuations in the $I(B)$ response upon sweeping B (see Fig. 3.1), which reflect the "individuality" [19, 20, 21] of the nuclear environments associated with the relevant recombination centers in the organic.

More quantitatively, if the number, N, of current paths that contribute to $I(B)$ is finite, then the statistical averaging over $\boldsymbol{b}_h$ is incomplete. The relative fluctuation $\frac{\delta I(B)}{\langle I \rangle} \sim N^{-1/2}$, while small, can still be experimentally obtained because of the high accuracy with which current can be measured. In the field of "dynamic spin chemistry," mesoscopic fluctuations cannot occur since the number of radical pairs that contribute to the observable characteristics is huge.

Obviously, the necessary condition to observe mesoscopic fluctuations in the $I(B)$ response of organic devices is slow nuclear spin dynamics, which should allow one to obtain $I(B)$ before the nuclear configuration changes. This is realistic, since the characteristic time for current passage is a PP recombination time, which for organic devices is 50μs, see Ref. [22]. It is generally accepted [2, 23] that the time for the change of the nuclear-spin configuration is orders of magnitude longer, although no accurate measurements of proton spin-spin relaxation time for organic devices have yet been reported in the literature.

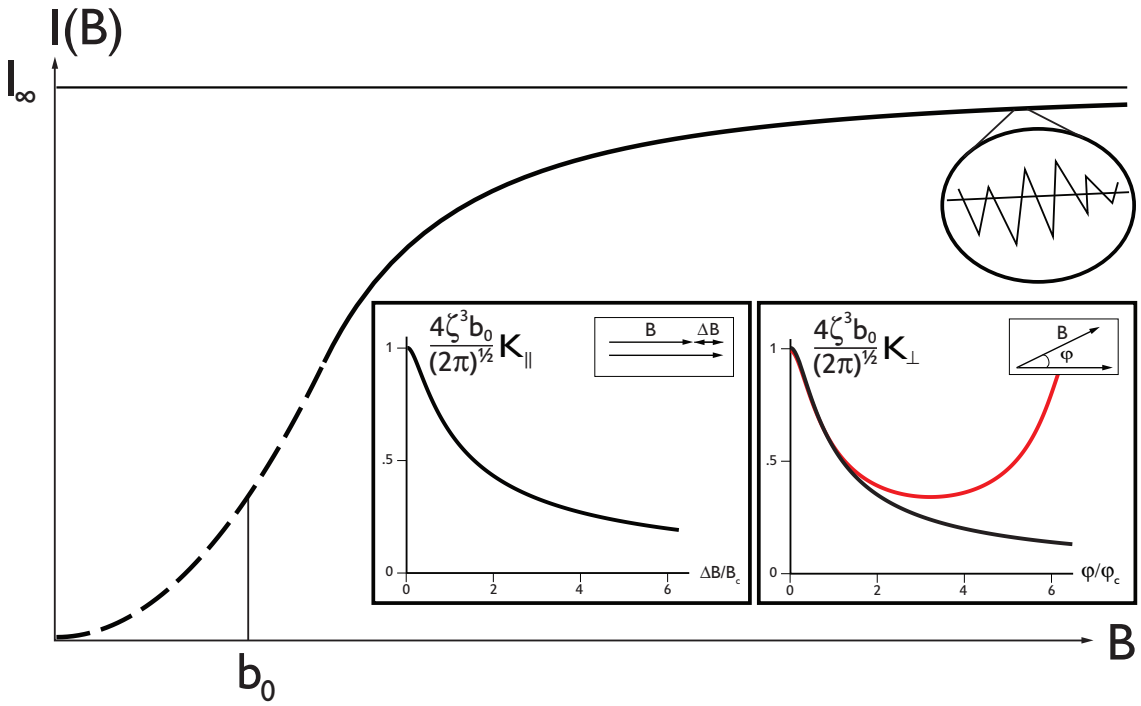

Figure 3.1: The dependence $I(B)$ of the device current on the applied magnetic field is shown schematically in the strong-field limit $B \gg b_0$. Enlargement illustrates mesoscopic fluctuations emerging in a small sample. Two insets are the correlators of the mesoscopic fluctuations for $\triangle \boldsymbol{B} \parallel \boldsymbol{B}$ and $\triangle \boldsymbol{B} \perp \boldsymbol{B}$ plotted from Eqs. (3.13) and (3.15), respectively .

3.2 PP dynamics in strong fields

3.2.1 Isolated PP

We start with a detailed account of the PP spin dynamics and recombination in the strong B-domain, which we then use to calculate mesoscopic contribution to $I(B)$ near saturation. For an isolated PP the spin Hamiltonian $\widehat{H} = \boldsymbol{\Omega}_1 \cdot \widehat{\boldsymbol{S}}_1 + \boldsymbol{\Omega}_2 \cdot \widehat{\boldsymbol{S}}_2$ describes the precession of the PP spins $\boldsymbol{S}_1$, $\boldsymbol{S}_2$ in the fields $\boldsymbol{\Omega}_1 = \boldsymbol{B} + \boldsymbol{b}_1$ and $\boldsymbol{\Omega}_2 = \boldsymbol{B} + \boldsymbol{b}_2$, respectively. If at $t = 0$ the PP is in the singlet state, then the probability, $P_{SS}(t)$, to find it in the singlet state at finite time later oscillates. $P_{SS}(t)$ oscillations contain two frequencies: $\Delta = |\boldsymbol{\Omega}_1| - |\boldsymbol{\Omega}_2|$ and $\Sigma = |\boldsymbol{\Omega}_1| + |\boldsymbol{\Omega}_2|$. The advantage in considering the strong-field limit is that since $|\boldsymbol{\Omega}_1| \approx |\boldsymbol{\Omega}_2|$, the frequencies Δ and Σ are very different from each other, so that the spin dynamics decouples into distinct "slow" and "fast" modes. Moreover, the slow mode involves predominantly S and T_0 states, while the admixture of T_+ and T_- states to this mode is relatively weak (of the order of b_0^2/B^2). The fast mode Σ has frequency $\approx 2B$ and describes the oscillations between S and T_+, T_-. However, the admixture of S to this mode is also suppressed as b_0^2/B^2 in the strong-field limit. We thus conclude that, with accuracy b_0^2/B^2, $P_{SS}(t)$ dynamics simplifies in the strong-field limit to $P_{SS}(t) = \cos^2 \Delta t$; namely the "beating" between S and T_0 states. Similarly, if in the strong-field limit the PP is initially in the T_0 state then the probability to find it in the S state at time t is $\sin^2 \Delta t$.

3.2.2 Recombination in the presence of $S - T_0$ beating

We now assume that the PP is still isolated from the "leads," but can recombine from S to the ground state, G. A crucial question for OMAR is: What are the waiting times $\langle t \rangle_S$, $\langle t \rangle_{T_0}$ for the recombination, if the system is initially in S and T_0, respectively. The simplified spin dynamics in the strong-field limit allows us to address this question analytically.

Upon restricting the basis to S, T_0 and the ground state, we have nine relevant elements of the density matrix for solving the Liouville-Lindblad equations of motion: $\dot{\rho} = -i[\hat{H}, \rho] + \hat{L}(\rho)$, where the operator $\hat{L}(\rho)$ describes the recombination. To find $\langle t \rangle_S$, the system should be solved with the initial conditions $\rho(0) = |S\rangle \langle S|$. Subsequently, $\langle t \rangle_S$ is found from the formula

$$\langle t \rangle_S = \int_0^\infty dt \; t \; \frac{\partial \rho_{GG}}{\partial t} = \int_0^\infty dt \left(\rho_{SS}(t) + \rho_{T_0 T_0}(t) \right). \tag{3.1}$$

Similarly $\langle t \rangle_{T_0}$ is obtained from Eq. (3.1) upon solving the equations of motion with initial conditions $\rho(0) = |T_0\rangle \langle T_0|$. These calculations yield

$$\langle t \rangle_S = \tau, \qquad \langle t \rangle_{T_0} = \tau + \frac{1}{2\tau\Delta^2}. \tag{3.2}$$

For a typical PP we have $\Delta = |\mathbf{\Omega}_1| - |\mathbf{\Omega}_2| \sim b_0$. Eq. (3.2) suggests that $\langle t \rangle_S \approx \langle t \rangle_{T_0} \approx \tau$. This is a natural result since recombination is preceded by many beatings between S and T_0 states; therefore, the recombination time does not depend on the initial PP state. The most striking consequence of Eq. (3.2) is that for *sparse* PP for which Δ is accidentally smaller than τ^{-1}, we have $\langle t \rangle_S \ll \langle t \rangle_{T_0} \approx \frac{1}{2\Delta^2\tau}$. This suggests that the smaller is Δ, the longer the pair stays "trapped" in T_0. Note that in the course of beating *without possibility of recombination*, such PP would cross from T_0 to S after a much shorter time $\Delta^{-1} \ll \langle t \rangle_{T_0}$. We can trace the origin of the "trapping" described by Eq. (3.2) to the complex eigenmodes of the system that consist of singlet and triplet components being mixed by the hyperfine field. This system may be described by the 2×2 non-hermitian matrix:

$$\begin{array}{cc} |S\rangle & |T\rangle \\ \begin{pmatrix} -i/\tau & \Delta \\ \Delta & 0 \end{pmatrix} & \end{array}, \tag{3.3}$$

where the nondiagonal elements describe the mixing, while $-i/\tau$ describes recombination from S to G. The eigenvalues of this matrix are

$$\lambda_{1,2} = -\frac{i}{2\tau} \pm \sqrt{\Delta^2 - \frac{1}{4\tau^2}}. \tag{3.4}$$

In the limit $\Delta \ll \tau^{-1}$ we have $\lambda_1 \approx -\frac{i}{\tau}$, while $\lambda_2 \approx i\tau\Delta^2$. We see that λ_2 is anomalously small, and the result of Eq. (3.2) for $\Delta \ll \tau^{-1}$ can be interpreted as $\langle t \rangle_{T_0} \sim \frac{1}{\lambda_2}$. We note in passing that the emergence of slow mode, λ_2, in a compound system with anomalously close levels was previously found in Refs. [24, 25, 26] in connection with resonant tunneling through pairs of localized states.

Eqs. (3.3) and (3.4) provide a semiqualitative derivation of our main result from Eq. (3.2). A detailed derivation which justifies the above procedure is presented in Ref. [27] for the case of arbitrary external field. In particular, this paper deals with a delicate fact that the eigenvectors of non-hermitian matrix Eq. (3.3) are not orthogonal to each other.

In the remainder of the paper we demonstrate that it is the sparse pairs with $\Delta \lesssim \tau^{-1}$ that are responsible for the mesoscopic part of the $I(B)$ response in the strong-field limit.

3.3 Transport model

We assume that the organic active layer in the device is strongly inhomogeneous and its width, W, is much larger than the distance, L, between the electrodes, see Fig. 3.2.

Under these conditions the minimal description of transport is to model the sample as $N \gg 1$ parallel conducting channels. Moreover, due to the film inhomogeneity, the current

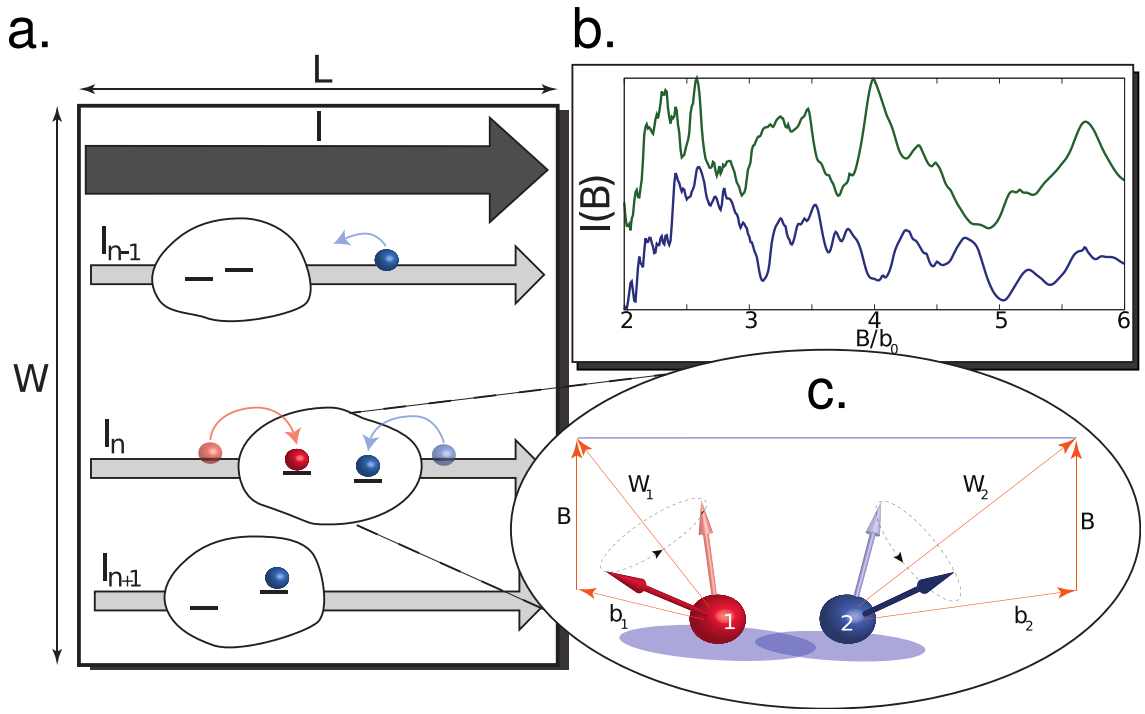

Figure 3.2: In a strongly inhomogeneous device with $W \gg L$ the current passage is dominated by the most conductive channels, $I = \sum_n I_n$. Each current component is limited by the most resistive junction, illustrated schematically (a). The current through this junction is sensitive to the spin dynamics of the constituting PP. "Slow" pairs, shown in the enlargement (c), are those in which the z-projections of their hyperfine fields coincide accidentally. The inset (b) shows $\sum_{n=1}^{N} I_n$ calculated for two realizations of $N = 10^4$ random hyperfine fields with rms $b_0 = 10^2\zeta^{-1}$.

through each channel is limited by a single, *most resistive* junction. The stronger is the inhomogeneity, the more realistic is the proposed model, see the review, Ref. [20]. The net current through the sample is the sum, $I = \sum_{n=1}^{N} I_n$, of the currents in each channel. Each junction, n, can be viewed as a pair of sites coupled to the nuclei environment. In the course of the current I_n through the junction, the pair of sites first gets occupied, is then emptied, and so on. In other words, the current passage can be viewed as a sequence of *cycles*, see Fig. 3.3. Each cycle consists of two steps, namely *assembly* of a pair on neighboring sites and disappearance of the pair through either dissociation or recombination, see Fig. 3.3. At this point we emphasize that it is the recombination stages of the cycles II and III (defined in Fig. 3.3) that are described by Eq. (3.2), and are thus sensitive to B.

The simplified transport model described in Fig. 3.2 encodes the same picture of transport put forward in Ref. [13]. It contains recombination and bypassing, if recombination takes too long. From Fig. 3.3 we may write the average duration $\langle t_n \rangle$ of the cycle as follows

$$\langle t_n \rangle = 2 \times \frac{1}{4}(2\tau_D) + \frac{1}{4}(\langle t \rangle_S + \tau_D) + \frac{1}{4}(\langle t \rangle_{T_0} + \tau_D). \tag{3.5}$$

The first term in Eq. (3.5) originates from the variants I and IV of the current cycle when the pair is assembled, and subsequently disassembled in T_+ and T_- states, respectively. Then the cycle lasts for time $2\tau_D$. The last two terms in Eq. (3.5) describe the current cycle variants II and III, in which the pair is assembled in either S or T_0. Eq. (3.5) takes into account that realization of each current cycle has equal probability of $\frac{1}{4}$. For simplicity we assume that processes involving leads, namely, assembly and dissociation, take equal time, τ_D. The current through the junction, which is the inverse cycle duration, can be then cast in the form

$$I_n = \frac{1}{\langle t_n \rangle} = 8\zeta^2\tau - \delta I_n(\boldsymbol{B}), \quad \delta I_n(\boldsymbol{B}) = \frac{8\zeta^4\tau}{\Delta_n(\boldsymbol{B})^2 + \zeta^2}, \tag{3.6}$$

where we used Eq. (3.2) and introduced the characteristic frequency

$$\zeta = \frac{1}{2\big[\tau(3\tau_D + \tau)\big]^{1/2}}. \tag{3.7}$$

We emphasize that the correction, $\delta I_n(\boldsymbol{B})$, in Eq. (3.6) originates from $S - T_0$ beating. For a *typical* nuclear environment we have $\Delta_n \sim b_0$, so that the relative magnitude of this correction is $\sim \frac{\zeta^2}{b_0^2} \ll 1$. However, *on average*, this term is much bigger, since it is dominated by sparse configurations with anomalously small $\Delta_n \sim \zeta$. This is because, while the portion of these sparse configurations is small, $\sim \zeta/b_0$, the δI_n value for these configurations exceeds the typical δI_n by a large factor $\frac{b_0}{\zeta}$. It can be demonstrated through a careful analysis [27]

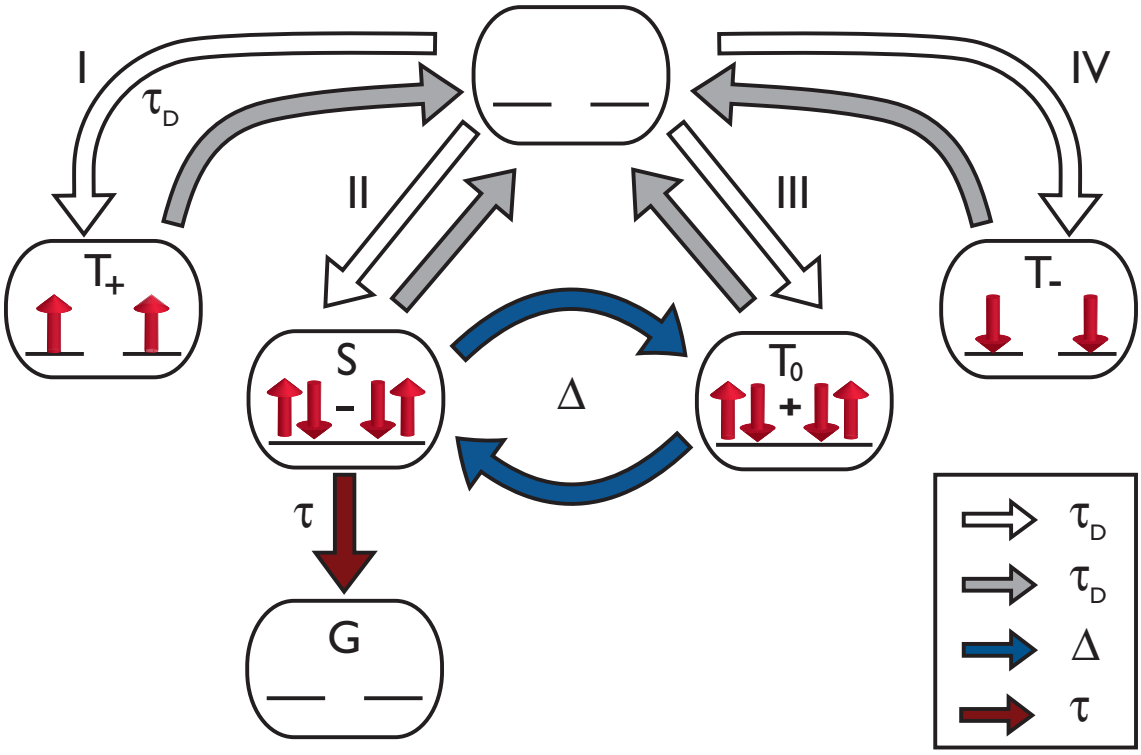

Figure 3.3: Schematic representation of the PP population dynamics in the strong-field domain. For variants of cycle I (IV) the pair is assembled and, subsequently, disassembled in T_+ (T_-) state. For variants II (III) the pair is assembled in S (T_0) state in which it undergoes slow dynamics prior to disassembly. In the course of the slow dynamics the pair can recombine; recombination is possible *only* from S. Since the transport is *unidirectional*, current is passed through a junction upon completion of each cycle variant.

that the correction $\delta I_n(\boldsymbol{B})$ is insensitive to $\boldsymbol{B}$ *on average*. The number of "slow" pairs decreases with B. It was established in Ref. [27] that the PP recombination time also decreases with B in such a way that the two tendencies compensate each other identically. In spite of this, it is the correction, Eq. (3.6), that gives rise to the mesoscopic fluctuations of current to which we now turn.

3.4 Mesoscopic fluctuations

If a *given* pair contributes to the correction $\delta I_n(\boldsymbol{B})$ in Eq. (3.6), then the $S-T_0$ splitting, $\Delta_n(\boldsymbol{B})$ for this pair is $\sim\zeta$. This suggests that, upon changing $\boldsymbol{B}$ by a small $\triangle\boldsymbol{B}$, the condition $\Delta_n(\boldsymbol{B})\sim\zeta$ for *this* pair is violated, while it becomes satisfied for *different* pairs. Such "switching" of pairs contributing to the correction, $\delta I(\boldsymbol{B})$ gives rise to the mesoscopic fluctuations of the current, which we may quantify by the correlator

$$K(\boldsymbol{B},\triangle\boldsymbol{B})=\left\langle \delta I(\boldsymbol{B}-\frac{\triangle\boldsymbol{B}}{2})\delta I(\boldsymbol{B}+\frac{\triangle\boldsymbol{B}}{2})\right\rangle-\langle\delta I(\boldsymbol{B})\rangle^2. \tag{3.8}$$

We consider two cases. In the first case, $\triangle\boldsymbol{B}\parallel\boldsymbol{B}$, the two magnetic fields are collinear. In the second case, $\triangle\boldsymbol{B}\perp\boldsymbol{B}$, the two magnetic fields have the same magnitude but are rotated through an angle φ with respect to each other.

For calculating the correlator in Eq. (3.8) we recast the factor $(\Delta^2+\zeta^2)^{-1}$ in δI_n as a Fourier transform

$$\frac{1}{\Delta^2+\zeta^2}=\frac{1}{2\zeta^2}\int_{-\infty}^{\infty}ds\exp\left(-|s|+i\frac{s\Delta}{\zeta}\right). \tag{3.9}$$

By virtue of this transformation, the beating frequency, Δ, which depends on the hyperfine fields, appears in the exponent of the integrand. Next we take advantage of the fact that the beating frequency, Δ, in the strong-field limit can be expanded as

$$\Delta=(\boldsymbol{b}_1-\boldsymbol{b}_2)\cdot\boldsymbol{n}+\frac{\boldsymbol{b}_1^2-\boldsymbol{b}_2^2-(\boldsymbol{b}_1\cdot\boldsymbol{n})^2+(\boldsymbol{b}_2\cdot\boldsymbol{n})^2}{2B}, \tag{3.10}$$

where $\boldsymbol{n}$ is the unit vector in the direction of $\boldsymbol{B}$. Now, since Δ contains only linear and quadratic terms in $\boldsymbol{b}_i$, the averaging of the exponential factor can be performed explicitly using the properties

$$\left\langle e^{i\kappa b_i}\right\rangle=e^{-\kappa^2b_0^2/4},\quad \left\langle e^{-\mu b_i^2}\right\rangle=\frac{1}{\sqrt{1+\mu b_0^2}}. \tag{3.11}$$

For the parallel case, this averaging yields

$$\left\langle\frac{1}{(\Delta(\boldsymbol{B}+\frac{\triangle\boldsymbol{B}}{2})^2+\zeta^2)(\Delta(\boldsymbol{B}-\frac{\triangle\boldsymbol{B}}{2})^2+\zeta^2)}\right\rangle$$

$$= \frac{1}{4\zeta^4} \int_{-\infty}^{\infty} ds_1 \int_{-\infty}^{\infty} ds_2 \frac{\exp\left(-(|s_1|+|s_2|) - \frac{b_0^2}{2\zeta^2}(s_1-s_2)^2\right)}{1+\frac{b_0^4}{4\zeta^2}\left(\frac{s_1}{B+\frac{\Delta B}{2}} - \frac{s_2}{B-\frac{\Delta B}{2}}\right)^2}. \quad (3.12)$$

The exponent $\exp\left[-\frac{b_0^2}{2\zeta^2}(s_1-s_2)^2\right]$ follows from the first identity, Eq. (3.11), while the denominator emerges from the second identity.

As a next step we perform the integration over the difference $s_1 - s_2$. This integration can be performed explicitly using the fact that $\zeta \ll b_0 \ll B$. Upon this integration, the average, Eq. (3.12), can be presented in the form $\frac{\sqrt{2\pi}}{4\zeta^3 b_0}\Phi_\parallel(\frac{\Delta B}{B_c})$, where the dimensionless function $\Phi_\parallel$ is defined as

$$\Phi_\parallel(z) = \int_0^\infty dx \ \frac{e^{-x}}{1+z^2x^2}, \quad (3.13)$$

and $B_c = 4B^2\zeta/b_0^2$. The argument of the function Φ imposes a characteristic "period" of mesoscopic fluctuations: $\delta B \sim \frac{B^2\zeta}{b_0^2}$.

Eq. (3.13) suggests that the period of the mesoscopic fluctuations grows quadratically with B. We tested this result by a numerical simulation. For this simulation we chose $N = 10^4$ random values of $\boldsymbol{b}$ with rms $b_0 = 10^2\zeta^{-1}$. For each set of the local hyperfine fields the sum $\sum_{n=1}^N \delta I_n(\boldsymbol{B})$, where δI_n is given by Eq. (3.6) was evaluated. The results of simulation are shown in Fig. 3.2. Mesoscopic fluctuations and growth of their period with B are apparent.

Our consideration applies for $\delta B \ll B$. This condition suggests that for measuring the fluctuations one must work in the domain $b_0 \ll B \ll b_0^2/\zeta$. The correlator Eq. (3.13) is plotted in Fig. 3.1. For small $\delta B \ll B_c$ it behaves as $1-(\frac{\delta B}{B_c})^2$, and falls off slowly, as $\frac{\pi B_c}{2\delta B}$, for $\delta B \gg B_c$.

For the perpendicular case, we can simplify Δ as $\Delta \approx (\boldsymbol{b}_1 - \boldsymbol{b}_2)\cdot\boldsymbol{n}$. This is because the $\boldsymbol{B}$-dependence of Δ enters via the orientation, $\boldsymbol{n}$. Performing the same decoupling (Eq. (3.9)) as for the parallel case, instead of the double integral in Eq. (3.12) we get now

$$\left\langle \frac{1}{(\Delta(\boldsymbol{B}+\frac{\Delta\boldsymbol{B}}{2})^2+\zeta^2)(\Delta(\boldsymbol{B}-\frac{\Delta\boldsymbol{B}}{2})^2+\zeta^2)} \right\rangle$$
$$= \int \frac{ds_1}{2\zeta^2} e^{-|s_1|} \int \frac{ds_2}{2\zeta^2} e^{-|s_2|} \exp\left\{-\frac{b_0^2}{2\zeta^2}\left(s_1^2+s_2^2-2s_1s_2\cos\varphi\right)\right\}. \quad (3.14)$$

We again see that by virtue of the relation $b_0 \gg \zeta$, the difference $(s_1 - s_2) \sim \frac{\zeta}{b_0}$ is small. This allows us to integrate over $s_1 - s_2$ and reduce Eq. (3.14) to $\frac{\sqrt{2\pi}}{4\zeta^3 b_0}\Phi_\perp(\frac{\varphi}{\varphi_c})$, where $\varphi_c = \frac{2\sqrt{2}\zeta}{b_0} \ll 1$ and the function $\Phi_\perp(z)$ is defined as

$$\Phi_\perp(z) = \int_0^\infty dx \ \exp\left[-x - z^2x^2\right]. \quad (3.15)$$

The correlator is plotted in Fig. 3.1. At $\varphi \gg \varphi_c$, it falls off as φ_c/φ. In general, the correlator, Eq. (3.14), is a periodic function of φ; had we not used the small-φ expansion it would go through a minimum at $\varphi = \pi/2$ and "revive" at $\varphi = \pi$.

Our results related to mesoscopics can be summarized in the following expression

$$\frac{\left\langle \delta I\left(\boldsymbol{B}-\frac{\triangle \boldsymbol{B}}{2}\right)\delta I\left(\boldsymbol{B}+\frac{\triangle \boldsymbol{B}}{2}\right)\right\rangle}{I(\infty)^2}=\frac{\sqrt{2\pi}\zeta}{4Nb_0}\begin{cases}\Phi_{\parallel}\left(\frac{\triangle B}{B_c}\right), \triangle \boldsymbol{B} \parallel \boldsymbol{B}\\ \Phi_{\perp}\left(\frac{\varphi}{\varphi_c}\right), \triangle \boldsymbol{B} \perp \boldsymbol{B}\end{cases} \tag{3.16}$$

3.5 Discussion

- By choosing a simple transport model for an organic semiconductor device, and adopting the assumption [13, 18] that recombination proceeds exclusively from the singlet state, we were able to demonstrate mesoscopic fluctuations in the OMAR response in the domain $B \gg b_0$, where the average current is saturated, and predict their characteristic magnitude and period. Our theory is based on an observation that in this B-domain there exists a strong separation between slow and fast components of the PP spin-dynamics. As a result of this separation, the S-T_0 beating becomes decoupled, which, in turn, leads to a dramatic recombination slow down which originates from PP "trapping" in the T_0 state. Since the underlying physics are so general, any transport model in a small device with few junctions should exhibit mesoscopic fluctuations. What is really required for mesoscopic features to emerge in $I(B)$ is that the transport is in the regime of "slow-hopping," namely, $b_0 \gg \zeta$. It is in this regime when sparse PPs, for which the $\boldsymbol{b}_h$ projections on the external field almost coincide, play a distinguished role.

  Mesoscopic effect persists when recombination from triplet is also allowed. Important is that the recombination times from singlet and triplet PPs differ.

- We assumed that the time, τ_D, of the pair formation is equal to the time of pair disassembly. This requirement is not restrictive for mesoscopics. What is important for mesosopics is that both times exceed the recombination time, τ. In fact, this requirement is a general requirement for spin-dependent recombination, which is at the core of the OMAR effect.

- As we mentioned above, the transport model adopted in the present paper is quite similar to bipolaron model of transport put forward in Ref. [13]. Replacement of bipolaron formation by recombination does not bring in any new qualitative features. Thus, the mesoscopic fluctuations demonstrated in the present paper can be viewed

as a correction due to the local environment to the average current emerging from the mechanism Ref. [13].

- Regarding experimental verification of the predicted mesoscopic fluctuations, we note that there might be an alternative (to decreasing the size) way to bring samples into a mesoscopic regime. It was demonstrated in Ref. [28] that tin-doped indium oxide (ITO) electrodes exhibit sharp pillars with areal density of $\sim 1\,\mu\mathrm{m}^{-2}$. These pillars may cause additional inhomogeneity of the local conductivity and even define high-conductivity channels in the active layer. If this is the case, one can estimate from the data in Ref. [28] that a small OLED with area of $\sim 10^{-2}\,\mathrm{cm}^2$ will show mesoscopic fluctuations of $\frac{\delta I}{I} \sim 10^{-3}$. Another example illustrating how the device fabrication can lead to preformed channels of the current paths can be found in Ref. [29], see Fig. 3.4. Ref. [29] coated LSMO with the organic semiconductor tetraphenyl porphyrin (TPP). The scale of inhomogeneities shown in the AFM image was $\sim$ 100nm. The pillars are $\sim$ 20nm in height.

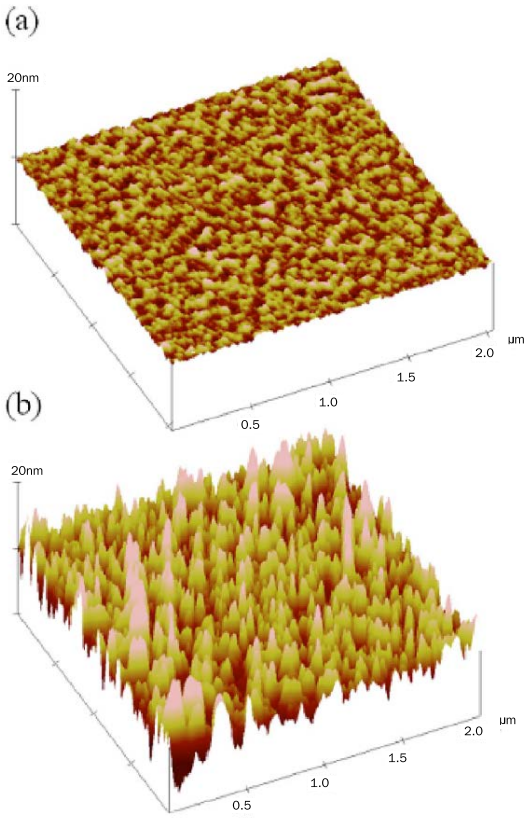

Figure 3.4: An AFM image of a ferromagnetic electrode (LSMO) is shown before (a) and after (b) the deposition of the organic semiconductor (TPP). The scale of inhomogeneities shown are about 100nm in diameter and can grow to be about 20nm in height. From Ref. [29].

3.6 References

[1] K. M. Salikhov, Y. N. Molin, R. Z. Sagdeev, and A. L. Buchachenko, in *Spin Polarization and Magnetic Effects in Radical Reactions*, edited by Y. N. Molin (Elsevier, Amsterdam, 1984), pp. 32116, and the review U. E. Steiner and T. Ulrich, Chem. Rev. **89**, 51 (1989).

[2] K. Schulten and P. G. Wolynes, J. Chem. Phys. **68**, 3292 (1978).

[3] T. L. Francis, Ö. Mermer, G. Veeraraghavan, and M. Wohlgenannt, New J. Phys. **6**, 185 (2004).

[4] Ö. Mermer, G. Veeraraghavan, T. L. Francis, Y. Sheng, D. T. Nguyen, M. Wohlgenannt, A. Khler, M. K. Al-Suti, and M. S. Khan, Phys. Rev. B **72**, 205202 (2005).

[5] Y. Sheng, T. D. Nguyen, G. Veeraraghavan, O. Mermer, M. Wohlgenannt, S. Qiu, and U. Scherf, Phys. Rev. B **74**, 045213 (2006).

[6] V. N. Prigodin, J. D. Bergeson, D. M. Lincoln, and A. J. Epstein, Synth. Met. **156**, 757 (2006).

[7] P. Desai, P. Shakya, T. Kreouzis, and W. P. Gillin, Phys. Rev. B **76**, 235202 (2007).

[8] F. J. Wang, H. Bässler, and Z. Valy Vardeny, Phys. Rev. Lett. **101**, 236805 (2008).

[9] T. D. Nguyen, G. Hukic-Markosian, F. Wang, L. Wojcik, X.-G. Li, E. Ehrenfreund, and Z. V. Vardeny, Nat. Mater. **9**, 345 (2010).

[10] T. D. Nguyen, B. R. Gautam, E. Ehrenfreund, and Z. V. Vardeny, Phys. Rev. Lett. **105**, 166804 (2010).

[11] Tho D. Nguyen, T. P. Basel, Y.-J. Pu, X-G. Li, E. Ehrenfreund, and Z. V. Vardeny, Phys. Rev. B **85**, 245437 (2012).

[12] F. L. Bloom, W. Wagemans, M. Kemerink, and B. Koopmans, Phys. Rev. Lett. **99**, 257201 (2007).

[13] P. A. Bobbert, T. D. Nguyen, F. W. A. van Oost, B. Koopmans, and M. Wohlgenannt, Phys. Rev. Lett. **99**, 216801 (2007).

[14] W. Wagemans, F. L. Bloom, P. A. Bobbert, M. Wohlgenannt, and B. Koopmans, J. Appl. Phys. **103**, 07F303 (2008).

[15] F. L. Bloom, M. Kemerink, W. Wagemans, and B. Koopmans, Phys. Rev. Lett. **103**, 066601 (2009).

[16] S. P. Kersten, A. J. Schellekens, B. Koopmans, and P. A. Bobbert, Phys. Rev. Lett. **106**, 197402 (2011).

[17] W. Wagemans, A. J. Schellekens, M. Kemper, F. L. Bloom, P. A. Bobbert, and B. Koopmans Phys. Rev. Lett. **106**, 196802 (2011).

[18] N. J. Harmon and M. E. Flatté, Phys. Rev. Lett. **108**, 186602 (2012); Phys. Rev. B **85**, 075204 (2012); Rev. B **85**, 245213 (2012).

[19] L. I. Glazman and K. A. Matveev, Zh. Eksp. Teor. Fiz. **94**, 332 (1988) [Sov. Phys. JETP **67**, 1276 (1988)].

[20] M. E. Raikh and I. M. Ruzin, in *Mesoscopic Phenomena in Solids*, edited by B. L. Altshuller, P. A. Lee, and R. A. Webb (Elsevier, New York, 1991), p. 315.

[21] R. J. F. Hughes, A. K. Savchenko, J. E. F. Frost, E. H. Linfield, J. T. Nicholls, M. Pepper, E. Kogan, and M. Kaveh, Phys. Rev. B **54**, 2091 (1996).

[22] D. R. McCamey, S.-Y. Lee, S.-Y. Paik, J. M. Lupton, and C. Boehme Phys. Rev. B **82**, 125206 (2010).

[23] A. V. Khaetskii, D. Loss, and L. I. Glazman, Phys. Rev. Lett. **88**, 186802 (2002).

[24] T. V. Shahbazyan and M. E. Raikh, Phys. Rev. B **49**, 17123 (1994).

[25] J. König, Y. Gefen, and G. Schön, Phys. Rev. Lett. **81**, 4468 (1998).

[26] M. G. Schultz and F. von Oppen, Phys. Rev. B **80**, 033302 (2009).

[27] R. C. Roundy and M. E. Raikh, Phys. Rev. B **87**, 195206 (2013).

[28] G. Liu, J. B. Kerr, and S. Johnson, Synth. Met. **144**, 1 (2004).

[29] W. Xu, G. J. Szulczewski, P. LeClair, I. Navarrete, R. Schad, G. Miao, H. Guo, and A. Gupta, Appl. Phys. Lett. **90**, 072506 (2007).

CHAPTER 4

ORGANIC MAGNETORESISTANCE UNDER RESONANT AC DRIVE

4.1 Introduction

The first papers reporting observation of spin injection into organic material (sexithienyl) [1] and spin-valve effect [2] with organic active layer (Alq_3) have launched a new field, organic spintronics, with numerous potential practical applications resulting from the high tunability of organic-based structures. In the quest for fabrication of functional spin valves it was noticed that organic layers with nonmagnetized electrodes exhibit anomalous sensitivity to weak magnetic fields. This is how the sensitivity dubbed organic magnetoresistance (OMAR) became a subject of extensive experimental and theoretical studies. [3, 4, 5, 6, 7, 8, 9, 10, 11, 12, 13, 14, 15] Until now, these studies were restricted to measurement of current change, $\delta I(B)$, and luminescence intensity change, $\delta I_L(B)$, with magnetic field, B, at different temperatures and applied voltages. However, $\delta I(B)$ and $\delta I_L(B)$ exhibit quite similar behaviors, and thus offer limited room for discriminating between different physical mechanisms. Partly because of this, a unique explanation and quantitative theory of OMAR is still debated. Meanwhile, there is a strong indication that the physics behind the OMAR phenomenon is fundamental. This is the because the effect itself is robust, while its magnitude and even the sign are sensitive to technological details, [10, 11, 12, 13] and intentionally imposed random fringe fields. [16]

The most "economic" theoretical description of OMAR so far was put forward in Ref. [8]. It is appealing, in the sense that it relates OMAR to spin-blocking, which is its natural origin, in a most direct way by reducing it to the Larmor precession of spins within a *single* pair of carriers. The model of Ref. [8] was originally titled a "bipolaron model," however, the basic physics of spin-selective processes which it captures is the same for either a bipolaron or an electron-hole pair. Still, to confirm or rule out the existing physical pictures of OMAR, it is desirable to supplement the measurements of $\delta I(B)$ and $\delta I_L(B)$ with probes of different aspects of OMAR. Viability of a certain OMAR model should be

judged by how successfully it can account for the results of these probes. One such probe was recently reported by Ref. [17]. They applied a transverse ac drive to an organic-based diode, with bipolar injection, placed in magnetic field B_0 in which OMAR was practically saturated, and observed a lively response in the form of a dip in $\delta I(B)$ at the resonance, $\omega_0 = \gamma B_0$, where γ is the gyromagnetic ratio, see Fig. 4.1. The dip got got progressively deeper upon increasing the drive intensity.

In the present paper we incorporate ac drive into the theory of OMAR, and demonstrate that the two-site model [8] offers very nontrivial predictions for the dependence of OMAR on the driving amplitude, B_1, and on detuning of ω_0 from the resonance. In particular, we predict that the dependence $\delta I(B_1)$ is *nonmonotonic*. This behavior is a fingerprint of the ac-induced *trapping*, which we demonstrate. Experimental verification of this behavior would provide a strong support to the adequacy of the two-site model.

4.2 Qualitative picture

It is commonly accepted that, in organic materials, where the spin-orbit coupling is weak, spin-dependent phenomena are due to the random hyperfine fields with rms $b_0 \sim 10$ mT created by the nuclei. To relate OMAR to the spin dynamics of a single pair of polarons, it is sufficient to adopt the simplest assumption [8, 14, 15] that bipolaron formation or recombination (in bipolar devices) proceed only when the pair-partners are in the singlet state, S. With equal probabilities of all initial states, the recombination time of a pair is determined by the hyperfine-field-induced admixture of the singlet to three other spin eigenstates.

It is a crucial ingredient of OMAR that the current response, $\delta I(B)$, at $B \sim b_0$ is governed by sparse *blocking* configurations [8] in which hyperfine fields "conspire" to protect the pair from crossing into S after its creation. As the field increases and exceeds b_0, these long-living states evolve into T_+ and T_- components of a triplet, and the current saturates.

From the perspective of blocking, the effect of ac drive on OMAR can be accounted for by considering the ac field as a mixing agent, which tends to scramble all three triplet states and, thus, to limit the trapping ability of T_+, T_-, see Fig. 4.2.

In this way, the ac field tends to change the current towards its value at zero magnetic field, which is what was observed in Ref. [17]. From this picture one would expect that the radiation-induced change of current, δI, is due to the change of the recombination rate, which, in turn, is proportional to B_1^2, i.e., to the power of the driving field.

The main finding which we report is that the dependence of δI on B_1 is much more intricate. In particular, it is *linear* for weak B_1. This effect stems from pairs in which one

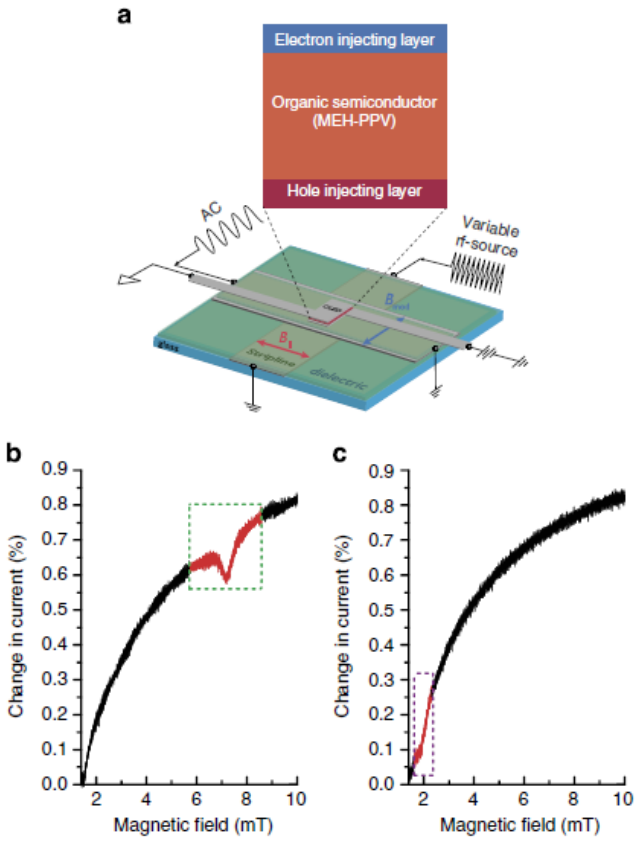

Figure 4.1: An experimental probe of the OMAR response under ac drive. (a) The device consists of an organic diode structure (inset, the layers are not to scale), which is located above two mutually perpendicular striplines required for on-chip spin resonant excitation and field modulation. Electron and hole polarons are injected from opposite sides into the diode structure and recombine spin dependently in the organic semiconductor. (b,c) The magnetic field response of a DC current (no modulation) in a bipolar MEH-PPV diode as a function of magnetic field as RF radiation (200 M MHz in (b); 50 M MHz in (c)) is applied. Reductions in the current are seen when MR conditions are satisfied. These are more pronounced when the applied field B_0 exceeds ΔB_{Hyp}, that is, where MR-induced spin mixing dominates. Adapted from Ref. [17].

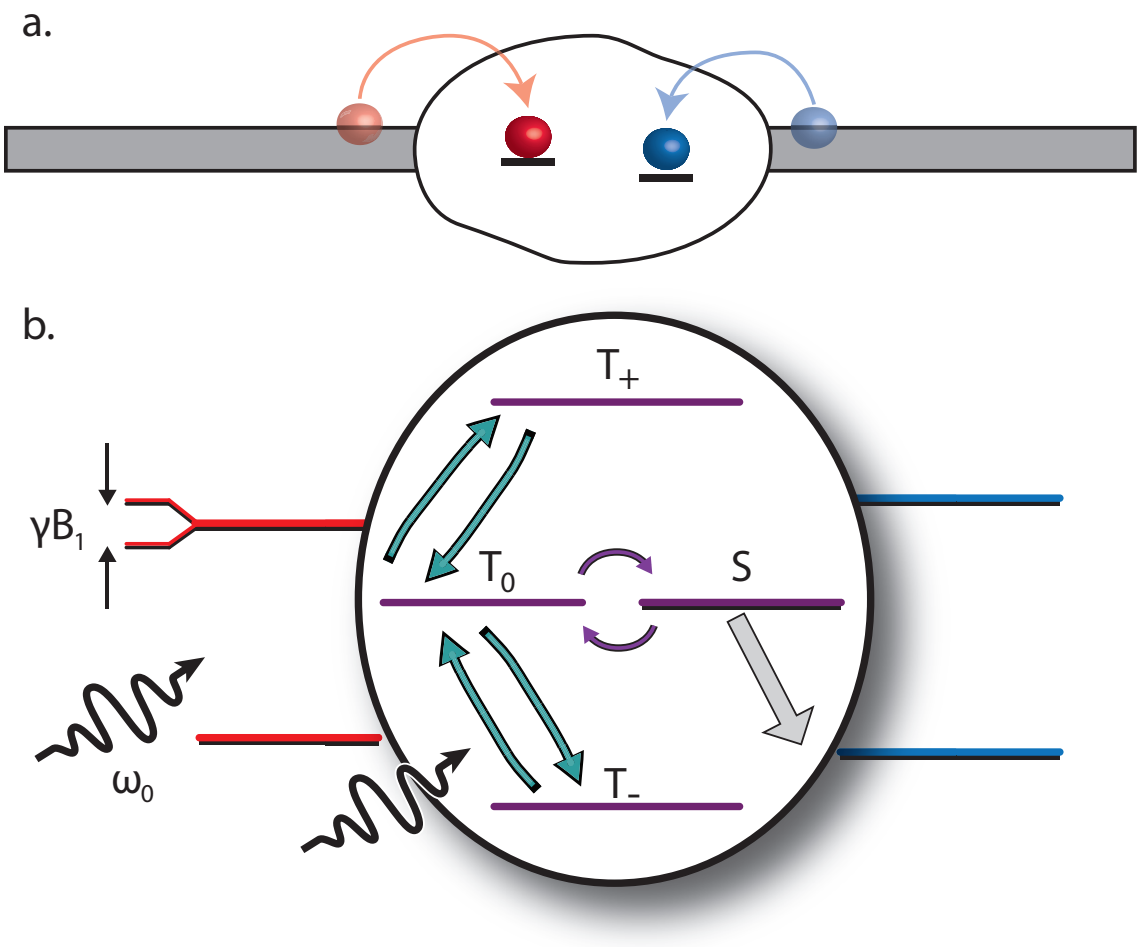

Figure 4.2: (Color online). (a) Current passage through a bipolar device involves recombination of electron (red) and hole (blue) which occupy the neighboring sites; (b) Example of a pair in which electron is on-resonance and hole is off-resonance. The bubble illustrates the efficient mixing of the triplet components by the ac field, which, in turn, affects the crossing rate $T_0 \leftrightarrows S$. The gray arrow indicates that recombination occurs exclusively from S.

of the partners is on-resonance, see Fig. 4.2. It appears that for these particular pairs the radiation-induced suppression of trapping by T_+ and T_- is especially efficient. However, such pairs determine $\delta I(B_1)$ only for weak driving fields, namely, for fields in which the nutation frequency is much smaller than γb_0. As we will proceed to show, a very nontrivial physics unfolds for higher B_1. Quite unexpectedly, a new *long-living mode*, $\frac{1}{\sqrt{2}}(T_+ - T_-)$, emerges in strong enough driving fields, see Fig. 4.3.

This mode, in which both pair-partners are on resonance, is fully analogous to subradiant state in the Dicke effect [18]. In this regard, we would like to note that although the Dicke physics for an ensemble of atoms in an excited state has been known for almost sixty years, the fact that it can emerge as a result of ac-drive has never been considered before. Trapping by this "subradiant" state also yields a linear correction to the current, but with *opposite slope*.

4.3 Driven spin-pair without recombination

To highlight the physics, we first neglect recombination. Since the experiment in Ref. [17] was performed on a bipolar device, we start with the Hamiltonian of a driven electron-hole pair

$$\widehat{H} = \omega_e S_e^z + \omega_h S_h^z + 2\Omega_R \left(S_e^x + S_h^x\right) \cos\omega_0 t, \tag{4.1}$$

where $\omega_{e,h} = \omega_0 + \delta_{e,h}$, $\Omega_R = \gamma B_1$ is the Rabi frequency, and $\delta_{e,h}$ are the z-components of the hyperfine fields acting on the electron and hole, respectively, i.e., the detunings of the pair-partners from the resonance. By retaining only z-components, we assumed that $B_0 \gg b_0$. We will also assume that $\gamma B_0 \gg \Omega_R$, which allows us to employ the rotating wave approximation. In the rotating frame, the amplitudes of T_+, T_-, T_0, and S-components of the wave function are related by a system

$$(\chi - \delta) A_{T_-} = \frac{\Omega_R}{\sqrt{2}} A_{T_0}, \tag{4.2}$$

$$(\chi + \delta) A_{T_+} = \frac{\Omega_R}{\sqrt{2}} A_{T_0}, \tag{4.3}$$

$$\chi A_S = -\delta_0 A_{T_0}, \tag{4.4}$$

$$\chi A_{T_0} = -\delta_0 A_S + \frac{\Omega_R}{\sqrt{2}} \left(A_{T_+} + A_{T_-}\right), \tag{4.5}$$

where χ is the quasienergy, see Fig. 4.4, while parameters δ_0 and δ are defined as

$$\delta_0 = \frac{1}{2}\left(\delta_e - \delta_h\right), \quad \delta = \frac{1}{2}\left(\delta_e + \delta_h\right). \tag{4.6}$$

The quasienergies satisfy the equation

$$\chi^2(\chi^2 - \delta^2 - \Omega_R^2) - \delta_0^2(\chi^2 - \delta^2) = 0 \tag{4.7}$$

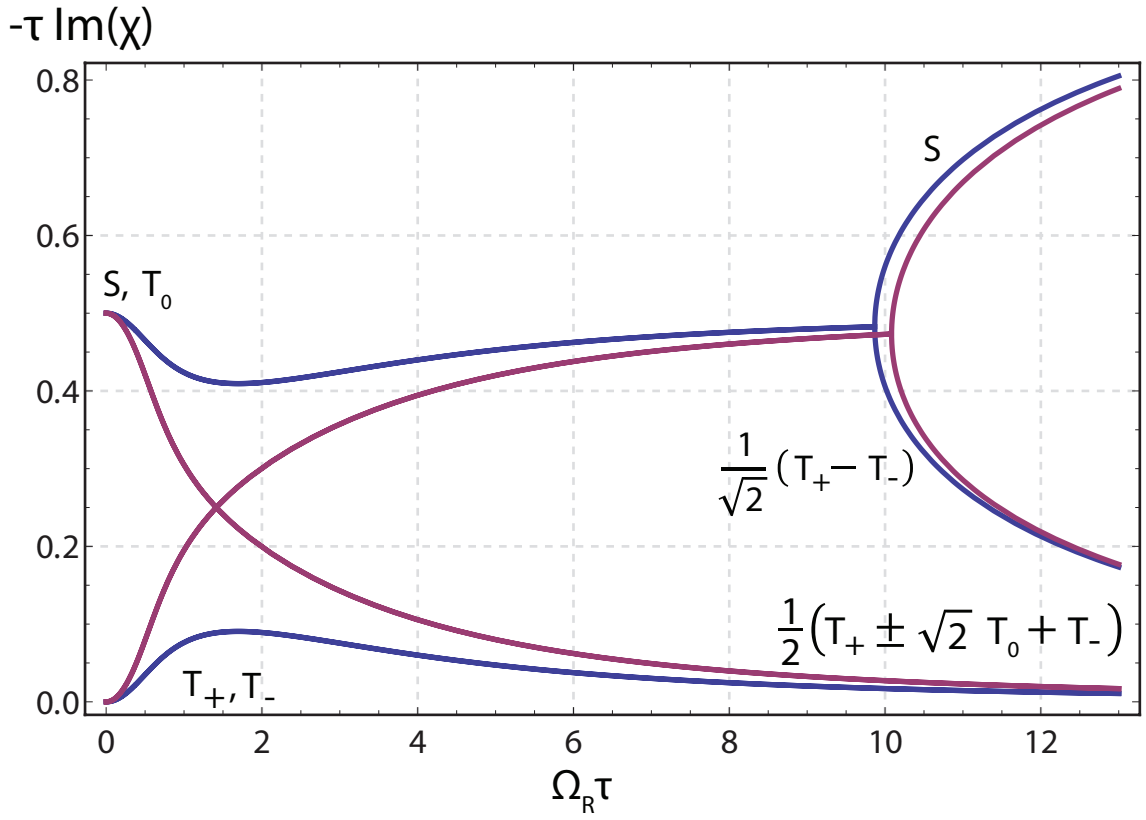

Figure 4.3: (Color online). The evolution of dimensionless decay rates of different modes with amplitude of the ac drive is plotted from Eq. (4.10) for two sets of parameters $(\delta\tau, \delta_0\tau)$: blue $(2.5, 2)$; purple $(2, 2.5)$. The content of the quasimodes evolves from T_+, T_- and linear combinations of S, T_0 at weak drive into the combinations, $\frac{1}{2}\left(T_+ \pm \sqrt{2}T_0 + T_-\right)$, one superradiant mode, S, and one subradiant mode, $\frac{1}{\sqrt{2}}\left(T_+ - T_-\right)$.

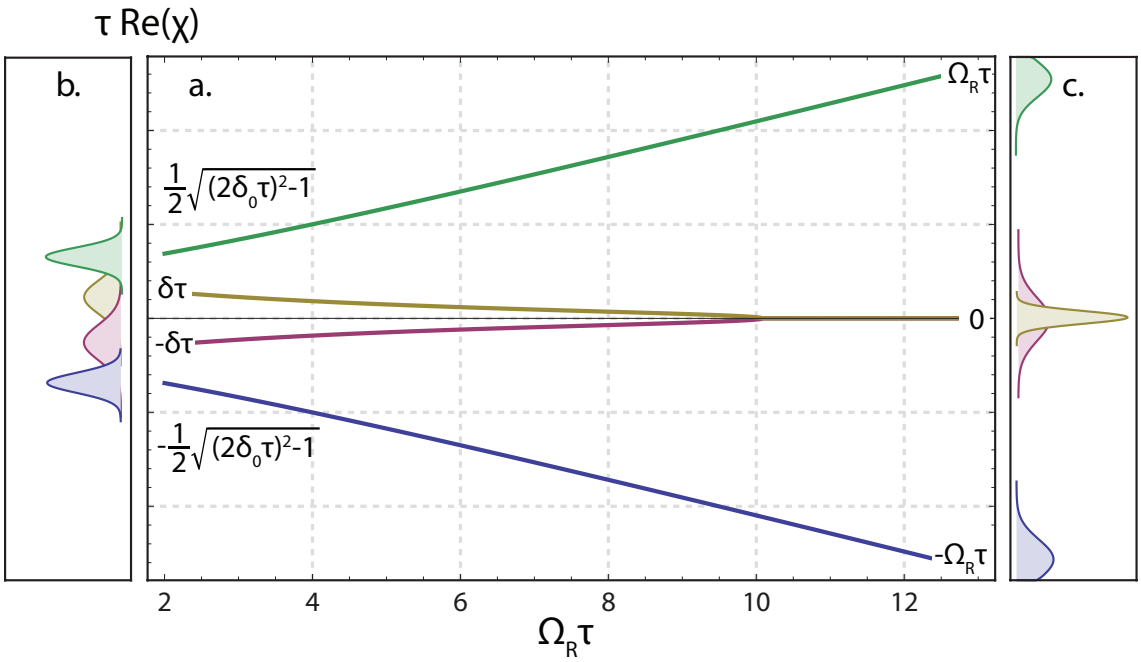

Figure 4.4: (Color online). (a) The evolution of quasienergies with amplitude of the driving field is plotted from Eq. (4.10) for parameters $(\delta\tau, \delta_0\tau) = (2, 2.5)$. Quasienergies evolve from $\pm\delta$, $\pm\frac{1}{2}\sqrt{(2\delta_0\tau)^2 - 1}$ to $0, \pm\Omega_R$. At small Ω_R, the quasienergies are well resolved (b). Merging of two quasienergies at large Ω_R is accompanied by splitting of their widths (c), which is a manifestation of the Dicke physics.

with obvious solutions

$$\chi = \pm\frac{1}{2}\left[(\delta_0+\delta)^2+\Omega_R^2\right]^{1/2} \pm \frac{1}{2}\left[(\delta_0-\delta)^2+\Omega_R^2\right]^{1/2}. \tag{4.8}$$

It follows from Eqs. (4.2), (4.7) that for large $\Omega_R \gg \delta_0, \delta$, the pair of quasienergies, which approach $\chi = 0$, (see Fig. 4.4), correspond to the modes S and $\frac{1}{\sqrt{2}}(T_+ - T_-)$, while the quasienergies that approach $\chi = \pm\,\Omega_R$ correspond to the combinations $\frac{1}{2}\left(T_+ \pm \sqrt{2}T_0 + T_-\right)$, respectively.

4.4 Driven spin-pair with recombination

Including recombination from S requires the analysis of the full equation for the density matrix,

$$i\dot{\rho} = [\widehat{H}, \rho] - \frac{i}{2\tau}\left\{\Pi_S, \rho\right\}, \tag{4.9}$$

where τ is the recombination time, and Π_S is the projector onto the singlet subspace. The matrix corresponding to this equation is 16×16. The 16 eigenvalues can be cast in the form $\chi_i - \chi_j^*$, where χ_i and χ_j satisfy the quartic equation

$$\chi\left(\chi + \frac{i}{\tau}\right)(\chi^2 - \delta^2 - \Omega_R^2) - \delta_0^2(\chi^2 - \delta^2) = 0, \tag{4.10}$$

which generalizes Eq. (4.7) to the pair with decay. For slow recombination, $b_0\tau \gg 1$, the quasienergies acquire small imaginary parts, which can be found perturbatively from Eq. (4.10)

$$\delta\chi = -\frac{i}{4\tau}\left(1 \pm \frac{\left|\delta_0^2 - \delta^2 - \Omega_R^2\right|}{\sqrt{(\delta^2+\delta_0^2+\Omega_R^2)^2 - 4\delta_0^2\,\delta^2}}\right). \tag{4.11}$$

Naturally, in the limit $\Omega_R \to 0$, Eq. (4.11) yields either $\delta\chi = -i/2\tau$ for S and T_0 states, and $\delta\chi = 0$ for the trapping states T_+ and T_-. Less trivial is that at large $\Omega_R \gg \delta_0, \delta$ the values $\delta\chi$ again approach $\delta\chi = -i/2\tau$ and $\delta\chi = 0$. The evolution of the imaginary parts of the quasienergies with Ω_R is illustrated in Fig. 4.3.

4.5 Current at a weak drive

Finite $\Omega_R \ll \delta, \delta_0 \sim b_0$ leads to finite lifetimes of the trapping modes. Expanding Eq. (4.11), we get

$$\tau_{tr} = \frac{1}{2|\chi|} = \frac{4\tau\left(\delta^2 - \delta_0^2\right)^2}{\Omega_R^2\delta_0^2}. \tag{4.12}$$

Once τ_{tr} is known, we can employ the simplest quantitative description of transport [15] based on the model of Ref. [8] to express the correction, $\delta I(\Omega_R)$, to the current caused by

the ac drive. Within this description, a pair at a given site is first assembled, then undergoes the pair-dynamics and either recombines or gets disassembled depending on which process takes less time, see Fig. 4.2 (a). These three steps are then repeated, so that the passage of current proceeds in cycles. Then the current associated with a given pair is equal to $\frac{1}{\langle t\rangle}$, where $\langle t\rangle$ is the average cycle duration. Importantly, all the initial spin configurations of the pair have equal probabilities. For simplicity, it is assumed [15] that, on average, the times of assembly and disassembly are the same $\tau_D \gg \tau$. This input is sufficient to derive the following expression for $\delta I(\Omega_R)$

$$\frac{\delta I(\Omega_R)}{I(0)} = \frac{\tau_{tr}^{-1}}{\tau_{tr}^{-1} + 2\tau_D^{-1}} = \frac{\Omega_R^2\delta_0^2}{\Omega_R^2\delta_0^2 + 8(\delta^2-\delta_0^2)^2\frac{\tau}{\tau_D}}, \tag{4.13}$$

where $I(0) = \frac{1}{\tau_D}$. The remaining task is to average Eq. (4.13) over the distributions of the hyperfine fields, or equivalently, over δ and δ_0. Since we consider a weak drive, this averaging is greatly simplified. Indeed, the major contributions to the average comes from narrow domains $|\delta-\delta_0| \sim \Omega_R\left(\frac{\tau_D}{\tau}\right)^{1/2}$ and $|\delta+\delta_0| \sim \Omega_R\left(\frac{\tau_D}{\tau}\right)^{1/2}$, much narrower than b_0. On the other hand, these domains are wider than Ω_R, which justifies the expansion Eq. (4.12). Replacing the distribution functions of $(\delta+\delta_0)$ and $(\delta-\delta_0)$ by $\frac{1}{\sqrt{\pi}b_0}$, we get

$$\frac{\langle\delta I(\Omega_R)\rangle}{I(0)} = \frac{\Omega_R^2}{(2\pi)^{1/2}b_0}\int\frac{d(\delta-\delta_0)}{\Omega_R^2+\frac{32\tau}{\tau_D}(\delta-\delta_0)^2} + \frac{\Omega_R^2}{(2\pi)^{1/2}b_0}\int\frac{d(\delta+\delta_0)}{\Omega_R^2+\frac{32\tau}{\tau_D}(\delta+\delta_0)^2} \tag{4.14}$$

$$= \left(\frac{\pi\tau_D}{2\tau}\right)^{1/2}\left(\frac{\Omega_R}{b_0}\right), \tag{4.15}$$

i.e., the radiation-induced correction is *linear* in Ω_R. To understand this anomalous behavior qualitatively, notice that small $(\delta+\delta_0)$ and $(\delta-\delta_0)$ correspond to small δ_e and δ_h, respectively. Therefore, the linear $\delta I(\Omega_R)$ comes from configurations of hyperfine fields in which one of the pair-partners is on-resonance [19, 20, 21]; this partner responds strongly to the ac drive. The ratio Ω_R/b_0 is the portion of such configurations. The upper boundary of the weak driving domain is set by the condition $\Omega_R\sqrt{\tau_D/\tau} \lesssim b_0$, which allowed us to replace the distribution functions of $\delta-\delta_0$, $\delta+\delta_0$ by a constant. It is also seen from Eq. (4.13) that for $\Omega_R \gg b_0\sqrt{\tau_D/\tau}$ the correction saturates at $\langle\delta I\rangle/I(0) = 1$. This saturation applies as long as T_+ and T_- are the trapping eigenmodes. As was mentioned above, upon increasing Ω_R, the trapping eigenmodes evolve into $\frac{1}{2}\left(T_+ \pm \sqrt{2}T_0 + T_-\right)$ and we enter the strong-driving regime.

4.6 Strong drive

Expanding Eq. (4.11) in the limit $\Omega_R \gg \delta, \delta_0$ yields the expression $\tau_{tr} \approx \tau\Omega_R^2/\delta_0^2$ for the lifetime of the trapping eigenmodes. The same steps that led to Eq. (4.13) give rise to the

following *negative* correction to the current

$$\frac{\delta I(\Omega_R)}{I(0)} = 1 - \left(\frac{\tau}{\tau_D}\right) \frac{\Omega_R^2}{\delta_0^2 + \frac{\tau}{\tau_D}\Omega_R^2}. \tag{4.16}$$

We see from Eq. (4.16) that at $\Omega_R \gg \left(\frac{\tau_D}{\tau}\right)^{1/2} b_0$ the current is the same as it was in the absence of the ac drive. This is due to the fact that both in the absence of drive and in this domain the number of long-living modes is two. The return of $\delta I(\Omega_R)$ to zero takes place over a parametrically broad interval $\sqrt{\frac{\tau}{\tau_D}} < \frac{\Omega_R}{b_0} < \sqrt{\frac{\tau_D}{\tau}}$. The slope is calculated upon averaging Eq. (4.16) over δ_0, which again can be carried out after replacing the distribution function by $\frac{1}{\sqrt{\pi}b_0}$ and yields

$$\frac{1}{I(0)} \frac{\partial \langle \delta I \rangle}{\partial \Omega_R} = -\left(\frac{\tau}{\pi \tau_D}\right)^{1/2} \frac{1}{b_0}. \tag{4.17}$$

We see that the strong-field slope is τ_D/τ times smaller than the weak-field slope given by Eq. (4.14); this is consistent with the fact that the domain of the current drop is τ_D/τ times broader than the domain of current growth.

In fact, the saturation predicted by Eq. (4.16) precedes another domain of change of current, which stems from bifurcation in lifetimes of S, T_0 modes at large Ω_R, see Fig 4.3. To capture this bifurcation analytically, notice that for large Ω_R Eq. (4.11) predicts for $\delta\chi = -\frac{i}{2\tau}$ for the $\frac{1}{\sqrt{2}}(T_+ - T_-)$-mode, while the zero-order value of quasienergy falls off with Ω_R as $\delta_0\delta/\Omega_R$. Therefore, when Ω_R exceeds $\delta\delta_0\tau$, the correction would exceed the zero-order value and the perturbative treatment becomes inapplicable. Instead, we must make use of the fact that quasienergy is small, which allows us to simplify the quartic equation Eq. (4.7) to

$$\chi^2 + \frac{i}{\tau}\chi - \frac{\delta_0^2\delta^2}{\Omega_R^2} = 0. \tag{4.18}$$

The bifurcation of the lifetimes is revealed in the imaginary parts of the quasienergies, which are given by

$$\chi_\pm = -\frac{i}{2\tau}\left[1 \pm \sqrt{1 - \frac{4\delta_0^2\delta^2\tau^2}{\Omega_R^2}}\right], \tag{4.19}$$

see Fig. 4.3. For large Ω_R, solution $\chi_+ \approx -i/\tau$ corresponds to the S-mode, while the solution $\chi_- \approx -i\delta_0^2\delta^2\tau/\Omega_R^2$ evolves into a long-living mode $\frac{1}{\sqrt{2}}(T_+ - T_-)$. In other words, strong ac drive *induces* a third long-living mode which decouples from S, and therefore, cannot recombine. At the same time, the decoupling of S from all other triplet states makes its lifetime two times shorter than in the absence of drive. Note that there is a full formal correspondence between the solutions χ_+, χ_- and the superradiant and subradiant modes in the Dicke effect [18]. On the physical level, in the Dicke effect, the subradiant mode

acquires a long lifetime due to weak overlap with a photon field, while the long lifetime of the mode $\frac{1}{\sqrt{2}}(T_+ - T_-)$ is due to weak overlap with the recombining state S. With trapping by the subradiant mode incorporated, the correction to current takes the form

$$\frac{\delta I(\Omega_R)}{I(0)} = -\frac{\Omega_R^2}{(\delta_0^2\delta^2\tau\tau_D + \Omega_R^2)}. \tag{4.20}$$

It can be seen that the denominator in Eq. (4.20) defines a narrow domain $\delta_0 \sim \delta \sim \Omega_R^{1/2}/(\tau\tau_D)^{1/4}$, which yields the major contribution to $\langle\delta I(\Omega_R)\rangle$. Physically, this corresponds to configurations of the hyperfine fields in which *both* pair-partners are on-resonance. This again leads to the linear correction to $\langle\delta I(\Omega_R)\rangle$, which can be rewritten in dimensionless units as

$$\frac{\langle\delta I(\Omega_R)\rangle}{I(0)} = -\frac{\Omega_R}{\pi b_0^2\sqrt{\tau\tau_D}}\int dx\int dy\frac{1}{x^2y^2+1}. \tag{4.21}$$

The double integral in Eq. (4.21) diverges, but only logarithmically, as $\ln\left[b_0^2(\tau\tau_D)^{1/2}/\Omega_R\right]$. In performing the averaging Eq. (4.21) we again replaced the distribution functions of δ, δ_0 by $\frac{1}{\sqrt{\pi}b_0}$. This replacement is justified provided the characteristic δ, δ_0 are much smaller than b_0. The latter condition is equivalent to the condition that the argument of the logarithm is big. We should also check the validity of the expansion of the square root in Eq. (4.19). For characteristic δ, δ_0 the combination $\delta^2\delta_0^2\tau^2/\Omega_R^2$ is $\sim \tau/\tau_D \ll 1$, i.e., the expansion is valid. Overall dependence of $\langle\delta I\rangle$ on Ω_R exhibiting three prominent domains, Eqs. (4.14), (4.16) and (4.21) is sketched in Fig. 4.5.

4.7 Discussion

The prime experimental finding reported in Ref. [17], which motivated the present paper, is that the current blocking responsible for the OMAR effect [8] is effectively lifted under magnetic-resonance conditions. We demonstrated that this lifting is a natural consequence of developing of the Rabi oscillations in one of the spin-pair partners. It is also known [19, 20, 21] that Rabi oscillations in organic semiconductors, detected by pulsed magnetic resonance techniques, are dominated by pairs with one partner on-resonance as well. The reason why both effects are due to the same sparse objects is that these objects are more responsive to the ac-drive than nonresonant pairs. At the same time, the phase volume of such pairs is linear in Ω_R. Unfortunately, in the device design in Ref. [17], the magnitude of ac drive in the sample could not directly be measured. This precludes more quantitative comparison of our predictions with the experimental results. We hope that this comparison will be possible in the future as the experimental technique used in Ref. [17] matures.

Besides the physical picture in the weak-driving domain, we also predict that the overall evolution of current with increasing B_1 is much more complex, and involves a maximum

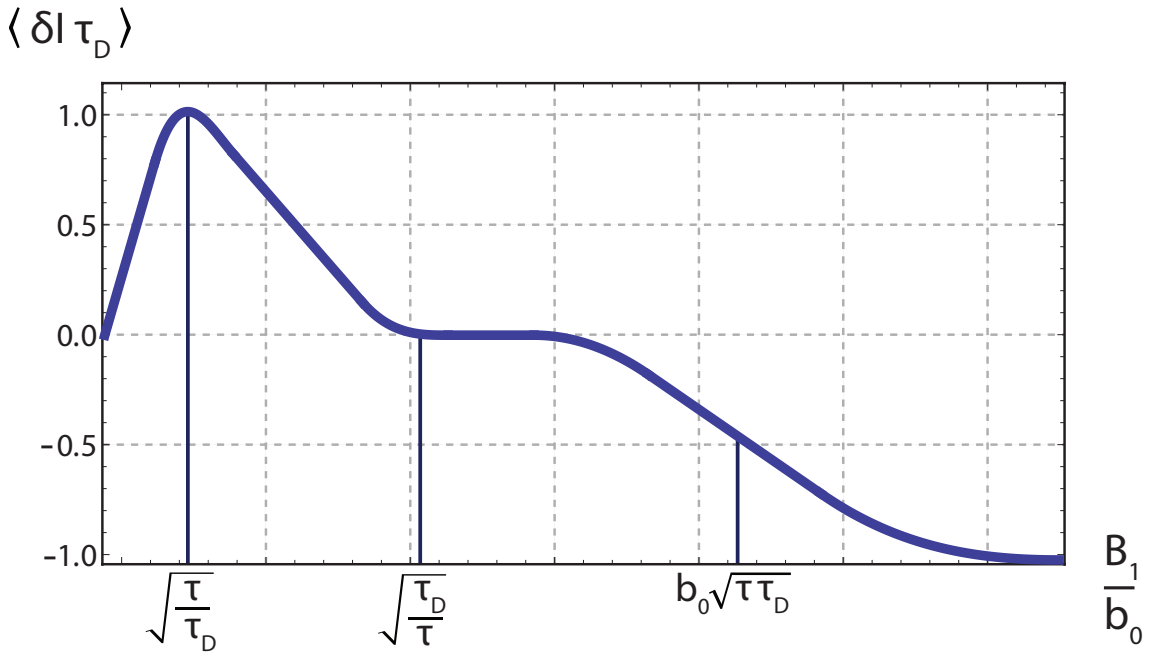

Figure 4.5: (Color online). Schematic dependence of the radiation-induced correction to the current on the amplitude of the ac drive. Three prominent domains (a), (b), and (c) are described by Eqs. (4.14), (4.20), and (4.21), respectively.

followed by a drop and subsequent saturation, see Fig. 4.5. Note that strong deviation from linear dependence of δI sets in already at weak driving fields, $B_1 \lesssim b_0$. The nonmonotonic behavior of current with ac drive is very unusual; its experimental verification would be a crucial test of radiation-induced trapping, which we predict.

Throughout the paper we assumed that the driving frequency exactly matches the Zeeman splitting γB_0. In fact, in Ref. [17] the sensitivity of OMAR to the ac drive extended over a sizable interval of applied dc fields centered at B_0. It is straightforward to generalize our consideration to a finite detuning $\Delta = \gamma B_0 - \omega_0$. Detuning enters the theory as a shift of the center of the Gaussian distribution of parameter δ from $\delta = 0$ to $\delta = \Delta$. Below we simply list the changes in the correction, δI, caused by strong detuning, $\Delta \gg \gamma b_0$. These changes are different in different domains of the driving field shown in Fig. 4.5. For weak driving the correction δI is given by

$$\frac{\delta I(\Omega_R)}{I(0)} = \frac{\Omega_R^2 b_0^2 \tau_D}{8\Delta^4 \tau}. \tag{4.22}$$

It emerges upon neglecting the Ω_R^2 term in the denominator of Eq. (4.13) and applies in the domain $\Omega_R \lesssim \Delta$ if Δ exceeds not only b_0 but also $b_0\sqrt{\frac{\tau_D}{\tau}}$. Then, unlike Fig. 4.5, the change $\frac{\delta I}{I(0)}$ does not reach one. The maximal change is $\sim b_0^2\tau_D/\Delta^2\tau \ll 1$. Interestingly, the domain (c) in Fig. 4.5 is affected much weaker by the detuning, Δ. Instead of Eq. (4.21) we have

$$\frac{\delta I(\Omega_R)}{I(0)} = -\frac{\Omega_R}{\Delta b_0\sqrt{\pi\tau\tau_D}}, \tag{4.23}$$

i.e., the linearity in Ω_R persists while the slope is suppressed by Δ/b_0.

In conclusion, we would like to note that one of our main findings, radiation-induced Dicke physics, goes way beyond the spin-dependent processes in organics. Previously the Dicke physics implied that one of the compound excited states of the system is orthogonal to the ground state, and hence the radiative decay is slow. We found that this orthogonalization of one of the excited states emerges in the "rotating frame" under strong enough ac drive and inhibits nonradiative recombination.

4.8 References

[1] V. Dediu, M. Murgia, F. C. Matacotta, C. Taliani, and S. Barbanera, Solid State Commun., **122**, 181 (2002).

[2] Z. H. Xiong, D. Wu, Z. Valy Vardeny, and J. Shi, Nature (London) **427**, 821 (2004).

[3] T. L. Francis, Ö. Mermer, G. Veeraraghavan, and M. Wohlgenannt, New J. Phys. **6**, 185 (2004).

[4] Ö. Mermer, G. Veeraraghavan, T. L. Francis, Y. Sheng, D. T. Nguyen, M. Wohlgenannt, A. Khler, M. K. Al-Suti, and M. S. Khan, Phys. Rev. B **72**, 205202 (2005).

[5] Y. Sheng, T. D. Nguyen, G. Veeraraghavan, O. Mermer, M. Wohlgenannt, S. Qiu, and U. Scherf, Phys. Rev. B **74**, 045213 (2006).

[6] V. N. Prigodin, J. D. Bergeson, D. M. Lincoln, and A. J. Epstein, Synth. Met. **156**, 757 (2006).

[7] P. Desai, P. Shakya, T. Kreouzis, and W. P. Gillin, Phys. Rev. B **76**, 235202 (2007).

[8] P. A. Bobbert, T. D. Nguyen, F. W. A. van Oost, B. Koopmans, and M. Wohlgenannt, Phys. Rev. Lett. **99**, 216801 (2007).

[9] A. J. Schellekens, W. Wagemans, S. P. Kersten, P. A. Bobbert, and B. Koopmans, Phys. Rev. B **84**, 075204 (2011).

[10] B. Hu and Y. Wu, Nature Mater. **6** 985 (2007).

[11] F. J. Wang, H. Bässler, and Z. V. Vardeny, Phys. Rev. Lett. **101**, 236805 (2008).

[12] F. L. Bloom, W. Wagemans, M. Kemerink, and B. Koopmans, Phys. Rev. Lett. **99**, 257201 (2007).

[13] T. D. Nguyen, G. Hukic-Markosian, F. Wang, L. Wojcik, X.-G. Li, E. Ehrenfreund, and Z. V. Vardeny, Nat. Mater. **9**, 345 (2010).

[14] N. J. Harmon and M. E. Flatté, Phys. Rev. Lett. **108**, 186602 (2012); Phys. Rev. B **85**, 075204 (2012); Phys. Rev. B **85**, 245213 (2012).

[15] R. C. Roundy and M. E. Raikh, Phys. Rev. B **87**, 195206 (2013); R.C. Roundy, Z. V. Vardeny, and M. E. Raikh, Phys. Rev. B **88**, 075207 (2013).

[16] F. Wang, F. Macià, M. Wohlgenannt, A. D. Kent, and M. E. Flatté, Phys. Rev. X **2**, 021013 (2012); N. J. Harmon, F. Macià, F. Wang, M. Wohlgenannt, A. D. Kent, and M. E. Flatté, Phys. Rev. B **87**, 121203 (2013).

[17] W. J. Baker, K. Ambal, D. P. Waters, R. Baarda, H. Morishita, K. van Schooten, D. R. McCamey, J. M. Lupton, and C. Boehme, Nature Commun. **3**, 898 (2012).

[18] R. H. Dicke, Phys. Rev. **93**, 99 (1954).

[19] C. Boehme and K. Lips, Phys. Rev. B 68, 245105 (2003).

[20] D. R. McCamey, K. J. van Schooten, W. J. Baker, S.-Y. Lee, S.-Y. Paik, J. M. Lupton, and C. Boehme, Phys. Rev. Lett. **104**, 017601 (2010).

[21] R. Glenn, W. J. Baker, C. Boehme, and M. E. Raikh, Phys. Rev. B **87**, 155208 (2013).

PART II

INTERFERENCE OF PARTIAL SPIN ROTATION AND ORGANIC SPIN VALVES

CHAPTER 5

INTRODUCTION

5.1 Preface

The focus of Part I was a basic physical scenario when an electron and a hole emitted from *unpolarized* electrodes arrive to neighboring sites and wait to recombine. The role of the random hyperfine fields is the mixing of the spin states of the pair during the waiting time. In part II we switch to the scenario where the electrodes are *spin-polarized*. Suppose that the polarization of the electrodes is full. The current between the electrodes will flow only when the directions of their magnetization are parallel. This remark illuminates the importance of the hyperfine field in such a *spin-valve* geometry. Indeed, even if the magnetizations of the electrodes are opposite, the spin of an injected electron would experience a number of random precessions in local hyperfine fields as it travels between the electrodes. These physics are certainly well understood and the effectiveness of such a spin-memory loss is usually encoded into the phenomenological parameter, L_s, spin diffusion length, which is the property of the spin-valve active layer. The reality is, actually, more complicated since the spin-memory loss can take place also at the interfaces between the electrodes and the active layer. Still, the interfacial effects alone cannot account for the spin-memory loss in the spin valves. Experimental evidence for that is found in numerous experiments where the efficiency of the spin valve is quantified by the parameter, dubbed tunnel magnetoresistance (TMR), falls off exponentially with the active-layer thickness, d. In fact, the parameter L_s is inferred from an experiment by fitting the TMR with $\exp(-d/L_s)$ behavior.

The focus of Part II is the in-depth examination of the concept of L_s. Following we list the reasons why such an investigation is warranted:

- Conventional expression for the spin diffusion length is $L_s = (D\tau_s)^{1/2}$, where D is the *charge* diffusion coefficient, while τ_s is the spin-relaxation time. For hopping over the isolated sites the diffusion coefficient is $D = \ell^2/\tau$, where ℓ is the distance between the sites, and τ is the waiting time for a hop. This definition immediately raises a

question: What is L_s in the deep hopping regime where *local* values of τ have an exponentially broad spread? This question is studied in the next section.

- Consider two subsequent hops exercised by a carrier. In the course of these hops its spin was subjected to two different on-site magnetic fields. In the standard calculation of L_s it is assumed that the corresponding spin rotations are uncorrelated. Our main finding is that, since the *matrices* describing these spin rotations do not commute, the net rotation after two hops does not reduce to the sum of partial rotations. It appears that this net rotation depends crucially on the mutual orientations of the local fields. This question is studied in detail in Chapter 6. Moreover, as it is demonstrated in Chapter 7, the net spin rotation after a large number of unidirectional hops is a fingerprint of the realization of hyperfine fields along the carrier path.

- In Chapter 8 we examine a text-book derivation of τ_s in the bulk material and find that τ_s might admit very nontrivial corrections. The origin of these corrections lies in the fact that the diffusive motion of a carrier leads to a correlated character of the hyperfine field "sensed" by the carrier spin. This is due to the self-intersections of the random-walk trajectories. In low dimensions the role of self-intersections is prominent, and these corrections manifest themselves in the acceleration of spin relaxation. However, in all dimensions these corrections lead to anomalous sensitivity of the spin relaxation to a weak external magnetic field.

5.2 Hyperfine-field limited spin transport in the deep hopping regime

The leading source of spin-relaxation in traditional semiconductors, like GaAs, is spin-orbit coupling. The time over which a diffusively moving electron "forgets" its initial spin orientaton is given by [1]

$$\tau_s = \frac{1}{\Omega^2 \tau}, \tag{5.1}$$

where Ω is spin-orbit magnetic field, and τ is the scattering time. The physical picture underlying the Dyakonov-Perel mechanism Eq. (5.1) implies that the spin rotation angle, $\delta\varphi \sim \Omega\tau$, in the course of one scattering act is small, $\delta\varphi \ll 1$. Spin relaxation time manifests itself in optical experiments, see Ref. [2], while in studies of spin-polarized transport [3] the relevant quantity is the spin diffusion length

$$L_s = \left(\frac{\tau_s}{\tau}\right)^{1/2} \ell = \frac{\ell}{\delta\varphi}, \tag{5.2}$$

where ℓ is the mean free path.

An alternative mechanism of spin relaxation is the spin precession in the random hyperfine field of nuclei. In traditional semiconductors this mechanism is inefficient as long as electrons are free; its role becomes more prominent for very low carrier densities [2]. Meanwhile, this mechanism plays a crucial role in organic semiconductors. As it was explained, this is because of the low atomic numbers of elements from which the organic semiconductor is made. Also different from more traditional semiconductors is that the carrier mobilities in organic semiconductors are extremely low, on the order of $10^{-2}\text{cm}^2/\text{Vs}$, so that the transport can be better modeled as a sequence of inelastic hops over sites than the elastic diffusion of a carrier between the scatterers [4]. Certainly, describing the transport in organic materials as "hard-core" hopping, as in amorphous Si or Ge [5], is a big stretch. This description is adequate when the material is truly insulating, exhibits exponential growth of conductivity with temperature, and a typical log-resistance is ~ 10. No such features are observed in organic semiconductors. Still, in this chapter we will adopt the assumption that hopping is an adequate description. The purpose for which we do it is the following: Spin relaxation in a deep insulating regime possesses unique *qualitative* features, which we intend to uncover in the present chapter and describe on a semiquantitative level. The most important outcome of our analysis is the modified, compared to Eq. (5.2), expression for the spin diffusion length. On a very basic level, the reason why L_s gets modified in the hopping regime is that, among the hops with exponentially broad distribution of waiting times, those responsible for current flow are the so-called critical hops, which are sparse. Meanwhile the carrier suffers a disproportionately big spin memory loss in course of these hops.

Our qualitative analysis uncovers delicate features of L_s in the hopping regime which are hard to deduce from numerical simulations (Ref. [8]). In particular, we find that L_s contains a correlation length, R, of the current-carrying cluster and thus the *critical exponent*, ν, of the percolation network [9]. This is unlike the charge transport, where the resistance is determined by much shorter length, r_c, of the critical hop. We also find that the dependence of L_s on magnetic field, B, is *nonmonotonic*.

5.2.1 L_s in the hopping regime.

The term spin diffusion implies that the carrier of spin exercises a random walk. For free electrons each step of the random walk is one mean free path length, ℓ. In the hopping regime, the electron changes direction after each hop of length r, so it is tempting to replace ℓ by r. Our main point is that, such a replacement would be incorrect. This is because the charge transport becomes diffusive only at scales much larger than r. This

is a delicate property of the random-resistor network, that at the percolation threshold it becomes spatially homogeneous only starting from distances $\mathcal{L}_c \gg r$, where $\mathcal{L}_c$ is the correlation radius of the critical cluster [9], see Fig. 5.1. To express it through r, the equivalent resistance, R_{ij} between the sites i and j is presented as $\exp \xi_{ij}$, where ξ_{ij} is either tunneling or activation exponent. Percolation threshold ξ_c is determined from the condition that subnetwork of resistors with $\xi_{ij} < \xi_c$ conducts. Upon approach to the threshold the size of critical cluster diverges as

$$\mathcal{L}(\xi) = r \left(\frac{\xi_c}{\xi_c - \xi} \right)^{\nu}, \tag{5.3}$$

where $\nu \approx 0.9$ is the critical exponent. Only clusters with $\xi - \xi_c \sim 1$ are important for transport, so that $\mathcal{L}_c = r\xi_c^{\nu}$. While the length $\mathcal{L}_c$ does not manifest itself in the charge transport, it can be germane for spin transport if the carrier "remembers" its spin direction while it hops over the distance $\mathcal{L}_c$. In the latter case $\mathcal{L}_c$ assumes the role of ℓ and we get

$$L_s = \frac{\mathcal{L}_c}{\delta\varphi_c}. \tag{5.4}$$

We will consider the nearest-neighbor hopping regime, which takes place at high temperatures. The log-resistance is given by $\xi = \frac{2r_c}{a}$, where a is the localization radius. Large value of ξ ensures that the correlation length and critical hopping length differ strongly, $R \sim \xi^{\nu} r_c$, see Fig. 5.1. Our main message is that R manifests itself in spin transport because spin "memory" is preserved over many hops. At scales larger than R the hopping system becomes homogeneous and the transport acquires a diffusion character. Thus, the length, R, assumes the role of the mean free path in Eq. (5.2), and we arrive to the following generalization of the spin-diffusion length to the hopping regime

$$L_s = \frac{R}{\delta\varphi}, \tag{5.5}$$

where $\delta\varphi$ is the rms spin rotation angle over the length R. Next we note that, unlike spin-orbit coupling when electron spin is rotated in course of tunneling to the neighboring site [10], hyperfine field rotates electron spin while it *waits* for the hop [11]. Since the waiting times are exponentially broadly distributed, the largest being $\tau_c = \tau_0 \exp(2r_c/a)$, where τ_0 is a prefactor, we conclude that $\delta\varphi$ is governed by a single critical hop.

To make the correlation length "visible" one needs to introduce a length scale much bigger than r_c. One example is an amorphous film [9] with thickness $L \gg r_c$. Then R enters the resistance via the correction $\delta\xi \sim (R/L)^{1/\nu}$. Our main message is that spin transport sets a large length-scale *internally* and allows R to manifest itself in the spin-diffusion

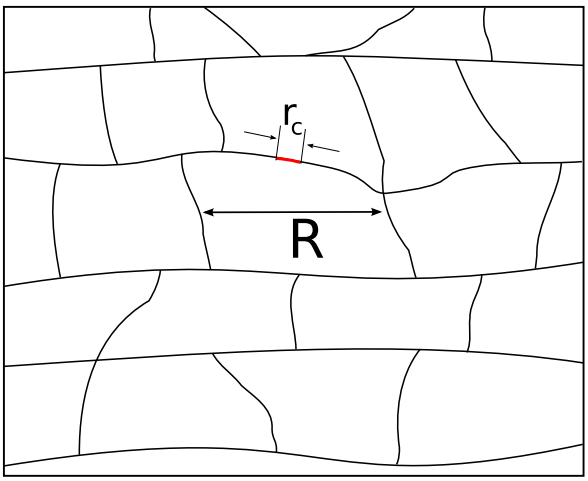

Figure 5.1: Schematic view of the backbone of a percolation cluster. R indicates the correlation radius, while r_c is the critical hopping distance within a "unit cell."

length, L_s. Indeed, the waiting times of the hops on the current-carrying cluster, Fig. 5.1 are broadly distributed, the largest being $\tau_c = \tau_0 \exp(2r_c/a)$, where τ_0 is a prefactor. Unlike spin-orbit coupling, when electron spin is rotated in the course of tunneling to the neighboring site [10], hyperfine field rotates electron spin while it *waits* for the hop [11].

If the spin of the hopping electron is rotated by $\delta\varphi \ll 1$ during the time τ_c, then the initial direction of spin will be nearly preserved up to the length, R, see Fig. 5.1. On the other hand, at scales bigger than R the system gets homogenized. The charge transport at these scales becomes diffusive, i.e. the length, R, assumes the role of the mean free path in Eq. (5.2). Then we arrive to the following generalization of the spin-diffusion length to the hopping regime

$$L_s = \frac{R}{\delta\varphi(\tau_c)}, \tag{5.6}$$

where $\delta\varphi(\tau_c)$ is the rms spin rotation angle during the time τ_c.

Note that Eq. (5.6) does not apply when the external field B exceeds the hyperfine field b_0. In the presence of $\boldsymbol{B}$ one should introduce *two* spin-diffusion lengths, $L_s^{\perp}$ and $L_s^{\parallel}$, depending on initial orientation of electron spin with respect to $\boldsymbol{B}$.

5.2.2 Calculation of $\delta\varphi$.

Even in a given hyperfine field, $\boldsymbol{b}$, the rotation angle, $\delta\varphi$, is a random quantity, since the waiting times are random with distribution $\frac{1}{\tau_c}\exp[-\tau/\tau_c]$. A rigorous definition of $\delta\varphi$ is $\langle\delta\varphi^2\rangle_\tau = p_{\uparrow\downarrow}(\tau_c)$, where $p_{\uparrow\downarrow}(\tau_c)$ is the spin-flip probability. For initial orientation of spin along the z-axis this probability is easy to find using the following expression for the time evolution of the operator $\widehat{S}_z$.

$$\widehat{S}_z(t) = \frac{1}{2}\Big\{[\sigma_z - n_z(\boldsymbol{n}\cdot\boldsymbol{\sigma})]\cos(\Omega t) + [\boldsymbol{n}\times\boldsymbol{\sigma}]_z \sin(\Omega t) + n_z(\boldsymbol{n}\cdot\boldsymbol{\sigma})\Big\}. \tag{5.7}$$

Here, $\boldsymbol{n}$, is the unit vector along the effective field $\boldsymbol{\Omega} = \boldsymbol{B} + \boldsymbol{b}$, and $\boldsymbol{\sigma}$ is the spin operator. Expressing $p_{\uparrow\downarrow}(t)$ as $\frac{1}{2} - \langle\uparrow|\,\widehat{S}_z(t)\,|\uparrow\rangle$, and performing the averaging over waiting times τ we get

$$p_{\uparrow\downarrow}(\tau_c) = \frac{1}{2}(1 - n_z^2)\frac{\Omega^2\tau_c^2}{1+\Omega^2\tau_c^2}. \tag{5.8}$$

In principle, the spin-flip probability upon hopping the distance, R, should account for all hops constituting a unit cell of the critical network, Fig. 5.1. The number of these hops can be estimated as $N \sim R/r_c$. The latter estimate neglects the tortuosity of the sides of the unit cells, which is permissible in three-dimensions [9]. Then the full spin-flip probability is given by

$$P_{\uparrow\downarrow}(\tau_c) = 1 - \prod_{i=1}^{N}\Big(1 - p_{\uparrow\downarrow}(\tau_i)\Big) \approx \sum_{i=1}^{N} p_{\uparrow\downarrow}(\tau_i). \tag{5.9}$$

The second identity in Eq. (5.9) accounts for the fact that spin diffusion length has a meaning when the product in Eq. (5.9) is close to 1. It also justifies neglecting double spin flips.

As we alluded to in the Introduction, in a zero external field when the sum in Eq. (5.9) reduces to $\sum_{i=1}^{N} b_i^2\tau_i^2$, one can restrict the summation to a single term corresponding to the critical hop. This is because the waiting times $\tau_i = \tau_0 \exp[2r_i/a]$ are broadly spread. Then, after averaging Gaussian distribution of hyperfine fields with rms b_0, we get

$$L_s = \frac{R}{b_0\tau_0} \exp\Big[-\frac{2r_c}{a}\Big]. \tag{5.10}$$

Eq. (5.10) is the main result of the present chapter. It should be compared to the "metallic" expression, Eq. (5.2), for L_s. The difference amounts to

$$\frac{\ell}{\delta\varphi_{\text{typical}}} \to \frac{R}{\delta\varphi_c}. \tag{5.11}$$

As a side remark, we note that the spin-diffusion length limited by the hyperfine fields gets longer upon increasing temperature, since the waiting times become shorter.

Full summation in Eq. (5.9) becomes necessary in strong external field such that $B\tau_c \gg 1$. In this limit the denominator in Eq. (5.8) is big, while $\boldsymbol{n}_z$ is close to 1. Then the waiting times drop out of Eq. (5.9), and we get $p_{\uparrow\downarrow}(\tau_i) \approx \frac{1}{B^2}\left(b_{ix}^2 + b_{iy}^2\right)$, which leads to the following result for L_s.

$$L_s^{\parallel} = \frac{R}{\sqrt{N\frac{b_0^2}{B^2}}} = \sqrt{R\,r_c}\Big(\frac{B}{b_0}\Big). \tag{5.12}$$

We see that, unlike the case $B = 0$, the spin-diffusion length is proportional to $R^{1/2}$. We also note that both the prefactor and the magnetic field dependence in our result Eq. (5.12) differ from the empirical expression for L_s in Ref. [8], where it was inferred from numerical simulations. With regard to $L_s^{\perp}$, in the limit $B\tau_c \gg 1$, there is no spin diffusion, since the spin memory is lost while waiting for the critical hop.

As was mentioned above, the deep hopping regime is not particularly adequate for description of transport in realistic organic semiconductors. What does apply from the above description is that the carrier does move from site to site and each site is characterized by a random hyperfine field. However, there is no exponential spread of the waiting times over different hops. In the chapters that follow we demonstrate that within the scenario where spin-relaxation is still due to hyperfine fields, but all of the hops are essentially

equivalent, the description of spin-relaxation becomes quite delicate. This leads to such phenomena as sign-reversal of local tunnel magnetoresistance [TMR] (Chapter 6), giant fluctuations of local TMR (Chapter 7), and even *nonexponential* time dependence of spin relaxation (Chapter 8).

5.3 References

[1] M. I. Dyakonov and V. I. Perel, Sov. Phys. Solid State **13**, 3023 (1971).

[2] R. I. Dzhioev, K. V. Kavokin, V. L. Korenev, M. V. Lazarev, B. Y. Meltser, M. N. Stepanova, B. P. Zakharchenya, D. Gammon, and D. S. Katzer, Phys. Rev. B **66**, 245204 (2002).

[3] I. Zutić, J. Fabian, and S. Das Sarma, Rev. Mod. Phys. **76**, 323 (2004).

[4] N. J. Harmon and M. E. Flatté, Phys. Rev. Lett. **108**, 186602 (2012); Phys. Rev. B **85**, 075204 (2012); Phys. Rev. B **85**, 245213 (2012).

[5] J. J. Hauser, Phys. Rev. Let. **29**, 476 (1972).

[6] P. A. Bobbert, T. D. Nguyen, F. W. A. van Oost, B. Koopmans, and M. Wohlgenannt, Phys. Rev. Lett. **99**, 216801 (2007).

[7] S. P. Kersten, S. C. J. Meskers, and P. A. Bobbert, Phys. Rev. B **86**, 045210 (2012).

[8] P. A. Bobbert, W. Wagemans, F. W. A. van Oost, B. Koopmans, and M. Wohlgenannt, Phys. Rev. Lett. **102**, 156604 (2009).

[9] B. I. Shklovskii and A. L. Efros, *Electronic Properties of Doped Semiconductors* (Springer-Verlag, Berlin, 1984).

[10] B. I. Shklovskii, Phys. Rev. B **73**, 193201 (2006).

[11] N. J. Harmon, M. E. Flatté, arXiv:1304.3400.

CHAPTER 6

TUNNEL MAGNETORESISTANCE IN ORGANIC SPIN VALVES IN THE REGIME OF MULTISTEP TUNNELING

6.1 Introduction

A spin valve is a device the resistance of which, $R_{\uparrow\uparrow}$ or $R_{\uparrow\downarrow}$, depends on the mutual orientation ($\uparrow\uparrow$ or $\uparrow\downarrow$) of magnetization directions in ferromagnetic electrodes. Quantitative measure of the effectiveness of a spin valve is the tunnel magnetoresistance [1, 2] which is expressed via the electrode polarizations, $\mathcal{P}_1$ and $\mathcal{P}_2$, as follows

$$\mathrm{TMR} = \frac{\Delta R}{R_{\uparrow\uparrow}} = \frac{R_{\uparrow\downarrow} - R_{\uparrow\uparrow}}{R_{\uparrow\uparrow}} = \frac{2\mathcal{P}_1\mathcal{P}_2}{1 - \mathcal{P}_1\mathcal{P}_2}, \tag{6.1}$$

If the thickness, L, of the active layer is large enough, the spin orientation of injected electrons is "forgotten" in the course of transport between the electrodes. Usually this effect is taken into account by multiplying the product $\mathcal{P}_1\mathcal{P}_2$ by a factor $\exp(-L/l_s)$, where l_s is the spin-diffusion length.

The use of the concept of spin diffusion implies that while traveling between the electrodes, the electron experiences many scattering events, and for each event the spin rotation is weak. Under these conditions the spin polarization is a continuous function of the coordinate. More generally, the product $\mathcal{P}_1\mathcal{P}_2$ should be multiplied by $(1 - 2P_{\mathrm{sf}})$, so that

$$\mathrm{TMR} = \frac{2\mathcal{P}_1\mathcal{P}_2(1 - 2P_{\mathrm{sf}})}{1 - \mathcal{P}_1\mathcal{P}_2(1 - 2P_{\mathrm{sf}})}, \tag{6.2}$$

where P_{sf} is the probability that the electron flips its spin over the distance L. Then Eq. (6.2) applies even when the spin rotation in the course of a scattering event is not small, i.e., the initial spin orientation is "forgotten" after only a few events. The factor $(1 - 2P_{\mathrm{sf}})$ emerges in Eq. (6.2) if one takes into account that, as a result of spin-flips in the active layer, the states with spin, say, $\uparrow$, in the left electrode are coupled to the states $\uparrow$ in the right electrode with probability $1 - P_{\mathrm{sf}}$ and to the states $\downarrow$ with probability P_{sf}. Although

Eq. (6.2), for the particular case $(1-2P_{\rm sf}) = \exp(-{\rm L}/l_s)$ appears in many sources, for completeness, we present its derivation in Appendix 6.5.

In the present chapter we assume that the underlying mechanism responsible for $P_{\rm sf}$ is the spin rotation in hyperfine magnetic fields. This situation is generic for organic spin valves [3, 4, 5, 6, 7, 8, 9, 10]. In Ref. [11] experimental data on spin valves with an organic active layer were analyzed. The results were interpreted within a model in which the tunnel transport through the active layer proceeds in two steps: First tunneling from the left electrode L (see Fig. 6.1) to a localized state in the middle, and, subsequently, to the right electrode R. This "stop" near the middle of the active layer increases the overall tunnel probability from $\exp(-{\rm L}/a)$ to $\exp(-{\rm L}/2a)$, where a is the under-barrier tunneling length. At the same time, while the electron waits to tunnel into R, its spin is subject to a hyperfine magnetic field created by surrounding nuclei. If the average waiting time is τ, the expression for $P_{\rm sf}$ takes the form

$$P_{\rm sf}^{(0)} = \frac{1}{2}\frac{\left(\Omega^2 - \Omega_z^2\right)\tau^2}{1+\Omega^2\tau^2}, \tag{6.3}$$

where Ω is the total magnetic field at the site (in frequency units), and Ω_z is the projection of this field on the direction of magnetization; z-direction is determined by the magnetization in the electrode L.

Upon gradual increase of the thickness, the transport will be dominated by three-step tunneling, then four-step tunneling, and so on [12]. Rigorous treatment [13] demonstrates that the number of steps, N, grows with the thickness, L, as $N = \sqrt{L/a}$. In the present chapter we study in detail the domain of lengths where the transport is via three-step tunneling, as illustrated in Fig. 6.1. This regime is still analytically tractable, and yet reveals fundamental features which are germane to multistep transport and are lacking in the two-step regime. These features are:

(i) TMR is strongly affected by the fact that the *amplitude* for the net spin rotation is the sum of amplitudes for the rotations taking place when the electron waits for the hop on site 1 and on site 2. We show that this addition of amplitudes rather than probabilities can lead to *negative* TMR, and explore the domain in which the sign reversal of TMR occurs.

(ii) If the waiting time for the hop $2 \to R$ is long, the electron *bounces* between the sites 1 and 2 while awaiting the hop $2 \to R$. This bouncing, which has absolutely no effect on the current, can strongly affect the spin rotation.

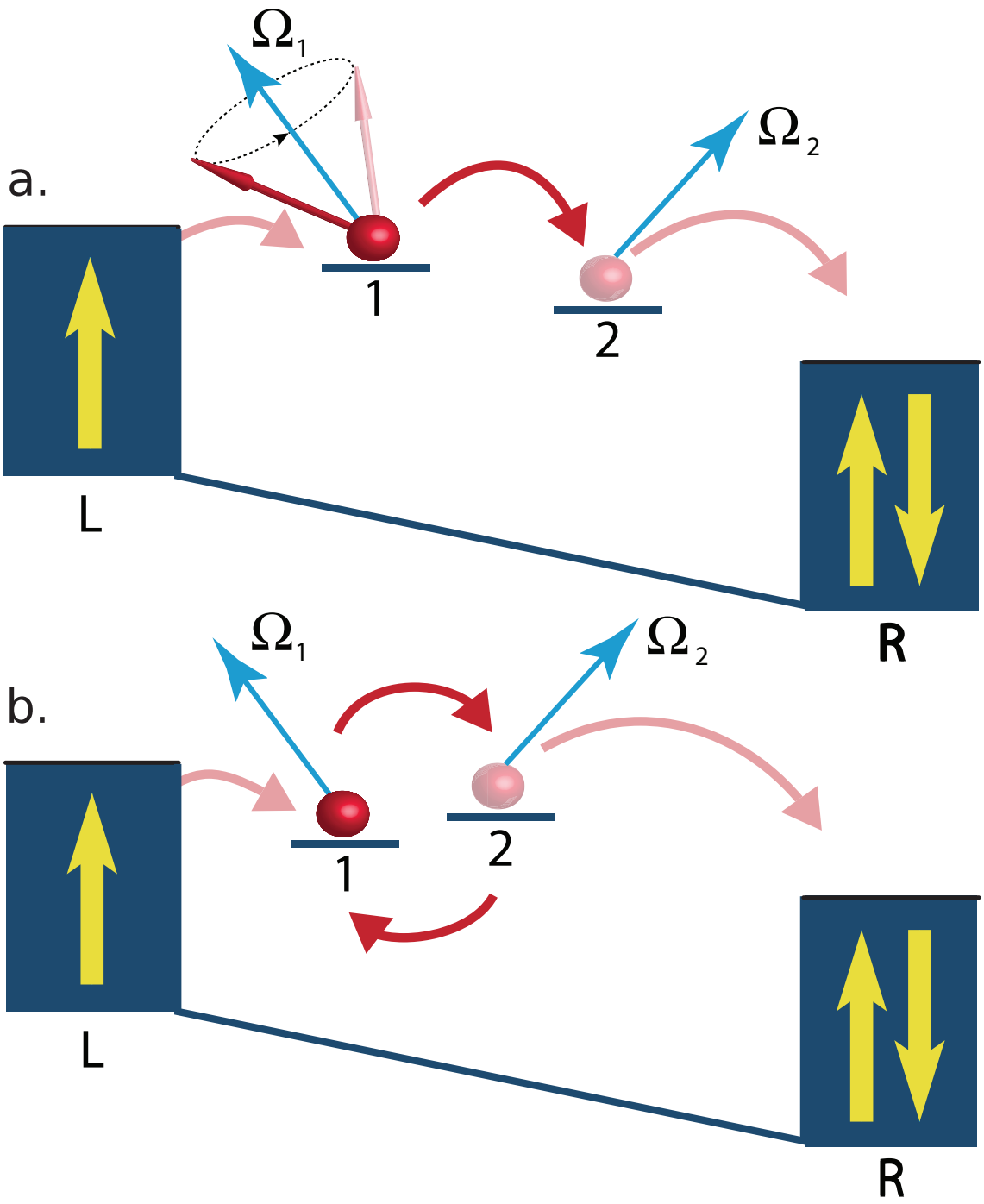

Figure 6.1: Schematic illustrations of the regimes of hopping transport between the electrodes: (a) Illustration of the regime of transport between ferromagnetic electrodes, L and R, dominated by hops via intermediate sites 1 and 2. Spin precession in the hyperfine fields takes place while the electron waits for the hops $1 \to 2$ and $2 \to R$. Bias is assumed large, so that all hops are unidirectional; (b) When the sites 1 and 2 are close in energy, electron bounces $2 \to 1 \to 2$ many times while waiting for the "long" hop $2 \to R$.

Both of the above findings have quantum interference at their core. In this regard note that, while electron hops are incoherent, the spin evolution in the course of these hops remains *fully coherent*. The fact that the times spent by the electron on each site are random tends to average out the interference effects. It is thus nontrivial that interference effects survive this averaging, and manifest themselves in the limit $\Omega\tau \gg 1$, when the typical spin rotation is strong.

The chapter is organized as follows. In Sect. 6.2 we consider the transport via two sites at high bias when the electron moves only forward. In Sect. 6.3 we relax this condition and allow fast backward hops while awaiting the slow forward hop. For both situations we calculate $P_{\rm sf}$ averaged over the random durations of the waiting periods, which should be substituted into Eq. (6.2). We pay special attention to $P_{\rm sf}$ in the presence of external magnetic field in view of mysterious absence of the Hanle effect in spin valves reported recently [14, 15]. In Sect. 6.4 we discuss the implications of our findings for true multistep or bulk transport.

6.2 Interference correction to the two-step spin-flip probability

6.2.1 Analytical expression for $P_{\rm sf}$

Under a strong applied bias the motion of the electron is unidirectional. The hops proceed in a sequence $L \to 1 \to 2 \to R$. Denote with t_1 and t_2 the random times spent by electron on sites 1 and 2, respectively. The evolution of spin is described by the product of the unitary matrices $U(t_2)U(t_1)$, where the matrix $U(t)$ is defined as

$$U(t) = \begin{bmatrix} \cos\alpha - i\frac{\Omega_z}{\Omega}\sin\alpha & -i\frac{\Omega_-}{\Omega}\sin\alpha \\ -i\frac{\Omega_+}{\Omega}\sin\alpha & \cos\alpha + i\frac{\Omega_z}{\Omega}\sin\alpha \end{bmatrix}, \ \alpha = \frac{\Omega t}{2}, \tag{6.4}$$

where $\Omega_\pm = \Omega_x \pm i\Omega_y$. The spin-flip amplitude is given by a nondiagonal element, $A_{\uparrow\downarrow} = -i\frac{\Omega_+}{\Omega}\sin\left(\frac{\Omega t}{2}\right)$. Averaging of $p_{\uparrow\downarrow} = |A_{\uparrow\downarrow}|^2$ over the Poisson distribution, $\frac{1}{\tau}\exp(-t/\tau)$, of the waiting time, t, reproduces Eq. (6.3).

The spin-flip amplitude after two steps is given by the nondiagonal element of $U(t_2)U(t_1)$. It can be written in the form

$$\tilde{A}_{\uparrow\downarrow} = A^{(1)}_{\uparrow\downarrow}A^{(2)}_{\downarrow\downarrow} + A^{(1)}_{\uparrow\uparrow}A^{(2)}_{\uparrow\downarrow}, \tag{6.5}$$

where $A^{(1,2)}$ are the corresponding elements of the matrices $U(t_1)$ and $U(t_2)$. Averaging of $P_{\rm sf} = |\tilde{A}_{\uparrow\downarrow}|^2$ over random times t_1, t_2, can be easily carried out. First, it is convenient to present $P_{\rm sf}$ in the form

$$P_{\rm sf} = P_{\rm incoh} + \delta P_{\rm int} \tag{6.6}$$

of the sum of incoherent and interference contributions defined as

$$P_{\rm incoh} = p_{\rm sf}^{(1)}\left(1-p_{\rm sf}^{(2)}\right) + \left(1-p_{\rm sf}^{(1)}\right)p_{\rm sf}^{(2)}, \tag{6.7}$$

where $p_{\rm sf}^{(1)}$ and $p_{\rm sf}^{(2)}$ are the partial probabilities given by Eq. (6.3), and

$$\delta P_{\rm int} = 2\langle {\rm Re}\left(A_{\uparrow\downarrow}^{(1)}A_{\downarrow\downarrow}^{(2)}A_{\uparrow\uparrow}^{(1)*}A_{\uparrow\downarrow}^{(2)*}\right)\rangle_{t_1,t_2}. \tag{6.8}$$

Averaging of $\delta P_{\rm int}$ over t_1 and t_2 can be performed independently. The product of the terms depending on t_1 is

$$A_{\uparrow\downarrow}^{(1)}A_{\uparrow\uparrow}^{(1)*} = \left[-i\frac{\Omega_{1+}}{\Omega_1}\sin\left(\frac{\Omega_1 t_1}{2}\right)\right]\times\left[\cos\left(\frac{\Omega_1 t_1}{2}\right)+i\frac{\Omega_{1z}}{\Omega_1}\sin\left(\frac{\Omega_1 t_1}{2}\right)\right]. \tag{6.9}$$

Denote with τ_1 the average waiting time for the hop $1\to 2$. Averaging of Eq. (6.9) over t_1 yields a compact expression

$$\langle A_{\uparrow\downarrow}^{(1)}A_{\uparrow\uparrow}^{(1)*}\rangle_{t_1} = \frac{1}{2}\frac{\Omega_{1+}\tau_1(-i+\Omega_{1z}\tau_1)}{1+\Omega_1^2\tau_1^2}. \tag{6.10}$$

The same expression with τ_2 instead of τ_1 and Ω_2 instead of Ω_1 together with an additional complex conjugation describes the result of averaging over t_2. Altogether, the expression for $\delta P_{\rm int}$ can be cast in the form

$$\delta P_{\rm int} = \frac{1}{2}{\rm Re}\left(\frac{\Omega_{1+}\Omega_{2-}\tau_1\tau_2(1+i\Omega_{1z}\tau_1)(1-i\Omega_{2z}\tau_2)}{(1+\Omega_1^2\tau_1^2)(1+\Omega_2^2\tau_2^2)}\right). \tag{6.11}$$

At this point note that, within the probabilistic approach, the result for $P_{\rm sf}$ would be simply $P_{\rm incoh}$. Indeed, within this approach the net spin flip corresponds to flipping on the first site and preserving spin on the second site or vice versa. Since these are mutually exclusive events their probabilities simply add. Because of this, $\delta P_{\rm int} = P_{\rm sf} - P_{\rm incoh}$ is a measure of quantum interference of the amplitudes of two rotations that took place at site 1 and at site 2.

Throughout this subsection we implicitly identified $P_{\rm sf}$ with the spin-flip probability which appears in Eq. (6.2). It is, however, not entirely obvious that the quantum-mechanical quantity $P_{\rm sf}(t_1,t_2)$ averaged over the Poisson distribution of the waiting times is the same quantity which appears in Eq. (6.2). Formal justification is presented in Appendix 6.5.

In the next subsection we analyze several particular cases when the interference term has dramatic consequences for TMR.

6.2.2 Limiting cases

It is instructive to express the result Eq. (6.9) via the partial probabilities $p_{\rm sf}^{(1)}$ and $p_{\rm sf}^{(2)}$ as follows

$$\delta P_{\rm int} = \sqrt{p_{\rm sf}^{(1)}\left(1-2p_{\rm sf}^{(1)}\right)p_{\rm sf}^{(2)}\left(1-2p_{\rm sf}^{(2)}\right)}\cos\phi, \tag{6.12}$$

where the phase ϕ is defined as

$$\phi = \varphi_1 - \varphi_2 + \tan^{-1}(\Omega_1\tau_1\cos\vartheta_1) - \tan^{-1}(\Omega_2\tau_2\cos\vartheta_2). \tag{6.13}$$

The angles ϑ_1, φ_1 (ϑ_2, φ_2) are the spherical angles describing the polar and azimuthal orientations of the vector $\mathbf{\Omega}_1$ ($\mathbf{\Omega}_2$). Eqs. (6.12), (6.13) indicate that interference can be either constructive of destructive depending on the mutual orientations of the fields $\mathbf{\Omega}_1$, $\mathbf{\Omega}_2$. When $\Omega_1\tau_1$ and $\Omega_2\tau_2$ are of the same order, the interference correction is of the order of $P_{\rm incoh}$.

6.2.2.1 Identical fields, $p_{sf}^{(1)} = p_{sf}^{(2)}$

The role of interference is maximal when the vectors $\mathbf{\Omega}_1$ and $\mathbf{\Omega}_2$ are collinear and $\Omega_1\tau_1 = \Omega_2\tau_2$. Then we have

$$P_{\rm sf} = 2p_{\rm sf}(1-p_{\rm sf}) + p_{\rm sf}(1-2p_{\rm sf}) = 3p_{\rm sf} - 4p_{\rm sf}^2. \tag{6.14}$$

To illuminate the nontriviality of Eq. (6.14), note that the single-scattering value, $p_{\rm sf}$, never exceeds 1/2. Equally the incoherent part of the two-scattering probability, $P_{\rm incoh}$, never exceeds 1/2. The physical meaning of these restrictions is obvious: $p_{\rm sf} = 1/2$ implies a full loss of the spin memory. Therefore, if *either* of two values of $p_{\rm sf}$ in Eq. (6.7) is equal to 1/2, we get $P_{\rm incoh} = 1/2$ regardless of the value of the other $p_{\rm sf}$. Interestingly, the exact $P_{\rm sf}$ does not satisfy this restriction. Similarly to $P_{\rm incoh}$, Eq. (6.14) does yield 1/2, for $p_{\rm sf} = 1/2$, when the interference term vanishes. However, the value of $P_{\rm sf}$ can actually *exceed* 1/2 for smaller $p_{\rm sf}$. Namely, at $p_{\rm sf} = 3/8$, Eq. (6.14) has a maximum and assumes the value $P_{\rm sf} = 9/16$. This implies that the TMR, defined by Eq. (6.1), is *negative* for this $p_{\rm sf}$. Moreover, it retains negative value within the domain $1/4 < p_{\rm sf} < 1/2$. Physically, this means that the resistance for antiparallel orientations of magnetization in the electrodes is *smaller* than for the parallel orientation.

In fact, negative values of TMR happen not only when the vectors $\mathbf{\Omega}_1$ and $\mathbf{\Omega}_2$ coincide. For illustration, assume that the product $\Omega_1\tau_1$ is still equal to $\Omega_2\tau_2$, but the vectors $\mathbf{\Omega}_1$ and $\mathbf{\Omega}_2$ are skewed by an angle ϕ. The domain $P_{\rm sf} = 1/2$ on the $(p_{\rm sf}, \phi)$-plane is shown in Fig. 6.2. The "allowed" values of ϕ range from 0 at $p_{\rm sf} = 1/4$ to $\pm\pi/2$ at $p_{\rm sf} = 1/2$.

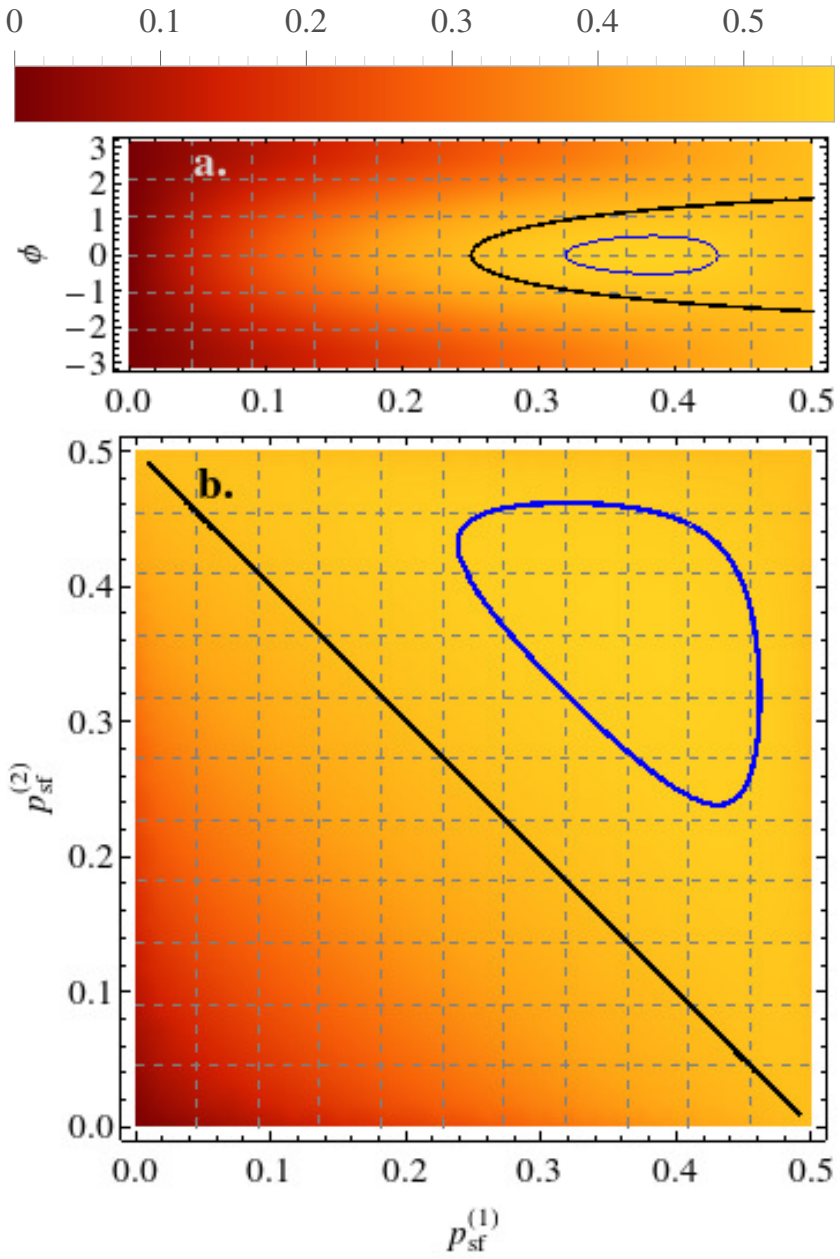

Figure 6.2: Calculated spin flip probabilities for a two step process are shown: (a) Contour plot of the cumulative spin-flip probability, P_{sf}, calculated from Eqs. (6.7) and (6.12). It is assumed that partial probabilities, $p_{sf}^{(1)}$ and $p_{sf}^{(2)}$, are the same (horizontal axis), while the hyperfine fields at sites 1 and 2 are skewed by angle ϕ (vertical axis). Black curve separates the domains with positive TMR (to the left) and negative TMR (to the right). Blue curve is a contour $P_{sf} = 0.55$. (b) Same as (a) for the limiting case when hyperfine fields are parallel, $\phi = 0$, but have different magnitudes, so that the partial probabilities $p_{sf}^{(1)}$)(horizontal axis) and $p_{sf}^{(2)}$ (vertical axis) are different. As ϕ increases, the domain of negative TMR shrinks and completely disappears at $\phi = \pi/2$.

To what degree is the assumption that the field magnitudes are precisely equal to each other crucial for negative TMR? To answer this question we have plotted in Fig. 6.2b, the contour plot of $P_{\rm sf}$ for configurations with $\phi = 0$ when $p_{\rm sf}^{(1)}$ and $p_{\rm sf}^{(2)}$ vary over their allowed values. We see that negative TMR corresponds to the domain above the diagonal of the square. This domain shrinks upon increasing ϕ.

6.2.2.2 Identical fields, many hops

In the example considered above the TMR was "most negative" when both hyperfine fields were equal, i.e., the hopping of the electron does not interrupt the spin precession at all. It might seem that this case should be reducible to the precession in one given field for which the result of Eq. (6.3) never goes above 1/2. The resolution lies in the fact that Eq. (6.3) was obtained upon averaging over exponential distribution of the waiting times. When *two* hops are performed in the same magnetic field, the distribution function of the two-hop waiting times is different: $F_2(T) = T/\tau^2 \exp(-T/\tau)$. It is because of this difference that $P_{\rm sf} > 1/2$ emerges. In this regard, it is interesting to consider what happens if an electron performed $N > 2$ steps in the same magnetic field. Then the distribution function of the waiting time is

$$F_N(T) = \frac{T^{N-1}}{\tau^N (N-1)!} \exp(-T/\tau). \tag{6.15}$$

With this distribution, the expression for spin-flip probability can be easily shown to take the form

$$P_{\rm sf} = \frac{|\Omega_+|^2}{2\Omega^2} \left[1 - \frac{\cos\left(N \sin^{-1} \frac{\Omega\tau}{\sqrt{1+\Omega^2\tau^2}} \right)}{(1+\Omega^2\tau^2)^{N/2}} \right]. \tag{6.16}$$

The situation most favorable for negative TMR is an in-plane orientation of magnetic field, when the prefactor in Eq. (6.16) is equal to 1/2. Then we have $P_{\rm sf} > 1/2$ in the domains of $\Omega\tau$ when the cosine is negative. These domains are shown in Fig. 6.3 for several values of N. We see that the net width of the domains with negative TMR does not change much with N, while the magnitude of negative TMR grows with increasing N.

Another message of Eq.(6.16) is that $P_{\rm sf}$ saturates with damped oscillations upon increasing N. The saturation value is $|\Omega_+|^2/2\Omega^2$. This saturation is the result of quantum interference. To illuminate this point, let us compare it to the result obtained via probabilistic treatment, i.e., neglecting interference

$$P_{\rm sf} = \frac{1}{2} \left(1 - \exp\left\{ -N \left| \ln\left(1 - \frac{|\Omega_+|^2\tau^2}{1+\Omega^2\tau^2} \right) \right| \right\} \right). \tag{6.17}$$

We see that neglecting quantum evolution leads to the intuitively obvious prediction that in the limit of large N, $P_{\rm sf}$ approaches 1/2 exponentially. The logarithm in the exponent

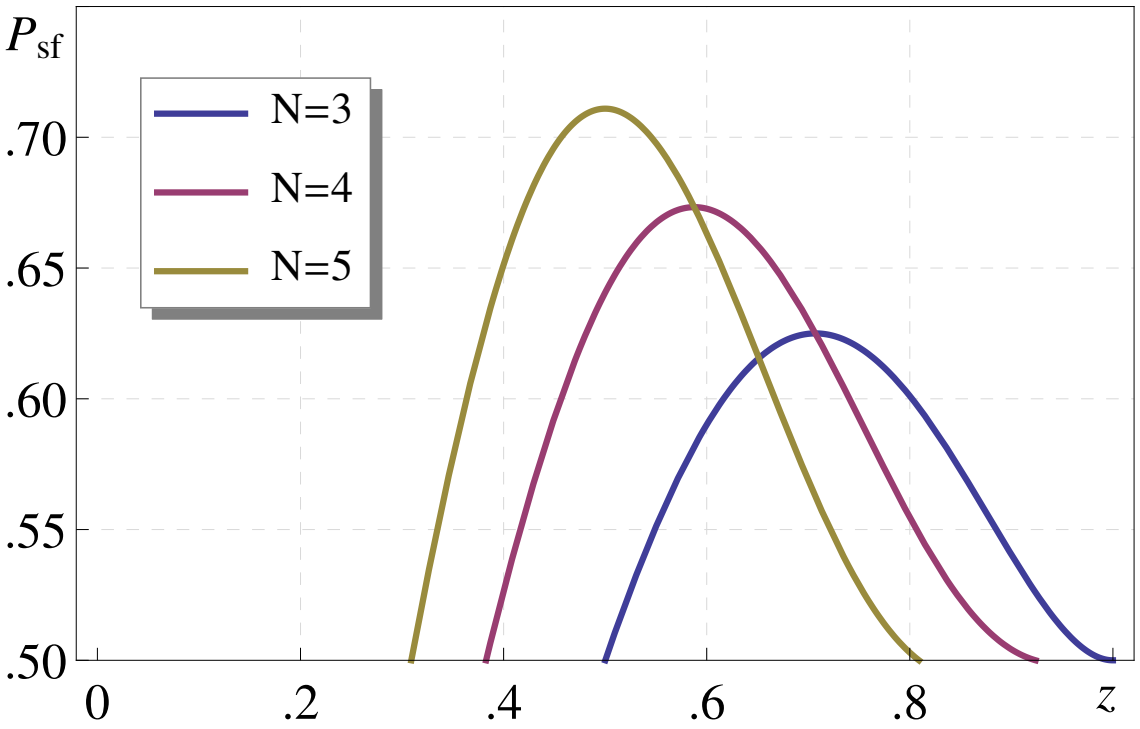

Figure 6.3: The spin-flip probability for N-step process is plotted from Eq. (6.16) versus dimensionless combination $z = \Omega\tau/(1+\Omega^2\tau^2)^{1/2}$ for $N = 3, 4, 5$. It is assumed that in-plane hyperfine fields, Ω, and waiting times, τ, are the same at all $(N-1)$ sites. Only the parts of the curves for which TMR is negative are shown.

relates the "time" of spin-memory loss to the hyperfine field magnitude [16]. The dramatic difference between Eq. (6.16) and Eq. (6.17) indicates that interference survives in spite of the fact that the individual hopping times are random. The fact that rotation of spin in a constant magnetic field can be nontrivial due to the randomness in the waiting times for subsequent hops was previously pointed out in Ref. [17].

6.2.2.3 Averaging over hyperfine fields

It is apparent from Eq. (6.12) that, since $\cos\phi$ is zero on average, the interference correction to $P_{\rm sf}$ vanishes upon averaging over hyperfine field distribution. This explains why the D'yakonov-Perel (DP) result of Ref. [18] for the spin relaxation time derived from probabilistic treatment remains valid in spite of the fact that spin rotations for subsequent electron steps are strongly correlated; a large number of electron collisions, each of which is accompanied by a small spin rotation [18], guarantees that the averaging takes place. Equally, the averaging happens for a spin valve with large area of the active layer. For a given path through the layer, $\delta P_{\rm int}$ can be of the order of $P_{\rm sf}$, but it will not contribute to the average spin-flip probability coming from many channels. If the area is finite, so that the number of channels, $N \gg 1$, is also finite, the averaging will be incomplete. The TMR will acquire a random correction of the order $\Delta/\sqrt{N}$, where Δ^2 is the variance of $P_{\rm sf}$, which we calculate below.

It follows from Eqs. (6.6), (6.12) that the variance has two contributions

$$\Delta^2 = \overline{P_{\rm sf}^2} - \left(\overline{P_{\rm sf}}\right)^2 = \Delta_{\rm incoh}^2 + \Delta_{\rm int}^2, \tag{6.18}$$

where $\Delta_{\rm incoh}^2$ and $\Delta_{\rm int}^2$ are the variances of the incoherent and coherent contributions, respectively. The overline stands for hyperfine averaging over the Gaussian distribution, $\frac{1}{\sqrt{\pi}b_0}\exp[-b_i^2/b_0^2]$, of the hyperfine-field components, b_i. Then the variance $\Delta_{\rm incoh}^2$ can be expressed through averages $\overline{p}_{1,2}$ and partial variances $\Delta_{1,2}^2 = \overline{p^2}_{1,2} - \left(\overline{p}_{1,2}\right)^2$ as follows

$$\Delta_{\rm incoh}^2 = (1-2\overline{p}_2)^2\Delta_1^2 + (1-2\overline{p}_1)^2\Delta_2^2 + 4\Delta_1^2\Delta_2^2. \tag{6.19}$$

The corresponding expression for the interference contribution, $\Delta_{\rm int}^2$, reads

$$\Delta_{\rm int}^2 = \frac{1}{2}\left[(\overline{p}_1+2\overline{p}_1^2)(\overline{p}_2+2\overline{p}_2^2) - 2(\overline{p}_2+2\overline{p}_2^2)\Delta_1^2 \ -2(\overline{p}_1+2\overline{p}_1^2)\Delta_2^2 + 4\Delta_1^2\Delta_2^2\right]. \tag{6.20}$$

Analytical expressions for $\overline{p}_{1,2}$ and $\Delta_{1,2}^2$ take a simple form in the limits of strong ($\Omega\tau \gg 1$) and weak ($\Omega\tau \ll 1$) magnetic fields:

$$\overline{p}_{1,2} = \begin{cases} b_0^2\tau_{1,2}^2, & \Omega_{1,2}\tau_{1,2} \ll 1 \\ \frac{1}{2}\int\limits_0^\infty \frac{ds}{(1+s)^{5/2}}\exp\left[-\frac{s}{1+s}\frac{B^2}{b_0^2}\right], & \Omega_{1,2}\tau_{1,2} \gg 1 \end{cases} \tag{6.21}$$

$$\Delta_{1,2}^2 = \begin{cases} b_0^4\tau_{1,2}^4, & \Omega_{1,2}\tau_{1,2} \ll 1 \\ -\overline{p}_{1,2}^2 + \frac{1}{2}\int\limits_0^\infty \frac{s\,ds}{(1+s)^{7/2}} \exp\left[-\frac{s}{1+s}\frac{B^2}{b_0^2}\right], & \Omega_{1,2}\tau_{1,2} \gg 1 \end{cases} \tag{6.22}$$

Here, B is the external field directed along the z-axis. Eq. (6.21) describes the fall-off of the disorder-averaged spin-flip probability with B. For weak hyperfine field, $b_0\tau \ll 1$, the dependence $\overline{p}_{1,2}(B)$ evolves from small value, $b_0^2\tau_{1,2}^2$, to $b_0^2/2B^2$. In the opposite limit, $b_0\tau \gg 1$, the evolution starts from $\overline{p}_{1,2}(0) = 1/3$ and converges to $b_0^2/2B^2$ when B exceeds b_0.

In the first case we have $\Delta_{\rm int}^2 \approx \overline{p}_1\overline{p}_2/2$, while $\Delta_{\rm incoh}^2 \approx \Delta_1^2 + \Delta_2^2$, so that for the ratio $\Delta_{\rm int}^2/\Delta_{\rm incoh}^2$ we get $\tau_1^2\tau_2^2/\left(\tau_1^4 + \tau_2^4\right)$, i.e. the interference contribution is of the same order as $\Delta_{\rm incoh}^2$. For strong hyperfine field, $\Delta_{\rm int}^2$ and $\Delta_{\rm incoh}^2$ do not depend on τ. At $B = 0$ Eq. (6.22) yields $\Delta_{1,2}^2 = \frac{1}{45}$. Using this value, we get for the contributions to the variance: $\Delta_{\rm incoh}^2 = \frac{7}{2}\left(\frac{2}{45}\right)^2$ and $\Delta_{\rm int}^2 = \frac{1}{2}\left(\frac{23}{45}\right)^2$, i.e., the interference contribution is almost 20 times bigger than the incoherent contribution. Finally, consider the limit of strong hyperfine field and $B \gg b_0$. In this limit Eq. (6.22) yields $\Delta_{1,2}^2 = b_0^4/2B^4$, and we thus have:

$$\Delta_{\rm int}^2 = \frac{\overline{p}_{1,2}^2}{2} = \frac{b_0^4}{8B^4}, \quad \Delta_{\rm incoh}^2 = 2\Delta_{1,2}^2 = \frac{b_0^4}{B^4} = 8\Delta_{\rm int}^2. \tag{6.23}$$

In summary, for all the domains of change of the dimensionless parameters, $b_0\tau$ and b_0/B, the variance, Δ, of the spin-flip probability is of the order of average $P_{\rm sf}$, and the interference contribution to Δ is comparable to Δ itself.

In conclusion of this section, note that for $\tau_2 \gg \tau_1$, the hops $1 \to 2$ between the sites do not affect the current. Except for anomalous configurations of hyperfine fields, when $\Omega_{2\perp}$ is much smaller than $\Omega_{1\perp}$, these hops also do not affect the spin memory. In the next section we will demonstrate that multiple *bounces* of electron within a pair of sites, while not affecting the current, can significantly affect the spin memory. This effect, caused by interference, is most pronounced in the presence of an external magnetic field.

The partial spin-flip probabilities obviously fall off with magnetic field, B, which is parallel to the polarization in the injector. The result of the probabilistic approach, $P_{\rm incoh}$, also falls off with B. As it is easy to see from Eq. (6.3), the probability $p_{\rm sf}$ is proportional to $1/B^2$ for $\Omega\tau \gg 1$. Concerning the magnitude of the interference term, Eq. (6.9), it can actually grow with B if both partial probabilities, $p_{\rm sf}$, exceed $1/4$. However, when they are both small, the magnitude of interference term also drops with B as $1/B^2$. In the next section we will demonstrate that electron bounces can transform the $1/B^2$ to a much weaker dependence.

6.3 Effect of bouncing on the spin-flip probability

Assume that τ_2 is much bigger than τ_1, and the activation energy for the back-hop $2 \to 1$ is small, Fig. 6.1b. In this case, as it was explained in the Introduction, while awaiting the hop $2 \to R$, the electron performs $m = \tau_2/\tau_1 \gg 1$ hops $2 \to 1$ and back. This bouncing strongly affects the spin-rotation and enhances the interference contribution to $P_{\rm sf}$.

Note first that, within the probabilistic description, taking bounces into account is equivalent to modifying the partial probability $p_{\rm sf}^{(1)}$

$$\tilde{p}_{\rm sf}^{(1)} = \frac{1}{2} - \frac{1}{2}(1 - 2p_{\rm sf})^m, \tag{6.24}$$

where m is odd. Eq. (6.24) expresses the fact that $\tilde{p}_{\rm sf}^{(1)}$ is the sum of probabilities to flip spin *only* once in the course of all bounces, only three times in the course of all bounces, and so on. Accumulation of the powers of $(1 - 2p_{\rm sf})$ with m is natural since $(1 - 2p_{\rm sf})$ is the probability of spin preservation for one step. In reality, while bouncing, electron spin experiences an *alternating* magnetic field, which takes only two values. This favors the interference processes, and the result of Eq. (6.24) should be compared to the result of treatment with interference taken into account. Within the latter treatment, the spin-flip amplitude is given by the nondiagonal elements of the matrix product $U_m(t_m)...U_2(t_2)U_1(t_1)$, where $U_j(t_i)$ is the matrix (Eq. (6.4)) in which the fields corresponding to U_1 and U_2 are $\mathbf{\Omega}_1$ and $\mathbf{\Omega}_2$, respectively. The times, t_i, are random, but have the same distribution.

To illuminate the importance of interference in the course of bouncing, consider the following simple example. Suppose that $m = 3$ and that the external field is strong, i.e. $\Omega_\perp \ll \Omega$. Assume as well that the in-plane field components for all three steps are equal in magnitude and differ only in azimuthal orientations, χ_i. Then the nondiagonal matrix element of the product

$$\begin{pmatrix} u & -ive^{i\chi_3} \\ -ive^{-i\chi_3} & u \end{pmatrix} \begin{pmatrix} u & -ive^{i\chi_2} \\ -ive^{-i\chi_2} & u \end{pmatrix} \begin{pmatrix} u & -ive^{i\chi_1} \\ -ive^{-i\chi_1} & u \end{pmatrix} \tag{6.25}$$

takes a simple form

$$\tilde{A} = iv^3 e^{-i(\chi_3 - \chi_2 + \chi_1)} - iu^2 v \left(e^{-i\chi_1} + e^{-i\chi_2} + e^{-i\chi_3}\right). \tag{6.26}$$

Here, $u^2 + v^2 = 1$. For a sequential hopping all χ_i are random. Then the average value of $|\tilde{A}|^2$ is given by

$$|\tilde{A}|^2 = v^6 + 3u^4 v^2. \tag{6.27}$$

On the other hand, if the hops constitute a single bounce $1 \to 2 \to 1$, we have $\chi_1 = \chi_3$, which leads to the following expression for average $|\tilde{A}|^2$.

$$|\tilde{A}|^2 = v^6 + 5u^4 v^2. \tag{6.28}$$

The result of Eq. (6.27) can be brought in correspondence with probabilistic description of Eq. (6.24), if we identify $|v|^2$ with $p_{\rm sf}$. The fact that Eq. (6.28) yields a bigger value for $|\tilde{A}|^2$ is due to interference of the spin-flip amplitudes which arises as a result of visiting site 1 *twice*. Multiple bouncing would amplify the role of interference. It is easier to capture this effect quantitatively by starting directly from the Schrödinger equation for electron spin in a time-dependent magnetic field.

In the next two subsections we will separately consider the effect of bouncing on the spin preservation in a zero, and in strong external fields. We will demonstrate that in these two limits the effects of bouncing are *opposite*.

6.3.1 Bouncing in a zero external field

The amplitudes a_1 and a_2 for an electron to have an $\uparrow$ and $\downarrow$ projections of spin satisfy the system

$$\begin{aligned} i\dot{a}_1(t) &= \frac{1}{2}\Big[b_z(t)a_1(t) + b_\perp^*(t)a_2(t)\Big], \\ i\dot{a}_2(t) &= \frac{1}{2}\Big[b_\perp(t)a_1(t) - b_z(t)a_2(t)\Big]. \end{aligned} \tag{6.29}$$

Suppose that at time $t = 0$ electron spin is directed $\uparrow$, so that $a_2 = 0$. A formal solution of the system Eq. (6.29) reads

$$a_2(t) = \frac{-i}{2}\int\limits_0^t dt'\, b_\perp(t')a_1(t') \exp\left[\frac{-i}{2}\int\limits_0^{t'} dt''\, b_z(t'')\right]. \tag{6.30}$$

If the net spin rotation during the time, τ_2, when the electron waits for the hop $2 \to R$ is small, we can set $a_1(t) = 1$ and $\exp[-\int_0^t b_z(t')] = 1$ in the integrand. This leads to the following result for the spin-flip probability

$$P_{\rm sf} = \left|b_{1\perp}\left(t_1 + t_3 + \cdots\right) + b_{2\perp}\left(t_2 + t_4 + \cdots\right)\right|^2, \tag{6.31}$$

where $t_1, t_3, \ldots$ are the time intervals spent by the electron on the site 1, while $t_2, t_4, \ldots$ are the time intervals spent by the electron on site 2; each time interval is $\sim \tau_1$. It is an important consequence of bouncing that these time intervals add up, instead of averaging out, which would be the case for hopping over multiple sites. The big parameter τ_2/τ_1 allows us to replace these sums by $\tau_2/2$. Then we get

$$P_{\rm sf} = \frac{\tau_2^2}{2}\left|\frac{b_{1\perp} + b_{2\perp}}{2}\right|^2 = \frac{\tau_2^2\left|\bar{b}_\perp\right|^2}{2}. \tag{6.32}$$

The meaning of Eq. (6.32) is obvious: As a result of performing multiple "short" hops while awaiting the "long" hop, the electron spin "sees" the average hyperfine field, $\bar{b}_\perp$. If the

number of sites visited in the course of waiting was big, the averaging of the corresponding hyperfine fields would lead to the suppression of $P_{\rm sf}$.

We assumed that the net spin rotation is small, $b_0\tau_2 \ll 1$. However, the above derivation suggests that we could impose a much weaker requirement, $b_0\tau_1 \ll 1$. This is because the effective averaging takes place over time $\sim \tau_1$. If under the condition $\Omega\tau_1 \ll 1$ the product $b_0\tau_2$ is not small, then $P_{\rm sf}$ is given by the full Eq. (6.3) with $\mathbf{\Omega}$ replaced by the average of the vectors $\boldsymbol{b}_1$ and $\boldsymbol{b}_2$.

6.3.2 Bouncing in a strong external field

In a strong external field, $B \gg b_0$, the net spin rotation is small both for weak, $b_0\tau_2 \ll 1$, and for strong, $b_0\tau_2 \gg 1$, hyperfine fields. In the limit $B\tau_2 \gg 1$, when the electron spin rotates many times around the external field while waiting for the hop $2 \to R$, the waiting time drops out of $P_{\rm sf}$, see Eq. (6.3). The effect of bouncing on $P_{\rm sf}$ can be studied perturbatively with respect to hyperfine field. In a zeroth order we have, $a_1(t) = \exp\left(-\frac{iBt}{2}\right)$, $a_2 = 0$. In the first order the expression for $a_2(t)$ takes the form

$$a_2(t) = -\frac{i}{2}\int\limits_0^t dt'\, b_\perp(t') \exp\left(-iBt'\right). \tag{6.33}$$

It is convenient to subtract $\bar{b}_\perp$ from $b_\perp(t')$ in the integrand and rewrite Eq. (6.33) as

$$a_2(t) = -\bar{b}_\perp \frac{1-\exp\left(-iBt\right)}{2B} + \tilde{a}_2(t), \tag{6.34}$$

where $\tilde{a}_2(t)$ is determined by Eq. (6.33) in which $b_\perp(t')$ in the integrand is replaced by the difference $\left(b_\perp(t') - \bar{b}_\perp\right)$. The term $\tilde{a}_2(t)$ captures the effect of bouncing. Next, it is convenient to divide the domain of integration in Eq. (6.33) into $N = Bt/2\pi$ intervals $\frac{2\pi}{B}n < t' < \frac{2\pi}{B}(n+1)$, and reduce the integration to a single interval $0 < t' < \frac{2\pi}{B}$. This yields

$$\tilde{a}_2(t) = -\frac{i}{2}\sum_{n=0}^{N}\int\limits_0^{2\pi/B} dt'\, \exp\left(-iBt'\right)\left[b_\perp\left(t' + \frac{2\pi}{B}n\right) - \bar{b}_\perp\right]. \tag{6.35}$$

In the domain $\frac{1}{\tau_2} < B < \frac{1}{\tau_1}$ the right-hand side of Eq. (6.35) is a sum of N statistically-equivalent and independent terms, each being zero on average. In each term the integrand changes sign $2\pi/B\tau_1$ times with magnitude $\Delta b_\perp = \frac{1}{2}|b_{1\perp} - b_{2\perp}|$. This allows us to estimate $|\tilde{a}_2(t)|^2$ as follows

$$|\tilde{a}_2(t)|^2 \sim |\Delta b_\perp|^2\tau_1^2\left[N^{1/2}\left(\frac{2\pi}{B\tau_1}\right)^{1/2}\right]^2 \sim |\Delta b_\perp|^2 t\tau_1. \tag{6.36}$$

The factor $N^{1/2}$ accounts for the fact that all N terms in the sum (6.35) are random. The factor $\left(\frac{2\pi}{B\tau_1}\right)$ accounts for the fact that *each* term is the sum of $2\pi/B\tau_1$ random contributions.

We see that the magnetic field has dropped out of the "bouncing" estimate for $|\tilde{a}_2(t)|^2$. It dominates over the "regular" part, given by the first term in Eq. (6.34), if $t\tau_1 \gg 1/B^2$. Since the characteristic t is $\sim \tau_2$, this defines a characteristic field

$$B_c = \frac{1}{(\tau_1\tau_2)^{1/2}}. \tag{6.37}$$

At $B \sim B_c$ the spin-flip probability crosses over from $P_{\rm sf} \sim b_0^2/B^2$ to a plateau value

$$P_{\rm sf} \sim b_0^2\tau_1\tau_2. \tag{6.38}$$

In deriving Eq. (6.38) we assumed that many bounces took place during the period, $2\pi/B$, of the in-plane spin rotation. This assumption is justified since $B_c\tau_1 \sim (\tau_1/\tau_2)^{1/2} \ll 1$. As magnetic field increases above $1/\tau_1$, the spin will execute many in-plane rotations in course of every bounce. Then the integral in the expression for $\tilde{a}_2$ can be viewed as a sum of τ_2/τ_1 random contributions, each being of the order of $\Delta b_\perp/B$. Then we can again estimate $\tilde{a}_2$, and subsequently, $P_{\rm sf}(B)$, from the variance. The result reads

$$P_{\rm sf}(B)\Big|_{B\gg 1/\tau_1} \sim \frac{|\Delta b_\perp|^2}{B^2}\left(\frac{\tau_2}{\tau_1}\right). \tag{6.39}$$

Note that the bouncing-related spin-flip probability, Eq. (6.39), exceeds the result $P_{\rm sf} \sim b_0^2/B^2$ in the absence of bouncing by a large factor $\frac{\tau_2}{\tau_1}$, which is the number of bounces.

Thus, unlike the case $B = 0$, the bouncing causes the growth of the spin-flip probability. The probability Eq. (6.39) for strong fields matches $P_{\rm sf}$ for intermediate fields, Eq. (6.38), at $B \sim \frac{1}{\tau_1}$.

In conclusion of this subsection we summarize the results for $P_{\rm sf}$ in different domains of magnetic field

$$P_{\rm sf}(B) = \begin{cases} \bar{b}_\perp^2\tau_2^2, & 0 < B < \frac{1}{\tau_2} \\ (\Delta b_\perp)^2\tau_1\tau_2 + \frac{\bar{b}_\perp^2}{B^2}, & \frac{1}{\tau_2} < B < \frac{1}{\tau_1} \\ \frac{(\Delta b_\perp)^2}{B^2}\frac{\tau_2}{\tau_1}, & B > \frac{1}{\tau_2} \end{cases} \tag{6.40}$$

The evolution of the spin-flip probability with magnetic field is illustrated in Fig. 6.4.

6.4 Discussion

- Conventional treatments of spin relaxation neglect interference effects. This happens at the stage when the exact equation for the density matrix is solved using the "tau-approximation," see e.g. the review Ref. [19]. Concerning the effect of bouncing

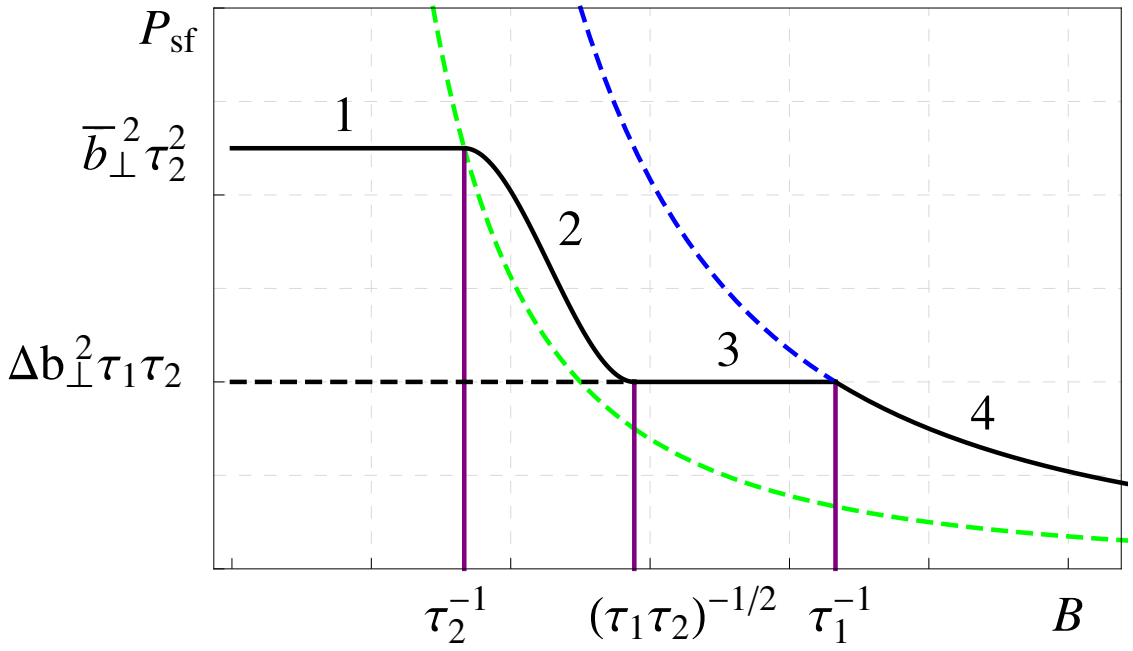

Figure 6.4: Schematic illustration of the enhancement of the spin-flip probability due to multiple bounces. In the absence of bouncing, the plateau (**1**) at small external fields crosses over to the $1/B^2$ behavior (green dashed line) at $B \sim 1/\tau_2$, where τ_2 is the waiting time for the hop $2 \to R$. When the waiting time, τ_1, for the hops $1 \to 2$ and $2 \to 1$ is much shorter than τ_2, the spin-flip probability decreases (**2**), develops a second plateau (**3**) at $B \sim (\tau_1\tau_2)^{-1/2}$, see Eq. (6.40), and crosses over (**4**) to $1/B^2$ behavior (blue dashed line) at $B \sim 1/\tau_1$.

considered in the present paper, there is an analog of bouncing in spin relaxation caused by spin-orbit coupling. In the course of the *orbital* electron motion in a strong magnetic field, it keeps returning to the origin after undergoing the same sequence of scattering events. This "memory" results in shortening of the spin relaxation time [19]. Similarly, Eq. (6.24), where bouncing is treated probabilistically, predicts that $P_{\rm sf}$ approaches to 1/2 faster as the number, m, of bounces grows. We emphasize that the quantum treatment of bouncing leads to the opposite result.

- Absence of the Hanle effect reported in Refs. [14] and [15] can be interpreted as independence of $P_{\rm sf}$ on the *magnitude* of the external field. In this regard, we note that the partial $p_{\rm sf}$ values given by Eq. (6.3) increase monotonically with increasing magnetic field, for any field orientation. However, in Sect. 6.2 we demonstrated that when the partial probabilities $p_{\rm sf}$ are in the vicinity of 1/2, the dependence of the net two-step probability, $P_{\rm sf}$, on these partial probabilities is *nonmonotonic*. Moreover, the derivative of $P_{\rm sf}$ with respect to the magnetic field, passes through zero. This indicates that, for a range of parameters where $P_{\rm sf}$ is near its maximum, there is no sensitivity to the magnitude of the applied field. Note, however, that since this behavior is a consequence of interference, it does not survive averaging over hyperfine field distributions.

- The fact that the electron flips its spin as it travels between the electrodes constitutes an additional source of shot noise [20] and, thus, affects the Fano factor. The above calculation of $P_{\rm sf}$ is insufficient to find the Fano factor of "two-site" transport with spin flip. The reason for this is that the transport of charge is incoherent while the spin-transport is fully coherent. Qualitatively, the complexity of description of noise follows from the fact that the Fano factor must depend on *both* $P_{\rm sf}$ and the magnetizations $\mathcal{P}_1, \mathcal{P}_2$ of the electrodes. The latter conclusion can be inferred from the reasoning presented in Ref. [20]. Suppose that magnetizations of the electrodes are antiparallel, and $P_{\rm sf}$ is small. Then, no matter what is the actual mechanism of transport, the Fano factor should be 1, which is the Poissonian value. This is because in order to be transferred between the electrodes, the electron must flip the spin. For small $P_{\rm sf}$ it is waiting time for the spin-flip which is the bottle-neck for transport, since it is much longer than the waiting time for all hops. All we can say is that, if one electrode changes from oppositely polarized to nonpolarized, the Fano factor changes from 1 to $\frac{\tau_1^2+\tau_1\tau_2+\tau_2^2}{(\tau_1+\tau_2)^2}$, which is the Fano factor for *spin-independent* transport

through the same sites. Rigorous evaluation of the Fano factor with magnetization of electrodes taken into account requires solving the equation for time evolution of the full density matrix.

- In a number of experimental papers, see Fig. 6.5, it was reported that the observed TMR has a "wrong" sign. This sign has been attributed to interfacial effects like the reversal of the carrier spin upon entering the active layer from the polarized electrode. We would like to emphasize that the emergence of negative TMR demonstrated above has nothing to do with interfacial effects. More specifically, the expression Eq. (6.2) contains the product $\mathcal{P}_1\mathcal{P}_2$ and the factor $(1-2P_{\rm sf})$. Previous reports of the sign reversal of TMR, both experimental [21, 22] and theoretical [23, 24], related this reversal with the fact that changing the properties of interface, e.g., by introducing an intermediate spacer, can effectively convert positive $\mathcal{P}_{1,2}$ into negative and vice versa. The mechanism of negative TMR uncovered in the present paper comes from the sign reversal of the "survival probability" $(1-2P_{\rm sf})$. As was discussed in Ref. [25], for a spin-valve with metallic active layer negative TMR can occur as a result of exchange spin-flip of tunneling electrons by pairs of magnetic impurities.

- As was mentioned in the Introduction, in diffusive transport, spin-memory loss is incorporated via the "survival" probability, $\exp(-\mathrm{L}/l_s)$, which we replaced by $1-2P_{\rm sf}$. The probabilistic description, on the other hand, predicts that $P_{\rm sf}$ falls off exponentially with the number of steps, N, see Eq. (6.17), or equivalently with time, but *not* with length. The exponential dependence $\exp(-\mathrm{L}/l_s)$ is recovered upon the transformation

$$P_{\rm sf}(\mathrm{L}) = \int dN\, P_{\rm sf}(N) \exp\left(-\frac{\mathrm{L}^2}{Nr^2}\right), \tag{6.41}$$

where r is the length of a diffusion step. This yields

$$l_s = \frac{r}{\sqrt{|\ln(1-2p_{\rm sf})|}}. \tag{6.42}$$

Here, we would like to emphasize that the concept of spin diffusion length does not apply for multistep transport [11, 12]. The reason for this is twofold. Unlike diffusion, the relationship between L and r in multistep transport is $r=\sqrt{\mathrm{L}a}$, and $N=\mathrm{L}/r=\sqrt{\mathrm{L}/a}$, where a is the under-barrier decay length. [13] Secondly, also unlike diffusion, the waiting time for the next step, which is the time for spin precession, is also a function of L and N, specifically, $\tau=\tau_0\exp(2\mathrm{L}/Na)$. As a result we get

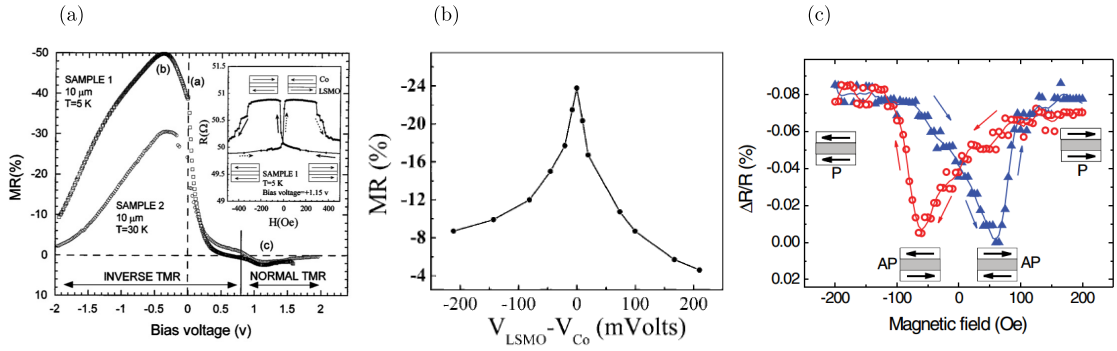

Figure 6.5: Experimental curves (taken from Ref. [21] (a), Ref. [22] (b), and from Ref. [23] (c)) where negative tunnel magnetoresistance in a spin valve was observed. The valve represented $Co/SrTiO_3/La_{0.7}Sr_{0.3}MnO_3$ in (a), $La_{0.67}Sr_{0.33}MnO_3$/ organic molecule / Co junctions in (b), and $CoPt/TIPS\text{-}pentacene/AlO_x/Co$ in (c).

$$P_{\rm sf} = \frac{1}{2}\left[\frac{b_0^2\tau_0^2 \exp\left(\sqrt{\frac{\rm L}{a}}\right)}{1 + b_0^2\tau_0^2 \exp\left(\sqrt{\frac{\rm L}{a}}\right)}\right]. \tag{6.43}$$

We see from Eq. (6.43) that for multistep transport the spin-memory falls off with thickness of the active layer, L, slower than for diffusive transport. Anomalous dependence of TMR on the device thickness was reported in Ref. [26]. However Eq. (6.43) does not explain the established facts that TMR vanished with increasing bias and temperature [26, 27].

6.5 Appendix

For spin-independent unidirectional transport the current between the electrodes can be viewed as a sequence of cycles

$$I(T) = \delta(T - T_1) + \delta(T - T_1 - T_2) + \delta(T - T_1 - T_2 - T_3) + \cdots, \tag{6.44}$$

where T_i is a random waiting time for the next electron to be transferred between L and R. Suppose now that the left electrode is polarized $\uparrow$, while the right electrode is polarized $\downarrow$. Then the electron transfer requires a spin-flip, and Eq. (6.44) should be modified as

$$I_{\uparrow\downarrow}(T) = P_{\rm sf}(T_1)\delta(T - T_1) + P_{\rm sf}(T_2)\delta(T - T_1 - T_2) + P_{\rm sf}(T_3)\delta(T - T_1 - T_2 - T_3) + \cdots, \tag{6.45}$$

where $P_{\rm sf}(T)$ is a quantum-mechanical probability that after a composite process with duration T the electron flips its spin. For the situation considered in this paper the composite process is an inelastic two-hop tunneling. To calculate the average current one should take the limit of large T and average over the compound waiting times, T_i, with distribution function $F(T)$. This averaging is convenient to perform [28] using the integral representation of the δ-function. Then the sum Eq. (6.45) turns into a geometrical progression, the summation of which yields

$$\langle I_{\uparrow\downarrow}(T)\rangle = \int \frac{d\alpha}{2\pi} e^{i\alpha T} \frac{\langle P_{\rm sf}(T')\exp\left(-i\alpha T'\right)\rangle}{1 - \langle\exp\left(-i\alpha T'\right)\rangle}. \tag{6.46}$$

In the limit $T \to \infty$ one can set $\alpha = 0$ in the numerator and expand the denominator to the lowest order. After that the integration over α can be easily performed leading to the natural result

$$\langle I_{\uparrow\downarrow}\rangle = \frac{\langle P_{\rm sf}\rangle}{\langle T\rangle}, \tag{6.47}$$

where $\langle P_{\rm sf}\rangle$ is defined as

$$\langle P_{\rm sf}\rangle = \int P_{\rm sf}(T)F(T)dT. \tag{6.48}$$

For a particular case of a two-hop transport we have $T = t_1 + t_2$, where t_1 and t_2 are distributed with $f_{1,2}(t) = \frac{1}{\tau_{1,2}}\exp(-t/\tau_{1,2})$. Then Eq. (6.48) assumes the form

$$\langle P_{\rm sf}\rangle = \int_0^\infty dt_1 \int_0^\infty dt_2\; P_{\rm sf}(t_1,t_2)f_1(t_1)f_2(t_2). \tag{6.49}$$

This is exactly the quantity calculated in Sect. 6.2 From Eq. (6.47) we conclude that for calculation of average current one should multiply this quantity by $1/\langle T\rangle$, which is the current between unpolarized electrodes.

From the same reasoning we confirm that opposite directions of polarization of the electrodes, the current is equal to $I_{\uparrow\uparrow} = (1 - \langle P_{\rm sf}\rangle)/\langle T\rangle$. Therefore, the expression for TMR with completely polarized electrodes takes the form

$$\mathrm{TMR} = \frac{I_{\uparrow\uparrow} - I_{\uparrow\downarrow}}{I_{\uparrow\downarrow}} = \frac{1}{P_{\rm sf}} - 2. \tag{6.50}$$

For partial polarization of electrodes with concentrations $\mathcal{N}_\uparrow$, $\mathcal{N}_\downarrow$ of $\uparrow$ and $\downarrow$ electrons in the left electrode and $n_\uparrow$, $n_\uparrow$ in the right electrode, the general expressions for $I_{\uparrow\uparrow}$ and $I_{\uparrow\downarrow}$ can be presented as

$$I_{\uparrow\uparrow} = \Gamma_{\uparrow\uparrow}\left(\mathcal{N}_\uparrow n_\uparrow + \mathcal{N}_\downarrow n_\downarrow\right) + \Gamma_{\uparrow\downarrow}\left(\mathcal{N}_\uparrow n_\downarrow + \mathcal{N}_\downarrow n_\uparrow\right), \tag{6.51}$$

$$I_{\uparrow\downarrow} = \Gamma_{\uparrow\uparrow}\left(\mathcal{N}_\uparrow n_\downarrow + \mathcal{N}_\downarrow n_\uparrow\right) + \Gamma_{\uparrow\downarrow}\left(\mathcal{N}_\uparrow n_\uparrow + \mathcal{N}_\downarrow n_\downarrow\right), \tag{6.52}$$

where $\Gamma_{\uparrow\uparrow}$ and $\Gamma_{\uparrow\downarrow}$ are the rates for the transfer processes from $\uparrow$ to $\uparrow$ and from $\uparrow$ to $\downarrow$. These rates are the characteristics of the active layer and do not depend on the polarizations of the electrodes. Naturally, we have $\Gamma_{\uparrow\uparrow} = \Gamma_{\downarrow\downarrow}$ and $\Gamma_{\uparrow\downarrow} = \Gamma_{\downarrow\uparrow}$. The expression Eq. (6.2) follows from Eqs. (6.51) and (6.52) in two steps. We relate the concentration via the degrees of polarization as

$$\mathcal{P}_1 = \frac{\mathcal{N}_\uparrow - \mathcal{N}_\downarrow}{\mathcal{N}_\uparrow + \mathcal{N}_\downarrow}, \quad \mathcal{P}_2 = \frac{n_\uparrow - n_\downarrow}{n_\uparrow + n_\downarrow}, \tag{6.53}$$

yielding

$$\mathrm{TMR} = \frac{2\mathcal{P}_1\mathcal{P}_2\left(\Gamma_{\uparrow\uparrow} - \Gamma_{\uparrow\downarrow}\right)}{\left(\Gamma_{\uparrow\uparrow} + \Gamma_{\uparrow\downarrow}\right) - \mathcal{P}_1\mathcal{P}_2\left(\Gamma_{\uparrow\uparrow} - \Gamma_{\uparrow\downarrow}\right)}. \tag{6.54}$$

Finally, we relate the rates $\Gamma_{\uparrow\uparrow}$, $\Gamma_{\uparrow\downarrow}$ via $P_{\rm sf}$ as

$$\frac{\Gamma_{\uparrow\uparrow} - \Gamma_{\uparrow\downarrow}}{\Gamma_{\uparrow\uparrow} + \Gamma_{\uparrow\downarrow}} = 1 - 2P_{\rm sf}, \tag{6.55}$$

and arrive at Eq. (6.2).

6.6 References

[1] M. Julliére, Phys. Lett. **54A**, 225 (1975).

[2] I. Zutic, J. Fabian, and S. Das Sarma, Rev. Mod. Phys. **76**, 323 (2004).

[3] F. J. Jedema, A. T. Filip, B. J. van Wees, Nature **410**, 345 (2001).

[4] Z. H. Xiong, D. Wu, Z. V. Vardeny, and J. Shi, Nature (London) **427**, 821 (2004).

[5] S. Pramanik, C.-G. Stefanita, S. Patibandla, S. Bandyopadhyay, K. Garre, N. Harth, and M. Cahay, Nat. Nanotechnol. **2**, 216 (2007).

[6] V. A. Dediu, L. E. Hueso, I. Bergenti, and C. Taliani, Nat. Mater. **8**, 850 (2009).

[7] A. J. Drew, J. Hoppler, L. Schulz, F. L. Pratt, P. Desai, P. Shakya, T. Kreouzis, W. P. Gillin, A. Suter, N. A. Morley, V. K. Malik, A. Dubroka, K. W. Kim, H. Bouyanfif, F. Bourqui, C. Bernhard, R. Scheuermann, G. J. Nieuwenhuys, T. Prokscha, and E. Morenzoni, Nat. Mater. **8**, 109 (2009).

[8] T. Nguyen, G. Hukic-Markosian, F. Wang, L. Wojcik, X. Li, E. Ehrenfreund, Z. Vardeny, Nat. Mater. **9**, 345 (2010).

[9] T. D. Nguyen, F, Wang, X.-G. Li, E. Ehrenfreund, and Z. V. Vardeny, Phys. Rev. B **87**, 075205 (2013).

[10] M. Grünewald, J. Kleinlein, F. Syrowatka, F. Würthner, L.W. Molenkamp, and G. Schmidt, arXiv:1304.2911.

[11] J. J. H. M. Schoonus, P. G. E. Lumens, W. Wagemans, J. T. Kohlhepp, P. A. Bobbert, H. J. M. Swagten, and B. Koopmans, Phys. Rev. Lett. **103**, 146601 (2009).

[12] T. L. A. Tran, T. Q. Le, J. G. M. Sanderink, W.G. van der Wiel, and M. P. deJong, Adv. Funct. Mater., **22**, 1180 (2012).

[13] A. V. Tartakovskii, M. V. Fistul', M. E. Raikh, and I. M. Ruzin, Sov. Phys. Semicond. **21**, 603 (1987); M. E. Raikh and I. M. Ruzin, in *Mesoscopic Phenomena in Solids*, edited by B. L. Altshuller, P. A. Lee, and R. A. Webb (Elsevier, New York, 1991), p. 315.

[14] A. Riminucci, M. Prezioso, C. Pernechele, P. Graziosi, I. Bergenti, R. Cecchini, M. Calbucci, M. Solzi, V. A. Dediu, Appl. Phys. Lett. **102**, 092407 (2013).

[15] M. Grünewald, R. Göckeritz, N. Homonnay, F. Würthner, L. W. Molenkamp, and G. Schmidt, arXiv:1304.6583.

[16] P. A. Bobbert, W. Wagemans, F. W. A. van Oost, B. Koopmans, and M. Wohlgenannt, Phys. Rev. Lett. **102**, 156604 (2009).

[17] N. J. Harmon and M. E. Flatté, Phys. Rev. Lett. **110**, 176602 (2013).

[18] M. I. D'yakonov and V. I. Perel, Sov. Phys. JETP **33**, 1053 (1971).

[19] M. M. Glazov, E. Ya. Sherman, and V. K. Dugaev, Physica E **42**, 2157 (2010).

[20] E. G. Mishchenko, Phys. Rev. B **68**, 100409 (2003).

[21] J. M. De Teresa, A. Barthélémy, A. Fert, J. P. Contour, R. Lyonnet, F. Montaigne, P. Seneor, and A. Vaurès, Phys. Rev. Lett. **82**, 4288 (1999).

[22] W. Xu, G. J. Szulczewski, P. LeClair, I. Navarrete, R. Schad, G. Miao, H. Guo, and A. Gupta, Appl. Phys. Lett. **90**, 072506 (2007).

[23] S. Mooser, J. F. K. Cooper, K. K. Banger, J. Wunderlich, and H. Sirringhaus, Phys. Rev. B **85**, 235202 (2012).

[24] S. Mandal and R. Pati, ACS Nano, **6**, 3580 (2012).

[25] M. A. Tanaka, T. Hori, K. Mibu, K. Kondou, T. Ono, S. Kasai, T. Asaka, and J. Inoue, J. Appl. Phys. **110**, 073905 (2011).

[26] T. D. Nguyen, F. Wang, X.-G. Li, E. Ehrenfreund, and Z. V. Vardeny, Phys. Rev. B **87**, 075205 (2013).

[27] J. S. Jiang, J. E. Pearson, and S. D. Bader, Phys. Rev. B **77**, 035303 (2008).

[28] J. Koch, M. E. Raikh, and F. von Oppen, Phys. Rev. Lett. **95**, 056801 (2005).

CHAPTER 7

GIANT FLUCTUATIONS OF LOCAL MAGNETO-RESISTANCE OF ORGANIC SPIN VALVES AND NON-HERMITIAN 1D ANDERSON MODEL

7.1 Introduction

Organic spin valves (OSVs), being one of the most promising applications of organic spintronics, are actively studied experimentally [1, 2, 3, 4, 5, 6, 7, 8, 9]. The organic active layer of an OSV is sandwiched between two magnetized electrodes. Due to long spin-relaxation times of carriers in organic materials, the net resistance of OSV is sensitive to the relative magnetizations of the electrodes. Among many advantages that OSVs offer is wide tunability due to, e.g., chemical doping, and enormous flexibility. The processes that limit the performance of OSVs can be conventionally divided into two groups: (i) interfacial, which take place at the interfaces between the electrodes and active layer [11, 12, 13, 14, 15, 16, 17, 18], and (ii) intralayer, which exist even if the interfaces are ideal [19, 20]. Due to the latter processes, the injected polarized electrons, Fig. 7.1, lose memory about their initial spin orientation while traveling between the electrodes. One of the most prominent mechanisms of this spin-memory loss is the precession of a carrier spin in random hyperfine fields of hydrogen nuclei [5, 19, 20]. The effectiveness of OSV performance is quantified by tunnel magnetoresistance (TMR) given by a so-called modified Julliere's formula [22], see, e.g., the review of Ref. [21],

$$\mathrm{TMR} = \frac{2P_1P_2\exp(-d/\lambda_s)}{1-P_1P_2\exp(-d/\lambda_s)}, \tag{7.1}$$

where P_1, P_2 stand for polarizations of the electrodes. The difference from the original Julliere's formula [22] is the exponential factor $Q = \exp(-d/\lambda_s)$ describing the spin-memory loss over the active layer of thickness, d. Processes (i) can be incorporated into Eq. (7.1) by appropriately modifying P_1, P_2. For example, in Ref. [11] replacement of P_1, P_2 by "effective" spin polarizations reflects the relative position of the Fermi level with respect to

interfacial donor (acceptor) level. In this way, the "effective" polarization depends on bias, which might explain the sign reversal of TMR [11, 12, 13, 14, 15, 16, 17, 18]. Processes (ii), on the other hand, are reflected in Eq. (7.1) via the factor $Q = \exp(-d/\lambda_s)$, where λ_s is the spin diffusion length. The meaning of Q is the polarization of electrons at $x = d$, provided that at $x = 0$ they are fully polarized. Encoding the processes (ii) into $Q = \exp(-d/\lambda_s)$ implies that the spin polarization of electrons falls off *homogeneously and monotonically* with coordinate x, see Fig. 7.1.

The prime message of the present paper is that strong local fluctuations of TMR, including the local sign reversal, is a generic property of the OSV even with ideal interfaces. In other words, the factor Q captures the spin memory loss only *on average*. The *local* value of Q fluctuates strongly from point to point and takes values in the domain $-1 < Q < 1$. On the physical level, the local value of TMR in the absence of interfacial effects is the fingerprint of hyperfine-field configuration along a given current path.

The origin of strong local fluctuations of TMR is quantum-mechanical interference of *amplitudes* [23] of subsequent spin rotations accompanying the inelastic hops of the electron, which has been routinely neglected in earlier studies. Formally, this interference, in course of a *time* evolution of spin in random hyperfine field can be mapped on *spatial* propagation of an electron along a 1D disordered chain [26, 29, 27, 28]. In this regard, it is important to realize that as an electron enters the OSV, its spatial coherence is lost after a single inelastic hop. At the same time, the spin evolution of a given electron remains absolutely coherent all the way between the electrodes.

Experimental relevance of local TMR, which motivated our study, was demonstrated in a recent paper by Ref. [12], see Fig. 7.2, where an STM tip played a role of one of magnetized electrodes, while the other electrode was a Cr(001) substrate with alternating magnetization directions. The role of active layer was played by isolated C_{60} molecules attached to the substrate. By scanning the tip, the authors were able to recover the surface map of the conductance through a single molecule, and its evolution with bias. In this way, the sign reversal of TMR was demonstrated on the *local* level.

7.2 Recurrence relation for the spin transport

We will illustrate our message using the simplest model [19, 20, 24, 23] depicted in Fig. 7.1. As shown in this figure, electron hops along the parallel chains. The waiting times, τ_n, for each subsequent hop are Poisson-distributed as $\frac{1}{\tau^*}\exp[-\tau/\tau^*]$. While residing on a site, the electron spin precesses around a local hyperfine field. Hyperfine fields are random, their Gaussian distribution is characterized by rms value, b_0.

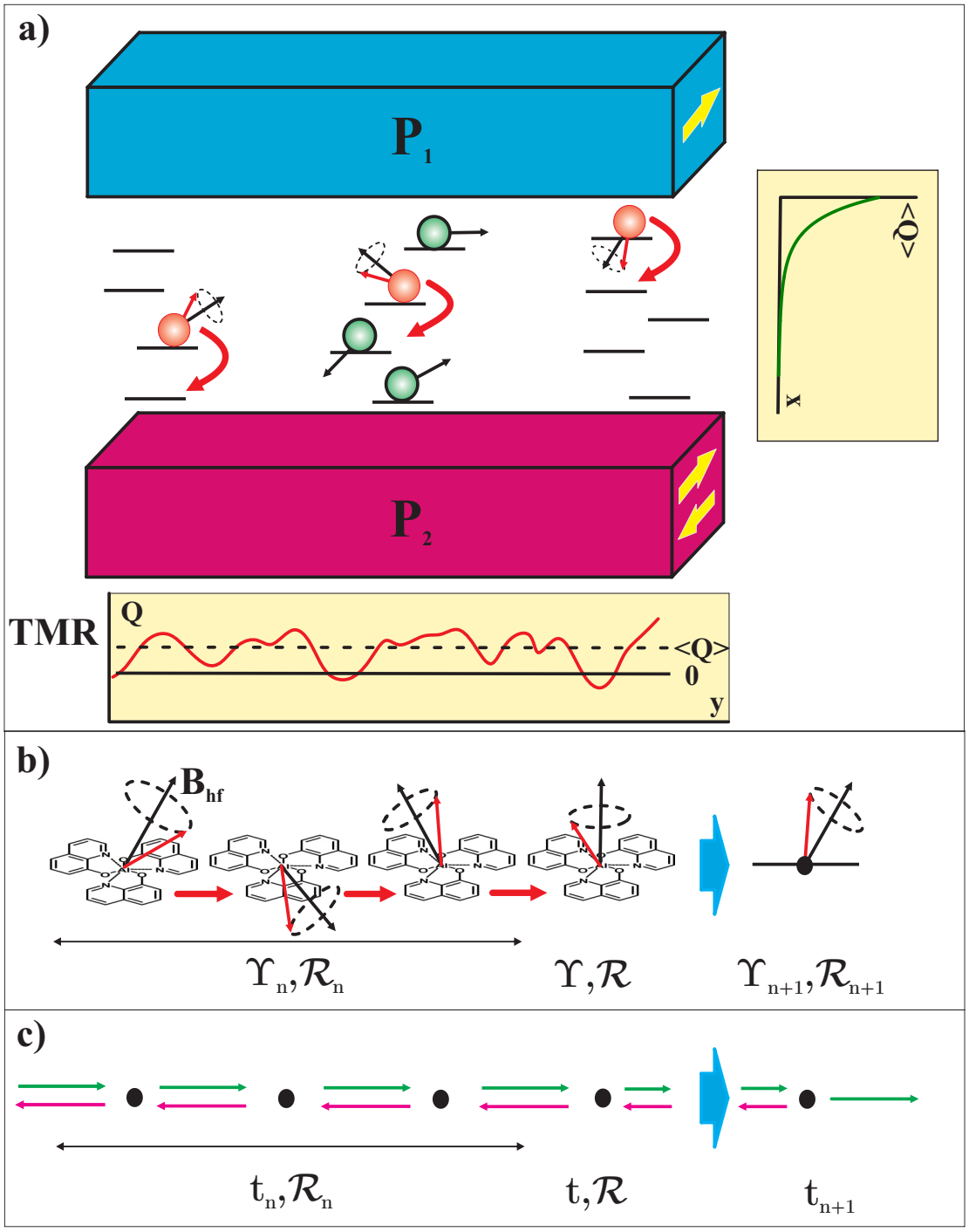

Figure 7.1: Depictions of an OSV with a thin active layer. (a). Schematic illustration of an OSV with a thin active layer, so that the transport is along independent chains. Electrode polarizations, $P_{1,2}$, are indicated in yellow. The in-plane components of hyperfine fields are depicted with black arrows. Below: A cartoon of *local* TMR along the y-direction; the classical value is indicated with a dashed line. Right: Decay of the *average* polarization across the active layer is shown. (b) and (c). Illustration of the mapping of *temporal* spin evolution in course of hopping onto the *spatial* propagation of an electron through a chain of random scatterers.

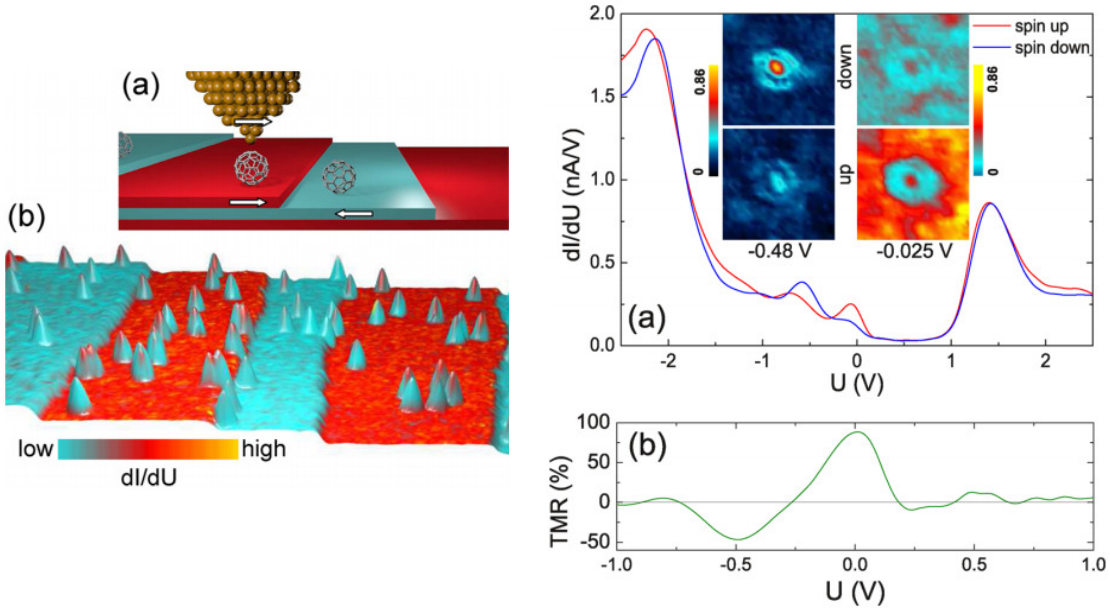

Figure 7.2: Experimental measurement of fluctuating *local* TMR. (left) Map of the local TMR measured in Ref. [12] with the help of an STM. The tip of the STM played the role of the upper electrode, while the substrate with alternating magnetization played the role of the lower electrode. The role of organic spacer layer was played by individual C_{60} molecules. (a) schematic illustration of the operational device; (b) illustration of local areas with both positive and negative TMR. (right) The sign reversal of *local* TMR is illustrated. (a) The resistance, dI/dU, is plotted against the energy U; (b) The TMR as a function of U is plotted. Adapted from Ref. [12].

In the course of hopping, the values $b_\perp$ change abruptly after each time interval, τ_n. The evolution of the amplitudes a_1, a_2 of $\uparrow$ and $\downarrow$ spin projections is described by the unitary evolution matrix defined as

$$\begin{Bmatrix} a_1(\tau_{n+1}) \\ a_2(\tau_{n+1}) \end{Bmatrix} = \widehat{U}_n \begin{Bmatrix} a_1(\tau_n) \\ a_2(\tau_n) \end{Bmatrix}, \; \widehat{U} = \begin{bmatrix} \Upsilon e^{-i\chi} & -i\mathcal{R}e^{-i\phi} \\ -i\mathcal{R}e^{i\phi} & \Upsilon e^{i\chi} \end{bmatrix}. \tag{7.2}$$

Microscopic expressions for $\mathcal{R}$, Υ, and the phases χ and ϕ are elementary: $\mathcal{R} = \frac{|b_{n,\perp}|\tau_n}{2}$, $\Upsilon = \sqrt{1-\mathcal{R}^2}$, $\chi = \frac{b_z\tau_n}{2}$, and $\phi = \tan^{-1}\frac{b_{n,y}}{b_{n,x}}$. Here, b_z and $b_\perp = (b_x, b_y)$ are the tangetial and normal (with respect to the initial spin orientation) components of the hyperfine field.

Coherent evolution of the electron spin over n steps is described by the product, $\prod_{i=0}^{n} \widehat{U}_i$, of matrices Eq. (7.2). Naturally, after n steps, this product can also be reduced to the form Eq. (7.2) with Υ replaced by some effective Υ_n. This observation suggests that Υ_n and Υ_{n+1} are related via a recurrence relation which we choose to cast into the form

$$\frac{1}{\Upsilon_{n+1}^2} = \frac{\dfrac{1}{\Upsilon_n^2}\dfrac{1}{\Upsilon^2}}{1 + \left(\dfrac{1}{\Upsilon^2}-1\right)\left(\dfrac{1}{\Upsilon_n^2}-1\right) - 2\sqrt{\left(\dfrac{1}{\Upsilon^2}-1\right)\left(\dfrac{1}{\Upsilon_n^2}-1\right)}\cos\left((-\phi_n+\phi)-(\chi_n+\chi)\right)}. \tag{7.3}$$

7.3 Mapping on a 1D Anderson model

Consider now a different physical situation: *Spinless* electron propagates *coherently* along a line of impurities randomly positioned at points, x_n, see Fig. 7.1c. As shown in the figure, the energy-conserving wave function on the interval (x_n, x_{n+1}) is a combination of two counterpropagating waves. Denote with t the amplitude transmission coefficient of the impurity. Then the relation between the net transmission coefficient, t_n, of the system with n impurities satisfies the famous Fabry-Perrot-like recurrence relation

$$t_{n+1}^2 = \frac{t_n^2 t^2}{1 + (1-t^2)(1-t_n^2) + 2\sqrt{(1-t^2)(1-t_n^2)}\cos 2\eta}, \tag{7.4}$$

where η is the phase accumulation upon passage through the interval (x_n, x_{n+1}).

At this point we make our main observation that the recurrence relations Eq. (7.4) and Eq. (7.3) map onto each other upon replacement, $\Upsilon^{-1} \leftrightarrow t$. On the other hand, it is known that the distribution function of t_n can be found exactly. In particular, the average $\ln(t_n^2)$ increases linearly [27] with n, which is the manifestation of the Anderson localization in 1D. Anderson localization is the result of quantum interference of multiply-scattered waves [26]. The very existence of the mapping of Eq. (7.3) onto Eq. (7.4) suggests that the interference effects are equally important for the *temporal* evolution of spin. We will see, however, that

replacement t_n by $1/\Upsilon_n$ rules out the Anderson localization but causes giant fluctuations of Υ_n with n. In addition, the mapping allows one to employ well-developed techniques, see the review by Ref. [28], who describe these fluctuations analytically.

7.4 Distribution of local spin polarization after n steps.

In the mapping of Eq. (7.3) onto Eq. (7.4) the randomness of the impurity positions, x_n, is taken over by the random azimuthal orientations of the hyperfine fields. Following Ref. [27], this randomness allows one to write down the recurrence relation for the distribution function of the effective transmission coefficient. In our case it is more convenient to analyze the distribution of the related quantity $Q = 2\Upsilon^2 - 1 = 1 - 2\mathcal{R}^2$, which is the local spin polarization, as mentioned in the Introduction. Then the functional recurrence relation reads

$$\mathcal{F}_{n+1}(Q_{n+1}) = \int_{-1}^{1} dQ_n \mathcal{F}_n(Q_n) \int_0^{2\pi} \frac{d\phi}{2\pi} \delta\left[Q_{n+1} - Q_n(1-2\mathcal{R}^2) + 2\sqrt{1-Q_n^2}\mathcal{R}\Upsilon\cos\phi\right] \quad (7.5)$$

$$= \frac{1}{\pi}\int_{-1}^{1} dQ_n \frac{\mathcal{F}_n(Q_n)}{\sqrt{\left[2\sqrt{1-Q_n^2}\mathcal{R}\Upsilon\right]^2 - [Q_{n+1} - Q_n(1-2\mathcal{R}^2)]^2}}.$$

An immediate consequence of Eq. (7.5) is the relation, $\langle Q_{n+1}\rangle = (1-2\mathcal{R}^2)\langle Q_n\rangle$ between the averages. This, in turn, implies that, on average, spin-memory loss follows the classical prediction $\exp(-n/\lambda_s)$, where $\lambda_s = 1/\ln(1-2\mathcal{R}^2)$.

From now on we consider the limit of large n and small $\mathcal{R}$. The latter allows us to expand the denominator in Eq. (7.5) to the first order in $\mathcal{R}^2$, which, upon integration by parts, yields the following Fokker-Planck equation

$$\frac{\partial \mathcal{F}}{\partial x} = \frac{\partial}{\partial Q}\left[\left(1-Q^2\right)\frac{\partial \mathcal{F}}{\partial Q}\right], \quad (7.6)$$

where $x = n\mathcal{R}^2$ is assumed to be a continuous variable. It is not surprising that Eq. (7.6) is *exactly* the Fokker-Planck equation for 1D localization. The important difference, however, is that for spin evolution it should be solved in the domain $|Q| < 1$ rather than [28] $Q > 1$. The latter is a direct consequence of the mapping $t \leftrightarrow \Upsilon^{-1}$.

For a restricted domain $|Q| < 1$ the separation of variables in Eq. (7.6) reveals that the eigenfunctions with respect to Q are the Legendre polynomials, $P_m(Q)$, the corresponding eigenvalues, $m(m+1)$, define the x-dependence, $\exp[-m(m+1)x]$, for a given m. The coefficients in the linear combination of the Legendre polynomials are fixed by the "initial"

condition $\mathcal{F}(0,Q)=\delta(Q+1)$, which corresponds to a full polarization at $x=0$. This yields the following solution $\mathcal{F}(x,Q)$

$$\mathcal{F}(x,Q)=\sum_{m=0}^{\infty}\left(m+\frac{1}{2}\right)(-1)^m P_m(Q)e^{-m(m+1)x}. \tag{7.7}$$

Summation over m in Eq. (7.7) can be performed explicitly by using the integral presentation

$$e^{-m^2x}=\int\frac{d\kappa}{\sqrt{\pi x}}\exp\left(-\frac{\kappa^2}{x}+2im\kappa\right), \tag{7.8}$$

and the identity

$$\sum_{m=0}^{\infty}(2m+1)\,P_m(Q)\zeta^m=\frac{1-\zeta^2}{(1-2Q\zeta+\zeta^2)^{3/2}}, \tag{7.9}$$

which can be easily derived from the generating function for the Legendre polynomials. Substituting $\zeta=-\exp(x-2i\kappa)$ and integrating by parts leads to the final result

$$\mathcal{F}(x,Q)=\frac{e^{x/2}}{i\sqrt{\pi x^3}}\int dk(k+ix)\frac{\exp\left(-\frac{k^2}{4x}-\frac{ik}{2}\right)}{\sqrt{2Q+e^{x-ik}+e^{-(x-ik)}}}. \tag{7.10}$$

The imaginary part of the integrand is odd in k. Therefore, we can ultimately present Eq. (7.10) as a purely real integral

$$\mathcal{F}(x,Q)=\frac{e^{x/2}}{4\sqrt{\pi x^3}}\int_0^{\infty}\frac{dk\,\exp\left(-k^2/4x\right)}{\left\{\left[(\cos k+Q\cosh x)^2+(1-Q^2)\sinh^2 x\right]^{1/2}+\left[e^{-x}\cos^2 k+Q\cos k+\sinh x\right]\right\}^{1/2}}$$
$$\times\left(x-\frac{(e^{-x}\cos k+Q)\,(k\sin k-x\cos k)-x\sinh x}{\left[(\cos k+Q\cosh x)^2+(1-Q^2)\sinh^2 x\right]^{1/2}}\right). \tag{7.11}$$

The difference between Eq. (7.11) and its counterpart [28] in the 1D Anderson model stems from the fact that the denominator in the identity (Eq. (7.9)) in our case, is complex.

7.5 Numerical results and analysis

The parameter $x=n\mathcal{R}^2$ in the argument of the distribution, Eq. (7.11), is related to the sample thickness, d and *classical* spin-diffusion length as $x=d/2\lambda_s$. It is seen from Fig. 7.3 that, as x passes through $x\sim 1$ the distribution evolves from δ-function (at $x\ll 1$) to linear and, eventually, to flat. Flat distribution manifests complete spin-memory loss. Still, even when this loss is small on average, a sizable part of the distribution lies in the domain $Q>0$, which corresponds to negative TMR. Note that, upon neglecting interference in Eq. (7.5), the distribution becomes $\delta\left(Q+e^{-2x}\right)$, i.e., infinitely narrow.

Until now we neglected the effects caused by the randomness of the waiting times, τ_i. With regard to the distribution $\mathcal{F}(x,Q)$, this randomness amounts to replacement

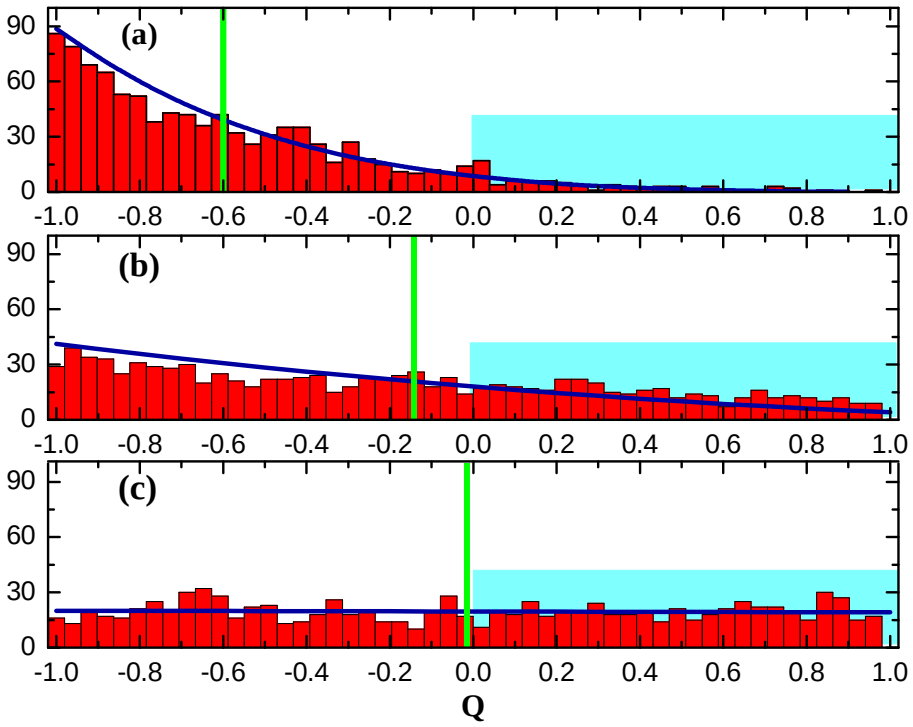

Figure 7.3: Solid lines denote the distribution function of the local degree of polarization, Q, for different rotation strengths on the sites plotted from Eq. (7.11) for values $x = n\mathcal{R}^2 = 0.20(a), 0.58(b)$, and $2.45(c)$. Red bins are the result of numerical simulation of the system for 10^4 random realizations of hyperfine fields, with $n = 20$ and $n\mathcal{R}^2$ as above. Classical values of polarization are shown with green bars. Blue rectangles highlight the domains of negative TMR.

of $\mathcal{R}^2$ by $\langle \mathcal{R}^2 \rangle_{\tau_i}$ in the parameter x. A much more delicate issue is whether or not the randomness in τ_i affects the local value of TMR. Naturally, the TMR, measured by a local probe, is the average over all τ_i. Then the question arises whether this averaging washes out the difference between the points at which the TMR is measured, i.e., replaces the local Q by $\exp(-d/\lambda_s)$ or, on the contrary, the averaged TMR is a unique signature of the actual realization of the hyperfine fields along a given current path. We argue that the second scenario holds. Our argument is two-fold. Firstly, we performed direct numerical simulation of local spin polarization along a *given* path with randomness in τ_i incorporated, see Appendix 7.7. The results shown in Fig. 7.4 demonstrate that while this randomness broadens the histograms, their center, which is the observable quantity, depends dramatically on actual orientations of the hyperfine fields along the path. Secondly, our analytical calculation, which is given in Appendix 7.7, demonstrates that while the disorder due to random orientations is short-ranged, $\langle b_x(\tau) b_x(\tau') \rangle_{b_{i,x}} = \exp\left(-\frac{|\tau-\tau'|}{\tau^*}\right)$, the same correlator calculated with *given* hyperfine-field realization but with random τ_i falls off very slowly, as a power law. On the basis of the two preceding arguments we conclude that at time scales where nuclear spin-spin interaction does not rearrange the hyperfine-field configuration, the TMR remains specific for this configuration.

7.6 Concluding Remarks

Our theory applies for OSVs with thin inhomogeneous active layers, depicted in Fig. 7.1, in which the transport can be modeled with directed noncrossing paths [9].

In this paper we treated the time evolution of the amplitudes (a_1, a_2) in terms of a product of matrices. An alternate approach would be to start from the Schrödinger equations, namely, $i\dot{a}_1 = \frac{1}{2} b_\perp(\tau) a_2(\tau)$, and $i\dot{a}_2 = \frac{1}{2} b_\perp^*(\tau) a_1(\tau)$. These two equations can be reduced to a single second-order equation for, say, a_1. This equation can then be reduced to the Schrödinger-like form. This procedure would formally demonstrate why the spin evolution maps on *non-hermitian* 1D Anderson model: The effective potential, $\frac{1}{2b_\perp^2}\left(\ddot{b}_\perp b_\perp - \frac{3}{2}\dot{b}_\perp^2\right)$, in the Schrödinger equation appears to be *complex* [29].

7.7 Appendix

In this appendix we present the derivations of numerous results which are used in the chapter.

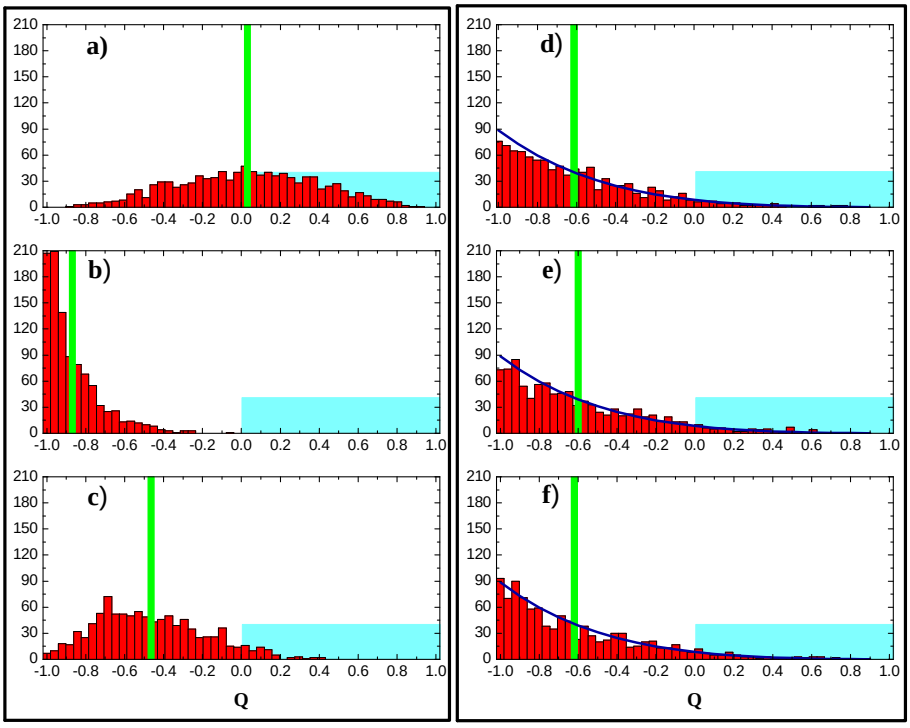

Figure 7.4: Histograms of the spin polarization, Q, from simulation of the system with $n = 20$, $\langle \mathcal{R}^2 \rangle = 0.01$. a-c: In each of three histograms the orientations of hyperfine fields are *fixed*; the spread of Q-values is due to the randomness in the waiting times. d-f: Three histograms generated for the same number (10^3) of realizations as in the left, but with allowance for randomness in the hyperfine-field orientations. Values of TMR in a-c, which are the averages of the histograms (green), are specific for the configuration of the hyperfine field. On the contrary, the histograms in d-f approach the theoretical result, Eq. (7.11), shown with solid line. These histograms would represent the evolution of local TMR when field configuration slowly rotates due to, e.g. spin-spin interaction.

7.7.1 Distribution of off-diagonal element of the evolution matrix

The expression $\mathcal{R} = |b_{n,\perp}|\,\tau_n/2$ for the off-diagonal element of the evolution matrix applies in the limit of weak rotation, $\mathcal{R} \ll 1$. The spread in the local values of $\mathcal{R}$ originates from the randomness of $b_{n,\perp} = (b_x, b_y)$ as well as from the randomness of the waiting times, τ_n. Therefore, the calculation of the distribution function of $\mathcal{R}$ involves averaging over three random variables

$$H(\mathcal{R}) = \int \frac{d^2 b_\perp}{\pi b_0^2} \exp\left(-\frac{b_\perp^2}{b_0^2}\right) \int_0^\infty d\tau F(\tau)\delta\left(\mathcal{R} - \frac{|b_\perp|\,\tau}{2}\right), \tag{7.12}$$

where $F(\tau) = \frac{1}{\tau^*}\exp\left(-\frac{\tau}{\tau^*}\right)$ is the Poisson distribution. Introducing dimensionless variables, $x = b_\perp/b_0$, and integrating over τ with the help of the δ-function yields

$$H(\mathcal{R}) = \frac{4}{b_0\tau} \int_0^\infty dx\ \exp\left(-x^2 - \frac{2\mathcal{R}}{b_0\tau^* x}\right). \tag{7.13}$$

For $\mathcal{R} > b_0\tau^*$ the above integral can be calculated using the steepest-descent method

$$H(\mathcal{R}) = \frac{2}{\sqrt{3}}\left(\frac{2\sqrt{\pi}}{b_0\tau^*}\right)\exp\left[-3\left(\frac{\mathcal{R}}{b_0\tau^*}\right)^{2/3}\right]. \tag{7.14}$$

It turns out that Eq. (7.14) provides an excellent approximation for *all* values of $\mathcal{R}$. For example, for $\mathcal{R} = 0$ the difference between the exact value and Eq. (7.14) amounts to a factor $2/\sqrt{3}$. We checked numerically that, with the latter distribution, the histograms of local polarization do not differ from box-like distribution.

Another effect of randomness in the waiting times originates from the phase $\chi = \frac{b_z\tau}{2}$ in the matrix Eq. (2). Thus, a rigorous account of the spread in τ_i requires generating random χ_i and $\mathcal{R}_i$ from the joint distribution

$$\tilde{H}(\mathcal{R},\chi) = \int \frac{d^3 b}{(\pi b_0^2)^{3/2}} \exp\left(-\frac{b^2}{b_0^2}\right) \int_0^\infty d\tau F(\tau)\delta\left(\mathcal{R} - \frac{|b_\perp|\,\tau}{2}\right)\delta\left(\chi - \frac{|b_z|\,\tau}{2}\right). \tag{7.15}$$

Since typical $\mathcal{R}$ and χ are of the same order, we again used in the simulations the $\mathcal{R}_i$-values uniformly distributed between 0 and $\mathcal{R}$ and χ_i values uniformly distributed between $-\frac{\mathcal{R}}{2}$ and $\frac{\mathcal{R}}{2}$. The results are shown in Fig 7.3.

7.7.2 Temporal correlators of the random fields

Consider a hopping chain containing $N \gg 1$ sites. For concreteness we will consider only the correlation of the x-projections of the hyperfine fields. In the course of transit between the electrodes, the carrier spin "sees" this projection in the form of a telegraph signal

$$b_x(t) = \sum_{i=0}^{N} (b_{i+1} - b_i)\theta(\tau - \sum_{j=0}^{i} \tau_j), \tag{7.16}$$

where $\theta(\tau)$ is a step-function, b_i is the x-projection on site i, and τ_i are the random waiting times for the hop $i \to (i+1)$. As was mentioned in the main text, there are two correlators, $\langle b_x(\tau) b_x(\tau + T)\rangle$, relevant for TMR. The first is

$$K_1(T) = \Big\langle b_x(\tau) b_x(\tau + T) \Big\rangle_{\{\tau_i\}}, \tag{7.17}$$

for a *fixed* realization, $\{b_i\}$, and randomness coming only from the Poisson distribution of τ_i. The second correlator, K_2, is K_1 averaged over all possible realizations of hyperfine fields

$$K_2(T) = \Big\langle b_x(\tau) b_x(\tau + T) \Big\rangle_{\{b_i\},\{\tau_i\}} = \langle K_1(T)\rangle_{\{b_i\}}. \tag{7.18}$$

It is easy to see that $K_2(T)$ has a simple form,

$$K_2(T) = b_0^2 \exp(-T/\tau^*), \tag{7.19}$$

and decays on the time scale of a single hop $\sim \tau^*$. On the other hand, as we will see below, $K_1(T)$ persists at much longer times. The result, Eq. (7.19), can be established from the simple reasoning: The product $b_x(\tau) b_x(\tau + T)$ contains the terms of the type b_i^2 and the terms $b_i b_j$ with $j \neq i$. The latter terms vanish upon configurational averaging. The terms b_i^2 are nonzero only if T is smaller than τ_i. The corresponding probability can be expressed as $\theta(\tau_i - T)$. Subsequent averaging over τ_i leads us to Eq. (7.19).

Turning to the correlator K_1, in order to perform averaging over τ_i in Eq. (7.17), we use the integral representation of the θ-function and cast $b_x(\tau)$ in the form

$$b_x(\tau) = \int \frac{d\omega\ e^{-i\omega\tau}}{-2\pi i\omega} \left(b_1 e^{i\omega\tau_1} + (b_2 - b_1) e^{i\omega(\tau_1+\tau_2)} + \cdots \right). \tag{7.20}$$

In a similar way the product $b_x(\tau) b_x(\tau + T)$ can be presented as a double integral

$$b_x(\tau) b_x(\tau + T) = \int \frac{d\omega\ e^{-i\omega\tau}}{-2\pi i\omega} \int \frac{d\omega'\ e^{-i\omega'(\tau+T)}}{-2\pi i\omega'} \left(b_1 e^{i\omega\tau_1} + (b_2 - b_1) e^{i\omega(\tau_1+\tau_2)} + \cdots \right) \times \left(b_1 e^{i\omega'\tau_1} + (b_2 - b_1) e^{i\omega'(\tau_1+\tau_2)} + \cdots \right). \tag{7.21}$$

The advantage of the above representation is that it allows averaging over τ_i in the integrand using the relation

$$\langle e^{i\omega\tau_i}\rangle = \int_0^\infty d\tau\, e^{i\omega\tau} F(\tau) = \frac{1}{1-i\omega\tau^*}. \tag{7.22}$$

Obviously, the average $\langle b_x(\tau)b_x(\tau+T)\rangle$ does not depend on τ, since it should be understood as $\lim\limits_{\mathcal{T}\to\infty} \frac{1}{\mathcal{T}}\int_0^{\mathcal{T}} d\tau\langle b_x(\tau)b_x(\tau+T)\rangle$. Then the integration over τ sets $\omega = -\omega'$.

The coefficient in front of b_ib_j-term in the product, Eq. (7.21), is given by

$$\frac{\exp(-i\omega T)}{2\pi\omega^2}\left[\exp\left(i\omega\sum_{k=0}^{i}\tau_k\right) - \exp\left(i\omega\sum_{k=0}^{i-1}\tau_k\right)\right]\left[\exp\left(-i\omega\sum_{k=0}^{j}\tau_k\right) - \exp\left(-i\omega\sum_{k=0}^{j-1}\tau_k\right)\right]. \tag{7.23}$$

Assume that j is smaller than i, then all terms with $k < (j-1)$ do not enter into Eq. (7.23). As a result, the averaging over remaining $i-j+1$ random times leads to the following result for the coefficient in front of b_ib_j

$$\frac{\exp(-i\omega T)}{2\pi}\begin{cases}\dfrac{1}{(1-i\omega\tau^*)^{i-j+1}}, & i \geq j\\ \dfrac{1}{(1+i\omega\tau^*)^{j-i+1}}, & i < j\end{cases}. \tag{7.24}$$

The remaining step is the integration over ω in Eq. (7.21). This integration is carried out straightforwardly by closing the contour in the bottom half of the complex ω-plane. The ω-integral is nonzero only for $j \leq i$. The final expression for the coefficient in front of b_ib_j reads

$$\int \frac{d\omega}{2\pi}\frac{e^{-i\omega T}}{(1-i\omega\tau^*)^{i-j+1}} = \frac{1}{(i-j)!}\left(\frac{T}{\tau^*}\right)^{(i-j)}\exp\left(-\frac{T}{\tau^*}\right). \tag{7.25}$$

Thus, the final result for the correlator K_1 acquires the form

$$K_1(T) = K_2(T) + \frac{1}{N}\sum_{i=1}^{N}\sum_{j<i} b_ib_j\left[\frac{1}{(i-j)!}\left(\frac{T}{\tau^*}\right)^{(i-j)}\exp\left(-\frac{T}{\tau^*}\right)\right]. \tag{7.26}$$

Note that if we perform averaging over b_i-s, the second term will vanish, and we will recover the expected result, Eq. (7.19). For nonaveraged K_1 the term in the square brackets restricts the domain of summation over $(i-j)$ to $\left|i-j-\frac{T}{\tau^*}\right| \leq \sqrt{\frac{T}{\tau^*}}$. Therefore, if the length of the chain, N, is smaller than $\frac{T}{\tau^*}$ the above condition will *never* be satisfied, and K_1 will fall off exponentially with T with characteristic decay time τ^*. In the opposite limit, the summation over i, j within the allowed domain will eliminate T dependence from $K_1(T)$. We can now restate the above observation as follows: $K_1(T)$ weakly depends on T for $T < N\tau^*$, and decays exponentially with T for $T > N\tau^*$. Since the transport of electron between the electrodes takes the time $N\tau^*$, we conclude that the realization of the hyperfine field does not change during this time interval.

Finally, to estimate the magnitude of $K_1(T)$ for $T < N\tau^*$, we calculate the quantity K_1^2 and average it over hyperfine fields. This averaging can be performed analytically. The result is conveniently expressed through the modified Bessel function, I_0, as

$$\langle K_1(T)^2\rangle_{\{b_i\}} = b_0^4 I_0\left(2\frac{T}{\tau^*}\right)\exp\left(-2\frac{T}{\tau^*}\right). \tag{7.27}$$

For $T > \tau^*$ Eq. (7.27) simplifies to $K_1(T)^2 = b_0^4/\sqrt{4\pi T/\tau^*}$.

7.7.3 Broadening of the classical distribution

As was mentioned in the main text, neglecting the interference in Eq. (7.5) leads to the infinitely sharp distribution, $\tilde{\mathcal{F}}(x,Q) = \delta(Q + e^{-2x})$. This conclusion, however, implies that the magnitudes of $\mathcal{R}$ are the same on each site. In reality the magnitudes of $\mathcal{R}$ are distributed according to Eq. (7.14). This will cause a broadening of the classical distribution function, $\tilde{\mathcal{F}}(x,Q)$, which we estimate below.

We begin with the recurrence relation for $\tilde{\mathcal{F}}_n(Q)$

$$\tilde{\mathcal{F}}_{n+1}(Q_{n+1}) = \int_{-1}^{1} dQ_n\, \tilde{\mathcal{F}}_n(Q_n) \int d\mathcal{R}\; H(\mathcal{R})\, \delta\left(Q_{n+1} - Q_n(1-\mathcal{R}^2)\right). \tag{7.28}$$

The explicit form of $\tilde{\mathcal{F}}_n(Q)$ can be found exactly for arbitrary distribution $H(\mathcal{R})$. For this purpose we introduce a new variable $z = \ln Q$ and rewrite Eq. (7.28) in terms of the function $G(z) = e^z\tilde{\mathcal{F}}(e^z)$,

$$G_{n+1}(z) = \int d\mathcal{R}\; H(\mathcal{R}) G_n\left(z - \ln(1-2\mathcal{R}^2)\right). \tag{7.29}$$

The right-hand-side of Eq. (7.29) is a convolution and turns into a product upon the Fourier transform. This readily yields

$$G_n(k) = G_0(k)\left[\int d\mathcal{R}\; H(\mathcal{R})\exp\left(2ik\mathcal{R}^2\right)\right]^n. \tag{7.30}$$

For large n the form of $G_n(k)$ and, correspondingly, the form of the distribution $G_n(z)$ approaches to the Gaussian. Thus, the distribution $\tilde{\mathcal{F}}(Q)$ is essentially log-normal

$$\tilde{\mathcal{F}}_n(Q) = \frac{1}{|Q|\sqrt{\pi n\sigma_{\mathcal{R}^2}}}\exp\left[\frac{\left(\ln|Q| + n\langle R^2\rangle\right)^2}{n\sigma_{\mathcal{R}^2}}\right], \tag{7.31}$$

where $\sigma_{\mathcal{R}^2} = \left(\langle R^4\rangle - \langle R^2\rangle^2\right)$. It follows from Eq. (7.31) that the center of the distribution, $\tilde{\mathcal{F}}_n(Q)$, moves linearly with n, which is the same as the average of the quantum distribution, while the width slowly grows with n as $\delta Q = \sqrt{n\sigma_{\mathcal{R}^2}}\exp(n\langle\mathcal{R}^2\rangle)$. Strong local *quantum* fluctuations of TMR persist up to $n\mathcal{R}^2 \lesssim 1$. For such n the width of the classical distribution

remains smaller than $\mathcal{R}$. Note also that probabilistic treatment of the spin rotation encoded in Eq. (7.28) forbids negative TMR, i.e., restricts the domain of $\tilde{\mathcal{F}}_n(Q)$ to negative Q.

If, however, we proceed from the classical limit of Eq. (7.5) to the Fokker-Planck equation, then the classical limit of the Fokker-Planck equation would correspond to neglecting Q^2 in the right-hand side of Eq. (7.6). Note that by doing so, we also remove the restriction that Q is negative. The Fokker-Planck equation in this limit reduces to a heat equation, and, similarly to the quantum result, yields a flat distribution at large x. This corresponds to "temperature equilibration" at long times. Even though the classical and quantum Fokker-Plank results share limiting behavior and have the same average at all times, their shapes are visibly distinct.

In this subsection we have demonstrated that there are two different classical limits of the quantum spin evolution. They predict two dramatically different shapes for the distribution of spin polarization.

7.8 References

[1] Z. H. Xiong, D. Wu, Z. V. Vardeny, and J. Shi, Nature (London) **427**, 821 (2004).

[2] S. Pramanik, C.-G. Stefanita, S. Patibandla, S. Bandyopadhyay, K. Garre, N. Harth, and M. Cahay, Nat. Nanotechnol. **2**, 216 (2007).

[3] V. A. Dediu, L. E. Hueso, I. Bergenti, and C. Taliani, Nat. Mater. **8**, 850 (2009).

[4] A. J. Drew, J. Hoppler, L. Schulz, F. L. Pratt, P. Desai, P. Shakya, T. Kreouzis, W. P. Gillin, A. Suter, N. A. Morley, V. K. Malik, A. Dubroka, K. W. Kim, H. Bouyanfif, F. Bourqui, C. Bernhard, R. Scheuermann, G. J. Nieuwenhuys, T. Prokscha, and E. Morenzoni, Nat. Mater. **8**, 109 (2009).

[5] T. Nguyen, G. Hukic-Markosian, F. Wang, L. Wojcik, X. Li, E. Ehrenfreund, Z. Vardeny, Nat. Mater. **9**, 345 (2010).

[6] T. D. Nguyen, F, Wang, X.-G. Li, E. Ehrenfreund, and Z. V. Vardeny, Phys. Rev. B **87**, 075205 (2013).

[7] M. Grünewald, J. Kleinlein, F. Syrowatka, F. Würthner, L.W. Molenkamp, and G. Schmidt, arXiv:1304.2911.

[8] A. Riminucci, M. Prezioso, C. Pernechele, P. Graziosi, I. Bergenti, R. Cecchini, M. Calbucci, M. Solzi, V. A. Dediu, Appl. Phys. Lett. **102**, 092407 (2013).

[9] M. Grünewald, R. Göckeritz, N. Homonnay, F. Würthner, L. W. Molenkamp, and G. Schmidt, Phys. Rev. B **88**, 085319 (2013).

[10] T. D. Nguyen, F. Wang, X.-G. Li, E. Ehrenfreund, and Z. V. Vardeny, Phys. Rev. B **87**, 075205 (2013).

[11] C. Barraud, P. Seneor, R. Mattana, S. Fusil, K. Bouzehouane, C. Deranlot, P. Graziosi, L. Hueso, I. Bergenti, V. Dediu, F. Petroff, and A. Fert, Nat. Phys. **6**, 615 (2010).

[12] S. L. Kawahara, J. Lagoute, V. Repain, C. Chacon, Y. Girard, S. Rousset, A. Smogunov, and C. Barreteau, Nanoletters **12**, 4558 (2012).

[13] S. H. Liang, D. P. Liu, L. L. Tao, X. F. Han, and Hong Guo, Phys. Rev. B **86**, 224419 (2012).

[14] J. M. De Teresa, A. Barthélémy, A. Fert, J. P. Contour, R. Lyonnet, F. Montaigne, P. Seneor, and A. Vaurès, Phys. Rev. Lett. **82**, 4288 (1999).

[15] W. Xu, G. J. Szulczewski, P. LeClair, I. Navarrete, R. Schad, G. Miao, H. Guo, and A. Gupta, Appl. Phys. Lett. **90**, 072506 (2007).

[16] S. Mooser, J. F. K. Cooper, K. K. Banger, J. Wunderlich, and H. Sirringhaus, Phys. Rev. B **85**, 235202 (2012).

[17] S. Mandal and R. Pati, ACS Nano, **6**, 3580 (2012).

[18] M. A. Tanaka, T. Hori, K. Mibu, K. Kondou, T. Ono, S. Kasai, T. Asaka, and J. Inoue, J. Appl. Phys. **110**, 073905 (2011).

[19] J. J. H. M. Schoonus, P. G. E. Lumens, W. Wagemans, J. T. Kohlhepp, P. A. Bobbert, H. J. M. Swagten, and B. Koopmans, Phys. Rev. Lett. **103**, 146601 (2009).

[20] N. J. Harmon and M. E. Flatté, Phys. Rev. Lett. **110**, 176602 (2013).

[21] K. M. Alam and S. Pramanik, arXiv:1005.1118.

[22] M. Julliére, Phys. Lett. **54A**, 225 (1975).

[23] R. C. Roundy and M. E. Raikh, arXiv:1308.3801.

[24] T. L. A. Tran, T. Q. Le, J. G. M. Sanderink, W.G. van der Wiel, and M. P. deJong, Adv. Funct. Mater., **22**, 1180 (2012).

[25] R. N. Mahato, H. Lülf, M. H. Siekman, S. P. Kersten, P. A. Bobbert, M. P. de Jong, L. De Cola, W. G. van der Wiel, Science **341**, 257 (2013).

[26] N. F. Mott and W. D. Twose, Adv. Phys. **10**, 107 (1961); V. L. Berezinskii, Zh. Eksp. Teor. Fiz. **65**, 1251 (1973) [Sov. Phys. JETP **38**, 620 (1974)].

[27] P. W. Anderson, D. J. Thouless, E. Abrahams, and D. S. Fisher, Phys. Rev. B **22**, 3519 (1980).

[28] F. M. Izrailev, A. A. Krokhin, and N. M. Makarov, Phys. Rep. **512**, 125 (2012).

[29] Potential with imaginary component emerges also in the study of light propagation through a random medium in the presence of absorption, see e.g. V. Freilikher, M. Pustilnik, and I. Yurkevich, Phys. Rev. Lett. **73**, 810 (1994); J. C. J. Paasschens, T. Sh. Misirpashaev, and C. W. J. Beenakker, Phys. Rev. B **54**, 11887 (1996); L. I. Deych, A. Yamilov, and A. A. Lisyansky, Phys. Rev. B **64**, 024201 (2001); M. S. Rudner and L. S. Levitov Phys. Rev. Lett. **102**, 065703 (2009). It should be noted that in our case the structure of the complex potential and ensuing physics are completely different.

CHAPTER 8

SPIN RELAXATION OF A DIFFUSIVELY MOVING CARRIER IN A RANDOM HYPERFINE FIELD

8.1 Introduction

One of the reasons why organic semiconductors are promising candidates for the active layers of spin valves [1, 2, 3, 4, 5] is a long spin lifetime, τ_s, in these materials. Due to long τ_s, spin-polarized carriers, injected from one ferromagnetic electrode into the active layer, preserve their spin orientation while traveling towards the other ferromagnetic electrode. As a result, the resistance of the device depends on the mutual orientations of magnetizations of the electrodes (the spin-valve effect). The origin of slow spin relaxation in organic semiconductors is that they are composed from light atoms with weak spin-orbit coupling.

In the absence of spin-orbit coupling the leading mechanism of the spin memory loss is a precession of spin in random hyperfine fields created by surrounding protons on the sites visited by the carrier in the course of traveling between the electrodes. With mobility in organic semiconductors being very low, the charge transport in them is via random inelastic hops of carriers between the sites. Then the waiting time, τ, for a subsequent hop plays the role of the correlation time for the random magnetic field, with rms b_0 acting on the carrier spin. As a result, the Dyakonov-Perel (DP) expression of Ref. [6] for τ_s assumes the form

$$\tau_s = \frac{1}{b_0^2 \tau}. \tag{8.1}$$

Naturally, for long τ_s, a typical partial rotation of spin, $\delta\varphi = b_0\tau$, during the waiting time is weak, $\delta\varphi \ll 1$. Assuming that all partial rotations are completely uncorrelated, the spin polarization, averaged over realizations of the hyperfine fields, falls off with the number of hops, N, as $\langle S_z(N)\rangle = S_z(0)\exp\left(-N\delta\varphi^2\right)$. This suggests that the evolution of $\langle S_z\rangle$ with time $t = N\tau$ is a simple exponent

$$\langle S_z(t)\rangle = S(0)\exp\Big(-\frac{t}{\tau_s}\Big). \tag{8.2}$$

The main message of the present paper is that the random walk of a carrier over the sites induces the correlation in hyperfine fields "sensed" by the carrier spin. This correlation

modifies the decay law Eq. (8.2). The origin of correlation is the self-intersections of the random-walk trajectories, see Fig. 8.1. These self-intersections imply multiple visits of the carrier to the *same* site. Then the corresponding partial rotations *add up*, which leads to acceleration of the spin relaxation. The effect is most dramatic if the carrier moves in one dimension. Then, in the course of N hops, the carrier visits $N^{1/2}$ sites, and the number of visits to a given site is also $N^{1/2}$. The N-dependence of $\langle S_z \rangle$ can be found from the above derivation of Eq. (8.2) upon replacement $N \to N^{1/2}$ and $\delta\varphi \to N^{1/2}\delta\varphi$. This yields $\langle S_z(N) \rangle = S_z(0) \exp\left(-N^{3/2}\delta\varphi^2\right)$, and, correspondingly, the time dependence

$$\langle S_z(t) \rangle = S(0) \exp\Big(-\frac{t^{3/2}}{\tau^{1/2}\tau_s}\Big). \tag{8.3}$$

In higher dimensions, $d = 2$ and $d = 3$, the number of self-crossings of an N-step random-walk trajectory is $\sim N$ and $\sim N^{1/2}$, respectively, i.e., each site is visited twice with probability ~ 1 for $d = 2$, and with probability $N^{-1/2}$ for $d = 3$. As a result, the change, $\langle \delta S_z(t) \rangle$, of the decay law Eq. (8.2) due to accumulation of the partial rotations is of the order of $\langle S_z(t) \rangle$ for $d = 2$ and of the order of $(\tau/t)^{1/2} \langle S_z(t) \rangle$ for $d = 3$. Hover, even in the latter case the correction to Eq. (8.2) can be important since it induces a sensitivity of $\langle S_z(t) \rangle$ to a *weak* external magnetic field directed along z. Recall that without self-intersections the B-dependence of τ_s is given by the Hanle-type expression

$$\tau_s = \frac{1 + B^2\tau^2}{b_0^2\tau}, \tag{8.4}$$

which applies for $B \gg b_0$ and predicts that sensitivity to B emerges at $B \sim \tau^{-1} \gg b_0$. We will demonstrate that with self-crossings of the random-walk trajectories taken into account, the sensitivity to B develops at much smaller field $B \sim (\tau\tau_s^2)^{-1/3} \ll \tau^{-1}$ in one dimension and at $B \sim \tau_s^{-1} \ll \tau^{-1}$ for $d = 2$ and $d = 3$. Remarkably, the returns to the same site after a long time, t, give rise to the *oscillatory* correction $\propto \cos Bt$ to $\langle S_z(t) \rangle$, which is most pronounced for $d = 1$.

8.2 Diagrammatic expansion

To illustrate our main message, consider first a simplified situation, when the hyperfine field is located in the x, y-plane. Moreover, we will assume that the randomness in the in-plane field, $b_\perp = (b_x, b_y)$, is exclusively due to randomness in the azimuthal angle ϕ, i.e. $b_x = b_0 \cos\phi$, $b_y = b_0 \sin\phi$, see Fig. 8.1.

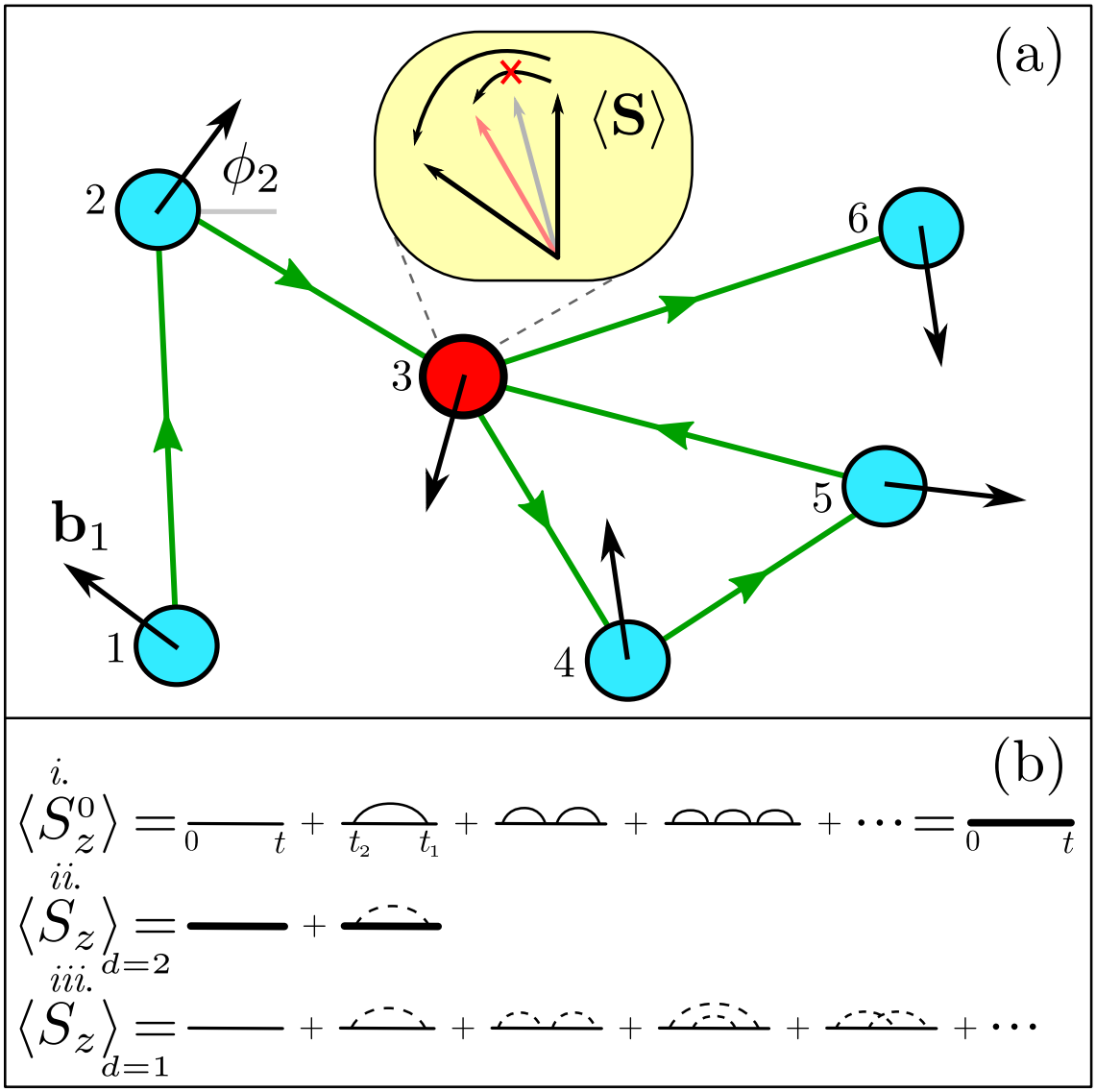

Figure 8.1: Depiction of spin memory loss for self intersecting paths. (a) In course of diffusion $1 \to 2 \to 3 \to 4 \to 5 \to 3 \to 6$ over sites hosting random hyperfine fields (black arrows) a carrier visits site 3 *twice*. As a result, the partial spin rotation doubles, see enlargement; (b) *i.* For a trajectory without self-intersections $\langle S_z(t) \rangle$ is given by sequence of *nonintersecting* solid arcs encoding the correlator C_0, *ii.* Graphical representation of Eq. (8.11) for the $d = 2$ spin relaxation; self-intersections are captured by a single dashed arc encoding the correlator C_D, *iii.* Spin relaxation for $d = 1$ is described by diffusive diagrams *only*.

The spin operator satisfies the equation of motion, $i\frac{d\widehat{S}}{dt} = [\widehat{S}, \widehat{H}]$, with Hamiltonian $\widehat{H} = \widehat{S} \cdot \boldsymbol{b}(t)$. Excluding the in-plane components of the operator $\widehat{S}$, the equation of motion for S_z takes the form

$$S_z(t) = 1 - b_0^2 \int_0^t dt_1 \int_0^{t_1} dt_2 \ \cos(\phi(t_1) - \phi(t_2)) S_z(t_2). \tag{8.5}$$

To find the time evolution of the average, $\langle S_z(t) \rangle$, it is necessary to iterate Eq. (8.5) as

$$\begin{aligned} S_z(t) = 1 - b_0^2 \int_0^t dt_1 \int_0^{t_1} dt_2 \cos(\phi(t_1) - \phi(t_2)) \\ + b_0^4 \int_0^t dt_1 \int_0^{t_1} dt_2 \int_0^{t_2} dt_3 \int_0^{t_3} dt_4 \cos(\phi(t_1) - \phi(t_2)) \cos(\phi(t_3) - \phi(t_4)) - \cdots \end{aligned} \tag{8.6}$$

and perform averaging over the random azimuthal angle, $\phi(t)$. Without self-intersections of the random-walk trajectories, this averaging is straightforward since the angles $\phi(t)$, $\phi(t')$ are correlated only for $|t - t'| \lesssim \tau \ll t$, i.e.

$$\langle \cos(\phi(t) - \phi(t')) \rangle = \exp\left[-|t - t'|/\tau\right] = C_0(t, t'). \tag{8.7}$$

The exponential character of C_0 expresses the Poisson distribution of the waiting times.

Each term of the expansion Eq. (8.6) can be graphically expressed as a diagram, see Fig. 8.1. Because of the short-time decay of C_0, the arcs corresponding to C_0 terms are not allowed to cross. More precisely, each crossing of arcs gives rise to a small factor $\tau/t \ll 1$. On the other hand, averaging of each term with n nonintersecting arcs yields $(-1)^n (b_0\tau)^{2n}/n!$, and we restore Eq. (8.2).

As a consequence of self-intersections of the random-walk path, the difference $(\phi(t) - \phi(t'))$ can be small even if the moments t and t' are well separated in time. Quantitatively, this is captured by the diffusive contribution, C_D, to the correlator

$$\langle \cos(\phi(t) - \phi(t')) \rangle = \left[\frac{1}{\pi D(t + t')}\right]^{d/2} = C_D(t, t'), \tag{8.8}$$

where the diffusion coefficient D is $1/\tau$ assuming that the separation between neighboring sites is unity. The form of Eq. (8.8) is established from the following reasoning. Denote with $P(\boldsymbol{r}, t) = \frac{1}{(\pi D t)^{d/2}} \exp\left(-\frac{\boldsymbol{r}^2}{Dt}\right)$ the distribution function of position of a particle in the course of a random walk. Then the probability that the particle visits the same site, $\boldsymbol{r}$, at time t and at time t' is given by $\int d\boldsymbol{r} P(\boldsymbol{r}, t) P(\boldsymbol{r}, t')$, which immediately leads to Eq. (8.8).

The correlator C_D should also be incorporated into the diagrammatic expansion; we denote it with dashed arcs, see Fig. 8.1. For example, the diagram involving only one dashed arc is given by

$$\lambda_d(t) = b_0^2 \int_0^t dt_1 \int_0^{t_1} dt_2 \left[\frac{1}{\pi D\,(t_1+t_2)}\right]^{d/2} = A_d \frac{b_0^2\, t^{2-\frac{d}{2}}}{D^{d/2}}, \tag{8.9}$$

where

$$A_1 = \frac{4(2^{1/2}-1)}{3\pi^{1/2}},\ A_2 = \frac{\ln 2}{\pi},\ A_3 = \frac{2^{3/2}\left(2^{1/2}-1\right)}{\pi^{3/2}}. \tag{8.10}$$

Expression Eq. (8.9) confirms the qualitative argument given in the Introduction. Namely, for $d = 1$, the averaged expansion Eq. (8.6) becomes a series in the dimensionless combination $b_0^2 t^{3/2}\tau^{1/2}$. Note also, that for $d = 1$ the diffusive contribution Eq. (8.9) exceeds by $(t/\tau)^{1/2}$ the contribution coming from a single solid-arc. This illustrates the fact that each site is visited many times in the course of a $d = 1$ random walk.

In 2D the contributions from the solid and dashed arcs are comparable. While we cannot find the averaged spin-dynamics analytically, we can still take advantage of the fact that $A_2 \approx .22$ is small and sum up *all* diagrams containing only zero or one dashed arc. The most delicate ingredient of this procedure is that decorating the dashed arc with all possible arrangements of solid arcs amounts to the replacement $C_D(t_1+t_2) \to C_D(t_1+t_2)\exp\left[-\frac{(t_1-t_2)}{2\tau_s}\right]$. Physically, this means that between the two subsequent visits to the same site at time moments t_1 and t_2, the spin polarization is "forgotten" in the course of many short-time hops. The emergence of the nontrivial factor $1/2$ in the exponent is demonstrated in Appendix 8.6 where we also show that the presence of a z-component of the hyperfine field amounts to the replacement $C_D(t_1+t_2) \to C_D(t_1+t_2)\exp\left[-\frac{3(t_1-t_2)}{4\tau_s}\right]$.

To present the final result it is convenient to measure the intermediate times t_1 and t_2 in units of t. Then we have

$$\langle S_z(t)\rangle = e^{-t/\tau_s} - \frac{g_2 t}{2\tau_s} e^{-t/\tau_s} \int_0^1 dx_1 \int_0^{x_1} dx_2 \frac{\exp\left[-\frac{t}{2\tau_s}(x_1-x_2)\right]}{x_1+x_2}. \tag{8.11}$$

The second term is responsible for the deviation from a simple exponential decay. Upon rescaling $x_2 = sx_1$ and changing the order of integration, the result can be written as a single integral

$$\langle S_z(t)\rangle = e^{-t/\tau_s}\left(1 - g_2 \int_0^1 ds \frac{1-\exp\left[-\frac{t(1-s)}{2\tau_s}\right]}{1-s^2}\right). \tag{8.12}$$

At times $t \gg \tau_s$ the logarithmical divergence of the integral is cut off at $(1-s) \lesssim \frac{\tau_s}{t}$, leading to the long-time behavior $\langle S_z(t)\rangle = \exp\left(-\frac{t}{\tau_s}\right)\left[1 - \frac{g_2}{2}\ln\left(\frac{2t}{\tau_s}\right)\right]$. The prefactor g_2 calculated using the prefactor in the diffusive propagator appears to be $g_2 = 2/\pi$.

The expression for $\langle S_z(t)\rangle$ for the case of $d = 3$ random walk can be presented in the form similar to Eq. (8.12)

$$\langle S_z(t)\rangle = e^{-t/\tau_s} - \frac{2^{1/2}e^{-t/\tau_s}}{\pi}\int\limits_0^1 \frac{ds\ \mathrm{erf}\left\{[t(1-s)/2\tau_s]^{1/2}\right\}}{(1+s)^{3/2}(1-s)^{1/2}}, \tag{8.13}$$

where $\mathrm{erf}(z)$ is the error-function. In agreement with qualitative reasoning, the diffusive correction crosses over from $-\lambda_3(t)$ at small times to $-\frac{1}{\pi}(2\tau/\tau_s)^{1/2}\exp(-t/\tau_s)$ at large times.

8.3 Sensitivity to the magnetic field along the z-axis

Incorporating the constant, $\boldsymbol{B} = \boldsymbol{z}_0 B$, and random, $b_z(t)$, components of the magnetic field amounts to the replacement

$$\Big[\phi(t_1) - \phi(t_2)\Big] \to \left[\phi(t_1) - \phi(t_2) + B(t_1 - t_2) + \int\limits_{t_1}^{t_2} dt' b_z(t')\right] \tag{8.14}$$

in Eq. (8.6). As discussed in the Introduction, the solid-arc diagrams describing the hops to nearest neighbors during the time intervals $\sim \tau$ develop the sensitivity to B only for strong $B \sim \tau^{-1}$. On the other hand, the dashed-arc diagrams are defined by much longer times, and are thus sensitive to much weaker B. The most interesting domain of B for $d = 2, 3$ is $(b_0\tau)^{-1} \gg \frac{B}{b_0} \gg (b_0\tau)$, where $B\tau$ is small but $B\tau_s$ is large. In this domain the decay of $\langle S_z(t)\rangle$ is predominantly exponential while the B-dependence comes from the diffusive correction. For $d = 1$ the corresponding domain of B is $(b_0\tau)^{-1} \gg \frac{B}{b_0} \gg (b_0\tau)^{1/3}$. Technically, in this domain, one can neglect the decoration of the diffusive propagator by solid arcs and rewrite the diffusive contribution Eq. (8.9) as

$$\delta\langle S_z(t)\rangle = -b_0^2\tau^{\frac{d}{2}}\int\limits_0^t dt_1\int\limits_0^{t_1} dt_2 \frac{\cos B\,(t_1 - t_2)}{(t_1 + t_2)^{d/2}} = -b_0^2\tau^{\frac{d}{2}}t^{2-\frac{d}{2}}F_d\,(Bt)\,, \tag{8.15}$$

where the function $F_d\,(v)$ is defined as

$$F_d\,(v) = \int\limits_0^1 dx\int\limits_0^x dy\ \frac{\cos v(x-y)}{(x+y)^{d/2}}. \tag{8.16}$$

The form of the function, $F_d(v)$, suggests that the diffusive correction contains both smooth and *oscillating* contributions. The meaning of the smooth contribution is that, upon visiting the same site at times t_1 and t_2, partial spin rotations add up only if $|t_1 - t_2| \lesssim 1/B$. The oscillatory contribution originates from their "phase shift," $B(t_2 - t_1)$.

Analysis of Eqs. (8.15), (8.16) yields the following asymptotes describing the B-dependent correction to $\langle S_z(t)\rangle$

$$F_d(v)|_{v\gg 1} = \frac{\varkappa_d}{v^{2-d/2}} - \frac{\cos v}{v^2}, \tag{8.17}$$

where $\varkappa_d = (\pi/8)^{1/2}$, $\pi/4$, and $(\pi/2)^{1/2}$ for $d = 1, 2$, and 3, respectively. It follows from Eq. (8.17) that the magnetic field causes a cutoff of the diffusive correction, Eq. (8.15), so that the value $\delta\langle S_z(t)\rangle$ approaches the value $\sim -b_0^2\tau^{d/2}/B^{2-d/2}$ at large times. With regard to oscillations, their amplitude falls off with time as $\left(b_0^2/B^2\right)(\tau/t)^{d/2}$, i.e., the oscillations are more pronounced in lower dimensions.

8.4 Numerical results

We simulated the spin evolution numerically using the discrete version of the equation of motion

$$\boldsymbol{S}_i = \Big[\boldsymbol{S}_{i-1} - \boldsymbol{n}_i\,(\boldsymbol{n}_i\cdot\boldsymbol{S}_{i-1})\Big]\cos b_0\tau + (\boldsymbol{n}_i\times\boldsymbol{S}_{i-1})\sin b_0\tau + \boldsymbol{n}_i\,(\boldsymbol{n}_i\cdot\boldsymbol{S}_{i-1})\,, \tag{8.18}$$

so that the local hyperfine field had the same magnitude, b_0, on all sites while the directions, $\boldsymbol{n}_i$, were defined by either a random azimuthal angle, ϕ_i, or by two spherical angles, ϕ_i and θ_i. The diffusive motion of a carrier was simulated by randomly choosing $\boldsymbol{n}_i$ at the next step from one of the nearest neighbors of $\boldsymbol{n}_i$ at the previous step.

Our numerical results are shown in Figs. 8.2 and 8.3. We started by verifying that, for a directed walk, when *all* $\boldsymbol{n}_i$ are uncorrelated, $\langle S_z(i)\rangle$ decays as a simple exponent. It is seen from Fig. 8.2 that, upon allowing self-intersections, the numerical curve $\langle S_z(t)\rangle$ drops below the result for uncorrelated $\boldsymbol{n}_i$ after several steps. For a spherical hyperfine field, $\ln\langle S_z(t)\rangle$ remains essentially linear at large t, but with bigger slope, i.e., the evolution of $\langle S_z(t)\rangle$ exhibits a crossover from one simple exponent at short times to another simple exponent at long times. By contrast, for planar hyperfine field, $\langle S_z(t)\rangle$ is strongly nonlinear in the log-scale at all times. This completely nonexponential decay is very well described by Eq. (8.12) with $g_2 = 1.8$ instead of $2/\pi \approx 0.64$. In Appendix 8.6 we speculate about the microscopic origin of this enhanced decay by detailing the consequence of the trajectory self-intersection for the spin rotation.

As we argued, self-intersections give rise to the sensitivity of the spin relaxation to magnetic field $B \sim \frac{1}{\tau_s} \ll \frac{1}{\tau}$. Evolution of the numerical curves with B is shown in Fig. 8.2. A significant slowing down of the relaxation starts from $B \sim \frac{5}{\tau_s}$. We have also plotted an analytical dependence of $\langle S_z(t)\rangle$ obtained by introducing $\cos Bt(x_1 - x_2)$ into the integrand of Eq. (8.11). Qualitatively, the numerical and analytical curves exhibit similar behavior.

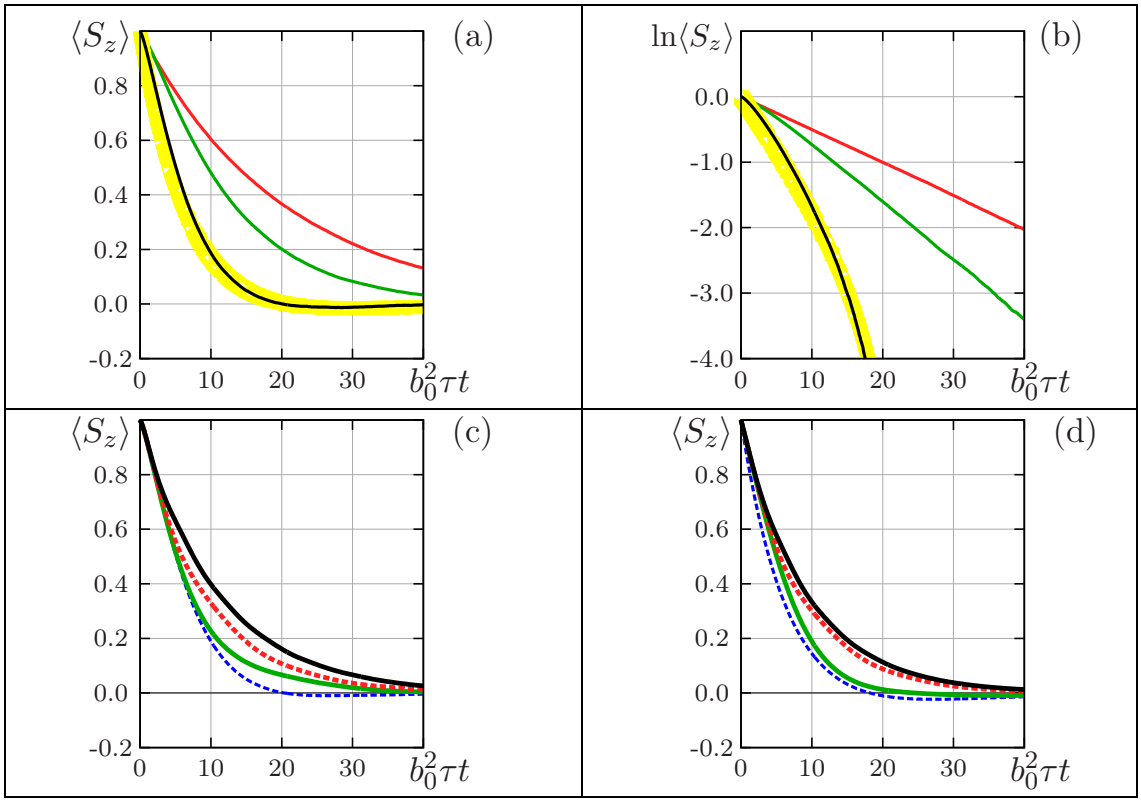

Figure 8.2: Numerical results for 2d random walk. (a) $d = 2$ spin relaxation for uncorrelated (no self-crossings) hyperfine fields $\boldsymbol{b}_i$ (red), with self-intersections and spherically distributed $\boldsymbol{b}_i$ (green), and with self-intersections and planar $\boldsymbol{b}_i$ (black); (b) same as (a) but in log-scale. The decay $\langle S_z(t)\rangle$ is a simple exponent (red), shows crossover between two simple exponents (green), strongly nonexponential (black). Yellow line is plotted from Eq. (8.11) with $g_2 = 1.8$; (c) and (d): weak external field $B \sim \tau_s^{-1}$ suppresses the effect of self-intersections. Numerical (c) and analytical (d) results illustrate how a simple-exponent decay is restored upon increasing $B\tau_s$. Results for $B = 0$ (blue), $B\tau_s = 2$ (green), $B\tau_s = 5$ (red), and $B\tau_s = 10$ (black) are shown.

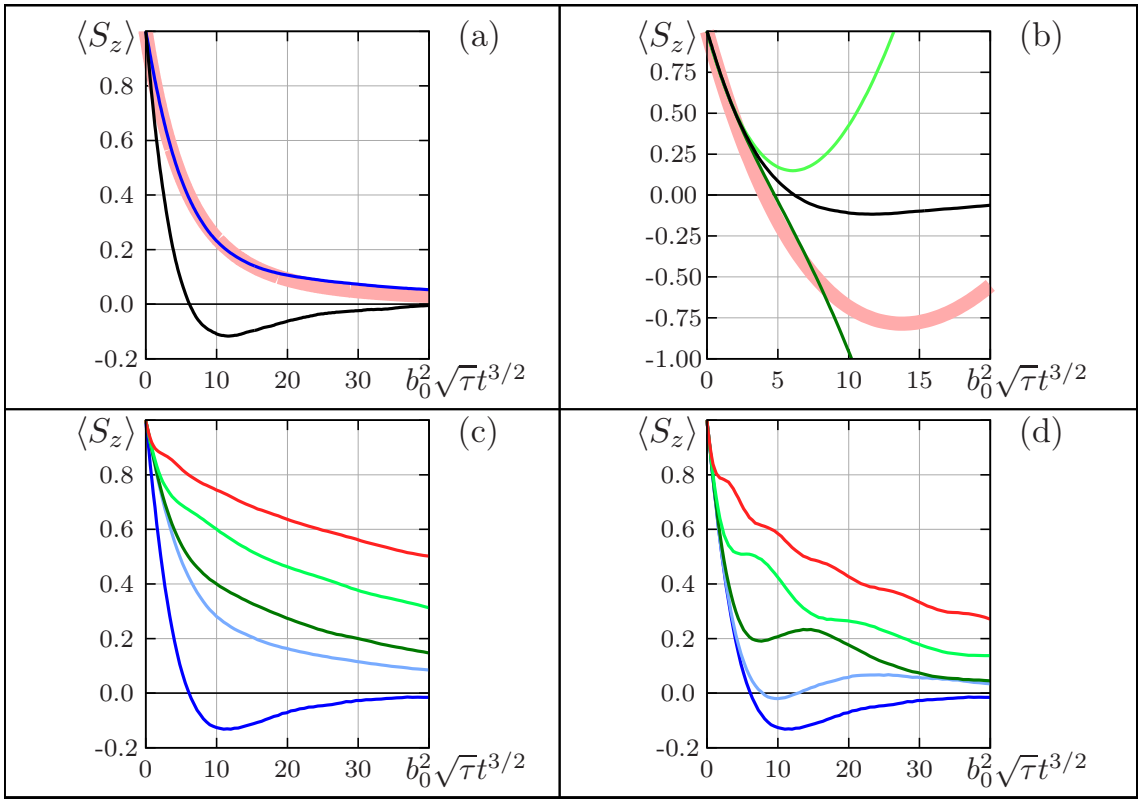

Figure 8.3: Numerical results for 1d random walk. For $d = 1$ random walk $\langle S_z(t)\rangle$ is a universal function of $b_0^2\sqrt{\tau}t^{3/2}$. Numerical results for a planar hyperfine field (black curves in (a) and (b)) exhibit spin reversal at intermediate time. For a spherically distributed $\boldsymbol{b}_i$ (blue curve in (a)) the decay is monotonic but nonexponential and is accurately captured by the solution of the self-consistent equation Eq. (8.19) (pink curve in (a)). (b) Results of the different variants of partial summation of diffusive diagrams, see text, are shown with dark-green, pink, and light-green lines. Weak external field slows down the decay of $\langle S_z(t)\rangle$ for both spherical (c) and planar $\boldsymbol{b}_i$ (d). Numerical results are shown for the following values of $\frac{B}{b_0^{4/3}\tau^{1/3}}$: 0 (dark blue), 1 (light blue), 2 (dark green), 4 (light green), and 8 (red).

Note, however, that the analytical curves saturate at $B\tau_s \sim 15$, while the numerical curves flatten progressively with increasing B. This discrepancy is simply due to the fact that the analytical curves correspond to a vanishing product $B\tau$, and thus cannot capture the conventional spin relaxation Eq. (8.4). With regard to the oscillating correction $\propto \cos Bt$ predicted by Eq. (8.17) they show up in simulations, but their magnitude is too small to be resolved in Fig. 8.2.

Numerical results for random walk in 1D are shown in Fig. 8.3. Firstly, we established that these numerical results perfectly satisfy the scaling relation predicted from the qualitative reasoning. Namely, when plotted versus $t^{3/2}b_0^2\tau^{1/2}$, they all fall on a single curve. We also see that the empirical prediction, Eq. (8.3), does not apply. In fact, for purely planar hyperfine field, the numerical curve, $\langle S_z(t)\rangle$, drops to a *negative* value $\langle S_z\rangle \approx -0.16$ before approaching zero. As we explained above, only the dashed arcs are responsible for the spin relaxation for $d = 1$. Therefore, capturing the nontrivial decay of $\langle S_z\rangle$ analytically, requires summation of at least a part of dashed-arc-diagrams to *all* orders.

In Appendix 8.6 we present two variants of such summation. They essentially reduce to exponentiating of one-dashed-arc contribution, $\lambda_1(t)$, Eq. (8.9), and differ by the way the numerical factors in the diagrams with crossings are counted. Two ways of approximate counting yield $\langle S_z(t)\rangle = \exp\left[-\lambda_1(t)\right]$ and $\langle S_z(t)\rangle = 2\exp\left[-\frac{\lambda_1(t)}{2}\right] - 1$, which lie above and below the numerical results. An alternative approach is to sum only the contributions from nonoverlapping diffusive diagrams, Fig. 8.1. We show that this summation leads to a self-consistent equation

$$\frac{d\langle S_z\rangle}{du} = -\frac{4}{9\pi^{1/2}u^{1/3}} \times \int_0^u \frac{du_1 \exp\left[-\left(u^{2/3} - u_1^{2/3}\right)^{3/2}\right] \langle S_z(u_1)\rangle}{u_1^{1/3}\left(u^{2/3} + u_1^{2/3}\right)^{1/2}}, \tag{8.19}$$

where $u = b_0^2\tau^{1/2}t^{3/2}$. When the hyperfine field is planar, the numerator in Eq. (8.19) is 1, and, as shown in Appendix 8.6, the solution is an oscillatory function which, at large times, is well approximated by the Bessel function, $J_0(\frac{4b_0\tau^{1/4}t^{3/4}}{3(2\pi)^{1/4}})$. Then a single sign reversal of $\langle S_z(t)\rangle$ in Fig. 8.3 can be viewed as a first surviving minimum of the Bessel function. For a spherical hyperfine field the simulated decay of $\langle S_z(t)\rangle$ does not follow the prediction Eq. (8.3), but is very accurately described by the solution of Eq. (8.19). Unlike $d = 2$, the oscillations in $\langle S_z(t)\rangle$ in a finite magnetic field are clearly seen in the numerical data. They develop at $B \approx b_0^{4/3}\tau^{1/3}$.

8.5 Discussion

The effect of returns to the origin on the spin relaxation was previously discussed in Refs. [7, 8, 9]. It was assumed that the mechanism of relaxation is the spin-orbit coupling [6]. For this mechanism, the random field "sensed" by electron depends on the direction of its velocity. Then the effect of accumulation of the spin rotation upon multiple visits to the same site, which is central to the present paper, does not apply. For a unidirectional motion there are no returns and the *average* spin polarization decays as a simple exponent. At the same time, the *local* spin polarization exhibits very strong fluctuations [10, 11]. To interpret the anomalous sensitivity of $\langle S_z(t)\rangle$ to the external magnetic field, $\boldsymbol{B} = \boldsymbol{z}_0 B$, it is instructive to draw an analogy to the anomalous sensitivity of the resistance of metals to a weak magnetic field (weak localization [12]). Namely, the phase, Bt, of the spin rotation is analogous to the orbital Aharonov-Bohm phase. In weak localization, weak B restricts the area within which counter-propagating random-walk trajectories interfere constructively. In spin relaxation, weak B limits the time interval within which accumulation of spin rotation due to self-intersections takes place.

8.6 Appendix

8.6.1 Modification of the diffusive correlator by the short-time correlators

In order to establish how the short-time correlations modify the correlations due to self-intersections of the diffusive trajectories, consider the second term of Eq. (8.6). This term contains the combination

$$-\cos\big(\phi(t_1)-\phi(t')\big)\cos\big(\phi(t'')-\phi(t_2)\big) \tag{8.20}$$

of four azimuthal angles. Assume that the carrier visits the same site at distant times moments t_1 and t_2, while t' and t'' are the initial and final moments of some hop that takes place between t' and t''. Then the averaging over t', t'' should be performed using the correlator Eq. (8.7). To perform this averaging it is convenient to decompose the product Eq. (8.20) into a sum

$$-\frac{1}{2}\cos\big(\phi(t_1)-\phi(t_2)+\phi(t'')-\phi(t')\big)-\frac{1}{2}\cos\big(\phi(t_1)+\phi(t_2)-\phi(t')-\phi(t'')\big). \tag{8.21}$$

The second term containing the sum, $\big(\phi(t')+\phi(t'')\big)$, is zero on average. The first term contains the difference, $\big(\phi(t')-\phi(t'')\big)$, and averages to

$$-\frac{1}{2}C_0(t',t'')\cos\big(\phi(t_1)-\phi(t_2)\big). \tag{8.22}$$

Consider now two intermediate hops taking place within the intervals $[t', t'']$ and, subsequently, $[t''', t'''']$, between the moments t_1 and t_2. The corresponding combination to be averaged over the initial and final moments of the hops reads

$$\cos\bigl(\phi(t_1)-\phi(t')\bigr)\cos\bigl(\phi(t'')-\phi(t''')\bigr)\cos\bigl(\phi(t'''')-\phi(t_2)\bigr).$$

To average over orientations of the on-site hyperfine fields we have to perform the above decomposition twice, which yields $\frac{1}{4}C_0(t',t'')C_0(t''',t'''')\cos\bigl(\phi(t_1)-\phi(t_2)\bigr)$.

Upon integration of Eq. (8.22) over t', t'' within the interval $t_1 < t' < t'' < t_2$, we conclude that a single hop, described by a solid arc, modifies the integrand in the expression for a diffusive arc by a factor of $-\frac{1}{2}\frac{(t_2-t_1)}{\tau_s}$. Similarly, for two hops, upon integrating over theit initial and final moments, we find that they modify the integrand by a factor of $\frac{1}{4}\frac{(t_2-t_1)^2}{2!\tau_s}$. Adding the contributions from zero, one, two, three, etc. hops, we conclude that intermediate hops lead to the factor $\exp\left[-\frac{(t_2-t_1)}{2\tau_s}\right]$ in the integrand.

In the presence of a z-component of the hyperfine field, the average, Eq. (8.22), assumes the form

$$-\frac{1}{2}C_0(t',t'')\cos\bigl(\phi(t_1)-\phi(t_2)\bigr)\left\langle\cos\left(-\int\limits_{t_2}^{t''}b_z(s)ds-\int\limits_{t'}^{t_1}b_z(s)ds\right)\right\rangle. \tag{8.23}$$

Recall now that $C_0(t',t'')$ restricts t' and t'' within τ from each other. Then the argument of the cosine in Eq. (8.23) reduces to a single integral, $\Phi=\int\limits_{t_2}^{t_1}b_z(s)ds$. Averaging of this cosine over the realizations of b_z can be performed analytically using the fact that the relevant times t_1 and t_2 are of the order of τ_s, which is much bigger than τ. Therefore, the phase, Φ, contains many random contributions, which allows us to use the relation $\langle\cos\Phi\rangle=\exp\left[-\frac{1}{2}\langle\Phi^2\rangle\right]$. The average, $\langle\Phi^2\rangle$, can be expressed via τ_s as $\langle\Phi^2\rangle=\frac{(t_2-t_1)}{4\tau_s}$. Thus, we conclude that, in addition to the factor $-\frac{(t_2-t_1)}{2\tau_s}$, a single arc brings an additional factor, $\exp\left[-\frac{(t_1-t_2)}{4\tau_s}\right]$, into the integrand.

Consideration of two hops leads to the *same* exponential factor, $\exp\left[-\frac{(t_1-t_2)}{4\tau_s}\right]$. This follows from the fact that the product $C_0(t',t'')C_0(t''',t'''')$ restricts t' within τ from t'' and t''' within τ from t'''', which again sets the phase of the cosine, caused by random b_z, equal to $\int\limits_{t_2}^{t_1}b_z(s)ds$. Thus, the modification, $\exp\left[-\frac{3(t_1-t_2)}{4\tau_s}\right]$, of the integrand of Eq. (8.9) used in the main text combines the contributions from in-plane and z components.

8.6.2 Partial summation of the diffusive diagrams for $d=1$

As discussed in the main text, the relevant terms of expansion, Eq. (8.6), for $\langle S_z(t)\rangle$ in 1D represent only diffusive arcs. We analyzed only a single-arc contribution, $\lambda_1(t)$, which

is proportional to b_0^2. The structure of the two-arc diagrams which are proportional to b_0^4 differs qualitatively from the b_0^2-term. To substantiate this point, consider a general case of the term $2n$ in the expansion of Eq. (8.6)

$$\left\langle \prod_{i,j=1}^{2n} \cos(\phi_i - \phi_j) \right\rangle. \tag{8.24}$$

The average in Eq. (8.24) is nonzero when ϕ_i and ϕ_j coincide pairwise. In the simplest case, $n = 1$, the only possible variant of pairing is $\phi_1 = \phi_2$. It corresponds to a single dashed arc. It is not entirely obvious that, already for $n = 2$, additional variants appear. Namely, the product $\cos(\phi_1 - \phi_2)\cos(\phi_3 - \phi_4)$ survives averaging when $\{\phi_1 = \phi_2,\ \phi_3 = \phi_4\}$, but also when $\{\phi_1 = \phi_3,\ \phi_2 = \phi_4\}$ and $\{\phi_1 = \phi_4,\ \phi_2 = \phi_3\}$. As we have shown in the previous subsection, the averaging Eq. (8.24) contains an extra $1/2$ for nontrivial pairings. Graphically, these nontrivial pairings are described by rainbow-like and crossed diffusive diagrams, see Fig. 8.4. Each of three diagrams in Fig. 8.4 is $b_0^4 \tau t^3$ times a numerical factor. Denote these factors with Γ_1, Γ_2, and Γ_3, so that the arcs in diagram Γ_1 do not overlap, the arcs in diagram Γ_2 form a rainbow, while the arcs in diagram Γ_3 cross. The explicit expressions for Γ_1, Γ_2, and Γ_3 read

$$\begin{aligned}
\Gamma_1 &= \frac{1}{\pi} \int_0^1 dx_1 \int_0^{x_1} dx_2 \frac{1}{\sqrt{x_1 + x_2}} \int_0^{x_2} dx_3 \int_0^{x_3} dx_4 \frac{1}{\sqrt{x_3 + x_4}}, \\
\Gamma_2 &= \frac{1}{2\pi} \int_0^1 dx_1 \int_0^{x_1} dx_2 \int_0^{x_2} dx_3 \frac{1}{\sqrt{x_2 + x_3}} \int_0^{x_3} dx_4 \frac{1}{\sqrt{x_1 + x_4}}, \\
\Gamma_3 &= \frac{1}{2\pi} \int_0^1 dx_1 \int_0^{x_1} dx_2 \int_0^{x_2} dx_3 \frac{1}{\sqrt{x_1 + x_3}} \int_0^{x_3} dx_4 \frac{1}{\sqrt{x_2 + x_4}}.
\end{aligned} \tag{8.25}$$

Note now that if all three coefficients in front of integrals were $1/2$, we would be able to present their sum as a single integral with an integrand being a *symmetric* function of all arguments. This integral can be easily evaluated since it decouples into a product. Thus, we have

$$\Gamma_1 + \Gamma_2 + \Gamma_3 = \frac{\Gamma_1}{2} + \frac{A_1^2}{4}. \tag{8.26}$$

Eq. (8.26) suggests that, upon neglecting $\frac{1}{2}\Gamma_1$, the sum of the terms containing zero, one, and two dashed arcs can be presented as $1 - \lambda_1(t) + \frac{1}{4}\lambda_1^2(t)$.

We can also look at the sum $\Gamma_1 + \Gamma_2 + \Gamma_3$ from a different perspective. Namely, it can be presented as $\frac{A_1^2}{2} - (\Gamma_2 + \Gamma_3)$, suggesting that, neglecting $(\Gamma_2 + \Gamma_3)$, the sum can be presented as $1 - \lambda_1(t) + \frac{1}{2}\lambda_1^2(t)$.

The situation with the terms of the order b_0^6 offers more options, see Fig. 8.4. There is one diagram with a coefficient in front of six-fold integral equal to 1, six diagrams with this coefficient equal to 1/2, and eight diagrams with coefficient equal to 1/4. Again, if all of the numerical coefficients were the same, the sum of all 15 terms reduces to a single 6-fold integral with a symmetric integrand, which can be decoupled into a product of three double integrals. Namely, if we set all the coefficients equal to 1/4 and neglect the remainder, the contribution of all 15 diagrams would be equal to $-\frac{1}{4}\left(\frac{A_1^3}{3!}\right)$. Conversely, if we put all the coefficients equal to 1 and neglect the remainder, the result would be $-\frac{A_1^3}{3!}$.

The above arguments can be applied to the higher-order terms proportional to b_0^{2n}. Setting all coefficients equal to 1, allows us to reduce the sum of diagrams with n dashed arcs to $\frac{(-1)^n\lambda_1^n}{n!}$, while setting them all equal to $\frac{1}{2^{n-1}}$ yields $\frac{(-1)^n\lambda_1^n}{2^{n-1}n!}$ for this sum.

Both partial sums can be evaluated analytically. Namely, the sum is equal to $\exp\left[-\lambda_1(t)\right]$ for the first choice of coefficients and is equal to $2\exp\left[-\lambda_1(t)/2\right]-1$ for the second one.

The difference between the partial and actual sums can be estimated by considering the first neglected terms. Within the first variant of the partial summation we neglected $\frac{1}{2}\Gamma_1$, so that

$$\delta\langle S_z\rangle = \frac{b_0^4\tau t^3}{2\pi}\int\limits_0^1 dx_1\int\limits_0^{x_1}\frac{dx_2}{\sqrt{x_1+x_2}}\int\limits_0^{x_2}dx_3\int\limits_0^{x_3}\frac{dx_4}{\sqrt{x_3+x_4}}. \tag{8.27}$$

The above integral can be evaluated analytically yielding

$$\delta\langle S_z\rangle = b_0^4\tau t^3\frac{\Gamma_1}{2} = \frac{b_0^4\tau t^3(\sqrt{2}-1)}{18\pi}(3\ln(1+\sqrt{2})-\sqrt{2}) \approx\ 9\times 10^{-3}b_0^4\tau t^3. \tag{8.28}$$

In a similar fashion we can estimate the accuracy of the second partial sum in which the first neglected term is $\Gamma_2+\Gamma_3$. One has

$$\delta\langle S_z\rangle = \left(b_0^4\tau t^3\right)\left(\frac{\sqrt{2}-1}{6\pi}-\frac{\Gamma_1}{2}\right) \approx\ 10^{-2}b_0^4\tau t^3 \tag{8.29}$$

Note that while the two corrections, Eq. (8.28) and Eq. (8.29), are almost equal in magnitude, the first one shifts the partial sum, $2\exp\left[-\lambda_1(t)/2\right]-1$, up, while the second one shifts the partial sum, $\exp\left[-\lambda_1(t)\right]$, down.

8.6.3 Self-consistent equation for $\langle S_z(t)\rangle$

Summation of the subset of diagrams with n nonoverlapping dashed arcs, Fig. 8.4, corresponds to retaining only the pairings $\phi(t_1)=\phi(t_2)$, $\phi(t_3)=\phi(t_4)$, ... in Eq. (8.6).

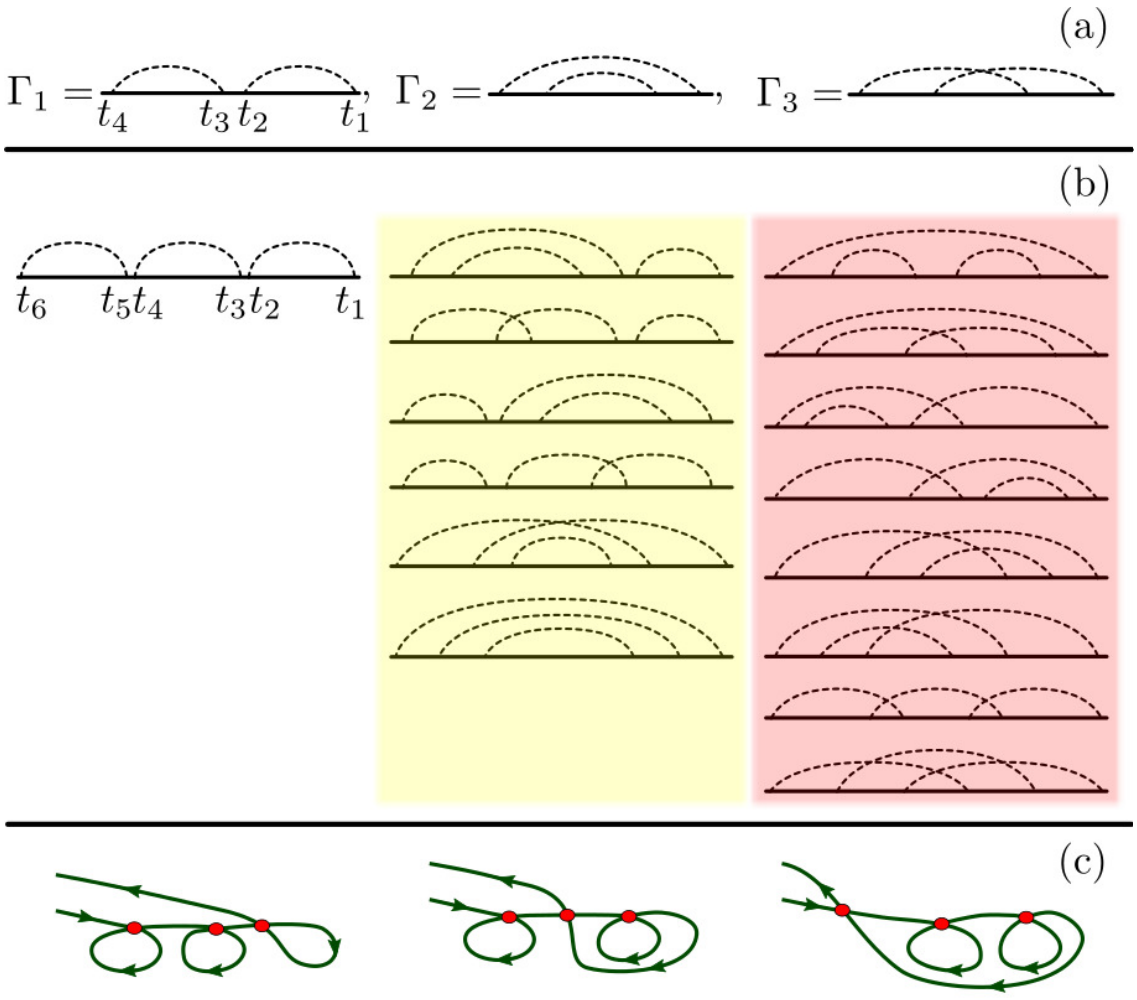

Figure 8.4: Diagrammatic representation of the diffusive propagator. (a) Three possible diagrams containing two dashed lines. Different pairings dictate the arguments of the diffusive propagators in the analytical expressions Eq. (8.25) for the diagrams. (b) Fifteen diagrams with three dashed lines arranged in three groups, white, yellow, and pink, according to their "complexity." Different groups correspond to different mutual arrangements of the self-intersections in the underlying diffusive trajectories. Corresponding trajectories for the first diagrams of each group are sketched in (c).

With these pairings, upon averaging of Eq. (8.6) over the hyperfine fields with the help of Eq. (8.8), the expression for the average $\langle S_z(t)\rangle$ assumes the form

$$\langle S_z(t)\rangle = \sum_{n=0}^{\infty}(-1)^n b_0^{2n}\mu^{(n)}(t), \tag{8.30}$$

where $\mu^{(n)}$ are the $2n$-fold integrals defined as

$$\mu^{(n)}(t) = \int_0^t dt_1 \int_0^{t_1} dt_2 C_D(t_1,t_2) \int_0^{t_2} dt_3 \int_0^{t_3} dt_4 C_D(t_3,t_4)\ldots. \tag{8.31}$$

It is apparent from Eq. (8.31) that these integrals satisfy the recurrence relation

$$\frac{d\mu^{(n+1)}}{dt} = \int_0^t dt_1 C_D(t,t_1)\,\mu^{(n)}(t_1). \tag{8.32}$$

Using this relation, the derivative $d\langle S_z\rangle/dt$ can be expressed via $\langle S_z\rangle$ as follows

$$\frac{d\langle S_z\rangle}{dt} = -\frac{b_0^2\tau^{1/2}}{\pi^{1/2}}\int_0^t \frac{dt'}{(t+t')^{1/2}}\langle S_z(t')\rangle, \tag{8.33}$$

where we have substituted the explicit form of the $1d$ diffusive correlator. Upon introducing a new variable $u = b_0^2\tau^{1/2}t^{3/2}$, Eq. (8.33) can be reduced to a dimensionless form

$$\frac{d\langle S_z\rangle}{du} = -\frac{4}{9\pi^{1/2}u^{1/3}}\int_0^u \frac{du_1}{u_1^{1/3}\left(u^{2/3}+u_1^{2/3}\right)^{1/2}}\langle S_z(u_1)\rangle. \tag{8.34}$$

The solution of Eq. (8.34) exhibits weakly decaying oscillations at $u \gg 1$. To demonstrate this analytically, we search for $\langle S_z(u)\rangle$ in the form of the expansion $\langle S_z(u)\rangle = \sum_{n=0}^{\infty} d_n u^n$. Substituting this expansion into Eq. (8.34) leads to following relation between d_{n+1} and d_n

$$d_{n+1} = -\frac{4\ d_n}{9\pi^{1/2}(n+1)}\int_0^1 \frac{dz\ z^{n-1/3}}{\left(1+z^{2/3}\right)^{1/2}}. \tag{8.35}$$

The behavior of $\langle S_z(u)\rangle$ at large u is determined by the terms of the expansion with $n \gg 1$. The asymptotic value of the integral for large n is $\frac{1}{2^{1/2}\left(n-\frac{1}{3}\right)}$, so that

$$\frac{d_{n+1}}{d_n}|_{n\gg 1} \approx -\frac{16}{9\,(2\pi)^{1/2}\,n^2}. \tag{8.36}$$

Comparing Eq. (8.36) with the Taylor expansion of the zero-order Bessel function $J_0(x) = \sum_{n=0}^{\infty}\frac{(-1)^n}{(n!)^2}\left(\frac{x}{2}\right)^{2n}$, we conclude that for $u \gg 1$ the asymptotic behavior of $\langle S_z(u)\rangle$ is $J_0\left(\frac{4u^{1/2}}{3(2\pi)^{1/4}}\right)$.

In the presence of b_z-component of the random hyperfine field $C_D(t_1,t_2)$ in Eq. (8.31) gets modified as

$$C_D(t_1,t_2) \to C_D(t_1,t_2)\left\langle \cos\left(-\int\limits_{t_2}^{t_1} b_z(s)ds\right)\right\rangle. \tag{8.37}$$

Averaging of the cosine again reduces to the exponent

$$\left\langle \cos\left(-\int\limits_{t_2}^{t_1} b_z(s)ds\right)\right\rangle = \exp\Big[-\frac{1}{2}\int\limits_{t_1}^{t_2}\int\limits_{t_1}^{t_2} dt'dt''\langle b_z(t')b_z(t'')\rangle\Big]$$

$$= \exp\Big[-\frac{b_0^2}{4}\int\limits_{t_1}^{t_2}\int\limits_{t_1}^{t_2} dt'dt'' C_D(t'+t'')\Big]. \tag{8.38}$$

Note that unlike modification of a single dashed arc, the exponent contains diffusive correlator, $C_D(t'+t'')$, rather than the short-time correlator $C_0(t',t'')$. With the above modification of $C_D(t_1+t_2)$, the self-consistent equation Eq. (8.33) takes the form

$$\frac{d\langle S_z\rangle}{dt} = -\frac{b_0^2\tau^{1/2}}{\pi^{1/2}}\int\limits_0^t \frac{dt' \exp\left[-b_0^2\tau^{1/2}(t-t')^{3/2}\right]}{(t+t')^{1/2}}\langle S_z(t')\rangle, \tag{8.39}$$

which leads to Eq. (8.19) of the main text.

8.6.4 Self-intersections in diffusion on the square lattice

In the main text we established that the analytical result Eq. (8.11) describes the results of simulations for $d = 2$ spin relaxation when the constant g_2 is chosen ≈ 3 times bigger than the value predicted by a continuous description of the random walk. To trace the origin of this enhancement let us consider a single self-intersection of a diffusive trajectory on a square lattice. It is illustrated in Fig. 8.5. The specifics of a self-intersection on a square lattice is that the random-walking particle returns to the origin (site 0) from one of four possible directions, say, from site 1, Fig. 8.5. This visit results in a doubling of the spin rotation on site 0. What remains beyond the continuous description, is that, at the next step after site 0, the particle can choose to go up. Then it will visit the site 1 *again*. This, in turn, will lead to additional accumulation of the spin rotation. Moreover, if the particle initially left site 0, say, to the right, i.e., it hopped on site 2, then, after revisiting site 0, it can choose to hop on site 2 again. This would also lead to the additional accumulation of the spin rotation. Finally, another source of accumulation is that, after leaving site 0, say, to site 2, the particle might choose to return back to 0. Accommodation of all the above processes into a continuous description would lead to the enhancement of the parameter g_2

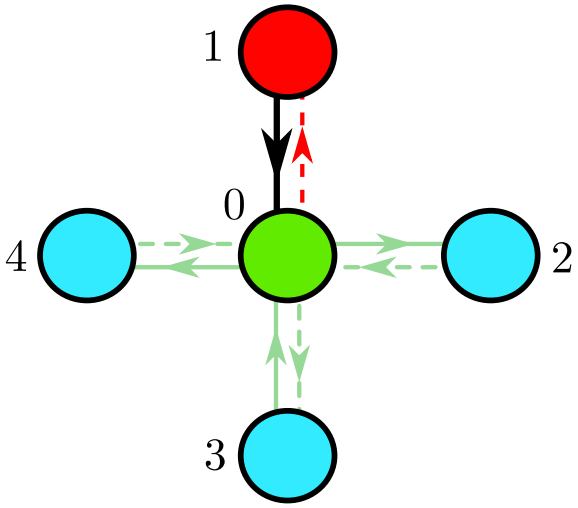

Figure 8.5: Peculiarity of a self-intersection of a random-walk trajectory on a square lattice. The particle returns to the origin, site 0, from site 1 and proceeds in one of the four directions. By choosing the vertical direction it visits site 1 again. If it proceeds towards either 2, 3, or 4, it can return to 0 at the next step. Finally, there is a chance that, it proceeds from 0 to the *same* site where it left from, 0, in the course of a previous visit. All these short-time processes cause additional acceleration of the spin decay.

in Eq. (8.11). However, a rough estimate of this enhancement yields an enhancement factor smaller than 3.

8.7 References

[1] Z. H. Xiong, D. Wu, Z. V. Vardeny, and J. Shi, Nature (London) **427**, 821 (2004).

[2] S. Pramanik, C.-G. Stefanita, S. Patibandla, S. Bandyopadhyay, K. Garre, N. Harth, and M. Cahay, Nat. Nanotechnol. **2**, 216 (2007).

[3] V. A. Dediu, L. E. Hueso, I. Bergenti, and C. Taliani, Nat. Mater.**8**, 850 (2009).

[4] A. J. Drew, J. Hoppler, L. Schulz, F. L. Pratt, P. Desai, P. Shakya, T. Kreouzis, W. P. Gillin, A. Suter, N. A. Morley, V. K. Malik, A. Dubroka, K. W. Kim, H. Bouyanfif, F. Bourqui, C. Bernhard, R. Scheuermann, G. J. Nieuwenhuys, T. Prokscha, and E. Morenzoni, Nat. Mater. **8**, 109 (2009).

[5] T. Nguyen, G. Hukic-Markosian, F. Wang, L. Wojcik, X. Li, E. Ehrenfreund, Z. Vardeny, Nat. Mater. **9**, 345 (2010).

[6] M. I. Dyakonov and V. I. Perel, Sov. Phys. Solid State **13**, 3023 (1971).

[7] I. S. Lyubinskiy and V. Y. Kachorovskii, Phys. Rev. B **73**, 041301 (2006).

[8] M. M. Glazov and E. Ya. Sherman, Europhys. Lett. **76**, 102 (2006).

[9] C. Echeverria-Arrondo and E. Ya. Sherman, Phys. Rev. B **85**, 085430 (2012).

[10] R. C. Roundy and M. E. Raikh, Phys. Rev. B **88**, 205206 (2013).

[11] R. C. Roundy, D. Nemirovsky, V. Kagalovsky, and M. E. Raikh, arXiv:1311.0338.

[12] B. L. Altshuler, D. Khmel'nitzkii, A. I. Larkin, and P. A. Lee, Phys. Rev. B **22**, 5142 (1980).